Universitat Autònoma de Barcelona

Unraveling new roles of geranylgeranyl diphosphate synthases and phytoene synthases in tomato

Miguel Ezquerro Urzanqui

ADVERTIMENT. L'accés als continguts d'aquesta tesi queda condicionat a l'acceptació de les condicions d'ús establertes per la següent llicència Creative Commons: http://cat.creativecommons.org/?page_id=184

ADVERTENCIA. El acceso a los contenidos de esta tesis queda condicionado a la aceptación de las condiciones de uso establecidas por la siguiente licencia Creative Commons: http://es.creativecommons.org/blog/licencias/

WARNING. The access to the contents of this doctoral thesis it is limited to the acceptance of the use conditions set by the following Creative Commons license: https://creativecommons.org/licenses/?lang=en

Unraveling new roles of geranylgeranyl diphosphate synthases and phytoene synthases in tomato

Miguel Ezquerro Urzanqui

2022

Universitat Autònoma de Barcelona

UNIVERSITAT AUTÒNOMA DE BARCELONA

FACULTAT DE BIOCIÈNCES

Programa de Doctorat en Biologia i Biotecnologia Vegetal

PhD thesis

Unraveling new roles of geranylgeranyl diphosphate synthases and phytoene synthases in tomato

Miguel Ezquerro Urzanqui

2022

UNIVERSITAT AUTÒNOMA DE BARCELONA

FACULTAT DE BIOCIÈNCES

Programa de Doctorat en Biologia i Biotecnologia Vegetal

PhD thesis

Unraveling new roles of geranylgeranyl diphosphate synthases and phytoene synthases in tomato

Dissertation presented by Miguel Ezquerro for the degree of Doctor of Plant Biology and Biotechnology at Autonomous University of Barcelona. This work was developed in the Centre for Research in Agricultural Genomics and the Institute for Plant Molecular and Cell Biology

Thesis Director	Thesis tutor	PhD candidate
Prof. Manuel Rodríguez Concepción	Dra. Mercè Llugany Olle	Miguel Ezquerro Urzanqui

Sueña el rico en su riqueza,
que más cuidados le ofrece;
sueña el pobre que padece
su miseria y su pobreza;
sueña el que a medrar empieza,
sueña el que afana y pretende,
sueña el que agravia y ofende,
y en el mundo, en conclusión,
todos sueñan lo que son,
aunque ninguno lo entiende.

Calderón de la Barca

Agradecimientos

Hace casi cinco años viajé a la ciudad de Barcelona a hacer la primera entrevista en el laboratorio donde finalmente he terminado mi tesis doctoral. En esa entrevista, me convencí (o más bien me convencieron) de que había elegido el sitio correcto para emprender un camino tan difícil, tan estresante, pero a la vez tan satisfactorio. Desde el primer momento en que me entrevisté con las personas que allí estaban, yo ya sabía que lo había conseguido.

En primer lugar, quiero agradecer a Manuel. Desde aquella entrevista (informal) en Valencia me abriste los ojos a una posibilidad que yo prácticamente no contemplaba, que era realizar la tesis. Gracias por confiar en mí, siempre recordaré esas palabras que me dijiste a posteriori, que había candidatos con un curriculum mejor y que hasta ahí podías leer. Gracias por todo lo que me has aportado a nivel científico, por ver como una mente brillante hace fácil lo difícil y por tu enorme positivismo cuando yo creía que no iba a poder con esto. Creo que hemos formado un dúo al nivel de las GGPPS con las PSY.

A Vicky, Miguel y Salva, por enseñarme que los verdaderos amigos se pueden hacer en el lugar de trabajo. Gracias por todos los buenos momentos, las fiestas, las excursiones, por hacer que cada día en el laboratorio el trabajo se haya hecho tan fácil. Pero sobre todo gracias por haber estado ahí, como una piña en los momentos malos, por habernos dado consejos, haber llorado juntos y haber crecido como personas. Esto, durará toda la vida.

Gracias a Laura y a Edison, compañeros infatigables durante la pandemia y verdaderos amigos después, aunque estemos separados yo nunca me olvido de vosotros.

A Rosa, Veni, Mireia, Ari, Luca, Di y el resto de compañeros y ex miembros del lab 2.01, gracias por vuestra compañía y por haberme hecho sentir tan cómodo y feliz allí. No me olvido de todos los colegas del CRAG de los que solo me llevo buenos recuerdos.

Ahora, en el IBMCP de Valencia, tan solo puedo agradecer a aquellas personas que me acogieron con los brazos abiertos cuando nuestro laboratorio estaba comenzando, a Vero, mi vecino Jordi, María, Patri, Bea, Beltrán, Buri y Mari Carmen, por esas comidas en las escaleras de emergencia, por esos partidos de pádel y esas (duras) clases de crossfit.

A Victoria, Victor, Carmen, Joaquín y Marta por hacer un grupo tan especial que me ha acogido con los brazos abiertos, juntos, podéis lograrlo todo.

A todos los nuevos miembros de los laboratorios 0.05 y 0.06, habéis hecho que un lugar que parecía vacío, ahora este lleno de risas y buen rollo, muchas gracias, os cuidáis Co.

Gracias al profesor Harro Bouwmeester por darme la oportunidad de formar parte de su laboratorio en Ámsterdam, y a todos los miembros de su equipo que me ayudaron cuando estaba perdido. Pero sobre todo gracias a Guillem, Diego, Javi y al grupo de gente que me acogió allí durante tres meses como si me conocieran de toda la vida.

Gracias a mis amigos de Calahorra y de biotecnología, aunque nos veamos poco, cada vez que lo hacemos es como si el tiempo no hubiera pasado, sois increíbles.

Gracias a Miguel Ángel y a María Ángeles, por la portada de esta tesis, pero sobre todo por la gran acogida que me habéis dado en vuestra familia.

A Julia, como un experimento se ha convertido en la historia de amor más maravillosa que recuerdo, no somos perfectos, pero nos compenetramos a las mil maravillas y vamos a poder con todo. Ahora me toca a mí aguantar los cuatro años de tu doctorado, ¡peta-ho!. Te quiero.

PD: Bali nos espera.

Gracias a mi familia, a mis tíos, a mis primos y gracias abuelos, os echo de menos. Pero en especial a mis abuelas porque, aunque no entendáis una palabra de lo que es una tesis doctoral si estoy aquí es gracias a todo vuestro cariño.

Gracias a mi hermana, aunque estemos separados, sé que nos acordamos el uno del otro todos los días, y que ambos estamos muy orgullosos de en qué nos hemos convertido. Ojalá sigas siendo igual de feliz en Madrid o donde te lleve la vida, solo recuerda que tienes un hermano que te adora.

A mis padres, os lo digo poco, pero os quiero mucho. Tengo demasiado que agradeceros y no sé si encontraré las palabras. Sois el principio y el final de esta historia, me lo habéis enseñado todo, dado todo y regalado todo. Espero que sigáis muchos años conmigo para disfrutar de todo lo que está por llegar. Sois los mejores padres que he podido tener y por eso me siento muy afortunado.

Summary

Carotenoids are isoprenoid compounds essential for photosynthesis and photoprotection but also as precursors of growth regulators such as abscisic acid (ABA) and strigolactones (SLs). In some plants, including tomato (*Solanum lycopersicum*), carotenoids also function as pigments that provide color to flowers and ripe fruit to attract animals for pollination and seed dispersion. Carotenoids are derived from plastidial geranylgeranyl diphosphate (GGPP) synthetized by GGPP synthases (GGPPS). Two molecules of GGPP are condensed by phytoene synthases (PSY) to produce phytoene, the first committed intermediate of the carotenoid pathway. Combined activity of GGPPS and PSY enzymes channel the production of GGPP towards carotenoids and away from other downstream plastidial isoprenoids that also derive from GGPP (*e.g.* chlorophylls, tocopherols, plastoquinone, or gibberellins). Although GGPPS and PSY have been broadly studied in *Arabidopsis,* less is known about the gene families encoding these enzymes and their regulation in most crops, including tomato. In Arabidopsis, only one GGPPS isoform is essential in plastids, where it interacts with the only PSY enzyme present in this species. In tomato, however, there are three genes encoding GGPPS isoforms (herein named SlG1 to 3) and three for PSY isoforms (PSY1 to 3). The main objective of this thesis was to better understand the contribution of specific GGPPS and PSY isoforms for the production of carotenoids in different tissues of the tomato plant, with a particular interest in deciphering the relevance of coordinated expression profiles and direct protein-protein interactions for the channeling of GGPP into the carotenoid pathway. To this end, the work was organized in two main blocks: (1) to identify and characterize the plastidial members of the tomato GGPPS family, and (2) to confirm and explore functional roles for tomato PSY isoforms. We used CRISPR-Cas9 editing to generate tomato mutants defective in all three GGPPS isoforms and two PSY isoforms as the main tools to achieve our objectives. We found that SlG3 acts as a housekeeping GGPPS isoform providing most of the GGPP necessary to produce photosynthesis-related isoprenoids and fruit carotenoids, whereas SlG2 is upregulated during peak-demands of carotenoids to help in delivering GGPP substrates. Intriguingly, absence of both SlG2 and SlG3 results in lethal seed/embryo phenotypes. The role of SlG1 is mainly restricted to roots, where it produces GGPP for the synthesis of carotenoid-derived hormone SLs. As for the PSY family, our results confirmed that PSY2 is the main isoform producing carotenoids in photosynthetic tissues whereas PSY1 functions mainly in flower and fruit chromoplasts. They also unveiled a supporting role for PSY1 in

chloroplasts when plants are exposed to high light. A specific role for each of these isoforms in the production of ABA was found in different fruit tissues. In particular, PSY1 provides carotenoid precursors for ABA synthesis in the pericarp to regulate fruit growth and ripening whereas PSY2 acts in the seed and modulates ABA production to regulate germination. Loss of both PSY1 and PSY2 isoforms results in an albino seedling-lethal phenotype, indicating that PSY3 is not active in photosynthetic shoot tissues but its role is mainly restricted to roots. Co-immunoprecipitation experiments showed specific GGPPS-PSY interactions: SlG1 only interacts with PSY3, SlG2 with PSY1 and PSY2, and SlG3 does not interact with any PSY isoform. We therefore conclude that the SlG1-PSY3 pair ensures the supply of precursors for SL and other carotenoid-derived products in roots, whereas SlG2-PSY2 and SlG2-PSY1 pairs might efficiently channel GGPP production to the synthesis of carotenoids and ABA in shoot tissues. All the new information generated here will be very useful to further design strategies for crop enrichment in carotenoids and other health-promoting GGPP-derived metabolites of specific tissues or under challenging climate conditions.

Resumen

Los carotenoides son compuestos isoprenoides esenciales para la fotosíntesis, la fotoprotección, y como precursores de reguladores del crecimiento como el ácido abscísico (ABA) y las estrigolactonas (SL). En algunas plantas, como el tomate (*Solanum lycopersicum*), los carotenoides también funcionan como pigmentos que dan color a las flores y a los frutos para atraer a polinizadores y a los animales dispersores de semillas. Los carotenoides derivan del precursor geranil geranil difosfato (GGPP), sintetizado en los plastos por las GGPP sintasas (GGPPS). Dos moléculas de GGPP son después condensadas por las fitoeno sintasas (PSY) para producir fitoeno, el primer intermediario de la ruta de los carotenoides. La actividad combinada de las enzimas GGPPS y PSY canaliza la producción de GGPP hacia los carotenoides y la aleja de otros isoprenoides plastidiales que también derivan del GGPP (por ejemplo, clorofilas, tocoferoles, plastoquinona o giberelinas). Aunque las GGPPS y PSY se han estudiado ampliamente en *Arabidopsis thaliana*, nuestro conocimiento de las familias de genes que codifican estas enzimas y su regulación en la mayoría de los cultivos, incluido el tomate, es pobre. En Arabidopsis, sólo una isoforma de GGPPS es esencial en los plastos, donde, además interacciona con la única PSY presente en esta especie. Sin embargo, en tomate, hay tres genes que codifican GGPPS (denominadas en este manuscrito como SlG1-3) y tres para las isoformas de PSY (PSY1-3). El objetivo principal de esta tesis ha sido entender mejor la contribución específica de las isoformas GGPPS y PSY en la producción de carotenoides en diferentes tejidos de la planta de tomate, en especial, estudiando los perfiles de expresión de estas enzimas, así como la interacción directa entre las isoformas GGPPS y PSY a nivel proteico para facilitar la canalización de GGPP a la síntesis de carotenoides. Para ello, organizamos el trabajo en dos bloques principales: (1) identificar y caracterizar los miembros plastidiales de la familia GGPPS de tomate, y (2) confirmar y explorar los roles de las isoformas PSY de tomate. Utilizamos la tecnología CRISPR-Cas9 para generar mutantes de tomate defectivos en las tres isoformas GGPPS y en dos de las isoformas PSY como herramientas para alcanzar nuestros objetivos. Descubrimos que SlG3 funciona como una isoforma “housekeeping”, proporcionando la mayor parte del GGPP necesario para producir isoprenoides fotosintéticos en hojas y carotenoides en fruto, mientras que observamos que la expresión de SlG2 se activa en los momentos de mayor demanda de carotenoides para ayudar con GGPP extra. Curiosamente, la ausencia conjunta de SlG2 y de SlG3 produce fenotipos letales durante el desarrollo de la semilla y/o el

embrión. A su vez descubrimos que el papel de SlG1 se restringe principalmente a las raíces, donde produce GGPP para la síntesis de SL (fitohormonas derivadas de carotenoides) y que no puede compensar la pérdida de SlG2 y SlG3 durante el desarrollo de la semilla. Respecto a la familia de las PSY, nuestros resultados sugieren que PSY2 es la principal isoforma productora de carotenoides en los tejidos fotosintéticos, mientras que PSY1 funciona principalmente en los cromoplastos de flores y frutos. Nuestros datos, también han revelado una función parcialmente redundante por parte de PSY1 en los tejidos fotosintéticos cuando las plantas están expuestas a altas intensidades de luz. Además, estas isoformas tienen un papel diferente en la producción de ABA en distintos tejidos del fruto de tomate. En particular, observamos que PSY1 proporciona fitoeno para la síntesis de ABA en el pericarpio, el cual regula el crecimiento y la maduración del fruto, mientras que PSY2 tiene un papel en semilla donde regula la producción de ABA encargado de controlar la dormancia y la germinación de la misma. La pérdida conjunta de las isoformas PSY1 y PSY2 da lugar a un fenotipo albino letal a nivel de plántula, lo que indica que PSY3 no es activa en los tejidos fotosintéticos durante el desarrollo y que su función se limita principalmente a las raíces. Finalmente, nuestros experimentos de co-inmunoprecipitación proteica, han revelado interacciones específicas entre los miembros de las familias GGPPS-PSY: mientras SlG1 sólo interactúa con PSY3, SlG2 lo hace con PSY1 y PSY2, y curiosamente, SlG3 no interactúa con ninguna PSY. Con esos datos, concluimos, que el dúo SlG1-PSY3 es el encargado del suministro de precursores para la síntesis de SL y otros productos derivados de carotenoides en las raíces, mientras que los pares SlG2-PSY2 y SlG2-PSY1 podrían canalizar eficientemente la producción de GGPP hacia la síntesis de carotenoides y ABA en la parte aérea de la planta de tomate. Toda la información que hemos generado en esta tesis será de gran utilidad para mejorar nuestras herramientas en el diseño de nuevos cultivos enriquecidos en carotenoides y otros metabolitos derivados de GGPP beneficiosos para nuestra salud en las difíciles condiciones climáticas en las que nos encontramos actualmente.

Table of Contents

General Introduction 1

1 Isoprenoids 2

1.1 Biosynthesis of isoprenoid building blocks 2

1.2 Plastidial GPP and GGPP synthesis 4

1.3 GGPP synthases 5

2 Carotenoids 7

2.1 Carotenoid biosynthesis and degradation in plants 8

2.2 Phytoene synthases 10

2.3 GGPPS-PSY interaction 13

3 The tomato model 13

Objectives 16

Chapter I : Several geranylgeranyl diphosphate synthase isoforms supply metabolic substrates for carotenoid biosynthesis in tomato 19

1 Introduction 22

2 Results 24

2.1 SlG1, SlG2 and SlG3 are GGPP-producing plastidial enzymes with similar kinetic properties. 24

2.2 Gene expression profiles suggest a major role of SlG2 and SlG3 in chloroplasts and chromoplasts 25

2.3 SlG2, but not SlG3, can interact with PSY1 and PSY2 26

2.4 Loss of function mutants defective in SlG3, but not those impaired in SlG2, show lower levels of photosynthetic pigments and activity 27

2.5 Ripening-associated fruit pigmentation is altered in *slg2* and *slg3* mutants in correlation with their carotenoid profile 31

2.6 Double mutants defective in both SlG2 and SlG3 are not viable 33

2.7 The phenotypes of single *slg3* mutants are exacerbated in lines with the *SlG2* gene in heterozygosis. 35

3 Discussion 40

3.1 Subfunctionalisation of plastidial GGPPS paralogues in tomato might involve several mechanisms with a major role for differential gene expression 40

3.2 GGPPS isoforms SlG2 and SlG3 have functionally interchangeable roles in chloroplasts and chromoplasts 42

3.3 Concluding remarks 44

4 Materials and methods 45

4.1 Plant material and growing conditions 45

4.2 Generation of CRISPR-Cas9 defective mutants and tomato transformation 45

4.3 Sample collection and phenotypical analysis 46

4.4 Photosynthetic parameters and photography 46

4.5 RNA extraction, cDNA synthesis and RT-qPCR 47

4.6 Isoprenoid extraction and analysis 47

4.7 Determination of ABA and primary metabolites 48

5 Acknowledgements 49

6 References 50

7 Supplemental information 56

Chapter II: Tomato geranylgeranyl diphosphate synthase isoform 1 specifically interacts with phytoene synthase isoform 3 to produce strigolactones in tomato roots. 73

1 Introduction 76

2 Results and discussion 79

2.1 Generation of CRISPR lines defective in SlG1 79

2.2 Loss of SlG1 does not impair the production of photosynthesis-related isoprenoids in tomato leaves 80

2.3 SlG1 is not required for monoterpene synthesis in leaves. 82

2.4 SlG1 is dispensable for carotenoid biosynthesis in fruit. 84

2.5 Gene co-expression analyses suggest a major role of SlG1 in roots. 87

2.6 SlG1 specifically interacts with PSY3 89

2.7 SL synthesis is impaired in *slg1* and *psy1* mutants 91

2.8 SL reduction in *slg1* and *psy1* roots does not affect aerial plant architecture 92

3 Materials and methods 97

3.1 Plant material, sample collection and phenotypical analyses. 97

3.2 Generation of constructs and tomato transformation 98

3.3 Gene co-expression network (GCN) analyses 98

3.4 Photosynthetic parameters 98

3.5 *P.syringae* infection of tomato plants 99

3.6 Co-immunoprecipitation assays 99

3.7 RNA extraction and RT-qPCR analyses 99

3.8 GC-MS analysis of volatile organic compounds 100

3.9 Isoprenoid identification and quantification 100

3.10 ABA extraction and quantification 101

3.11 Strigolactones extraction and measurement 101

4 Acknowledgments 102

5 References 103

6 Supplemental information 109

Chapter III: Overlapping and specialized roles of tomato phytoene synthase isoforms PSY1 and PSY2 in carotenoid and ABA production 121

1 Introduction 124

2 Results 126

2.1 Loss of both PSY1 and PSY2 causes an albino-lethal phenotype 126

2.2 PSY2 is supported by PSY1 to produce carotenoids for photoprotection in leaves 128

2.3 PSY1 is supported by PSY2 to produce carotenoids for flower and fruit pigmentation . 129

2.4 PSY1 and PSY2 are major contributors to ABA synthesis in tomato fruit pericarp and seeds, respectively 132

3 Discussion 138

3.1 PSY1 supports PSY2 in the production of photoprotective carotenoids in leaves and PSY1, PSY2 defective mutants are albino lethal. 138

3.2 PSY1 is supported by PSY2 to produce carotenoids for flower pigmentation and to a lower extent in fruit flesh. 139

3.3 PSY1 and PSY2 are major contributors to ABA synthesis in tomato fruit pericarp and seeds, respectively. 140

3.4 Concluding remarks 142

4 Materials and methods 143

4.1 Plant material, treatments and sample collection. 143
4.2 Generation of CRISPR-Cas9 mutants and tomato transformation. 143
4.3 Photosynthetic parameters 144
4.4 RNA extraction and RT-qPCR analyses. 144
4.5 Pigment quantification. 145
4.6 Determination of ABA levels 145

5 Acknowledgments 146

6 References 147

7 Supplemental information 151

General Discussion 162

1 Evolution of GGPPS and PSY gene families in plants 163

2 The GGPPS family in tomato 166

3 The PSY family in tomato 167

4 The GGPPS and PSY interaction network to direct GGPP flux into the carotenoid pathway: an open question. 169

Conclusions 172

General References 175

Annex

List of Abbreviations

ABA Abscisic acid
AM Arbuscular mycorrhizal
At *Arabidopsis thaliana*
B Breaker
BRs Brassinosteroids
Ca *Capsicum annuum*
CCD Carotenoid cleavage dioxygenase
CHYB carotenoid β hydroxylase
CHYE carotenoid ε hydroxylase
CKs Cytokinins
CLD Chain-length determination
CRISPR Clustered Regularly Interspaced Short Palindromic Repeats
CrtISO carotene isomerase
DMAPP Dimethylallyl diphosphate
DPA Days post-anthesis
dpi Days post-infiltration
DXP Deoxyxylulose 5-phosphate
DXS DXP synthase
e.g. *exempli gratia* ('for example')
FARM First aspartate-rich motif
FPP Farnesyl diphosphate
FPPS FPP synthase
Fv/Fm Maximum quantum yield of photosystem II
GAs Gibberellins
GAP Glyceraldehyde 3-phosphate
GC-MS Gas chromatography mass spectrometry
GCN Gene co-Expression Network
GFPP Geranylfarnesyl diphosphate
GFPPS GFPP synthase
GGPP Geranylgeranyl diphosphate
GGPPS GGPP synthase
GGR Geranylgeranyl reductase
GPP Geranyl diphosphate
GPPS GPP synthase

HPLC High Performance Liquid Chromatography

HY5 Long Hypocotyl5

IDI IPP/DMAPP isomerase

i.e. *id est* (‘that is’)

IP Immunoprecipitation

IPP Isopentenyl diphosphate

KDa Kilodalton

LB Luria-Bertani

LC-MS Liquid-Chromatography – Mass Spectrometry

LSU Large subunit

LYCB Lycopene β-cyclase

LYCE Lycopene ε-cyclase

MEP Methylerythritol 4-phosphate

MG Mature green

MS Murashige and Skoog

MVA Mevalonic acid

NCED Nine-*cis* epoxycarotenoid dioxygenases

NP Normal phosphate Hoagland solution

NPP Neryl diphosphate

NPPS NPP synthases

NPQ Non-photochemical quenching

Os *Oryza sativa*

Or Orange

-P without phosphate

PCR Polymerase chain reaction

PDS Phytoene desaturase

PIFs Phytochrome-Interacting Factors

PPC Pearson correlation coefficients

PRK Phosphoribulokinase

ΦPSII Effective quantum yield of photosystem II

PSY Phytoene synthase

PT Prenyltransferase

R red

rpm Revolutions per minute

RT-qPCR Real time quantitative PCR

SARM Second aspartate-rich motif

SC-PT Short-chain prenyltransferase

SD Standard deviation

Sl *Solanum lycopersicum*

SLs Strigolactones

SPS Solanesyl diphosphate synthase

SSU Small subunit

SSU-I Type I SSU

SSU-II Type II SSU

TF Transcription factor

TPS Terpene synthase

UB-9 Ubiquinone-9

UPLC Ultra Performance Liquid Chromatography

VDE violaxanthin deepoxidase

WT Wild-type

ZDS ζ-carotene desaturase

ZEP Zeaxanthin epoxidase

Z-ISO ζ-carotene isomerase

Zm *Zea Mays*

General introduction

1 Isoprenoids

Isoprenoids (also known as terpenoids) form one of the largest family of metabolites of all living organisms, with more than 50,000 members (Tholl, 2015; Rodríguez-Concepción & Boronat, 2015). Among them, plants show the largest diversity and abundance of isoprenoids in all life kingdoms (Bouvier et al., 2005; Vickers et al., 2014). In plants, some isoprenoids are primary metabolites with fundamental functions irreplaceable in many vital processes. For example, several plastidial isoprenoids are key in the photosynthetic process (Bouvier et al., 2005; Kirby & Keasling, 2009; Vickers et al., 2014). Among them, plastoquinones and phylloquinones are found in the thylakoid membranes of chloroplasts and are essential for the electron transport chain; chlorophylls are the main pigments involved in light harvesting and energy transfer; and carotenoids and tocopherols are powerful antioxidants with a photoprotective role for the photosynthetic apparatus against intense light. In mitochondria, ubiquinone participates in the respiratory electron transport chain, thus required for ATP production (Rodriguez-Concepcion et al., 2018; Tanaka & Tanaka, 2006; Wang & Hekimi, 2016). Also phytosterols are isoprenoid lipids that serve as structural components of plant membranes (similar to cholesterol in animal cells) (García-Llatas & Rodríguez-Estrada, 2011). Other essential isoprenoids are plant hormones such as cytokinins (CKs), brassinosteroids (BRs), gibberellins (GAs), strigolactones (SLs) and abscisic acid (ABA). However, the highest diversity of plant isoprenoids are secondary metabolites in charge of specialized functions. For example, most volatiles with signaling and defensive functions against pathogens are isoprenoids (Vickers et al., 2014). Some isoprenoids have both primary (essential) and secondary (specialized) roles. This is the case of carotenoids, which besides their essential role in photoprotection and hormone (ABA and SL) precursors also serve as natural pigments in many flowers and fruits (Rodriguez-Concepcion et al., 2018). Carotenoids and other isoprenoids are economically-relevant metabolites as colorants, drugs and aromas that have been used in pharma and agrofood industries from a long time ago (Bouvier et al., 2005; Kirby & Keasling, 2009). Understanding how their synthesis is regulated is a must for the rational design of plants with improved contents that could help in meeting the challenges that we are facing under the current climate challenge scenario.

1.1 Biosynthesis of isoprenoid building blocks

Despite the incredible diversity of isoprenoid chemical structures, only two five-carbon (C5) molecules serve as precursors of the entire family. Isopentenyl diphosphate (IPP)

and its allylic isomer dimethylallyl diphosphate (DMAPP) are the building blocks of all isoprenoid compounds (Rodríguez-Concepción & Boronat, 2015). The biosynthesis of these precursors in plants involves two independent pathways, the mevalonic acid (MVA) pathway in the cytosol and the methylerythritol 4-phosphate (MEP) pathway in plastids. Whereas the MVA pathway produces IPP and DMAPP for the synthesis of triterpenes, sterols, BRs, ubiquinone, diterpenes, sesquiterpenes and polyterpenes, the MEP pathway produces precursors for monoterpenes, diterpenes, CKs, GAs and photosynthesis-related isoprenoids (*e.g.* chlorophylls, tocopherols, plastoquinone and carotenoids) (Figure 1) (Bouvier et al., 2005). Several works have demonstrated some exchange of IPP and DMAPP between cell compartments, although at a very small rate and insufficient to sustain the normal demands of substrates for isoprenoid biosynthesis. That causes that both pathways coexist in plants and provide isoprenoid precursors in different cell organelles (Hemmerlin et al., 2012; Schuhr et al., 2003; Vranová et al., 2013) (Figure 1)**.**

The synthesis of all isoprenoid compounds downstream IPP and DMAPP starts with the sequential condensation of a variable number of IPP units into one molecule of DMAPP. This reaction is catalyzed by prenyltransferases (PTs), also known as isoprenyl diphosphate synthases (Hivert et al., 2020; Tholl, 2015). PTs catalyze the elimination of the diphosphate moiety from IPP, to favor the addition of the prenyl unit (without the PPi) to a DMAPP molecule in a head-to-tail manner. This reaction generates a longer linear product with a new 1'-4 double bond. Depending on the stereochemical conformation of these new double bonds on the growing prenyl chains, PTs are classified as *trans*- or *cis*-PTs (Liang et al., 2002; Takahashi & Koyama, 2006; Vandermoten et al., 2009). While both *trans*- and *cis*-PTs catalyze similar enzyme reactions, they share little homology and form different genetically diverse protein families. All *trans*-prenyl transferases share two conserved aspartate-rich motifs $DD(X)_{2–4}D$ (with X corresponding to any amino acid) named FARM (first Asp-rich motif) and SARM (second Asp-rich motif) that are key for their catalytic activity (Bouvier et al., 2005; Dhar et al., 2013). Besides, the chain-length determination motif (CLD) upstream the FARM domain divides *trans*-PTs into short (C10-C20), medium (C25-C35), and long-chain PTs (C40 or longer prenyl diphosphates) depending on the length of their final products (Nagel et al., 2015; Wang et al., 2016). Most primary isoprenoids are made from precursors made by short-chain *trans*-PTs (SC-PTs). Among them, GPP synthases (GPPS) produce C10 GPP for monoterpenes; FPP synthases (FPPS) produce C15 FPP for sesqui- and triterpenes (including sterols); and GGPP synthases (GGPPS) produce C20 GGPP for di- and tetraterpenes (including carotenoids) (Figure 1) (Tholl, 2015; Vandermoten et al., 2009).

These prenyl diphosphates represent the starting point of biosynthetic pathways that involve multiple enzymatic modifications by hundreds of terpenes synthases (TPS) (*e.g.* cyclization, isomerization, conjugation, self-condensation and oxidation) and lead to the incredibly diverse portfolio of isoprenoid molecules found in plants (Tholl, 2015; Vandermoten et al., 2009). In this thesis, we focus on the synthesis and regulation of the carotenoid pathway in particular and plastidial isoprenoids in general, and hence we will not cover isoprenoid pathways derived from the MVA pathway via FPP (Figure 1).

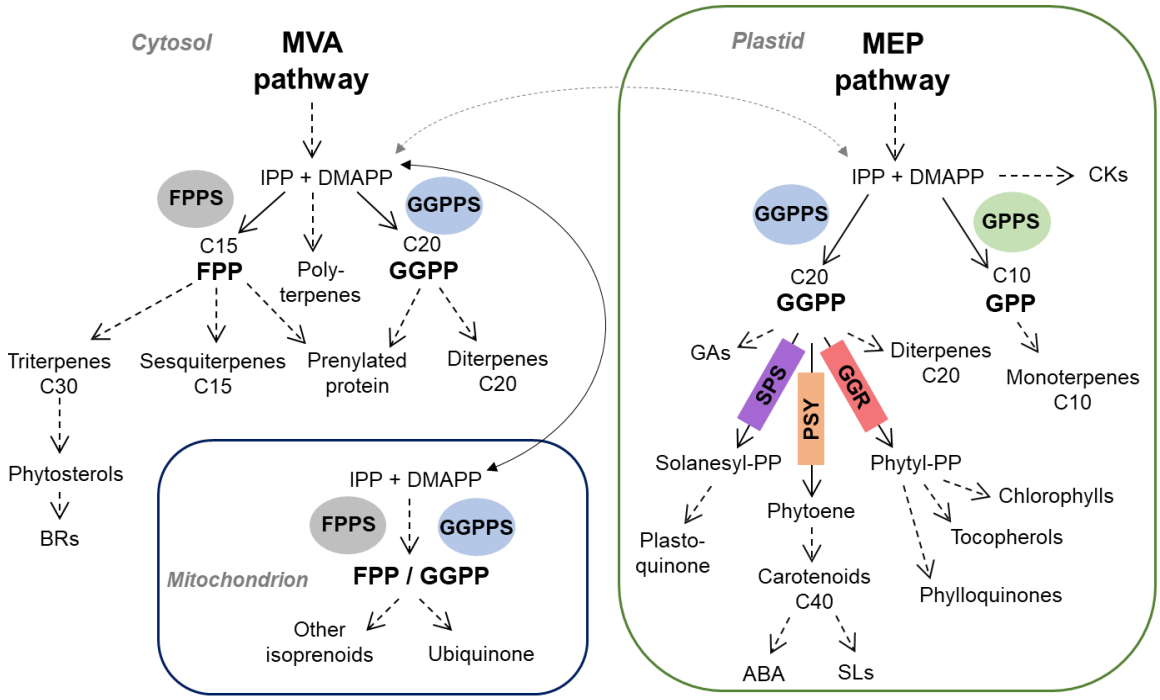

Figure 1. Isoprenoid synthesis in plant cells. IPP and DMAPP, the universal C5 isoprenoid units, are produced by the MVA pathway in the cytosol and the MEP pathway in plastids. Cytosolic IPP and DMAPP are imported into mitochondria, and some interchange exists between cytosol and plastids (gray arrow). Enzymes are shown in color: GPPS synthase (GPPS, in green), FPP synthase (FPPS, in grey) and GGPP synthase (GGPPS, in blue). Those catalyzing the first steps for the production of the main groups of plastidial isoprenoids are boxed; solanesyl diphosphate synthase (SPS) in purple, phytoene synthase (PSY) in orange and geranylgeranyl reductase (GGR) in red. Solid arrows represent single enzymatic steps and dashed arrows indicate multiple reactions. Abbreviations are listed in the Table of Contents at the beginning of the manuscript.

1.2 Plastidial GPP and GGPP synthesis

Plastidial GPPS catalyze the condensation of one IPP and one DMAPP unit to produce GPP, the precursor of most monoterpenes. Neryl diphosphate (NPP), the *cis*-isomer of GPP, can also be used as precursor of some monoterpenes (Schilmiller et al., 2009; Akhtar et al., 2013). NPP synthases (NPPS) are the *cis*-PTs that catalyze the synthesis of NPP from one molecule of IPP and one unit of DMAPP. The main physiological

functions of monoterpenes are defense, attraction of pollinators, and plant to plant communication (Degenhardt et al., 2009; Jansen et al., 2009). For example, oleoresin, a monoterpene synthetized by conifers, is released as a consequence of beetle attack and attracts the insect predators to the wounded trees (Celedon & Bohlmann, 2019). Many monoterpenes such as menthol or limonene also provide fresh aromas that are used as perfumes, while several have shown promising anti-cancer effects (Duetz et al., 2003; Sun, 2007).

GGPPS catalyze three sequential IPP condensations into one DMAPP molecule to produce GGPP (Barja & Rodriguez-Concepcion, 2021). GGPP is the precursor of a large variety of isoprenoids synthesized in different cell compartments, including plastids (Figure 1). Intriguingly, the same enzymes might be involved in the synthesis of both, GPP and GGPP. Homodimeric GPPS and GGPPS enzymes rely on the binding of two GPPS or GGPPS monomers to synthetize GPP or GGPP, respectively (Barja et al., 2021; Ruiz-Sola, Barja, et al., 2016; Vandermoten et al., 2009; Zhou et al., 2017). These GPPS and GGPPS monomers are also known as large subunits (LSUs) and share sequence homology (Wang & Dixon, 2009; Tholl, 2015). Two LSU units need to interact and homodimerize to form a catalytically active enzyme to produce GPP or GGPP. But GPPS or GGPPS activity are sometimes provided by heterodimeric enzymes. Small subunits (SSUs) are a group of proteins present in most plant species that partially share homology with LSUs but lack FARM and/or SARM domains and hence they are catalytically inactive (Wang & Dixon, 2009; Zhou & Pichersky, 2020). There are two types of SSU monomers in plant genomes. Type I SSUs (SSU-I) have been associated to the production of monoterpenes in most plant species. Heterodimerization of SSU-I and LSU-GGPS or LSU-GGPPS directs product specificity to GPP production (Coman et al., 2014; Wang et al., 2008; Zhou & Pichersky, 2020). Type II SSUs (SSU-II) are more complex. Heterodimerization of SSU-II with LSU-GPPS units enhances their ability to produce GPP (Wang & Dixon, 2009), while heterodimerization with LSU-GGPPS units typically enhances the production of GGPP compared to homodimeric GGPPS (Wang et al., 2018; Zhou et al., 2017; Zhou & Pichersky, 2020).

1.3 GGPP synthases

In most plants, different GGPP-demanding processes rely on differentially localized GGPPS isoforms, that normally form small gene families with different roles and spatio-temporal expression profiles (Barja et al., 2021; Kumar et al., 2020; Ruiz-Sola, et al., 2016b; Wang et al., 2019; Wang et al., 2018; Zhou et al., 2017). This coexistence of

different paralogs in the same species usually derives from duplication events of entire genomes or chromosomal segments. While duplication events are relatively normal in plant genomes, only sometimes the new isoforms generated are maintained because they provide an evolutive advantage. This evolutive advantage can come as neofunctionalization (*i.e*. acquiring new functions) or subfunctionalization (*i.e*. scission of the ancestral function between new paralogs). In *Arabidopsis* twelve GGPPS candidates were originally reported (Beck et al., 2013). Experimental lines of evidence, however, have now demonstrated that only isoforms AtGGPPS1 (At1g49530), AtGGPPS2 (At2g18620), AtGGPPS3 (At2g18640), AtGGPPS4 (At2g23800) and AtGGPPS11 (At4g36810) produce GGPP as their main product. The rest comprise a diverse family of SC-PTs but also medium chain-PTs (Beck et al., 2013). Of the true GGPPS enzymes, only two located in plastids: AtGGPPS2 and AtGGPPS11. The *AtGGPPS11* gene shows high expression levels in most plant tissues whereas *AtGGPPS2* is expressed at much lower levels and it shows co-expression with GA biosynthetic genes (Ruiz-Sola et al., 2016a). Further experimental evidence showed that AtGGPPS11 (from herein referred to as AtG11) can physically interact with SSU-I to change its product specificity to GPP production, with PSY for carotenoid production, with solanesyl diphosphate synthase 2 (SPS2) for plastoquinone biosynthesis, and with geranylgeranyl reductase (GGR) for phylloquinone, tocopherol and chlorophyll synthesis (Figure 1) (Ruiz-Sola et al., 2016b). Genetic approaches unraveled that alternative splicing in the *AtGGPPS11* gene produces two isoenzymes, one full-length with a plastid-targeting sequence that ensures chloroplast location for the production of GGPP-derived plastidial isoprenoids (including carotenoids) and another shorter version lacking the plastid-targeting sequence that is located in the cytosol and is required to produce an unidentified isoprenoid product required for embryo development (Ruiz-Sola et al., 2016a). Other GGPPS isoforms may participate in specialized processes in Arabidopsis but AtG11 is the hub isoform in charge of most (essential) GGPP production in plastid and cytosolic compartments (Ruiz-Sola et al., 2016a; Ruiz-Sola et al., 2016b).

Different from Arabidopsis, the rice (*Oryza sativa*) genome only harbors two genes encoding GGPPS-like enzymes. One is a bona fide plastid-targeted GGPPS named OsGGPPS1 (Os07g39270). The other candidate produced GPP as its main product and therefore it was designated as OsGPPS (Os01g14630) (You et al., 2020; Zhou et al., 2017). Rice SSU-II (OsSSU-II, Os02g44780) is able to interact with OsGGPPS1 to efficiently improve GGPP production. Intriguingly, OsSSU-II also recruits OsGGPPS1 from the chloroplast stroma to the thylakoid membranes, where it forms a large protein complex with GGR to channel GGPP into the chlorophyll biosynthesis pathway (Figure

1) (Zhou et al., 2017). The GGPPS family has also been studied in pepper (*Capsicum annuum*). From all SC-PTs candidates, two were found to localize in plastids and named CaGGPPS1 (Capana04g000412) and CaPTP1 (Capana05g000800). Of these, only CaGGPPS1 was experimentally found to produce GGPP *in vitro* (Wang et al., 2018). Yeast two hybrid and bimolecular fluorescence complementation assays demonstrated the heterodimerization of CaGGPPS1 with CaSSU-II (Capana09g002331), resulting in higher GGPP production (Wang et al., 2018). CaGGPPS1 alone (homodimers) and together with CaSSU-II (heterodimers) were also shown to interact with the fruit-predominant PSY isoform, probably to direct GGPP flux to specifically produce carotenoids required as pigments to change fruit color during ripening (Wang et al., 2018). It remains unknown how GGPP flux is directed towards other isoprenoid pathways in these crop systems.

2 Carotenoids

Carotenoids are a group of C40 isoprenoid molecules (tetraterpenes) synthetized by all photosynthetic organisms and some non-photosynthetic bacteria and fungi (Rodriguez-Concepcion et al., 2018; Sun et al., 2018; Torres-Montilla & Rodriguez-Concepcion, 2021). Plant carotenoids have essential roles in photosynthesis and in developmental processes. Carotenoids are important for the assembly of the photosynthetic apparatus and act as auxiliary pigments in light harvesting. But the main role of carotenoids in green tissues is photoprotection against excess light. Carotenoids dissipate excess light energy as heat and scavenge free radicals generated when light energy exceeds the photosynthetic capacity of the chloroplast (Rodriguez-Concepcion et al., 2018; Ruiz-Sola & Rodríguez-Concepción, 2012). Another primary function of carotenoids in plants is to act as precursors of phytohormones such as ABA (involved in plant responses to abiotic stress, seed dormancy and fruit growth) and SLs (involved in root mycorrhization, shoot branching and other developmental processes) (Al-Babili & Bouwmeester, 2015; Kuromori et al., 2018; Rodriguez-Concepcion et al., 2018). But perhaps the most widely known property of carotenoids is their role as natural pigments that provide appealing colors to some non-photosynthetic tissues such as flower petals and ripe fruit to attract animals for pollination and/or seed dispersal (Moreno et al., 2021; Sun et al., 2018).

Although mammals do not produce carotenoids (with only very few exceptions), they are taken in the diet as essential micronutrients (mainly as precursors of retinoids such as vitamin A). Carotenoids are also potent antioxidant compounds that have beneficial effects against sunburn, macular degeneration, some types of cancer and cardiovascular

diseases (Rao & Rao, 2007; Rodriguez-Concepcion et al., 2018). Besides, the characteristic yellow to red colors of carotenoids make them economically relevant as food quality parameters and as ingredients (natural pigments) for the pharma and agrofood industries (Jaswir et al., 2011). Most commercial carotenoids are produced by chemical synthesis. In order to produce these compounds in a more sustainable way (*e.g.*, in plant biofactories) or enrich plant tissues in health-promoting carotenoids (*e.g.*, via biotechnology-driven biofortification), it is essential to first fill the gaps in our understanding of how they are synthesized and how their production is regulated in plants.

2.1 Carotenoid biosynthesis and degradation in plants

Carotenoids in plants are produced in plastids from MEP pathway-derived GGPP (Figure 2). The first committed and main bottleneck step of carotenoid synthesis in plants is the condensation of two molecules of C20 GGPP into C40 phytoene catalyzed by PSY (Cao et al., 2019; Zhou et al., 2022). Several desaturation and isomerization steps subsequently catalyzed by phytoene desaturase (PDS), ζ-carotene isomerase (Z-ISO), ζ-carotene desaturase (ZDS) and carotene isomerase (crtISO) eventually convert uncolored phytoene into lycopene, a red carotenoid pigment that provides their characteristic color to ripe tomatoes. In most plant tissues, however, lycopene is a pathway intermediate that is rapidly converted into downstream products. From the linear lycopene molecule, carotenoid synthesis can diverge depending on the type of cyclization of the ends of the lycopene carbon chain (Figure 2). The production of two β rings (by lycopene β-cyclase, LYCB) produces β-carotene while the production of one ε ring (by lycopene ε-cyclase, LYCE) and one β ring (by LCYB) produces α-carotene. Further hydroxylation of the rings of carotenes by carotenoid β and/or ε hydroxylases (CHYB and/or CHYE, respectively) produces xanthophylls such as zeaxanthin (from β-carotene, β,β branch) or lutein (from α-carotene, β,ε branch) (Figure 2) (Rodriguez-Concepcion et al., 2018). Further epoxidation of zeaxanthin by zeaxanthin epoxidase (ZEP) produces violaxanthin, which can be converted back to zeaxanthin by violaxanthin deepoxidase (VDE). This interconversion, known as the xanthophyll cycle, is of key relevance for the photoprotective role of carotenoids as it contributes to heat dissipation by non-photochemical quenching (NPQ). Violaxanthin can also be transformed into neoxanthin, and both can act as precursors for ABA synthesis. The β,β branch is also

the origin of the carotenoid-derived hormones SLs, which are derived from β-carotene (Figure 2).

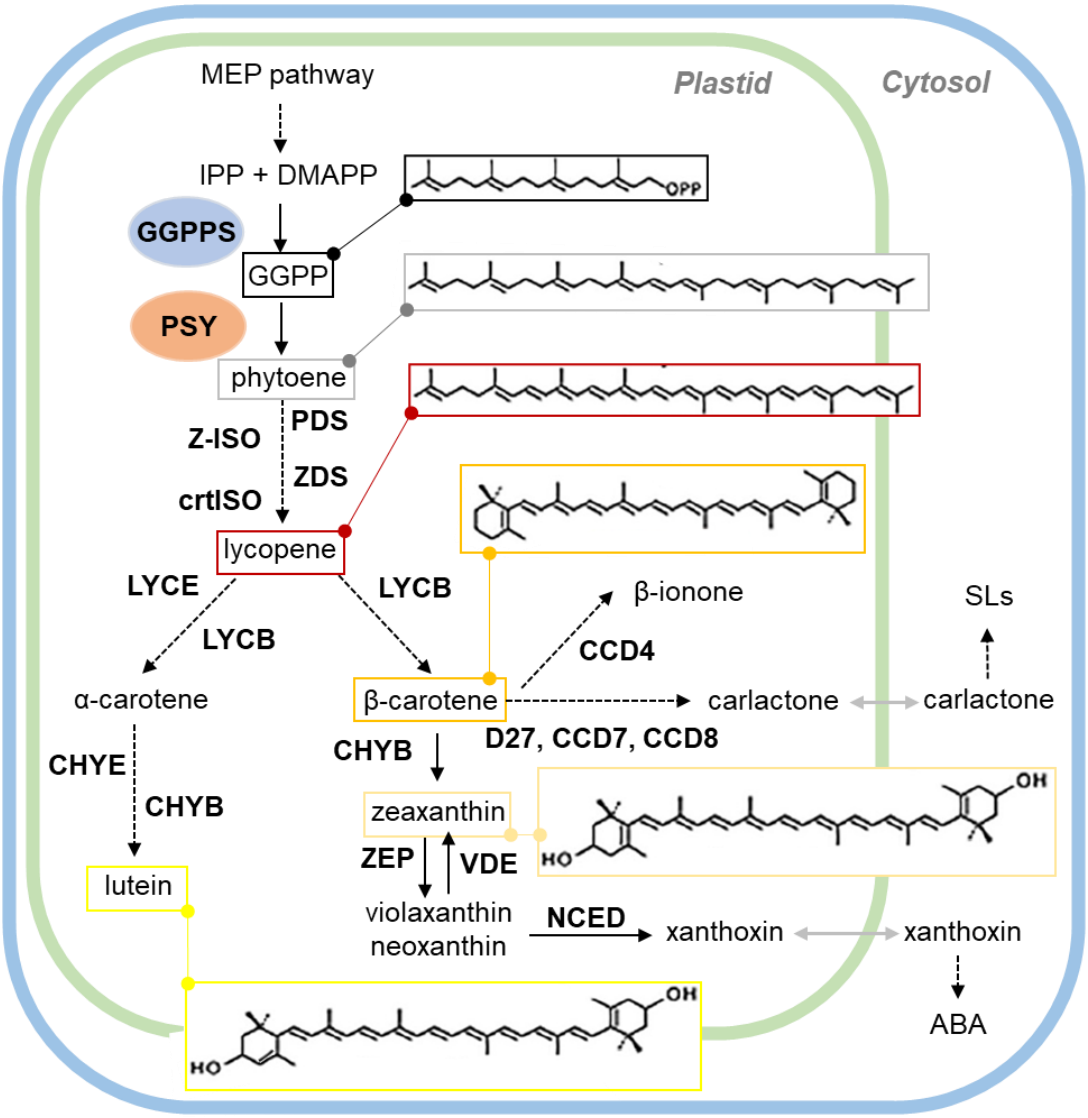

Figure 2. Carotenoid metabolism in plants. GGPPS and PSY enzymes are marked in blue and orange, respectively. The rest of enzymes are highlighted in bold (see text for acronyms). Dashed arrows represent multiple steps. The chemical structures of representative substrates, intermediates and products is shown.

Isomerization of β-carotene to 9-*cis* β-carotene by β-carotene *cis-trans* isomerase (D27) is the first committed step of SL biosynthesis. Subsequent cleavage by carotenoid cleavage dioxygenases 7 and 8 (CCD7 and CCD8) produce carlactone. Next, transport of carlactone to the cytosol for further transformation gives origin to the more than twenty different kinds of SLs (Matthys et al., 2016; Ruyter-Spira et al., 2013; Zhang et al., 2018). ABA biosynthesis also requires isomerization of its carotenoid precursors, violaxanthin or neoxanthin, but the responsible enzyme remains to be identified. Then, the C40 9-*cis*

isomers are cleaved by a particular subclass of CCD enzymes referred to as nine-*cis* epoxycarotenoid dioxygenases (NCEDs) into C15 xanthoxin, that is next transported to the cytosol for the final steps of ABA formation (Figure 2) (Nambara & Marion-Poll, 2005). Other CCD enzymes (including plastidial CCD4 and cytosolic CCD1) have been involved in the production of carotenoid-derived molecules collectively known as apocarotenoids. They include flower and fruit volatiles (flavors and aromas) and pigments mainly involved in attraction of pollinators and seed dispersing animals (Nawade et al., 2020; Rubio-Moraga et al., 2014; Simkin et al., 2004). Other apocarotenoids are biologically active molecules with signaling and regulatory roles. They include apocarotenoids involved in plastid-to-nucleus communication (*e.g.*, β-cyclocitral) and plant-herbivore communication (β-ionone).

2.2 Phytoene synthases

PSY catalyzes the condensation of two molecules of GGPP into phytoene in the first step of the carotenoid biosynthesis pathway (Figure 2). PSY has the highest flux control coefficient of the carotenoid pathway (Fraser et al. 2002), representing the main rate-controlling enzyme (Zhou et al., 2022). Because its pivotal role on controlling isoprenoid flux to carotenoid synthesis, several endogenous factors and environmental conditions control the amount of this important enzyme at transcriptional and translational levels (Arango et al., 2010; Ruiz-Lozano et al., 2016; Zhou et al., 2022). For example, at the transcriptional level environmental conditions such as high light, temperature, drought, or phosphate starvation are known to regulate *PSY* gene expression. In general, developmental events involving a burst in carotenoid synthesis (such as seedling de-etiolation, leaf and flower development and fruit ripening) positively regulate *PSY* expression (Barja et al., 2021; Fraser et al., 1994, 1999; Li et al., 2008; Welsch et al., 2008). Among the transcription factors (TFs) involved, Phytochrome-Interacting Factors (PIFs) and Long Hypocotyl 5 (HY5) negatively and positively influence *PSY* expression, respectively, by specifically binding the *PSY* promoter (Llorente et al., 2016; Toledo-Ortiz et al., 2010). Also several TFs related with fruit ripening have been found to transcriptionally regulate fruit-specific *PSYs* (Fujisawa et al., 2014; Lu et al., 2018). At the protein level, PSY function is regulated by direct binding to several proteins. For instance, binding to the OR chaperone promotes PSY activity by stabilizing the protein and avoiding PSY degradation, whereas binding to the ClpC1 chaperone results in PSY degradation by the Clp protease complex (D'Andrea & Rodriguez-Concepcion, 2019; Welsch et al., 2018). Interestingly, PSY enzymes have been shown to interact with GGPPS in different systems, as described in the next section.

PSY activity in plants is often provided by several paralogs or isoforms encoded by small gene families that produce phytoene for different environmental or developmental processes (Table 1). An exception to this rule is Arabidopsis. In Arabidopsis there is only one PSY-encoding gene (At5g17230) that provides phytoene for carotenoid biosynthesis in the whole plant (Rodríguez-Villalón et al., 2009; Pokhilko et al., 2015). Even though it has been postulated that alternative splicing can produce several PSY variants with distinct enzyme activity (Álvarez et al., 2016), complete inactivation of the Arabidopsis *PSY* gene generates an albino seedling-lethal phenotype (Pokhilko et al., 2015). The rice genome harbors three *PSY* paralogs in its genome (Welsch et al., 2008; You et al., 2020). *OsPSY1* (Os06g51290) and *OsPSY2* (Os12g43130) function predominantly in green tissues, and their expression is controlled by light responsive elements, while *OsPSY3* (Os09g38320) is up-regulated in roots in response to drought stress and high salt and it is associated with stress-induced ABA biosynthesis (Welsch et al., 2008) (Table 1). None of these active PSY isoforms is expressed in the seed endosperm, hence explaining why rice grains do not accumulate carotenoids and have a white color. As rice is the basis of the diet for most people in Asia and other parts of the world with Vitamin A deficiency, the development of carotenoid-rich cultivars of the controversial Golden Rice (probably the most famous genetically-engineered crop to date), appears as a good solution to fight this important problem (Al-Babili & Beyer, 2005; Beyer et al., 2002). In the Golden Rice 2 version, the PSY activity required to channel isoprenoid precursors into the carotenoid pathway was provided by maize (*Zea mays*) ZmPSY1, which is much more efficient than other plant PSY enzymes (Paine et al., 2005). In maize, as well in other monocot crops such as sorghum (*Sorghum bicolor*), PSY1 isoforms are involved in the synthesis of high levels of carotenoids specifically in the grain endosperm (Gallagher et al., 2004; Li et al., 2008). In these monocot species, PSY2 produces carotenoids in leaves and PSY3 in roots for ABA synthesis, similarly to rice (Li et al., 2008; Welsch et al., 2008).

In pepper and tomato, carotenoids are accumulated at high levels in the fruit pericarp (flesh) during ripening. In these two species, the PSY family also has three members. Pepper *CaPSY1* (Capana04g002519) and tomato *SlPSY1* (Solyc03g031860) are mainly involved in carotenoid production during fruit ripening, *CaPSY2* (Capana02g20350) and *SlPSY2* (Solyc02g081330) are mainly required for the synthesis of carotenoids involved in leaf photoprotection, and *CaPSY3* (Capana01g12040) and *SlPSY3* (Solyc01g005940) are proposed to be restricted to roots for SL (instead of ABA) synthesis (Jang et al., 2020; Kim et al., 2010; Wei et al., 2021) (Fraser et al., 1994; Giorio et al., 2008; Stauder et al., 2018).

Table 1. PSYs in plant species

Species	Gene ID	Name	Clade	Proposed function	Evidence	Supporting bibliography
Arabidopsis thaliana	*At5g17230*	*AtPSY*	*dicotPSY1*	essential	Seedling lethal knock out mutant	*Pokhilko et al. (2015)*
Sorghum bicolor	*SbGSStuc11-12-04.5154.*	*SbPSY1*	*monocot-PSY1*	Carotenoid accumulation in the endosperm	High expression in sorghum endosperm	*Gallagher et al. (2004)*
Sorghum bicolor	*SbGSStuc11-12-04.12062.1*	*SbPSY2*	*monocot-PSY2*	Carotenoid supply in green-tissue chloroplasts	Medium expression levels in leaves	*Gallagher et al. (2004)*
Sorghum bicolor	*SbGSStuc11-12-04.766.1*	*SbPSY3*	*monocot-PSY3*	Role in stress-induced ABA formation in roots	High expression during ABA synthesis	*Li et al. (2008)*
Oryza sativa	*Os06g51290*	*OsPSY1*	*monocot-PSY1*	Carotenoid supply in green-tissue chloroplasts	High expression levels in leaves	*Welsch et al. (2008)*
Oryza sativa	*Os12g43130*	*OsPSY2*	*monocot-PSY2*	Helper function in green-tissue chloroplasts	Medium expression levels in leaves	*Welsch et al. (2008)*
Oryza sativa	*Os09g38320*	*OsPSY3*	*monocot-PSY3*	Role in stress-induced ABA formation in roots	High expression during ABA synthesis	*Welsch et al. (2008)*
Zea mays	*GB: AAR08445*	*ZmPSY1*	*monocot-PSY1*	Carotenoid accumulation in the endosperm	High expression in maize endosperm	*Li et al. (2008)*
Zea mays	*GB: AAX13807*	*ZmPSY2*	*monocot-PSY2*	Carotenoid supply in green-tissue chloroplasts	Upregulation during seedling de-etiolation	*Li et al. (2008)*
Zea mays	*GB: DQ356430*	*ZmPSY3*	*monocot-PSY3*	Role in stress-induced ABA formation in roots	High expression during ABA synthesis	*Li et al. (2008)*
Crocus sativus	GB: MH124237	*CsPSY1a*	*monocot-PSY1*	Carotenoid supply in green-tissue chloroplasts	Mainly expressed in leaves	*Ahrazem et al. (2019)*
Crocus sativus	GB: MH124238	*CsPSY1b*	*monocot-PSY1*	Carotenoid supply in green-tissue chloroplasts	Mainly expressed in leaves	*Ahrazem et al. (2019)*
Crocus sativus	GB: MH124239	*CsPSY2*	*monocot-PSY2*	Synthesis of stigma crocins	High expression in the stigma	*Ahrazem et al. (2019)*
Crocus sativus	GB: MH124240	*CsPSY3*	*mono/di-PSY3*	Carotenoid synthesis in root mycorrhization	High expression in roots under stress conditions	*Ahrazem et al. (2019)*
Nicotiana benthamiana	*Niben261Chr17g0776007.1*	NbPSY1a	*dicotPSY1*	Carotenogenesis in green-tissue	Photobleaching when silencing PSY1 and PSY2	*Wang et al. (2021)*
Nicotiana benthamiana	*Niben261Chr14g0831007.1*	NbPSY1b	*dicotPSY1*	Carotenogenesis in green-tissue	Photobleaching when silencing PSY1 and PSY2	*Wang et al. (2021)*
Nicotiana benthamiana	*Niben261Chr16g0522010.1*	NbPSY2a	*dicotPSY1*	Helper function in green-tissue chloroplasts	Photobleaching when silencing PSY1 and PSY2	*Wang et al. (2021)*
Nicotiana benthamiana	Niben261Chr09g0804015.1	NbPSY2b	*dicotPSY1*	Helper function in green-tissue chloroplasts	Photobleaching when silencing PSY1 and PSY2	*Wang et al. (2021)*
Nicotiana benthamiana	Niben261Chr02g0433017.1	NbPSY3a	*dicot-PSY3*	No proposed function	Barely detected in any tissue	*Wang et al. (2021)*
Nicotiana benthamiana	Niben261Chr02g0115010.1	NbPSY3b	*dicot-PSY3*	No proposed function	Barely detected in any tissue	*Wang et al. (2021)*
Solanum lycopersicum	*Solyc03g031860*	*SlPSY1*	*dicotPSY1*	Carotenoid synthesis in petals and fruit	High expression in fruit and petals	*Bartley et al. (1992)*
Solanum lycopersicum	*Solyc02g081330*	*SlPSY2*	*dicotPSY1*	Carotenoid synthesis in leaves	Moderate expression in leaves and petals	*Bartley and Scolnik, (1993)*
Solanum lycopersicum	*Solyc01g005940*	*SlPSY3*	*dicot-PSY3*	Carotenoid synthesis in root mycorrhization	High up-regulation during root mycorrhization	*Walter et al. (2015)*
Solanum tuberosum	PGSC0003DMT400061846	*StPSY1*	*dicot-PSY1*	Unknown role		*Cao et al. (2019)*
Solanum tuberosum	PGSC0003DMT400043103	*StPSY2*	*dicotPSY1*	Carotenoid synthesis in tubers	High expression in potato tubers	*Pasare et al. (2013)*
Capsicum annuum	*Capana04g002519*	*CaPSY1*	*dicotPSY1*	Pepper fruit ripening	High expression in fruit, low in leaves	*Kim et al. (2010)*
Capsicum annuum	*Capana02g20350*	*CaPSY2*	*dicotPSY2*	Leaf photoprotection & pepper fruit ripening	High expression in leaves, low in fruits	*Jang et al. (2020)*
Capsicum annuum	*Capana01g12040*	*CaPSY3*	*dicot-PSY3*	root mycorrhization	Similar structure to other dicot-PSY3	*Jang et al. (2020)*
Medicago truncatula	Medtr5g076620	*MtPSY1*	*dicot-PSY1*	Carotenogenesis in green-tissue	High transcript levels in leaves	*Stauter et al. (2018)*
Medicago truncatula	Medtr3g450510	*MtPSY2a*	*dicot-PSY2*	Carotenogenesis in green-tissue	High transcript levels in leaves	*Stauter et al. (2018)*
Medicago truncatula	Medtr5g090780	*MtPSY2b*	*dicot-PSY2*	Carotenogenesis in green-tissue	High transcript levels in leaves	*Stauter et al. (2018)*
Medicago truncatula	Medtr3g083630	*MtPSY3*	*dicot-PSY3*	Carotenogenesis in root mycorrhization	Strong expression during root mycorrhization	*Stauter et al. (2018)*
Daucus carota	*Dq1921861515*	*DcPSY1*	*dicot-PSY2*	Carotenogenesis in green-tissue and root	High expression in leaves and moderate in roots	*Fuentes et al. (2012)*
Daucus carota	*Dq1921871939*	*DcPSY2*	*dicot-PSY1*	Carotenogenesis in roots and green-tissue	High expression in roots and moderate in leaves	*Fuentes et al. (2012)*
Manihot esculenta	*cassava30274*	MePSY1	*dicot-PSY1*	Carotenoid supply in green-tissue and nectaries	High expression in leaves and nectaries	*Arango et al. (2010)*
Manihot esculenta	*cassava35536*	MePSY2	*dicot-PSY1*	Carotenoid supply in petals and roots	High expression in petals and roots	*Welsch et al. (2010)*
Manihot esculenta	*cassava32745*	MePSY3	*dicot-PSY3*	Pseudo-gene	Abscense of MePSY3 transcript in all tissues	*Arango et al. (2010)*
Citrus sinensis	*GB: AB114648*	CsPSY1	*dicot-PSY1*	Carotenoid synthesis in leaves and fruit	High expression in leaves and fruit	*Tao et al. (2007)*
Cucumis melo	*GB: JF745118*	CmPSY1	*dicotPSY1*	Carotenoid synthesis in fruit, petal and leaves	High expression in fruits and moderate in petals	*Quin et al. (2011)*
Cucumis melo	ICuGI: MU16943	CmPSY2	*dicotPSY1*	Unknown role		*Harel-Beja et al. (2010)*
Cucumis melo	*GB: JF745117*	CmPSY3	*dicot-PSY3*	Unknown role	High expression in roots	*Quin et al. (2011)*

2.3 GGPPS-PSY interaction

Recent research has evidenced that PSY enzymes cannot use freely diffusible GGPP to make phytoene *in vitro* (Camagna et al., 2019). The authors proposed that membrane association of PSY might prevent access to GGPP produced by soluble GGPPS enzymes. A recombinant chimeric enzyme made by fusing GGPP and PSY together was much more efficient in transforming IPP and DMAPP into phytoene than when using two separate GGPPS and PSY enzymes *in vitro* (Camagna et al., 2019). These results suggest that physical interaction of GGPPS and PSY is necessary for efficient channeling of MEP-derived precursors into the carotenoid pathway. GGPPS-PSY interaction has been demonstrated in red algae (Deng et al., 2020) but also in some plant species. In Arabidopsis, AtG11 interacts with PSY, but also with other isoprenoid biosynthetic enzymes, presumably to direct GGPP to different downstream pathways (Ruiz-Sola et al., 2016b). Additionally, protein complexes containing unidentified isoforms of GGPPS and PSY enzymes have been found in tomato leaves but also in the carotenoid-overaccumulating ripe fruits from tomato and pepper (Fraser et al. 2000; Maudinas et al. 1977). More recently, yeast two hybrid and bimolecular fluorescence complementation assays demonstrated the interaction between pepper CaGGPPS1 and the fruit-predominant PSY isoform, CaPSY1 (Wang et al., 2018).

3 The tomato model

Tomato is a very well-suited model system to study carotenoid biosynthesis. Like all plants, tomato produces carotenoids for photosynthesis and photoprotection in chloroplasts and as precursors of ABA and SLs in photosynthetic and non-photosynthetic tissues (Rodriguez-Concepcion et al., 2018). But unlike other model plant systems such as Arabidopsis, tomato accumulates high levels of carotenoids in specialized plastids named chromoplasts, which are present in flower petals and ripe fruit, where carotenoids act as pigments that attract pollinators and seed dispersing animals (Torres-Montilla & Rodriguez-Concepcion, 2021). Besides, in tomato, SLs and other apocarotenoid molecules participate in the signaling and establishment of mycorrhizal symbiosis, that is extremely important for plant survival in poor nutritional soils (Fester et al., 2002; Nouri et al., 2021; Ruiz-Lozano et al., 2016).

When this thesis was started, the information about the GGPPS family in this plant was incomplete. Most of the members were not characterized (or even discovered) and their expression was never investigated in association with carotenoid accumulation (Bramley, 2002; Ament et al., 2006; Falara et al., 2011). By contrast, information on tomato the PSY

family was more abundant. Based on gene expression data and the phenotypic features of PSY1-defective lines, known as *yellow-flesh* (*r*) mutants (Fray and Grierson 1993; Kachanovsky et al., 2012; Kang et al., 2014; Karniel et al., 2022), it was proposed that *PSY1* supports carotenoid synthesis in flowers and fruits, *PSY2* in leaf chloroplasts, and *PSY3* in roots (Fraser et al., 1994, 1999; Kang et al., 2014; Stauder et al., 2018). This PhD project was started to provide an integrated view of these two important enzyme families in tomato.

Objectives

The main objective of this thesis is to better understand the contribution of specific GGPPS and PSY isoforms for the production of carotenoids in different tissues of the tomato plant, with a particular interest in deciphering the relevance of coordinated expression profiles and direct protein-protein interactions for the channeling of GGPP into the carotenoid pathway.

To this end, the work was organized in two main blocks and three chapters:

(1) to identify and characterize the plastidial members of the tomato GGPPS family

(2) to confirm and explore functional roles for tomato PSY isoforms.

Chapter I

Several geranylgeranyl diphosphate synthase isoforms supply metabolic substrates for carotenoid biosynthesis in tomato

Several geranylgeranyl diphosphate synthase isoforms supply metabolic substrates for carotenoid biosynthesis in tomato

Miguel EZQUERRO[1,a], M. Victoria BARJA[1,a] , Stefano BERETTA[1], Gianfranco DIRETTO[2], Igor FLOREZ-SARASA[1], Elisenda FEIXES[1], Alessia FIORE[2], Rumyana KARLOVA[3], Alisdair R. FERNIE[4], Jules BEEKWILDER[5], Manuel RODRIGUEZ-CONCEPCION[1,6,*]

1 Centre for Research in Agricultural Genomics (CRAG) CSIC-IRTA-UAB-UB, Campus UAB Bellaterra, 08193 Barcelona, Spain.

2 Italian National Agency for New Technologies, Energy, and Sustainable Development, Casaccia Research Centre, 00123 Rome, Italy.

3 Laboratory of Plant Physiology, Wageningen University and Research, 6700AA Wageningen, The Netherlands.

4 Max-Planck-Institut für Molekulare Pflanzenphysiologie, 14476 Potsdam-Golm, Germany.

5 BU Bioscience, Wageningen University and Research, 6700AA Wageningen, The Netherlands

6 Institute for Plant Molecular and Cell Biology (IBMCP), CSIC-Universitat Politècnica de València, 46022 Valencia, Spain.

a, These authors equally contributed to the work.

The results presented in this Chapter have been published in *New Phytologist* (Barja, Ezquerro et al., 2021 doi: 10.1111/nph.17283).

Note: The experiments included in this Chapter were co-designed and performed by the PhD candidate under the supervision of the PhD director and MVB. MVB started the research project and performed the initial experiments (results included but figures not shown here). MVB and the PhD candidate completed the presented results (figures shown in the chapter). The contribution of the rest of the authors is detailed in the published version of this chapter, which is attached as an annex.

Several geranylgeranyl diphosphate synthase isoforms supply metabolic substrates for carotenoid biosynthesis in tomato

Abstract

Geranylgeranyl diphosphate (GGPP) is a key metabolite precursor for the production of many cytosolic and plastidial isoprenoids in plants. GGPP is produced by GGPP synthases (GGPPS) and used to produce diterpenoids, gibberellins, tocopherols, chlorophylls, and carotenoids. GGPPS enzymes are encoded by small gene families in most plants, including *Arabidopsis thaliana* and tomato (*Solanum lycopersicum*), and localize to the cytosol, the endoplasmic reticulum, mitochondria and plastids. Three tomato GGPPS have plastidial location (SlG1, SlG2, and SlG3) and provide GGPP for carotenoid synthesis and other essential plastid isoprenoids. These three isoforms have different tissue expression where SlG1 is mainly expressed in roots and SlG2 and SlG3 are expressed both in photosynthetic tissues and ripening fruit. Based on expression profiles is difficult to assign specific roles to these isoforms, specially to SlG2 and SlG3.

Here we used biochemical, molecular, and genetic tools to characterize the plastidial members of the GGPPS family in tomato (*Solanum lycopersicum*) and their role in the production of plastidial isoprenoids in leaves and fruits.

By creating CRISPR-Cas9 mutants defective in SlG3 and SlG2 we found that SlG3 mutants showed a stronger impact on carotenoid levels and derived metabolic, physiological and developmental phenotypes that those impaired in SlG2. We also found that the double mutant defective in both genes were embryo lethal and could be rescued by one single copy of either SlG3 or SlG2. Our work demonstrates that the bulk of GGPP production in tomato chloroplasts and chromoplasts relies on two cooperating GGPPS paralogs, unlike other plant species such as *Arabidopsis thaliana*, rice or pepper, which produce their essential plastidial isoprenoids using a single GGPPS isoform.

1 Introduction

Isoprenoids are essential biological molecules in all living organisms. In particular, plants are the main source of the enormous structural and functional variety that characterizes this family of compounds (Pulido et al., 2012; Tholl, 2015). The building blocks for the biosynthesis of all isoprenoids are isopentenyl diphosphate (IPP) and its double-bond isomer dimethylallyl diphosphate (DMAPP). These five-carbon (C5) universal isoprenoid units are produced in plants by the mevalonic acid (MVA) pathway in the cytosol and the methylerythritol 4-phosphate (MEP) pathway in plastids (Vranová et al., 2013; Rodríguez-Concepción and Boronat, 2015). Short-chain prenyltransferases (SC-PTs) subsequently condense one or more molecules of IPP to one molecule of DMAPP giving rise to C10, C15, C20 and C25 prenyl diphosphates known as geranyl diphosphate (GPP), farnesyl diphosphate (FPP), geranylgeranyl diphosphate (GGPP), and geranylfarnesyl diphosphate (GFPP), respectively. These molecules are the immediate precursors for downstream pathways leading to the production of the main groups of isoprenoids. GPP is produced in plastids as the precursor of C10 monoterpenes. FPP is mainly produced in the cytosol and used to synthesize C15 sesquiterpenes and C30 triterpenes (including phytosterols). GGPP is mostly produced in plastids, serving as the precursor of gibberellins and photosynthesis-related isoprenoids such as chlorophylls, carotenoids, tocopherols, plastoquinone and phylloquinones. However, GGPP is also used for the production of C20 diterpenes in the cytosol, and both FPP and GGPP are produced in mitochondria for ubiquinone and diterpenoid biosynthesis. GFPP is used to produce C25 sesterterpenes in different cell compartments. SC-PTs are encoded by gene families in most plants and they are typically found in different cell compartments, consistent with the requirement of their specific prenyl diphosphate products in different subcellular locations. Prediction of specific products and cell targeting based solely on their protein sequences is still a challenge, making experimental evidence necessary to ascertain their biological role (Cunillera et al., 1996, 1997; Gaffe et al., 2000; Beck et al., 2013; Jones et al., 2013; Nagel et al., 2015; Wang et al., 2016a; Zhou et al., 2017; Zhou and Pichersky, 2020).

Carotenoids are one of the most studied groups of plant isoprenoids. These C40 tetraterpenes are greatly demanded by cosmetic and agro-food industries as natural red to yellow pigments and provide benefits for human health, *e.g.* as precursors of vitamin A and other biologically active molecules (Sandmann, 2015; Rodriguez-Concepcion et al., 2018). In plants, carotenoids have different functions. In photosynthetic tissues, they are required for the assembly of the photosynthetic apparatus, contribute to light harvesting and are essential for photoprotection by dissipating excess light energy as heat and by scavenging reactive oxygen species. They are also fundamental in growth regulation, since they are the

precursors of retrograde signals and phytohormones such as abscisic acid (ABA) and strigolactones. As a secondary role, carotenoids provide distinctive colors to flowers and fruits to attract pollinators and seed dispersal animals (Nisar et al., 2015; Yuan et al., 2015). In plants, carotenoids are produced and stored in plastids, including chloroplasts and chromoplasts (Ruiz-Sola and Rodríguez-Concepción, 2012; Sun et al., 2018). MEP-derived IPP and DMAPP are converted into GGPP by plastidial GGPP synthase (GGPPS) isoforms and then GGPP is transformed into phytoene by phytoene synthase (PSY) enzymes. The production of phytoene, the first committed intermediate of the carotenoid pathway, is considered to be a major rate-determining step regulating the metabolic flux through this pathway (Fraser et al., 2002). In tomato (*Solanum lycopersicum*), three PSY-encoding genes control carotenoid biosynthesis in different tissues. *PSY1* expression is boosted during ripening to produce carotenoids involved in the pigmentation of the fruit (Bartley et al., 1992; Fray and Grierson, 1993; Giorio et al., 2008; Kachanovsky et al., 2012). *PSY2* is expressed in all tissues, including fruits, but transcript levels are much higher than those of *PSY1* in photosynthetic tissues, where carotenoids are required for photosynthesis and photoprotection (Bartley and Scolnik, 1993; Giorio et al., 2008). Lastly, *PSY3* is mainly expressed in roots and it is induced during mycorrhization (Walter et al., 2015; Stauder et al., 2018), when carotenoid biosynthesis is up-regulated to produce strigolactones and apocarotenoid molecules essential for the establishment of the symbiosis (Fester et al., 2002, 2005; Baslam et al., 2013; Ruiz-Lozano et al., 2016; Stauder et al., 2018). Whether the corresponding PSY isoforms use GGPP supplied by different GGPPS isoforms remains unknown.

Several GGPP synthase (GGPPS) paralogs have been retained in plants during evolution (Beck et al., 2013; Zhang et al., 2015; Ruiz-Sola et al., 2016a, 2016b; Zhou et al., 2017; Wang et al., 2018). However, a single GGPPS isoform appears to produce the GGPP substrate needed for the production of carotenoids and other plastidial isoprenoids in the three plant species whose GGPPS families have been best characterized to date: *Arabidopsis thaliana,* rice (*Oryza sativa*) and pepper (*Capsicum annuum*) (Ruiz-Sola et al., 2016a, 2016b; Zhou et al., 2017; Wang et al., 2018). While tomato has become one of the best plant systems to study the biosynthesis of carotenoids and its regulation, we still have an incomplete picture of the GGPPS family in this plant. Recent work has determined that five genes encoding GGPPS homologs exist in the tomato genome, three of which were confirmed to produce GGPP *in vitro* and localize in plastids (Zhou and Pichersky, 2020; Barja et al., 2021). Which of these plastidial GGPPS isoforms are required for the production of carotenoids in photosynthetic tissues (*e.g.* for photoprotection), fruits (*e.g.* for pigmentation) or roots (*e.g.* for mycorrhization) remains unknown. Here we characterized the *in vivo* role of plastidial GGPPS enzymes located in green tissue and fruit and provide

clues to understand how the supply of plastidial GGPP for the synthesis of carotenoids with different biological functions in particular tomato tissues is regulated in this important crop plant.

2 Results

2.1 SlG1, SlG2 and SlG3 are GGPP-producing plastidial enzymes with similar kinetic properties.

Several genes encoding proteins with homology to GGPPS enzymes are found in the tomato genome (Ament et al., 2006; Fraser et al., 2007; Stauder et al., 2018; Zhou & Pichersky, 2020). From these, three have been found to localise in plastids and produce GGPP in vitro, namely GGPPS1 (Solyc11g011240), GGPPS2 (Solyc04g079960) and GGPPS3 (Solyc02g085700), here referred to as SlG1, SlG2 and SlG3. We confirmed the plastidial targeting of these three isoforms by expressing constructs encoding GFP fusions of the full-length SlG1-3 proteins in agroinfiltrated tobacco (Nicotiana benthamiana) leaves. In all three cases, fluorescence corresponding to the GFP fusion proteins co-localised with chlorophyll autofluorescence (Barja et al., 2021, annex I), and supported the conclusion that they were all efficiently targeted to chloroplasts. We also experimentally confirmed the ability of purified SlG1-3 proteins to produce GGPP in vitro. The three tomato isoforms were expressed in Escherichia coli cells without their predicted plastid-targeting sequences (Barja et al., 2021, annex I) and whole-cell protein extracts were directly used for activity assays in the presence of IPP and DMAPP followed by the analysis of the reaction products by LC-MS (Barja et al., 2021, annex I). As positive and negative controls, we used the Arabidopsis AtG11 (active) and AtG11s (inactive) proteins (Ruiz-Sola et al., 2016a). This experiment confirmed that SlG1, SlG2, SlG3 and AtG11 (but no AtG11s) produced only GGPP (Barja et al., 2021, annex I), in agreement with recently reported data (Zhou & Pichersky, 2020). To gain new knowledge on the biochemical properties of these enzymes, we used purified proteins to calculate their kinetic parameters. Enzymatic assays performed as described previously (Barja & Rodríguez-Concepción, 2020) showed that all tested GGPPS proteins exhibited a similar optimal pH around 7.5 (Barja et al., 2021, annex I), as expected for stromal enzymes (Höhner et al., 2016). The parameters Km (an estimator of the apparent affinity for the IPP and DMAPP substrates) and Vmax exhibited very similar values among the three tomato enzymes (Barja et al., 2021, annex I). They were also similar to those obtained for AtG11 here and elsewhere (Wang & Dixon, 2009; Camagna et al., 2019). We therefore concluded that tomato SlG1, SlG2 and SlG3 and Arabidopsis AtG11 are plastidial GGPPS enzymes with very similar kinetic properties.

2.2 Gene expression profiles suggest a major role of SlG2 and SlG3 in chloroplasts and chromoplasts

Analysis of public gene expression databases showed that the genes encoding SlG1-3 enzymes were expressed in roots, leaves and flowers (Figure S1). Of these, the most highly expressed gene was *SlG3* followed by *SlG2*, while *SlG1* transcripts were present at very low levels. *SlG2* and *SlG3*, but not *SlG1*, were also expressed at high levels in fruit pericarp and seed tissues (Figure S1). As an initial approach to gain an insight into the possible functions of these individual isoforms, we performed a GCN analysis. This is a powerful tool to infer biological functions that we previously used to identify AtG11 as the main GGPPS isoform for plastidial isoprenoid production in Arabidopsis (Ruiz-Sola et al., 2016b). By using publicly available databases for plant comparative genomics (*PLAZA 4.0, Phytozome*), we searched for tomato homologues of the plastidial pathways that supply GGPPS substrates (MEP pathway) and consume GGPP to produce carotenoids, chlorophylls, tocopherols, phylloquinone, plastoquinone, gibberellins, strigolactones and ABA (Barja et al., 2021, annex I). We retrieved their expression data from TomExpress database (Zouine et al., 2017) experiments carried out using either leaf or fruit samples at different developmental stages (Barja et al., 2021). Then, we calculated their correlation with *SlG1*, *SlG2* and *SlG3* expression using pairwise Pearson correlations. The results of the GCN analyses are shown in Barja et al., 2021 and annex I.

It was not possible to obtain correlation data for tomato roots as only two experiments using root samples are deposited in the TomExpress database. In leaves and fruits, *SlG1* was poorly co-expressed with the query genes. By contrast, and similar to that observed with AtG11 (Ruiz-Sola et al., 2016b), *SlG2* and, to a lower extent, *SlG3* were highly connected to plastidial isoprenoid biosynthetic genes in leaf tissues. Connectivity was lower in fruit and, in this case, it was a bit higher for *SlG3* (Barja et al., 2021, annex I). These results suggest that *SlG2* and *SlG3* might be the main GGPP-producing isoforms in leaf chloroplasts and fruit chromoplasts.

In tomato, carotenoids contribute to mycorrhizal associations, photoprotection and fruit pigmentation and, therefore, the levels of these GGPP-derived metabolites increase during root mycorrhization, seedling de-etiolation and fruit ripening. In agreement with the rate-determining role of PSY for carotenoid synthesis (Fraser et al., 2002), the expression levels of PSY-encoding genes also increase during such carotenoid-demanding developmental processes. By using real-time quantitative PCR (qPCR) analysis, we experimentally confirmed the upregulation of *PSY1* during fruit ripening and *PSY3* in mycorrhized roots (Barja et al., 2021, annex I). Furthermore, we found that the *PSY2* gene was more strongly upregulated than PSY1 during tomato seedling de-etiolation (Barja et al., 2021, annex I).

Using the same samples, we observed that only *SlG1* was upregulated during root mycorrhization, showing an expression pattern similar to that observed for *PSY3* (Barja et al., 2021, annex I). During fruit ripening, *SlG2* and, to a lower extent, *SlG3* were upregulated, but not as much as *PSY1* (Barja et al., 2021, annex I). *SlG2* was also the most strongly upregulated GGPPS-encoding gene during seedling de-etiolation, paralleling *PSY2* induction. Interestingly, *SlG3* and *PSY1* were also induced with a similar profile during this process, even though induction levels were much lower than those observed for *SlG2* and *PSY2* (Barja et al., 2021, annex I). Together, these data suggested that SlG1 might provide GGPP for PSY3 to produce carotenoids in roots, particularly when needed during mycorrhization, whereas both SlG2 and SlG3 would be required in leaves and fruits to support carotenoid production for photosynthesis (mostly by PSY2) and fruit pigmentation (by PSY1).

2.3 SlG2, but not SlG3, can interact with PSY1 and PSY2

A coordinated role for SlG1 and PSY3 in mycorrhization has already been proposed (Stauder et al., 2018), but the possible connection between the other plastidial GGPPS and PSY isoforms remains unclear. GGPPS proteins can physically interact with PSY and other enzymes catalysing both upstream and downstream biosynthetic steps in the plastids of different plant species (Maudinas et al., 1977; Dogbo & Camara, 1987; Camara, 1993; Fraser et al., 2000; Ruiz-Sola et al., 2016b; Zhou et al., 2017; Wang et al., 2018; Camagna et al., 2019). This mechanism may facilitate channelling of precursors towards specific groups of plastidial isoprenoids. Protein complexes containing both GGPPS and PSY enzymes were isolated from tomato chloroplasts and fruit chromoplasts (Maudinas et al., 1977; Fraser et al., 2000), but the specific isoforms forming these protein complexes were never identified. Given the co-regulation of SlG2 and SlG3 with PSY1 and PSY2 genes in chloroplasts (i.e. photosynthetic tissues) and chromoplasts (i.e. fruits), we decided to test possible interactions of these isoforms in co-immunoprecipitation assays (Figure 1). Constructs harbouring C-terminal Myc-tagged GGPPS and HA-tagged PSY sequences were combined and transiently co-expressed in N. benthamiana leaves. As a negative control, we used a Myc-tagged version of Arabidopsis phosphoribulokinase (PRK-Myc), a stromal enzyme of the Calvin cycle. Both PSY1-HA and PSY2-HA could be co-immunoprecipitated with SlG2-Myc, suggesting that they are present in the same complexes in vivo (Figure 1). By contrast, none of these PSY isoforms could be detected in the samples co-immunoprecipitated with either SlG3-Myc or PRK-Myc. The same Myc-tagged SlG2 and SlG3 proteins used in these experiments were able to co-immunoprecipitate their HA-tagged counterparts (Figure 1). This result, consistent with the ability of GGPPS proteins to form

homodimers and also heterodimers, confirms that the observed lack of interaction of SlG3 with PSY enzymes was not due to SlG3-Myc having lost its capacity to interact with other proteins.

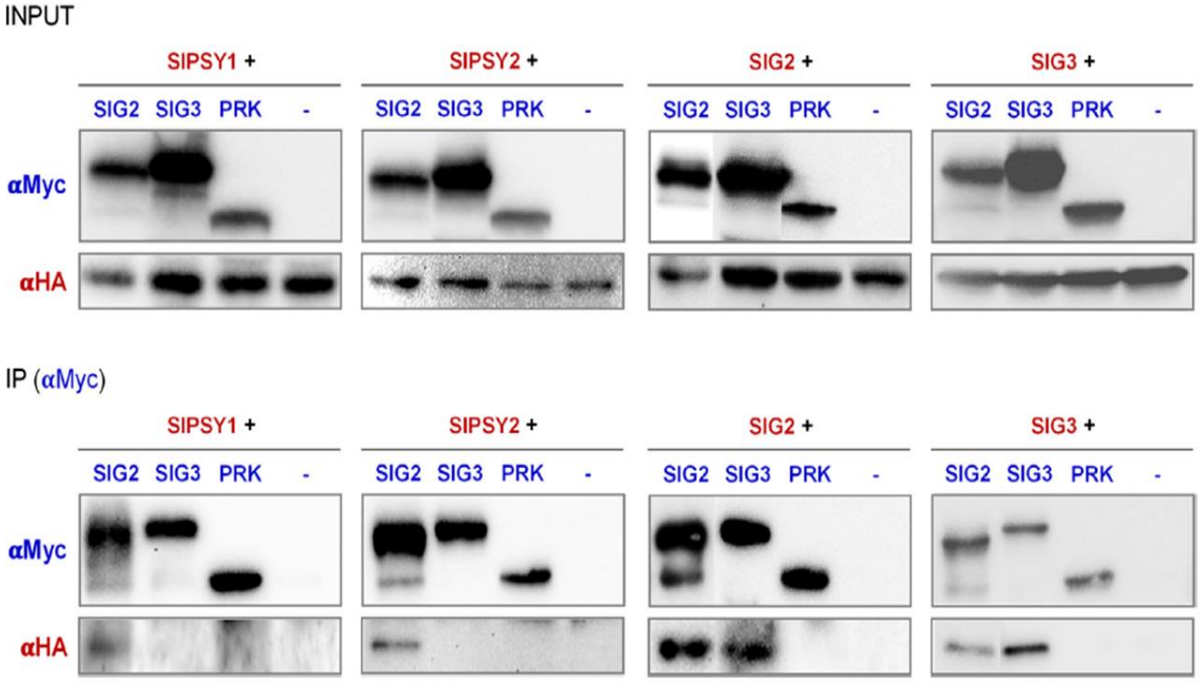

Figure 1. Co-immunoprecipitation analyses. *Nicotiana benthamiana* leaves were co-agroinfiltrated with the indicated proteins tagged with C-terminal Myc (in blue) or HA (in red) epitopes. Controls agroinfiltrated only with the HA-tagged protein are indicated as (-). A fraction of the protein extracts (INPUT) was used to test protein production using immunoblot analyses using antibodies against Myc (αMyc) and HA (αHA). After immunoprecipitation (IP) of the remaining protein extracts using αMyc, simples were used for immunoblot analyses with αMyc (to confirm successful IP) and αHA (to detect the presence of co-immunoprecipitated HA-tagged proteins)

2.4 Loss of function mutants defective in SlG3, but not those impaired in SlG2, show lower levels of photosynthetic pigments and activity

To provide genetic robust data that support the previous roles proposed for SlG2 and SlG3 in our laboratory (Barja et al., 2021, annex I), and elsewhere (Zhou & Pichersky, 2020) we generated CRISPR-Cas9 mutants defective in these enzymes (Figure 2, S2-3). We designed two single guide RNAs (sgRNA) for each gene with the aim of creating deletions encompassing unique restriction sites for rapid screening (Figure 2a). Two independent deletion alleles that created premature translation stop codons were selected for each gene and named *slg2-1*, *slg2-2*, *slg3-1* and *slg3-2* (Figure 2a) (Figures S2-S4). To confirm that the truncated proteins lacked GGPPS activity, we tested them in *E. coli* strains that synthesize the red carotenoid lycopene only when a source of GGPP is supplied (Ruiz-Sola et al., 2016a). Transformation with constructs harboring the mutant enzymes did not produce

more lycopene than empty plasmid controls, indicating that they lack GGPPS activity. (Figure 2b). Once confirmed that the selected mutant alleles produced non-functional proteins, homozygous lines without Cas9 were obtained and used for further experiments.

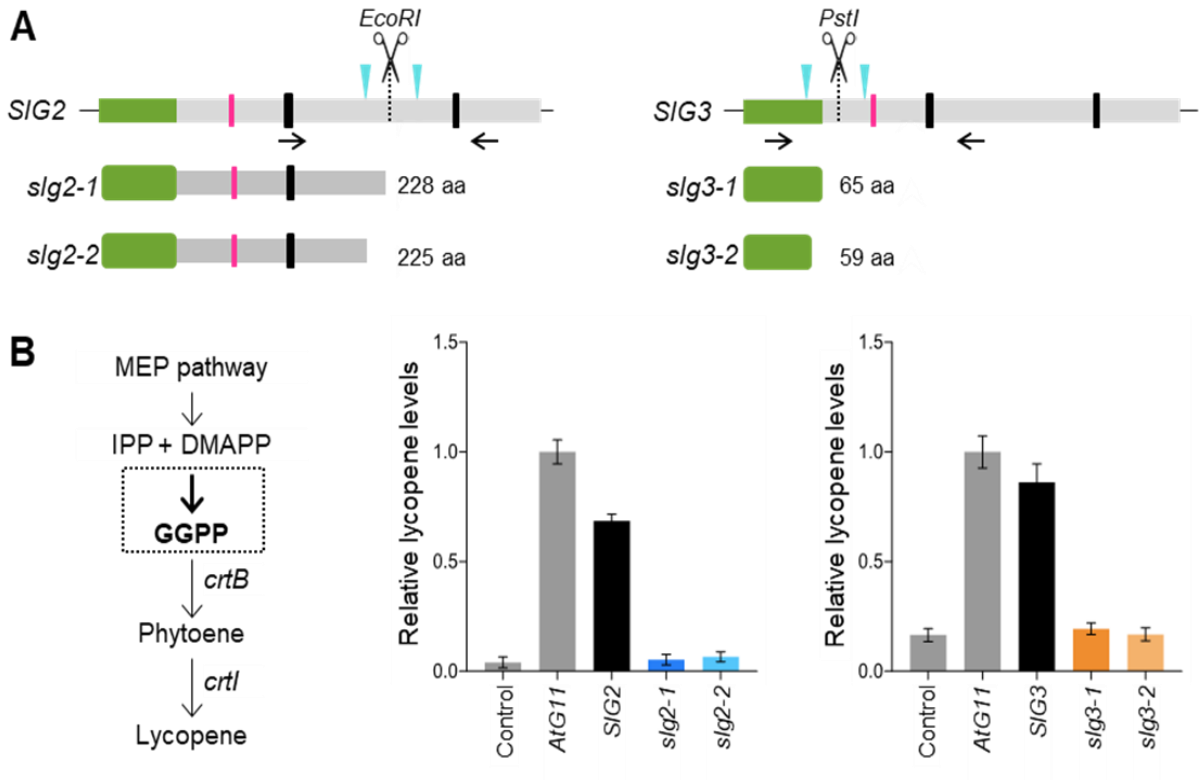

Figure 2. CRISPR-Cas9 mutagenesis of *SlG2* and *SlG3* genes. (A) Scheme representing the designed strategy to generate deletions on *SlG2* and *SlG3* genes and resulting proteins in selected mutant alleles (See Figures S2-4 for further details). Green, pink and black boxes represent transit peptides, protein-protein interaction motifs, and catalytic domains (FARM and SARM), respectively. Blue arrowheads indicate the position of the designed sgRNAs encompassing specific restriction sites, and black arrows represent primer pairs used for genotyping. **(B)** Activity assays of WT and mutant GGPPS enzymes in *E. coli* strains expressing bacterial genes for lycopene biosynthesis (*crtB* and *crtI*) but lacking GGPPS activity. Lycopene production after transformation with an empty vector (labelled as "Control" in the plots) or plasmid constructs harboring the indicated sequences is represented relative to the levels obtained with the bona-fide GGPPS enzyme AtG11. Values represent the mean±SD of at least three independent transformants (n=3).

The most obvious phenotype among the selected lines was the pale colour of *slg3* mutants compared with *slg2* alleles or azygous (wild-type (WT)) plants (Figure 3). This phenotype was clear in emerging and young leaves, but it weakened as leaves grew and became mature (Figure 3a). The pale colour correlated with significantly reduced levels of carotenoids and chlorophylls in young leaves of *sgl3-1* and *sgl3-2* lines compared with those of WT plants (Figure 3b; Table S3). The differences were less clear for tocopherols, another group of GGPP-derived plastidial isoprenoids (Figure 3b). Similar levels of carotenoids, chlorophylls and tocopherols were detected in mature leaves of WT, *slg2* and *slg3* plants (Figure 3b; Table S3). To test whether the reduced accumulation of photosynthesis-related isoprenoids in *slg3* lines had an impact on photosynthesis, we quantified the effective quantum yield of photosystem II (ϕPSII) in both young and mature leaves (Figure 3c). A 30% reduction in ϕPSII was observed in young leaves from *slg3* plants compared with those of WT or *slg2* lines, consistent with the *slg3*-specific reduction of GGPP-derived metabolites. Despite similar levels of photosynthetic pigments accumulated in the mature leaves of all genotypes tested, ϕPSII was slightly reduced in some mutants relative to WT lines (Figure 3c).

We further explored the possible effects that the loss of SlG2 or SlG3 function might have on other metabolic pathways using the same samples of young leaves used for isoprenoid and ϕPSII determination (Figure 4). GC-MS metabolite profiling showed strongly decreased levels of sucrose, glucose and fructose in SlG3-defective leaves, probably due to photosynthetic impairment. Mutant *slg3* leaves also displayed increased levels of amino acids derived from glycerate (Ser and Gly), shikimate (Phe, Trp and Tyr), pyruvate (Val, Ile and Ala), 2-oxoglutarate (Glu, Orn, His and GABA) and malate (Asp, Asn, Lys, Thr, Met, homoserine and beta-alanine). In line with some of these amino acid changes, SlG3-defective leaves displayed altered accumulation of tricarboxylic acid cycle-related intermediates (citrate and 2-oxoglutarate). Only a few common changes were detected in both *slg2* and *slg3* leaves. They included a decrease in putrescine and ascorbate levels (more pronounced in *slg3* leaves), as well as an altered accumulation of metabolites produced by the plastidial shikimate pathway, including the above-mentioned aromatic amino acids and phenylpropanoid derivatives such as caffeate and 3-caffeoyl-quinate (Figure 4). The levels of the carotenoid-derived hormone ABA were similar in WT and mutant samples (Table 1 and Figure 4).

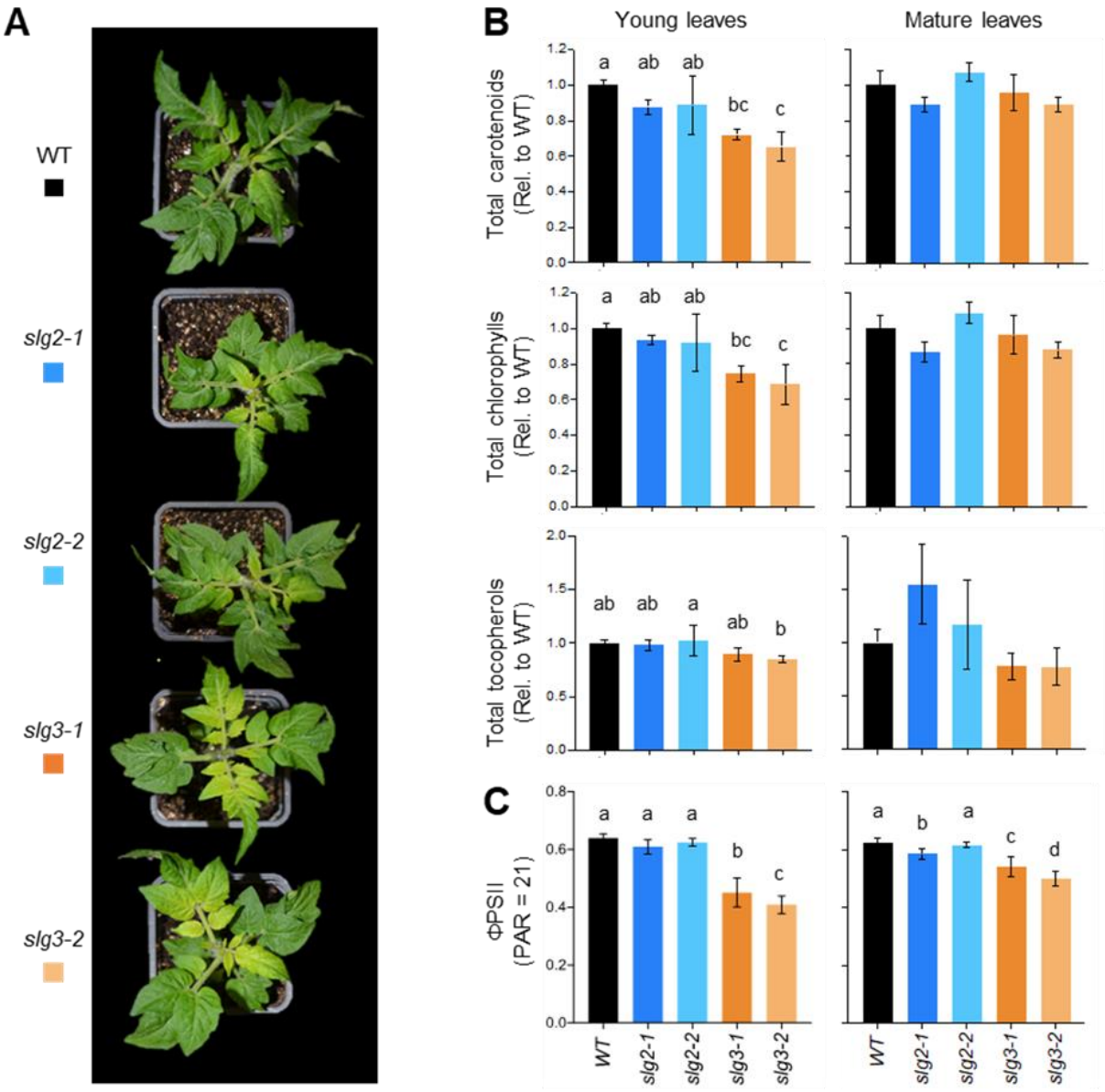

Figure 3. Leaf phenotypes of mutant lines defective in SlG2 or SlG3. (A) Representative images of 4-week-old plants of the indicated lines. **(B)** Relative levels of total carotenoids, chlorophylls and tocopherols in young and mature leaves of WT and mutant lines. Values are represented relative to WT levels and they correspond to the mean±SD of at least three independent biological replicates (n=3). See Table S3 for absolute values. **(C)** ϕPSII in young and mature leaves of the indicated lines. Values represent the mean±SD of four different leaf areas from three different plants. In all cases, different letters represent statistically significant differences ($p<0.05$) according to posthoc Dunnett's tests run when one-way ANOVA detected different means.

	Young leaves	B+10 fruit
WT	1.67 ± 0.19	0.63 ± 0.13
slg2-1	1.69 ± 0.10	0.55 ± 0.12
slg2-2	1.98 ± 0.39	**0.30 ± 0.08**
slg3-1	1.96 ± 0.09	**0.16 ± 0.04**
slg3-2	1.61 ± 0.29	**0.08 ± 0.01**

Table 1. ABA levels in GGPPS-defective leaves and fruit. Values (µg/g dry weight) correspond to the mean ± SD of four independent simples (n=4). Statistically significant changes in mutants compared to WT simples (t-test, p<0.01) are indicated in bold

2.5 Ripening-associated fruit pigmentation is altered in *slg2* and *slg3* mutants in correlation with their carotenoid profile

Lines with reduced levels of plastidial GGPPS activity also showed changes in reproductive development (Figure 5). Flowering time was similar in WT, *slg2* and *slg3* plants (Figure 5a). However, pigmentation changes associated to fruit ripening were visually delayed in mutant fruits (Figure 5b-c). Tomato fruits reach their final size at the mature green (MG) stage and then they start the ripening process. The first visual symptoms of ripening define the breaker (B) stage, when chlorophyll degradation and carotenoid biosynthesis change the fruit colour from green to yellow (Figure 5c). As ripening advances, accumulation of orange and red carotenoids (β-carotene and lycopene, respectively) progressively change the fruit colour and define the orange (O) and eventually red (R) stages (Figure 5c). The time from anthesis to B was similar in WT and SlG2-defective fruits, but it was longer in the *slg3* mutants (Figure 5b; S5). Fruits from lines defective in SlG3, but also those defective in SlG2, showed a pigmentation delay in the transition from B to O. The delay was observed both on vine (i.e. in fruits attached to the plant) and off vine (i.e. in fruits detached from the plant at the B stage; Figures 5b; S5). Both on-vine and off-vine measurements revealed that *slg2* mutants also took longer to reach the R stage compared with WT fruits (Figure S5), whereas *slg3* mutants did not reach a proper R stage, as they developed a dark-orange colour when ripe and never turned fully red (Figure 5c). WT and mutant fruits showed similar levels of carotenoids, chlorophylls and tocopherols at the MG stage (Figure S6), but clear differences were detected in ripe fruits at B + 10, i.e. 10 d after B (Figure 5d; Table S3).

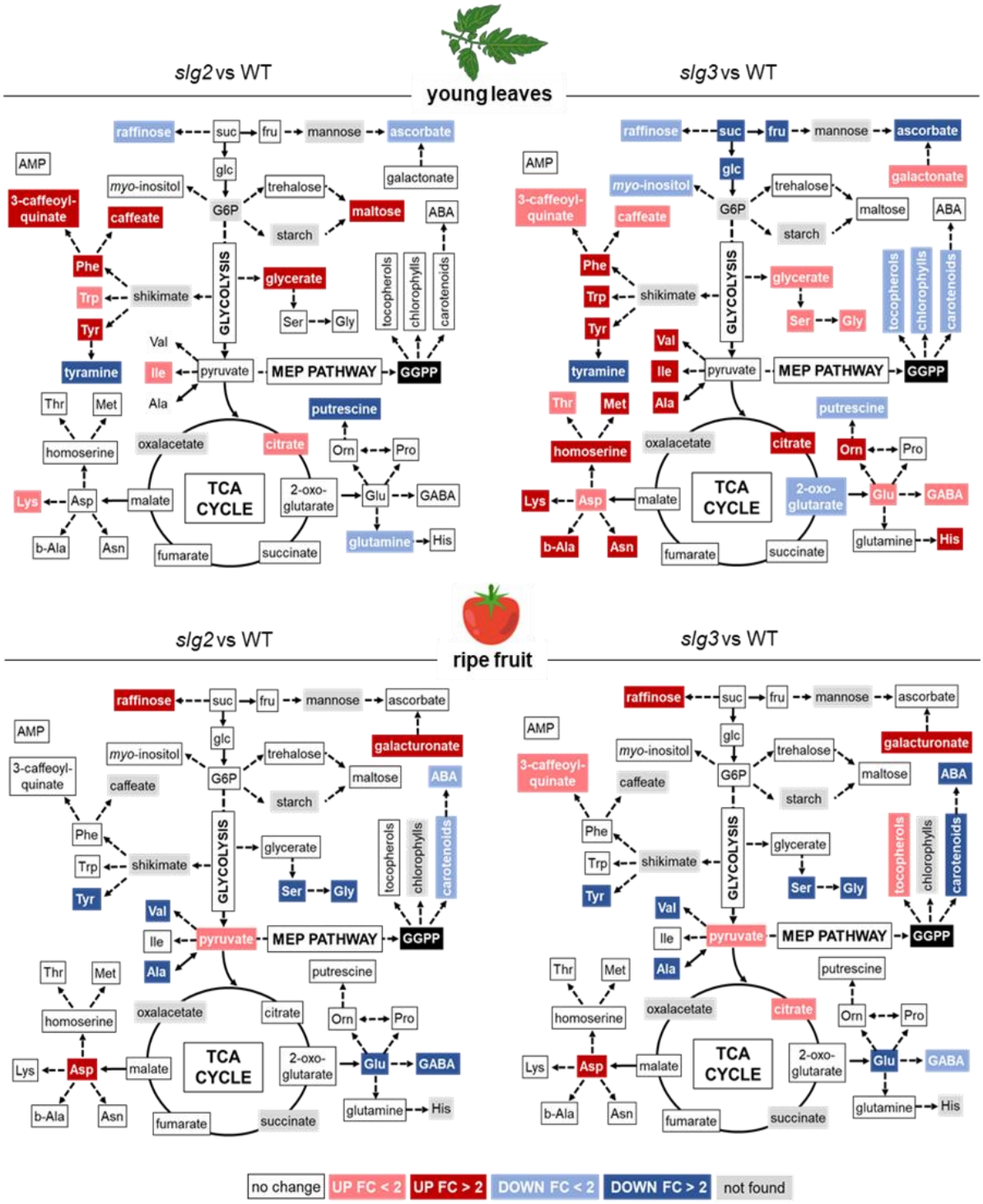

Figure 4. Metabolic changes in *slg2* and *slg3* mutants. Colors represent statistically significant fold-change (FC) values (t-test, p<0.05) of metabolite levels in young leaves or ripe fruit (B+10) from mutant plants relative to those in WT controls. Quantitative data are detailed in Table S4 for leaves and table S5 for fruit.

Phytoene and lycopene were decreased in all mutants, although the effect was higher for *slg3* fruits. No significant differences were found for β-carotene, although the levels of this orange carotenoid tended to be higher in *slg3* mutants. This, together with the lower levels of the red carotenoid lycopene, may explain the dark-orange colour of B + 10 *slg3* fruits (Figure 5c). Tocopherols also showed a trend towards higher abundance in SlG3-deficient fruits, a change that was statistically significant in the *slg3-1* allele (Figure 5d) or when *slg3-1* and *slg3-2* samples were considered together (Figure 4). Unlike that observed in young leaves, ABA levels were reduced in B + 10 fruits of *slg2* and, most strongly, *slg3* mutants compared with WT controls (Figure 4; Table 1). At the level of primary metabolites, B + 10 fruits from both *slg2* and *slg3* mutants exhibited increased levels of raffinose, galacturonate, pyruvate and Asp and lower levels of Ser, Gly, Tyr, Val, Ala, Glu and GABA compared with WT controls (Figure 4). The changes in these metabolites were typically stronger for *slg3* fruits, paralleling that observed for carotenoids and derived ABA levels.

2.6 Double mutants defective in both SlG2 and SlG3 are not viable

To assess the impact of simultaneous disruption of both *SlG2* and *SlG3* genes, alleles *slg2-2* and *slg3-1* were crossed using the former as female parent and the latter as male parent or vice versa. Double heterozygous F1 plants from each cross were allowed to self-pollinate and the resulting seeds were used to screen the F2 population for double homozygous plants, which were expected to occur at a Mendelian frequency of 6.25% (1 in 16). We performed two rounds of screening. In the first one, 200 seeds (100 from each cross) were plated and all of them germinated and produced green seedlings. In the second round, carried out with older seeds, 80 seeds were plated and 76 (95%) germinated (Table 2). The seeds that failed to germinate (four) were manually open and found to contain either albino/pale (three) or green (one) embryos (Figure S7). PCR genotyping of these embryos (Figure S7) and of the remaining 276 seedling did not identify double homozygous mutants (Table 2). A chi-squared goodness-of-fit test performed with 8 degrees of freedom and 95% interval of confidence confirmed that the observed genotype frequencies did not follow the expected Mendelian segregation in any of the two experiments or when considering all data together (Table 2). In addition to the absence of double *slg2-2 slg3-1* mutants (here referred to as *g2g2 g3g3*), lines with one of the two genes in homozygosis and the second one in heterozygosis (i.e. *g2g2 G3g3* and *G2g2 g3g3*) were found at lower frequencies than predicted (Table 2), suggesting a gene dosage effect.

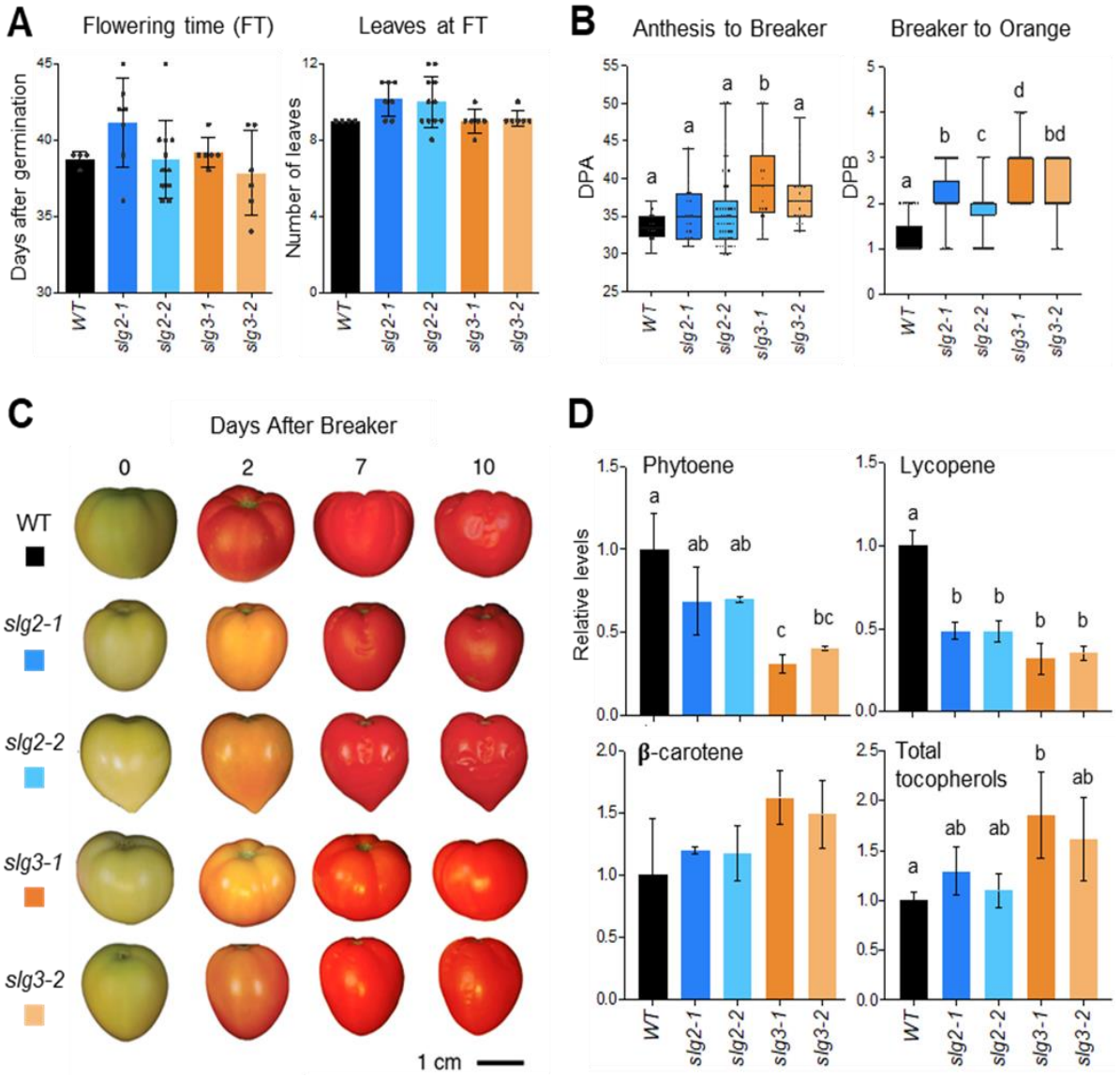

Figure 5. Flowering and fruit phenotypes of mutant lines defective in SlG2 or SlG3. (A) Flowering time measured as days after germination (left) or number of leaves (right). Values correspond to the mean±SD of at least n=4 independent biological replicates. **(B)** Number of days to reach the indicated ripening stages represented as days post-anthesis on-vine (left) and days post-breaker off-vine (right). **(C)** Representative images of fruit from WT and mutant lines harvested at the breaker stage. **(D)** Relative levels of individual carotenoids (phytoene, lycopene and β-carotene) and total tocopherols in B+10 fruits of WT and mutant lines. Values are represented relative to those in WT samples and correspond to the mean±SD of n=3 independent biological replicates. In all plots, different letters represent statistically significant differences (one-way ANOVA with Dunnett's multiple comparisons test, $p<0.05$).

Genotypes	Expected	Round 1		Round 2		Combined	
		#	%	#	%	#	%
G2g2 G3g3	25%	52	26%	15	20%	67	24%
G2g2 G3G3	12.5%	26	13%	18	24%	44	16%
G2G2 G3g3	12.5%	35	17.5%	10	13%	45	16%
g2g2 G3g3	12.5%	18	9%	6	8%	24	9%
G2g2 g3g3	12.5%	16	8%	5	7%	21	8%
g2g2 g3g3	6.25%	0	0%	0	0%	0	0%
g2g2 G3G3	6.25%	17	8.5%	5	7%	22	8%
G2G2 g3g3	6.25%	14	7%	8	11%	22	8%
G2G2 G3G3	6.25%	22	11%	9	12%	31	11%
Total plants (#)		200		76		276	
Chi-square			30.84		22.68		45.17
p-value			0.0002		0.0038		<0.0001

Table 2. Expected and observed frequencies of the F2 population from the crosses of *slg2-2* and *slg3-1* mutant plants. Mutant alleles are marked in red. A chi-squared goodness of fit test was performed with 8 degrees of freedom and 95% Interval of confidence to check the Mendelian segregation of the mutant alleles. #, number of plants

Our interpretation of these results is that the absence of both SlG2 and SlG3 results in a lethal phenotype that is partially rescued by incorporating one copy of any of these two genes (as in *g2g2 G3g3* or *G2g2 g3g3* plants), and fully rescued when two copies are present in the genome (as in double heterozygous or single homozygous mutants). These results, together with the similar expression levels of both genes in developing tomato seeds (Figure S1), suggest that SlG2 and SlG3 contribute similarly and additively to embryo or/and seed development.

2.7 The phenotypes of single *slg3* mutants are exacerbated in lines with the *SlG2* gene in heterozygosis.

Plants segregating from double heterozygous F1 plants (*G2g2 G3g3*) that showed a single mutant genotype (i.e *g2g2 G3G3* and *G2G2 g3g3*) or one of the two genes in homozygosis and the second one in heterozygosis (i.e *g2g2 G3g3* and *G2g2 g3g3*) were transferred to soil and used to carefully examinate their phenotype.

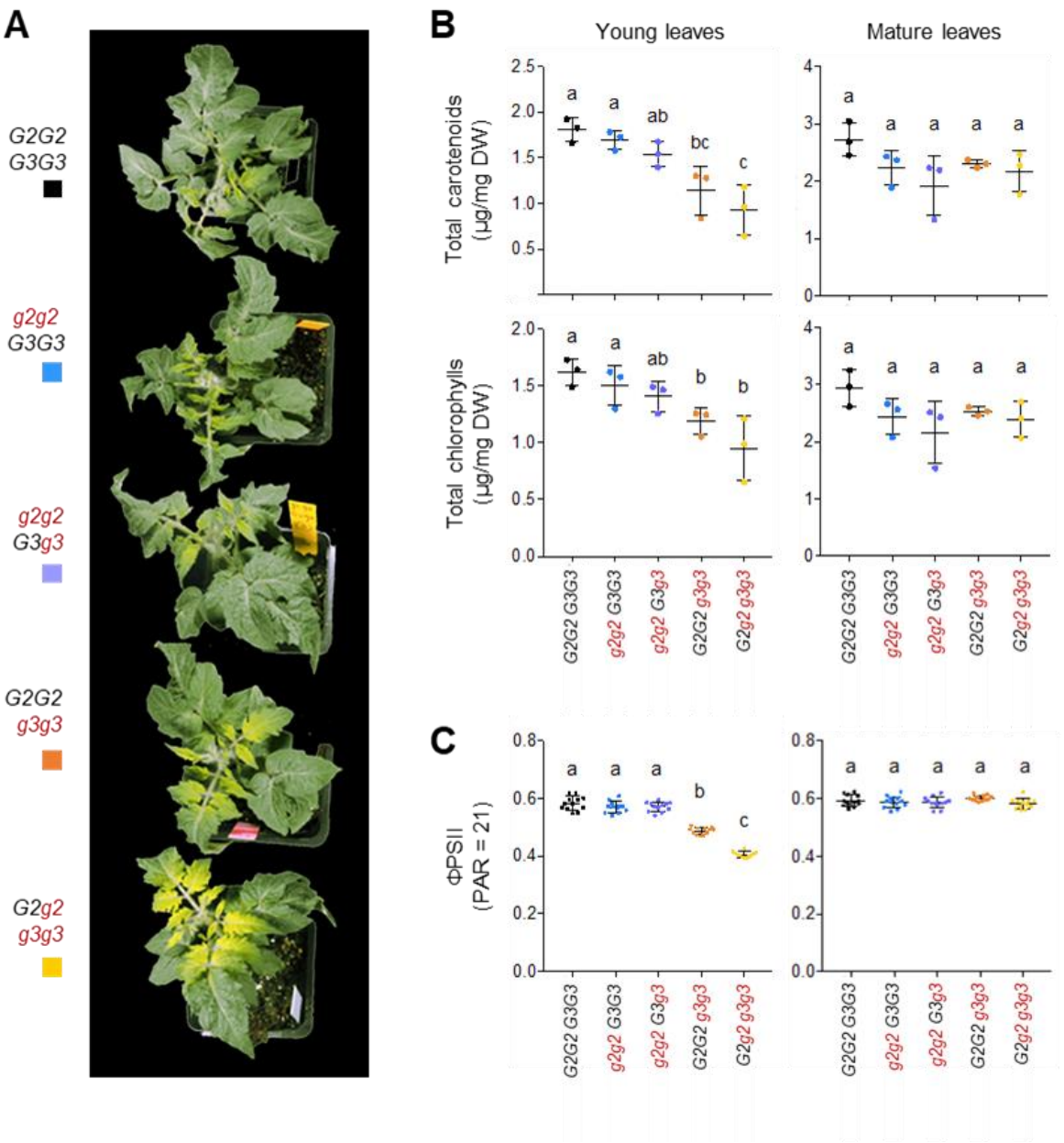

Figure 6. Leaf phenotypes of lines with different combinations of *slg2* and *slg3* mutations. (A) Representative images of 4-week-old plants of the indicated lines. Mutant alleles are marked in red. **(B)** Total levels of photosynthetic pigments (carotenoids and chlorophylls) in young and mature leaves of WT and mutant lines. Values, mean and SD of n=3 independent biological replicates are represented. **(C)** ϕPSII in young and mature leaves of the indicated lines. Values, mean and SD of four different leaf areas from three different plants are shown. In all plots, different letters represent statistically significant differences ($p<0.05$) according to posthoc Dunnett's tests that were run once the existence of different means was established by one-way ANOVA.

Consistent with that described for the *slg2-2* and *slg3-1* parentals (Figure 3), young leaves of *g2g2 G3G3* plants showed unchanged pigmentation and WT levels of photosynthetic

pigments (chlorophylls and carotenoids) and photosynthetic activity (ϕPSII), whereas *G2G2 g3g3* plants were paler and displayed reduced levels of photosynthetic pigments and activity (Figure 6b-c). Most interestingly, the phenotypes of the *slg3* mutants were intensified when one of the two genomic copies of *SlG2* was inactivated in the *G2g2 g3g3* line (Figure 6). Loss of a *SlG3* gene copy in the *slg2* mutant background, however, was not sufficient to trigger statistically significant changes in young leaves compared to WT or *slg2* lines. This result indicates that a single copy of the *SlG3* gene is sufficient to provide GGPP to produce photosynthetic pigments in chloroplasts, even when no SlG2 activity is available. In the case of mature leaves, no differences were observed between WT and any of the mutant lines (Figure 6).

At the level of fruit ripening, visual analysis and quantification of fruit color using the TomatoAnalyzer 4.0 tool (Gonzalo et al., 2009) confirmed the pigmentation delay previously observed in single mutants defective in SlG2 or, to a higher extent, SlG3 (Figures 5, 7, 8a) and further showed a stronger effect when one of the two genomic copies of *SlG2* was additionally inactivated in the *slg3* background (Figure 7, 8a).

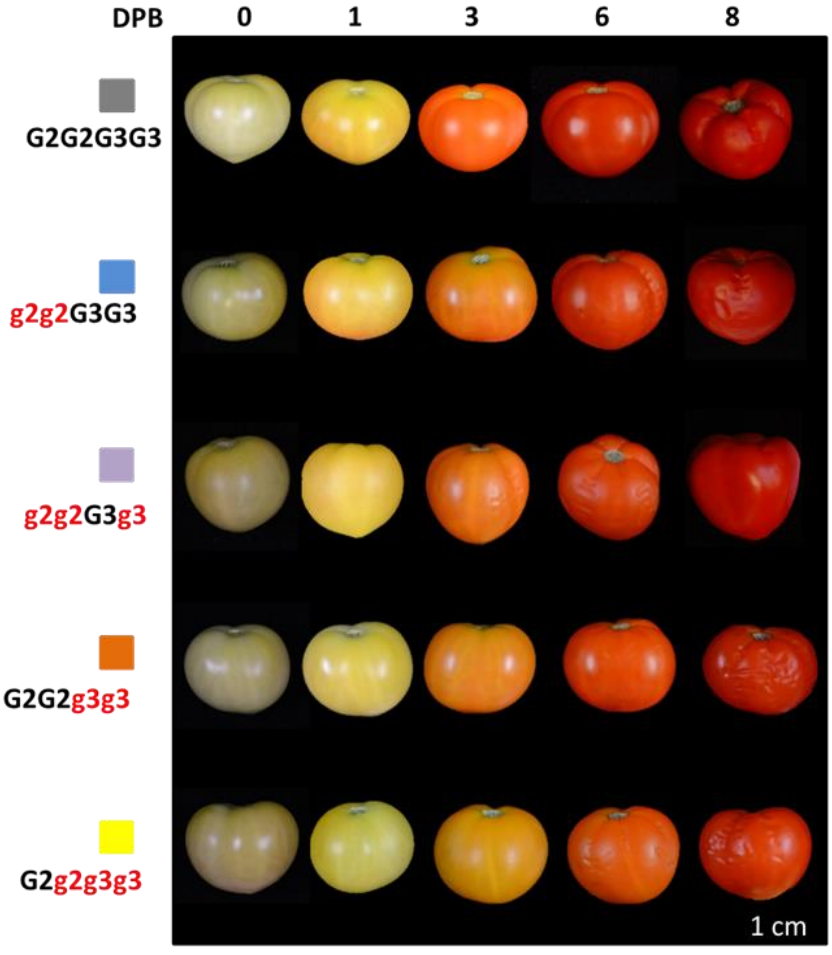

Figure 7. Fruit phenotypes of lines with different combinations of *slg2* and *slg3* mutations.
Representative images of fruit from WT and mutant lines harvested at the breaker stage and ripe off vine. Mutant alleles are marked in red.

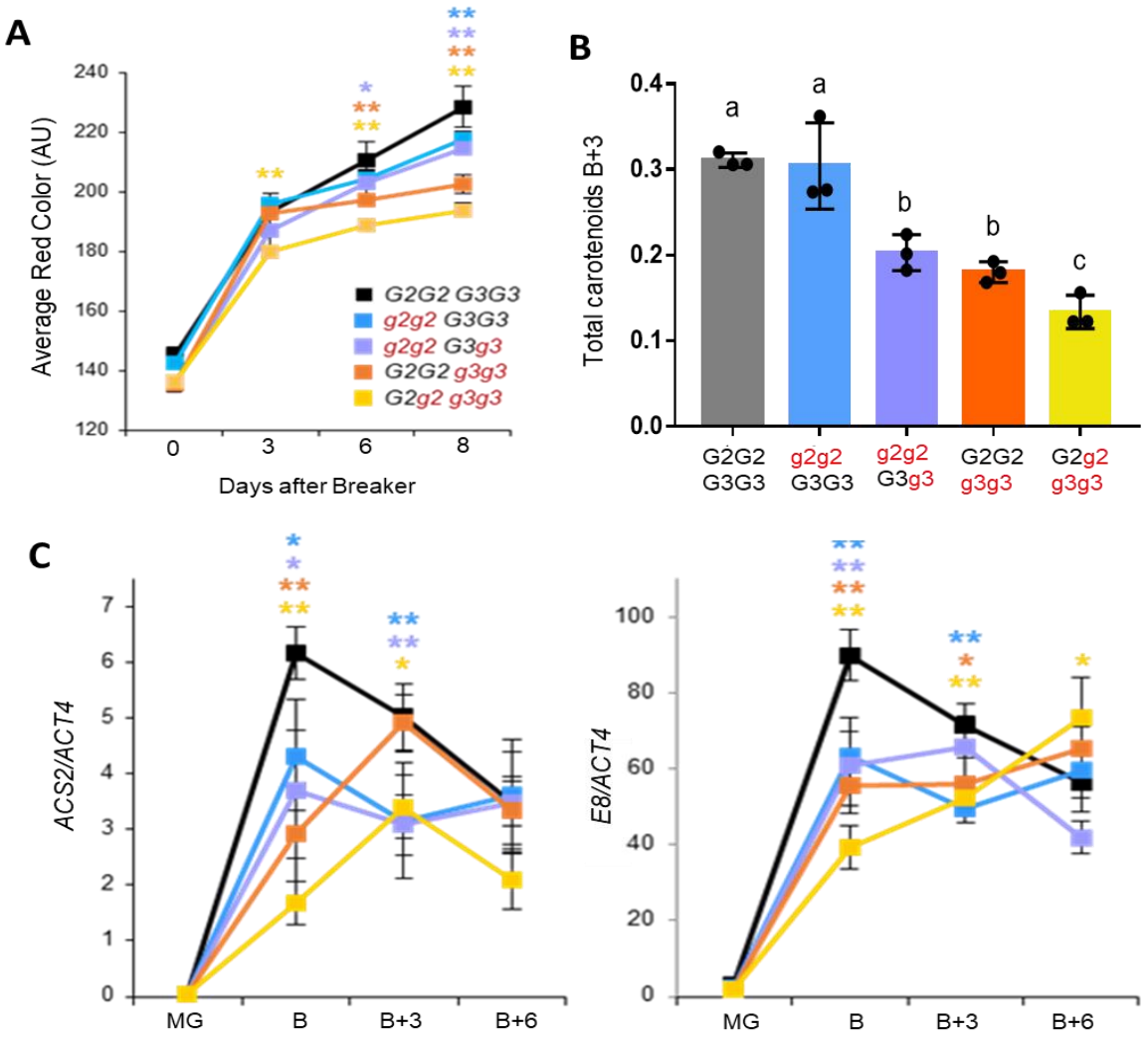

Figure 8. Ripening-associated pigmentation genotypes and marker gene expression in fruits with different combinations of *slg2* snd *slg3* mutations. (A) Average red color quantification (arbitrary units) of on-vine fruit from WT and mutant lines at the indicated times. Values represent the mean±SD of three different fruits (n=3) for each point. **(B)** Total carotenoid levels in B+3 fruits of WT and mutant lines. Values correspond to the mean±SD of n=3 independent biological replicates. In B, different letters represent statistically significant differences (one-way ANOVA with Dunnett's multiple comparisons test, $p<0.05$). **(C)** Abbreviations: MG, mature green; B, breaker. RT-qPCR analysis of *ACS2* and *E8* transcript levels in WT and mutant fruits collected at the indicated developmental stages. Expression values were normalized using *ACT4* and represent the mean±SD of n=3 independent biological replicates. In both plots, asterisks indicate statistically significant differences among means relative to WT samples (t-test, *$p<0.05$, **$p<0.01$). Asterisk color represents the genotype.

Measurement of carotenoid levels at B+3 (*i.e* 3 days after Breaker) further confirmed that the pigmentation delay observed in the *slg3* mutants brings together a reduction on the carotenoid levels during ripening (Figure 8b). Interestingly, *slg2* mutants with just one copy of *SlG3* presented reduced carotenoid levels when compared to *slg2* mutants or WT plants, suggesting that in the first stages of tomato fruit ripening, one single copy of *SlG3* is not sufficient to provide enough GGPP to produce carotenoid levels similar to those of WT in tomato chromoplast (Figure 8b). Analysis of the expression of ripening marker genes such as *E8* and *ACS2* (D'Andrea et al., 2018; Estornell et al., 2009; Llorente et al., 2016) showed that the peak of E8 and ACS2 expression observed at the onset of ripening (Figure S1) was reduced in the mutants (Figure 8c). Again, the stronger effect was observed in lines without SlG3 activity and tended to be higher in *G2g2 g3g3* compared to *G2G2 g3g3* lines (Figure 8c). We therefore conclude that reduced levels of plastidial GGPPS activity result in a delayed fruit ripening, with a higher contribution of the *SlG3* gene over *SlG2*.

3 Discussion

The fundamental basis for our knowledge of the regulation of GGPP biosynthesis in plants mainly comes from the characterization of the Arabidopsis GGPPS family (Zhu et al., 1997a, 1997b; Okada et al., 2000; Beck et al., 2013; Nagel et al., 2015; Ruiz-Sola et al., 2016a, 2016b; Wang et al., 2016b). In this model plant, there are two plastid-targeted GGPPS paralogs (AtG2 and AtG11) but only AtG11 appears to be required for the production of plastidial isoprenoids (Beck et al., 2013; Nagel et al., 2015; Ruiz-Sola et al., 2016a, 2016b). The gene encoding AtG11 is ubiquitously expressed at high levels and can generate long transcripts encoding the plastid-targeted isoform but also short transcripts encoding a cytosolic enzyme that retains enzymatic activity and is essential for embryo development (Ruiz-Sola et al., 2016b). The production of GGPP has also been studied in a few crop plants (Wang and Dixon, 2009; Zhang et al., 2015; Zhou et al., 2017; Wang et al., 2018, 2019). Similar to Arabidopsis, rice and pepper contain only one enzymatically active GGPPS isoform localized in plastids, named OsGGPPS1 (OsG1 in short) and CaGGPPS1 (CaG1), respectively (Zhou et al., 2017; Wang et al., 2018). Strikingly, only scattered information was available to date on the tomato GGPPS family despite this species being a well-established model plant that accumulates high amounts of GGPP-derived metabolites of human interest such as carotenoids in fruits. Here we demonstrate that, in tomato, two plastidial isoforms (SlG2 and SlG3) co-ordinately supply GGPP to produce carotenoids and other isoprenoids essential for photosynthesis, fruit pigmentation, and seed viability.

3.1 Subfunctionalisation of plastidial GGPPS paralogues in tomato might involve several mechanisms with a major role for differential gene expression

The three plastid-targeted GGPPS homologues present in tomato (SlG1-3) produce GGPP with similar kinetic parameters and an optimal pH around 7.5 (Barja et al., 2021, annex I). Several mechanisms might allow enzymatically similar GGPPS isoforms to acquire new functions, including: (a) localisation in distinct subcellular compartments, (b) specific interactions with other protein, and (c) diversification of spatio-temporal gene expression patterns. Despite the clear plastidial localisation observed here (Barja et al., 2021, annex I) and elsewhere (Zhou & Pichersky, 2020) for GFP fusions of the SlG1-3 isoforms, we cannot exclude the possibility that shorter extraplastidial versions of these proteins could also be produced in vivo, paralleling that observed for AtG11 (Ruiz-Sola et al., 2016a). Indeed, several M residues can be found in the N-terminal region of both SlG2 and SlG3 enzymes (Figure S4); they could be used as alternative translation start sites to produce catalytically

active GGPPS enzymes with an absent or shorter (i.e. dysfunctional) plastid-targeting domain.

In addition to localisation in distinct subcellular compartments, subfunctionalisation of GGPPS paralogues might also involve isoform-specific interactions with other proteins. The enzymatic properties of GGPPS proteins change to produce GPP upon heterodimerisation with members of the GPP synthase small subunit type I (SSU-I) subfamily (Orlova et al., 2009; Wang & Dixon, 2009). This occurs upon interaction of SlG1-3 enzymes with the tomato SSU-I protein (Solyc07g064660; Zhou & Pichersky, 2020). Multienzymatic complexes appear to be particularly important for metabolic channelling of GGPP. In particular, PSY cannot access freely diffusible GGPP or time-displaced GGPP supply by GGPPS (Camagna et al., 2019). Arabidopsis AtG11 and pepper CaG1 can directly interact with PSY proteins (Ruiz-Sola et al., 2016b; Wang et al., 2018; Camagna et al., 2019). We found that tomato SlG2, but not SlG3, is able to interact with PSY1 and PSY2 in planta (Figure 1). However, tomato SlG3 might deliver GGPP to PSY enzymes by heterodimerisation with PSY-interacting SlG2 (Figure 1). An alternative possibility involves interaction with members of another catalytically inactive SSU subfamily, named type II (SSU-II). Similar to AtG11 and CaG1, OsG1 is the only GGPPS enzyme producing GGPP for carotenoid biosynthesis in rice. Strikingly, OsG1 does not interact with PSY, but heterodimerises with a SSU-II homologue, resulting in its delivery to a large protein complex in thylakoid membranes (Zhou et al., 2017). The interaction with SSU-II proteins was also shown to enhance not only the GGPP-producing activity of rice OsG1 but also of pepper CaG1 (Wang et al., 2018) and tomato SlG1-3 isoforms (Zhou & Pichersky, 2020). Interestingly, the pepper SSU-II protein also interacts with PSY, suggesting that binding of CaG1 to SSU-II might stimulate both its GGPPS activity and its interaction with PSY (Wang et al., 2018). It is therefore possible that heterodimerisation with tomato SSU-II (Solyc09g008920) might also deliver SlG3 to PSY-containing protein complexes and enhance interaction of SlG2 with PSY isoforms.

Regardless of other possible mechanisms discussed above, it appears that a major determinant defining the biological roles of plastidial GGPPS isoforms in tomato is their distinct expression profiles. Mining of public tomato gene expression databases, GCN analyses and qPCR assays led us to conclude that *SlG1* is likely to contribute to carotenoid biosynthesis in roots together with *PSY3*. This conclusion is supported by a recent study showing that the expression of *PSY3* and *SlG1* co-ordinately responds to tomato root mycorrhization and phosphate starvation (Stauder et al., 2018). The SlG1–PSY3 tandem might be channeling the flux of MEP-derived precursors towards the synthesis of carotenoid-derived molecules, such as strigolactones and apocarotenoids, that are crucial for the

establishment of symbiosis (Stauder et al., 2018). Unlike *SlG1*, *SlG2* and *SlG3* are constitutively expressed, with *SlG3* being the paralogue with the highest expression level in all plant tissues (Figure S1). In leaves, *SlG2* is more strongly co-expressed than *SlG3* with genes from photosynthesis-related isoprenoid pathways (Barja et al., 2021, annex I). This suggests that the expression of the *SlG2* gene changes more than that of *SlG3* to adapt to conditions requiring a re-adjustment of the gene expression network regulating the metabolism of isoprenoids such as carotenoids. In agreement, *SlG2* is much more upregulated than *SlG3* during seedling de-etiolation (Barja et al., 2021, annex I) and leaf development (Figure S1c), in which an enhanced production of carotenoids and other photosynthesis-related isoprenoids contributes to assemble a functional photosynthetic machinery. *SlG2* was also much more induced than *SlG3* during fruit ripening, when carotenoid biosynthesis is boosted thanks to the upregulation of the *PSY1* isoform. *PSY1* and *SlG2*, but not *SlG3*, are co-ordinately regulated by FUL and RIN transcription factors that control the expression of ripening-related genes, including many of the MEP and carotenoid pathway genes (Fujisawa et al., 2013, 2014). All these expression data showed that *SlG2* expression is more responsive to sudden demands of precursors for the production of isoprenoids, including carotenoids. By contrast, *SlG3* expression is higher and does not change as much, suggesting a house-keeping role to maintain a continuous supply of GGPP in plastids for basal production of carotenoids and other isoprenoids. According to this model, *SlG1* and *SlG2* would help *SlG3* to supply GGPP when a boost in carotenoid production is needed. The very low and restricted expression level of *SlG1*, however, strongly suggests that *SlG2* is the main helper isoform for *SlG3* in chloroplasts of cotyledons and expanding leaves and chromoplasts of ripening fruit.

3.2 GGPPS isoforms SlG2 and SlG3 have functionally interchangeable roles in chloroplasts and chromoplasts

Analysis of tomato mutants defective in gene copies for *SlG2* or/and *SlG3* further suggested that these are functionally exchangeable isoforms that participate in the same biological processes. This might not be obvious when analysing leaves, as only *slg3* alleles were found to display reduced levels of GGPP-derived isoprenoids and subsequent inhibition of photosynthesis (Figures 3, 6). However, the effects of reduced isoprenoid synthesis could also be indirectly detected in *slg2* leaves. Our GC-MS analysis showed higher levels of all aromatic amino acids derived from the shikimate pathway (Trp, Tyr and Phe) as well as Phe-derived phenylpropanoids caffeate (caffeic acid) and 3-caffeoyl-quinate (chlorogenic acid) in both *slg2* and *slg3* mutant lines (Figure 4). This might be a physiological response to cope with photo-oxidative stress caused by lower levels of carotenoids in the mutants, as

phenylpropanoids (including Phe-derived flavonoids and anthocyanins) can also function as photoprotective metabolites (Muñoz & Munné-Bosch, 2018). Reduced levels of well-known metabolites associated with oxidative stress such as ascorbate and putrescine in leaves from both mutant lines would also support this view. Loss of one *SlG3* gene copy in the *slg2* mutant background failed to cause a statistically significant decrease in the levels of photosynthetic pigments or activity, even though a trend towards reduction of chlorophyll and carotenoid levels was observed (Figure 6). However, complete loss of SlG3 activity in lines with one or two functional *SlG2* copies was sufficient to reduce levels of GGPP-derived photoprotective isoprenoids such as carotenoids and tocopherols to an extent that became detectable and affected photosynthesis (Figures 3, 4), causing sugar starvation and the subsequent metabolic changes observed only in the *slg3* mutant (Figure 4). In agreement, the increased accumulation of most amino acids in *slg3* leaves suggested a high proteolytic activity to generate an alternative respiratory source, a probable response to sugar starvation derived from reduced photosynthesis and/or photo-oxidative stress (Araújo et al., 2011; Obata & Fernie, 2012; Galili et al., 2016).

The absence of any of the two individual enzymes also decreases plastidial GGPP production in fruit, as deduced from the levels of the main GGPP-derived metabolites (Figure 5d; Table S3). Tocopherol levels did not decrease in mutant fruit, perhaps because they are mostly produced by recycling the phytyl chain released from the chlorophylls degraded during fruit ripening. By contrast, lycopene (by far the most abundant carotenoid in ripe fruit) and, to a lower extent, phytoene, showed reduced levels in both mutants (Figure 5d; Table S3). Similar to that observed in leaves, the effect is stronger in *slg3* mutants, consistent with the higher expression levels of the *SlG3* compared with *SlG2* in young leaves and MG fruits (Figure S1). While altered levels of 3-caffeoyl-quinate and citrate were detected only in fruit of the *slg3* mutant, the rest of the metabolic changes were similar in *slg2* and *slg3* lines (Figure 4), again supporting the conclusion that these enzymes are redundant and interchangeable. In particular, both *slg2* and *slg3* fruit showed pigmentation defects that were associated with a decreased carotenoid accumulation (Figures 5, 8). Because ABA is synthesised from carotenoids, its reduced levels in GGPPS-defective ripe fruits, but not in leaves (Table 1), may be the result of a more substantial reduction in carotenoid contents in mutant fruit (Figure 5) compared with leaves (Figure 3; Table S3). A role for ABA in promoting tomato fruit ripening has been proposed based on the analysis of mutants or external application of hormones and inhibitors. This, together with the observed downregulation of ethylene-related ripening marker genes (E8 and ACS2) in GGPPS-defective fruit (Figure 8c), allowed us to speculate that reduced ABA levels in the mutant fruit may contribute to a delay in ripening, either directly or indirectly by ethylene (Zhang et al., 2009; McQuinn et al., 2020). Additionally, metabolic roles of SlG2 and SlG3 in addition

to their GGPPS activity in plastids might play a role in fruits but also in developing seeds, therefore explaining why we could not isolate a double *slg2 slg3* mutant (Table 2). The observation that the lethal phenotype is dose dependent in an isoform-independent fashion (i.e. can be rescued by a single genomic copy of either *SlG2* or *SlG3*) reinforces our conclusion that SlG2 and SlG3 have functionally interchangeable roles.

3.3 Concluding remarks

Retention of multiple gene copies after duplication events may allow the acquisition of new functions (neofunctionalisation) or partitioning the ancestral functions between duplicate partners (subfunctionalisation), by evolution of coding sequence and/or regulatory regions. The work reported here demonstrates that the bulk of GGPP production in tomato leaf chloroplasts and fruit chromoplasts relies on two redundant, but cooperating, GGPPS paralogues, SlG2 and SlG3. Additionally, the SlG1 isoform might contribute to GGPP synthesis in root plastids. This subfunctionalisation scenario contrasts with that described to date in other plant species such as Arabidopsis, rice or pepper, which produce their essential plastidial isoprenoids using a single GGPPS isoform. However, it is likely that tomato is not an exception. Examples of gene families encoding enzyme isoforms located in the same cell compartment but differing in gene expression profiles abound in the literature. They include deoxyxylulose 5-phosphate synthase (DXS) and PSY, the rate-determining enzymes of the MEP and carotenoid pathways, respectively (Walter et al., 2015). Both DXS and PSY are encoded by single genes in Arabidopsis, but several differentially expressed genes in tomato. Subfunctionalisation is also widespread beyond the isoprenoid pathway, contributing to the huge diversity of specialised metabolism in plants (Moghe & Last, 2015). Deciphering how different plants regulate plastidial GGPP production and channelling will be useful for future metabolic engineering approaches targeted to manipulate the accumulation of specific groups of GGPP-derived isoprenoids without negatively impacting the levels of others.

4 Materials and methods

4.1 Plant material and growing conditions

Tomato (Solanum lycopersicum var. MicroTom) plants were used for most of experiments. For seedling establishing, tomato seeds were surface-sterilized by a 30 min water wash, follow by 15 min incubation in 10 mL of 40% bleach containing a drop of Tween-20. Next, we performed 3 consecutive 10 min washes with sterilized milli-Q water under the fume hood. Sterile seeds were germinated on plates with solid 0.5x Murashige and Skoog medium containing 1% agar and no vitamins or sucrose. The medium was supplemented with kanamycin (100 µg/mL) when required to select transgenic plants. Plates were incubated in a climate-controlled growth chamber (Ibercex) at 26 °C with a photoperiod of 14 h of white light with a photon flux density of 50 µmol $m^{-2}s^{-1}$ followed by 10 h of darkness. After 10 to 14 days, seedlings were transferred to soil and grown under standard greenhouse conditions (14 h light at 25 ± 1 °C and 10 h dark at 22 ± 1 °C).

4.2 Generation of CRISPR-Cas9 defective mutants and tomato transformation

For CRISPR-Cas9-mediated disruption of *SlGGPPS2* and *SlGGPPS3*, two single guide RNAs (sgRNA) for each gene encompassing an *EcoRI* and a *PstI* restriction site for *SlG2* and *SlG3* genes, respectively (Figures S2 and S3) were designed gene using the online tool CRISPR-P 2.0 (Liu et al., 2017). A pair of primers for each guide was denaturalized and assembled into pENC1.1 (pENTRY) vector previously digested with *BbsI*. The entry vectors contained the corresponding sgRNA expression cassette flanked by *Bsu36I* and *MluI* restriction sites, and by GW recombinant sites to allow both types of interchange with a pDE-Cas9 plasmid providing kanamycin resistance (pDESTINY). The final binary vectors were generated in a two-step cloning process that involved *Bsu36I* and *MluI* digestion-ligation of the first sgRNA into the pDE-Cas9 vector followed by an LR reaction to subclone the second sgRNA of each gene into the pDE-Cas9 vector already containing the first sgRNA. Primers used for cloning and are detailed in Table S1. All constructs were confirmed by restriction mapping and DNA sequencing before tomato transformation (Table S2). Tomato plants were transformed as previously described (Fernandez et al., 2009). Surface-sterile MT seeds were sown in 50% MSO medium (50% MS salts; 30g/l sucrose; Vitamin B5; agar 8 g/l; pH=5.8) and grown during 10 days at 25 °C in long day conditions (16 h light; 8 h dark). Cotyledons were cut in two halves and incubated in KCMS medium (50% MS salts; 20g/l sucrose; KH2PO4 200 mg/l; Tiamin 0.9 mg/l; 2,4 D 2 mg/l, Kinetin 1 mg/l; acetosyringone 200 µM; agar 8 g/l; pH=5.8) during 24 h. Cotyledons were incubated during 30 min with an agrobacterium suspension in liquid KCMS harboring the desired plasmid. Cotyledons were

then transfer to a fresh solid KCMS medium and incubated in dark 48 h at 25 °C. Next, cotyledons were transferred to 2Z medium (50% MS salts; 30g/l sucrose; Nistch vitamins; Zeatin 2 mg/l; Timentin 250 mg/l; kanamycin 100 mg/l); agar 8 g/l; pH=5.8) during 15 days in long day conditions. Every 15 days cotyledons were refreshed by transferring to new 2Z medium until regenerated plants appeared (approximately 30 days). The re-generated explants were transferred to the rooting medium (50% MS salts; 10g/l sucrose; Nitsch vitamins; Zeatin 2 mg/l; Timentin 75 mg/l; kanamycin 100 mg/l); agar 8 g/l; pH=5.8). Once roots appeared, plants were transferred to soil and acclimated at the greenhouse. *In vitro* regenerated T1 lines were identified based on kanamycin resistance (100 µg/ml), PCR genotyping and restriction analyses. Homozygous T2 lines lacking Cas9 were obtained after segregation and stable T3 offspring was used for further experiments.

4.3 Sample collection and phenotypical analysis

Leaf samples were collected from four-week-old plants. Young leaf samples correspond to growing leaflets from the fifth and sixth true leaves, and mature leaf samples correspond to fully expanded leaflets from the third or fourth leaf. For the analysis of flowering time, at least five independent plants of each genotype were used. Flowering time was assessed by counting the number of days from germination until the first flower was fully opened (anthesis) or the number of leaves in the plant at this first anthesis day. For the counting of the number of days to reach breaker (B) stage, at least twenty flowers from each genotype in anthesis were marked and left to develop until they reach fruit B stage on vine. Next, the fruits were collected from the plant and off vine, number of days from breaker to orange (Or) was measured. Tomato fruit pericarp samples were collected at four ripening stages based on days post-anthesis (DPA) or days post-breaker (DPB): mature green (~30 DPA), breaker (~35 DPA), orange (~38-40 DPA) and red (~45-50 DPA or 10 DPB). Leaflets, and pericarp samples were frozen in liquid nitrogen immediately after collection, freeze-dried and stored at -80 °C. Fruit pigmentation was measured using the TomatoAnalyzer 4.0 software (https://vanderknaaplab.uga.edu/tomato_analyzer.html). Average Red Color of three different tomato fruits per genotype was quantified using the default red color calibrator sorted by the software as standard

4.4 Photosynthetic parameters and photography

Chlorophyll a fluorescence measurements were carried out with a MAXI-PAM fluorometer (Walz). Briefly, the effective quantum yield ϕPSII (ΔF/Fm') of young and mature tomato leaves was measured as (Fm'−Fs)/Fm', where Fm' is the maximum and Fs is the minimum

fluorescence of light exposed plants. Light intensity for ϕPSII was 21 PAR (actinic light, AL=2). The results show the average of three plants and four different leaf areas for each replicate. Plant pictures were done using a Nikon D7000 camera coupled to the objective AF-S NIKOR 18-70 MM 1:3.5-4.5G and AF-S MICRO NIKKOR 105 mm 1:2.8G.

4.5 RNA extraction, cDNA synthesis and RT-qPCR

Total RNA was isolated from tomato freeze-dried tissue (leaves or fruit pericarp) using the Maxwell® RSC Plant RNA Kit with the Maxwell® RSC Instruments (Promega) following the manufacturer's instructions. RNA was quantified using a NanoDropTM 8000 spectrophotometer (ThermoFischer Scientific) and checked for integrity by agarose gel electrophoresis. The Transcriptor First Strand cDNA Synthesis Kit (Roche) was used to reverse transcribe 0.5 µg of extracted RNA into 20 µL of cDNA, which was subsequently diluted ten-fold and stored at -20 °C for further analysis. Relative mRNA abundance was evaluated via Real-Time Quantitative Polymerase Chain Reaction (RT-qPCR) in a reaction volume of 20 µL containing 10 µL of the LightCycler 480 SYBR Green I Master Mix (Roche), 0.3 µM of each specific forward and reverse primer (Table S1) and 5 µL of cDNA. The RT-qPCR was carried out on a LightCycler 480 Real-Time PCR System (Roche). Three independent biological replicates of each condition and three technical replicates of each biological sample were performed. Primer efficiencies were calculated using serial dilutions of genomic or plasmidic DNA.

4.6 Isoprenoid extraction and analysis

Carotenoids, chlorophylls and tocopherols were extracted as follows. A mix was prepared in 2 mL Epperdorf tubes with 4 mg of freeze-dried leaf tissue, 375 µL of methanol as extraction solvent and 25 µL of a 10 % (w/v) solution of canthaxanthin (Sigma) in chloroform as internal control. After vortexing the samples for 10 s and lysing the tissue with 4 mm glass beads for 1 min at 30 Hz in the TissueLyser II (Qiagen), 400 µL of Tris-HCl pH:7.5 were added and the samples were again mixed for 1 min in the TissueLyser. Next, 800 µL of chloroform were added and the mixture was again shaken for 1 min in the TissueLyser. Samples were then centrifuged for 5 min at maximum speed at 4 ºC. The lower organic phase was placed in a new 1.5 mL tube and evaporated using a SpeedVac. Fruit isoprenoids were extracted using 15 mg of freeze-dried tissue and 1 ml of hexane/acetone/methanol 2:1:1 as extraction solvent. After vortexing and lysing the tissue with the TissueLyser as described for leaves, 100 µL of milli-Q water were added. Then, 1 min of TissueLyser was carried out again and samples were centrifuged for 3 min at 500 *g* and 4 ºC. The organic phase was transferred to a 1.5 mL tube and the rest was re-extracted by adding 1 mL of

hexane/acetone/methanol 2:1:1 solvent, TissueLyser-mixing for 1 min and centrifuging for 5 min at maximum speed and 4 ºC. The new organic phase was mixed with that previously extracted and evaporated using the SpeedVac system. Extracted metabolites from leaf and fruit pericarp samples were resuspended in 200 µL of acetone by using an ultrasound bath (Labolan) and filtered with 0.2 µm filters into amber-colored 2 mL glass vials. Separation and detection was next performed using an Agilent 1200 series HPLC system (Agilent Technologies). Eluting chlorophylls and carotenoids were monitored using a photodiode array detector whereas tocopherols were identified using a fluorescence detector. Peak areas of chlorophylls (650 nm), carotenoids (470 nm for lycopene, lutein, β-carotene, violaxanthin, neoxanthin and canthaxanthin or 280 nm for phytoene), and tocopherols (330 nm) were determined using the Agilent ChemStation software. Quantification was performed by comparison with commercial standards (Sigma).

4.7 Determination of ABA and primary metabolites

ABA levels in tomato leaves were determined as described previously (Diretto et al., 2020).Primary metabolites were extracted from 20mg of lyophilized young leaf tissue or 50 mg of freeze-dried tomato pericarp, respectively. Derivatization and gas chromatography-time of flight-mass spectrometry (GC-TOF-MS) analyses were carried out as described (Lisec et al., 2006; Llorente et al., 2020.). Metabolites were identified manually using the TagFinder software in combination with the reference library mass spectra and retention indices from the Golm Metabolome Database, http://gmd.mpimp-golm.mpg.de. Quantitative data are detailed in Tables S4 and table S5.

5 Acknowledgements

We greatly thank Juan Antonio López-Ráez for providing cDNA samples of nonmycorrhized and mycorrhized tomato roots; Ernesto Llamas for providing the pGWB417_AtPRK construct, and Albert Ferrer and Laura Gutiérrez for the pDE-Cas9 (with kanamycin resistance) plasmid. The technical support of M. Rosa Rodríguez-Goberna and all CRAG services is also appreciated. This work was funded by the European Regional Development Fund (FEDER) and the Spanish Agencia Estatal de Investigación (grants BIO2017-84041-P and BIO2017-90877-REDT) and Generalitat de Catalunya (2017SGR-710) to MRC. Support by the collaborative European Union's Horizon 2020 (EU-H2020) ERA-IB-2 (Industrial Biotechnology) BioProMo project to MRC (PCIN-2015-103), RK and JB (053-80-725) is also acknowledged. CRAG is financially supported by the Severo Ochoa Programme for Centres of Excellence in R&D 2016–2019 (SEV-2015-0533) and the Generalitat de Catalunya CERCA Programme. MVB was funded with a Spanish Ministry of Education, Culture and Sports PhD fellowship (FPU14/05142) and a EU-H2020 COST Action CA15136 (EuroCaroten) short-stay fellowship. ME is supported by a Spanish Agencia Estatal de Investigación (BES-2017-080652) PhD fellowship. IFS is supported by the EU-H2020 Marie S. Curie Action 753301 (Arcatom)

6 References

Ahrazem, O., Argandoña, J., Fiore, A., Aguado, C., Luján, R., Rubio-Moraga, Á., Marro, M., Araujo-Andrade, C., Loza-Alvarez, P., Diretto, G., and Gómez-Gómez, L. (2018). Transcriptome analysis in tissue sectors with contrasting crocins accumulation provides novel insights into apocarotenoid biosynthesis and regulation during chromoplast biogenesis. *Scientific. Reports*, 8, 1–17.

Ament, K., Van Schie, C.C., Bouwmeester, H.J., Haring, M.A., and Schuurink, R.C. (2006). Induction of a leaf specific geranylgeranyl pyrophosphate synthase and emission of (E,E)-4,8,12-trimethyltrideca-1,3,7,11-tetraene in tomato are dependent on both jasmonic acid and salicylic acid signaling pathways. *Planta,* 224, 1197–1208.

Araújo, W.L., Tohge, T., Ishizaki, K., Leaver, C.J., and Fernie, A.R. (2011). Protein degradation - an alternative respiratory substrate for stressed plants. *Trends Plant Science*, 16, 489–498.

Barja, M. V., Ezquerro, M., Beretta, S., Diretto, G., Florez-Sarasa, I., Feixes, E., Fiore, A., Karlova, R., Fernie, A. R., Beekwilder, J., & Rodríguez-Concepción, M. (2021). Several geranylgeranyl diphosphate synthase isoforms supply metabolic substrates for carotenoid biosynthesis in tomato. *New Phytologist*, 231(1), 255–272.

Barja, M.V. and Rodríguez-Concepción, M. (2020). A Simple In Vitro Assay to Measure the Activity of Geranylgeranyl Diphosphate Synthase and Other Short-Chain Prenyltransferases. *Methods in Molecular Biology*, pp. 27–38.

Bartley, G. and Scolnik, P. (1993). cDNA Cloning, Expression during Development, and Genome Mapping of a second phytoene synthase. *Biochemistry*, 268, 25718–25721.

Bartley, G.E., Viitanen, P. V, Bacot, K.O., and Scolnik, P.A. (1992). A tomato gene expressed during fruit ripening encodes an enzyme of the carotenoid biosynthesis pathway. *Journal of Biology and Chemistry,* 267, 5036–9.

Baslam, M., Esteban, R., García-Plazaola, J.I., and Goicoechea, N. (2013). Effectiveness of arbuscular mycorrhizal fungi (AMF) for inducing the accumulation of major carotenoids, chlorophylls and tocopherol in green and red leaf lettuces. *Applied Microbiology and Biotechnolonogy* ,97, 3119–3128.

Beck, G., Coman, D., Herren, E., Ruiz-Sola, M.A., Rodríguez-Concepción, M., Gruissem, W., and Vranová, E. (2013). Characterization of the GGPP synthase gene family in Arabidopsis thaliana. *Plant Molecular Biolog,y* 82, 393–416.

Bick, J.A. and Lange, B.M. (2003). Metabolic cross talk between cytosolic and plastidial pathways of isoprenoid biosynthesis: Unidirectional transport of intermediates across the chloroplast envelope membrane. *Archives of Biochemistry and Biophysics*, 415, 146–154.

Bradford, M.M. (1976). A rapid and sensitive method for the quantitation of microgram quantities of protein utilizing the principle of protein-dye binding. *Analitycal Biochemistry*, 72: 248–54.

Camagna, M., Grundmann, A., Bär, C., Koschmieder, J., Beyer, P., and Welsch, R. (2019). Enzyme Fusion Removes Competition for Geranylgeranyl Diphosphate in Carotenogenesis. *Plant Physiology*, 179, 1013–1027.

Camara, B. (1993). Plant phytoene synthase complex: Component enzymes, Immunology and Biogenesis. *Methods in Enzymology*, 214, 352–365.

Cao, H., Luo, H., Yuan, H., Eissa, M. A., Thannhauser, T. W., Welsch, R., Hao, Y. J., Cheng, L., & Li, L. (2019). A neighboring aromatic-aromatic amino acid combination governs activity divergence between tomato phytoene synthases. *Plant Physiology*, 180, 1988–2003.

Cunillera, N., Arró, M., Delourme, D., Karst, F., Boronat, A., and Ferrer, A. (1996). Arabidopsis thaliana Contains two differentially expressed farnesyl-diphosphate synthase genes. *Journal of Biology and Chemistry*, 271, 7774–7780.

Cunillera, N., Boronat, A., and Ferrer, A. (1997). The Arabidopsis thaliana FPS1 gene generates a novel mRNA that encodes a mitochondrial farnesyl-diphosphate synthase isoform. *Journal of Biology and Chemistry,* 272, 15381–15388.

D'Andrea, L., Simon-Moya, M., Llorente, B., Llamas, E., Marro, M., Loza-Alvarez, P., Li, L., and Rodriguez-Concepcion, M. (2018). Interference with Clp protease impairs carotenoid accumulation during tomato fruit ripening. *Journal of Experimental Botany*, 69, 1557–1568.

Diretto, G., Frusciante, S., Fabbri, C., Schauer, N., Busta, L., Wang, Z., Matas, A. J., Fiore, A., K.C. Rose, J., Fernie, A. R., Jetter, R., Mattei, B., Giovannoni, J., & Giuliano, G. (2020). Manipulation of β-carotene levels in tomato fruits results in increased ABA content and extended shelf life. *Plant Biotechnology Journal*, 18, 1185–1199.

Dogbo, O. and Camara, B. (1987). Purification of isopentenyl pyrophosphate isomerase and geranylgeranyl pyrophosphate synthase from Capsicum chromoplasts by affinity chromatography. *Archives of Biochemistry and Biophysics,* Acta (BBA)/Lipids Lipid Metab, 920, 140–148.

Emanuelsson, O., Brunak, S., von Heijne, G., and Nielsen, H. (2007). Locating proteins in the cell using TargetP, SignalP and related tools. *Proceedings of the National Academy of Sciences*, 2, 953–971.

Estornell, L.H., Orzáez, D., López-Peña, L., Pineda, B., Antón, M.T., Moreno, V., and Granell, A. (2009). A multisite gateway-based toolkit for targeted gene expression and hairpin RNA silencing in tomato fruits. *Plant Biotechnology Journal,* 7, 298–309.

Fernandez, A.I. et al. (2009). Flexible Tools for Gene Expression and Silencing in Tomato. *Plant Physiology*, 151, 1729–1740.

Fester, T., Schmidt, D., Lohse, S., Walter, M.H., Giuliano, G., Bramley, P.M., Fraser, P.D., Hause, B., and Strack, D. (2002). Stimulation of carotenoid metabolism in arbuscular mycorrhizal roots. *Planta,* 216, 148–154.

Fester, T., Wray, V., Nimtz, M., and Strack, D. (2005). Is stimulation of carotenoid biosynthesis in arbuscular mycorrhizal roots a general phenomenon? *Phytochemistry*, 66,1781–1786.

Fraser, P.D., Enfissi, E.M.A., Halket, J.M., Truesdale, M.R., Yu, D., Gerrish, C., and Bramley, P.M. (2007). Manipulation of Phytoene Levels in Tomato Fruit: Effects on Isoprenoids, Plastids, and Intermediary Metabolism. *Plant Cell*, 19, 3194–3211.

Fraser, P.D., Romer, S., Shipton, C.A., Mills, P.B., Kiano, J.W., Misawa, N., Drake, R.G., Schuch, W., and Bramley, P.M. (2002). Evaluation of transgenic tomato plants expressing an additional phytoene synthase in a fruit-specific manner. *Proceedings of the National Academy of Sciences*, 99, 1092–7.

Fraser, P.D., Schuch, W., and Bramley, P.M. (2000). Phytoene synthase from tomato (Lycopersicon esculentum) chloroplasts--partial purification and biochemical properties. *Planta,* 211, 361–369.

Fray, R.G. and Grierson, D. (1993). Identification and genetic analysis of normal and mutant phytoene synthase genes of tomato by sequencing, complementation and co-suppression. *Plant Molecular Biology*, 22, 589–602.

Fujisawa, M., Nakano, T., Shima, Y., and Ito, Y. (2013). A large-scale identification of direct targets of the tomato MADS box transcription factor RIPENING INHIBITOR reveals the regulation of fruit ripening. *Plant Cell,* 25, 371–386.

Fujisawa, M., Shima, Y., Nakagawa, H., Kitagawa, M., Kimbara, J., Nakano, T., Kasumi, T., and Ito, Y. (2014). Transcriptional regulation of fruit ripening by tomato FRUITFULL homologs and associated MADS box proteins. *Plant Cell,* 26, 89–101.

Gaffe, J., Bru, J.-P., Causse, M., Vidal, A., Stamitti-Bert, L., Carde, J.-P., and Gallusci, P. (2000). LEFPS1, a Tomato Farnesyl Pyrophosphate Gene Highly Expressed during Early Fruit Development. *Plant Physiology*, 123, 1351–1362.

Galili, G., Amir, R., and Fernie, A.R. (2016). The Regulation of Essential Amino Acid Synthesis and Accumulation in Plants. *Annual Review of Plant Biolology* , 67, 153–178.

Giorio, G., Stigliani, A. L., & D'Ambrosio, C. (2008). Phytoene synthase genes in tomato (Solanum lycopersicum L.) - New data on the structures, the deduced amino acid sequences and the expression patterns. *FEBS Journal,* 275(3), 527–535.

Goytia, E., Fernández-Calvino, L., Martínez-García, B., López-Abella, D., and López-Moya, J.J. (2006). Production of plum pox virus HC-Pro functionally active for aphid transmission in a transient-expression system. *Journal of General Virology,* 87, 3413–23.

Höhner, R., Aboukila, A., Kunz, H.-H., and Venema, K. (2016). Proton Gradients and Proton-Dependent Transport Processes in the Chloroplast. *Frontiers in Plant Science*, 7, 1–7.

Jones, M.O., Perez-Fons, L., Robertson, F.P., Bramley, P.M., and Fraser, P.D. (2013). Functional characterization of long-chain prenyl diphosphate synthases from tomato. *Biochemistry Journal*, 449, 729–740.

Kachanovsky, D.E., Filler, S., Isaacson, T., and Hirschberg, J. (2012). Epistasis in tomato color mutations involves regulation of phytoene synthase 1 expression by cis-carotenoids. *Proceedings of the National Academy of Sciences*, 109, 19021–6.

Koike-Takeshita, A., Koyama, T., Obata, S., and Ogura, K. (1995). Molecular cloning and nucleotide sequences of the genes for two essential proteins constituting a novel enzyme system for heptaprenyl diphosphate synthesis. *Journal of Biology and Chemistry,* 270, 18396–18400.

Lisec, J., Schauer, N., Kopka, J., Willmitzer, L., Fernie A.R. (2006) Gas chromatography mass spectrometry-based metabolite profiling in plants. *Nature Protocols*, 1, 387-96.

Liu, H., Ding, Y., Zhou, Y., Jin, W., Xie, K., & Chen, L. L. (2017). CRISPR-P 2.0: An Improved CRISPR-Cas9 Tool for Genome Editing in Plants. *Molecular Plant* 10, 530–532

Llorente, B., D'Andrea, L., Ruiz-Sola, M.A., Botterweg, E., Pulido, P., Andilla, J., Loza-Alvarez, P., and Rodriguez-Concepcion, M. (2016). Tomato fruit carotenoid biosynthesis is adjusted to actual ripening progression by a light-dependent mechanism. *The Plant Journal*, 85, 107–19.

Llorente, B., Torres-Montilla, S., Morelli, L., Florez-Sarasa, I., Ezquerro, M., D'andrea, L., Majer, E., Troncoso, A., Fernie, A.R., Daròs, J.A., and Rodriguez-Concepcion, M. (2020). Synthetic conversion of leaf chloroplasts into carotenoid-rich plastids reveals mechanistic basis of natural chromoplast development. *Proceedings of the National Academy of Sciences,* 117, 21796-21803.

Maudinas, B., Bucholtz, M.L., Papastephanou, C., Katiyar, S.S., Briedis, A. V., and Porter, J.W. (1977). The partial purification and properties of a phytoene synthesizing enzyme system. *Archives of Biochemistry and Biophysics,* 180, 354–362.

Muñoz, A. and Castellano, M.M. (2018). Coimmunoprecipitation of Interacting Proteins in Plants. In Two-hybrid systems: Methods and Protocols, *Methods in Molecular Biology*, 1794, 279–287.

Muñoz, P. and Munné-Bosch, S. (2018). Photo-oxidative stress during leaf, flower and fruit development. *Plant Physiology*, 176, 1004–1014.

Nagel, R., Bernholz, C., Vranová, E., Košuth, J., Bergau, N., Ludwig, S., Wessjohann, L., Gershenzon, J., Tissier, A., and Schmidt, A. (2015). Arabidopsis thaliana isoprenyl diphosphate synthases produce the C 25 intermediate, geranylfarnesyl diphosphate. *The Plant Journal*, 84, 847–859.

Nisar, N., Li, L., Lu, S., Khin, N.C., and Pogson, B.J. (2015). Carotenoid metabolism in plants. *Molecular Plant,* 8, 68–82.

Obata, T. and Fernie, A.R. (2012). The use of metabolomics to dissect plant responses to abiotic stresses. *Cellular and Molecular Life Sciences*, 69, 3225–3243.

Okada, K., Saito, T., Nakagawa, T., Kawamukai, M., and Kamiya, Y. (2000). Five geranylgeranyl diphosphate synthases expressed in different organs are localized into three subcellular compartments in Arabidopsis. *Plant Physiology*, 122, 1045–1056.

Oliver, S. (2000). Guilt-by-association goes global. *Nature* 403, 601–3.

Orlova I, Nagegowda DA, Kish CM, Gutensohn M, Maeda H, Varbanova M, Fridman E, Yamaguchi S, Hanada A, Kamiya Y, Krichevsky A, Citovsky V, Pichersky E, and Dudareva N. (2009). The small subunit of snapdragon geranyl diphosphate synthase modifies the chain length specificity of tobacco geranylgeranyl diphosphate synthase in planta. *Plant Cell*, 21, 4002-17

Phillips, M. a, D'Auria, J.C., Gershenzon, J., and Pichersky, E. (2008). The Arabidopsis thaliana type I Isopentenyl Diphosphate Isomerases are targeted to multiple subcellular compartments and have overlapping functions in isoprenoid biosynthesis. *Plant Cell* 20, 677–96.

Pulido, P., Perello, C., and Rodriguez-Concepcion, M. (2012). New Insights into Plant Isoprenoid Metabolism. *Molecular Plant* 5, 964–967.

Pulido, P., Toledo-Ortiz, G., Phillips, M. a, Wright, L.P., and Rodríguez-Concepción, M. (2013). Arabidopsis J-protein J20 delivers the first enzyme of the plastidial isoprenoid pathway to protein quality control. *Plant Cell,* 25, 4183–4194.

Quinet, M., Angosto, T., Yuste-Lisbona, F.J., Blanchard-Gros, R., Bigot, S., Martinez, J.P., and Lutts, S. (2019). Tomato Fruit Development and Metabolism. *Frontiers in Plant Science*, 10, 1–23.

Rodriguez-Concepcion, M., Avalos, J., Bonet, M. L., Boronat, A., Gomez-Gomez, L., Hornero-Mendez, D., Limon, M. C., Meléndez-Martínez, A. J., Olmedilla-Alonso, B., Palou, A., Ribot, J., Rodrigo, M. J., Zacarias, L., & Zhu, C. (2018). A global perspective on carotenoids: Metabolism, biotechnology, and benefits for nutrition and health. *Progress in Lipid Research* 70, 62–93

Rodríguez-Concepción, M. and Boronat, A. (2015). Breaking new ground in the regulation of the early steps of plant isoprenoid biosynthesis. *Current Opinion in Plant Biology*, 25, 17–22.

Ruiz-Lozano, J.M., Aroca, R., Zamarreño, Á.M., Molina, S., Andreo-Jiménez, B., Porcel, R., García-Mina, J.M., Ruyter-Spira, C., and López-Ráez, J.A. (2016). Arbuscular mycorrhizal symbiosis induces strigolactone biosynthesis under drought and improves drought tolerance in lettuce and tomato. *Plant, Cell Environment,* 39, 441–452.

Ruiz-Sola, M. Á., Coman, D., Beck, G., Barja, M. V., Colinas, M., Graf, A., Welsch, R., Rütimann, P., Bühlmann, P., Bigler, L., Gruissem, W., Rodríguez-Concepción, M., & Vranová, E. (2016b). Arabidopsis GERANYLGERANYL DIPHOSPHATE SYNTHASE 11 is a hub isozyme required for the production of most photosynthesis-related isoprenoids. *New Phytologis*t, 209, 252-64

Ruiz-Sola, M.Á., Barja, M.V., Manzano, D., Llorente, B., Schipper, B., Beekwilder, J., and Rodriguez-Concepcion, M. (2016b). A Single Arabidopsis Gene Encodes Two Differentially Targeted Geranylgeranyl Diphosphate Synthase Isoforms. *Plant Physiology*, 172, 1393–1402.

Ruiz-Sola, M. Á., & Rodríguez-Concepción, M. (2012). Carotenoid Biosynthesis in Arabidopsis: A Colorful Pathway. *The Arabidopsis Book*, 10, e0158.

Sandmann, G. (2015). Carotenoids of Biotechnological Importance. *Advances in Biochemical Engineering / Biotechnology*, 148, 449–467.

Sapir-Mir, M., Mett, A., Belausov, E., Tal-Meshulam, S., Frydman, A., Gidoni, D., and Eyal, Y. (2008). Peroxisomal Localization of Arabidopsis Isopentenyl Diphosphate Isomerases Suggests That Part of the Plant Isoprenoid Mevalonic Acid Pathway Is Compartmentalized to Peroxisomes. *Plant Physiology*, 148, 1219–1228.

Schiml, S., Fauser, F., and Puchta, H. (2016). CRISPR/Cas-Mediated Site-Specific Mutagenesis in Arabidopsis thaliana Using Cas9 Nucleases and Paired Nickases. *Methods in Molecular Biology*, 1469, 111–22.

Seymour, G.B., Chapman, N.H., Chew, B.L., and Rose, J.K.C. (2013). Regulation of ripening and opportunities for control in tomato and other fruits. *Plant Biotechnology Journal*, 11, 269–278.

Simon, P. (2003). Q-Gene: Processing quantitative real-time RT-PCR data. *Bioinformatics,* 19, 1439–1440.

Sparkes, I.A., Runions, J., Kearns, A., and Hawes, C. (2006). Rapid, transient expression of fluorescent fusion proteins in tobacco plants and generation of stably transformed plants. N*ature Protocols*, 1, 2019–25.

Stauder, R., Welsch, R., Camagna, M., Kohlen, W., Balcke, G.U., Tissier, A., and Walter, M.H. (2018). Strigolactone Levels in Dicot Roots Are Determined by an Ancestral Symbiosis-Regulated Clade of the PHYTOENE SYNTHASE Gene Family. *Frontiers in Plant Science*, 9, 1–18.

Sun, T., Yuan, H., Cao, H., Yazdani, M., Tadmor, Y., and Li, L. (2018). Carotenoid Metabolism in Plants: The Role of Plastids. *Molecular Plant*, 11, 58–74.

Tholl, D. (2015). Biosynthesis and Biological Functions of Terpenoids in Plants. *Advances in biochemical engineering/biotechnology* 148, 63–106.

Vranová, E., Coman, D., and Gruissem, W. (2013). Network analysis of the MVA and MEP pathways for isoprenoid synthesis. *Annual Review of Plant Biology*, 64, 665–700.

Walter, M.H., Stauder, R., and Tissier, A. (2015). Evolution of root-specific carotenoid precursor pathways for apocarotenoid signal biogenesis. *Plant Science*, 233, 1–10.

Wang, C., Chen, Q., Fan, D., Li, J., Wang, G., and Zhang, P. (2016). Structural Analyses of Short-Chain Prenyltransferases Identify an Evolutionarily Conserved GFPPS Clade in Brassicaceae Plants. *Molecular Plant*, 9, 195–204.

Wang, G. and Dixon, R. a (2009). Heterodimeric geranyl(geranyl)diphosphate synthase from hop (Humulus lupulus) and the evolution of monoterpene biosynthesis. *Proceedings of the National Academy of Sciences,* 106, 9914–9919.

Wang, J., Lin, H.-X., Su, P., Chen, T., Guo, J., Gao, W., and Huang, L.-Q. (2019). Molecular cloning and functional characterization of multiple geranylgeranyl pyrophosphate synthases (ApGGPPS) from Andrographis paniculata. *Plant Cell Reports*, 38, 117–128.

Wang, Q., Huang, X.-Q., Cao, T.-J., Zhuang, Z., Wang, R., and Lu, S. (2018). Heteromeric Geranylgeranyl Diphosphate Synthase Contributes to Carotenoid Biosynthesis in Ripening Fruits of Red Pepper (Capsicum annuum var. conoides). *Journal of Agriculture and Food Chemistry*, 66, 11691–11700.

Yuan, H., Zhang, J., Nageswaran, D., and Li, L. (2015). Carotenoid metabolism and regulation in horticultural crops. *Horticultural Research*. 2, 15036.

Zhang, M., Su, P., Zhou, Y.-J., Wang, X.-J., Zhao, Y.-J., Liu, Y.-J., Tong, Y.-R., Hu, T.-Y., Huang, L.-Q., and Gao, W. (2015). Identification of geranylgeranyl diphosphate synthase genes from Tripterygium wilfordii. *Plant Cell Reports*, 34, 2179–88.

Zhou, F., & Pichersky, E. (2020). The complete functional characterisation of the terpene synthase family in tomato. *New Phytologist*, 226, 1341–1360.

Zhou, F., Wang, C.-Y., Gutensohn, M., Jiang, L., Zhang, P., Zhang, D., Dudareva, N., and Lu, S. (2017). A recruiting protein of geranylgeranyl diphosphate synthase controls metabolic flux toward chlorophyll biosynthesis in rice. *Proceedings of the National Academy of Sciences,* 114, 6866–6871.

Zhu, X.F., Suzuki, K., Okada, K., Tanaka, K., Nakagawa, T., Kawamukai, M., and Matsuda, K. (1997a). Cloning and functional expression of a novel geranylgeranyl pyrophosphate synthase gene from Arabidopsis thaliana in Escherichia coli. *Plant Cell Physiology*, 38, 357–61.

Zhu, X.F., Suzuki, K., Saito, T., Okada, K., Tanaka, K., Nakagawa, T., Matsuda, H., and Kawamukai, M. (1997b). Geranylgeranyl pyrophosphate synthase encoded by the newly isolated gene GGPS6 from Arabidopsis thaliana is localized in mitochondria. *Plant Molecular Biology*, 35, 331–41.

Zouine, M., Maza, E., Djari, A., Lauvernier, M., Frasse, P., Smouni, A., Pirrello, J., and Bouzayen, M. (2017). TomExpress, a unified tomato RNA-Seq platform for visualization of expression data, clustering and correlation networks. *The Plant Journal*, 92, 727–735.

7 Supplemental information

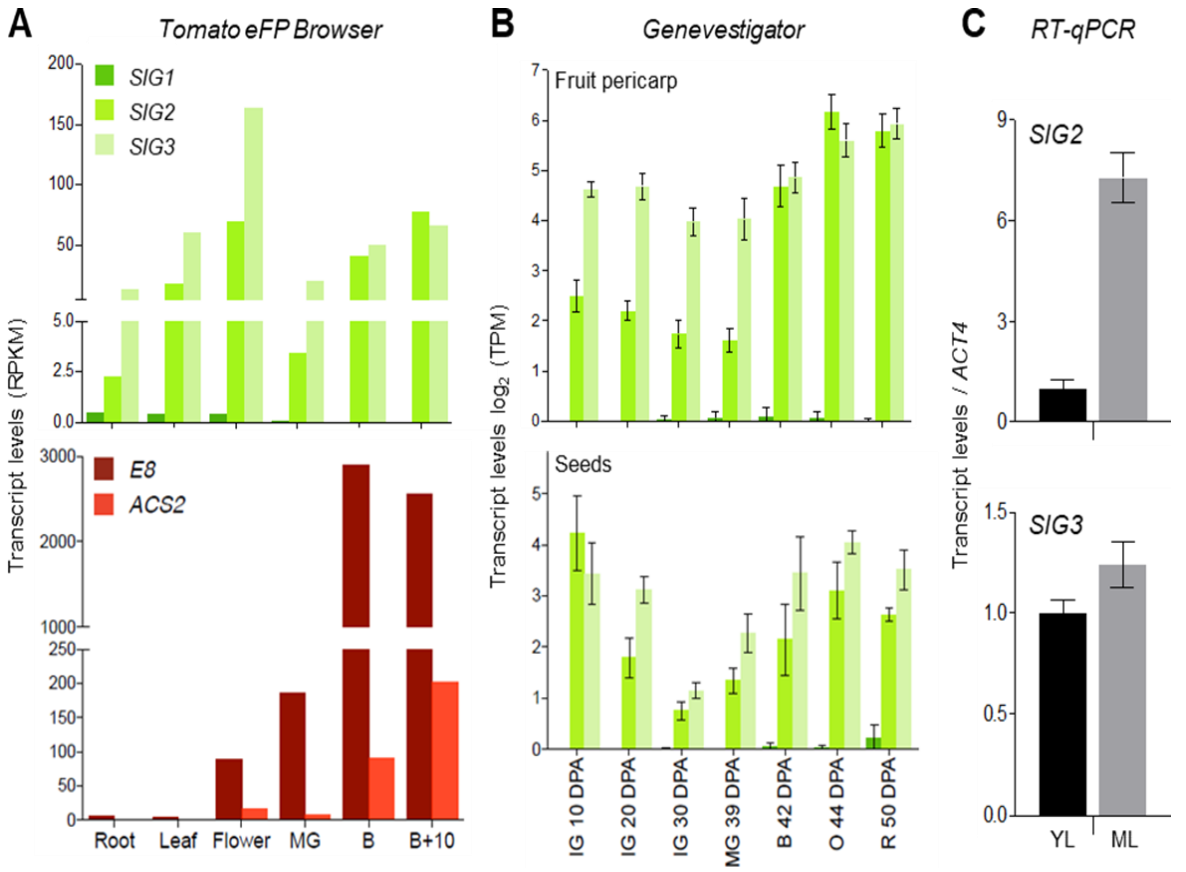

Figure S1. Transcript levels of tomato genes in different tissues. Abbreviations: DPA, days post-anthesis; IG, immature green; MG, mature green; B, breaker; O, orange,R, red; YL, young leaves; ML, mature leaves. (A) RNAseq data retrieved from the *Tomato eFP Browser* database (http://bar.utoronto.ca/efp_tomato/cgi-bin/efpWeb.cgi). (A)Plots show the transcript levels of *SlG1-3, E8 (Solyc09g089580)* and *ACS2 (Solyc01g095080)* genes in root, leaf, flower and fruit pericarp during ripening. Expression data are represented as RPKM (Reads per Kilobase of transcript per Million mapped reads). **(B)** RNAseq data obtained from GeneInvestigator (https://genevestigator.com/). Plots show the transcript levels of *SlG1-3* genes in fruit pericarp and seeds during development. Levels are represented as $\log_2$ TPM (Transcripts per Million mapped reads). **(C)** RT-qPCR analysis of *SlG2* and *SlG3* transcript levels in young and mature leaves from WT plants. Expression values were normalized using *ACT4* and and they are shown relative to YL samples. Data correspond to the mean±SD of n=3 independent biological replicates.

```
SlG2        ATGAGATCTATGAACCTTGTTGATTCATGGGGTCAAGCTTGTTTAGTTATCAATCAATCT    60
slg2-1      ATGAGATCTATGAACCTTGTTGATTCATGGGGTCAAGCTTGTTTAGTTATCAATCAATCT    60
slg2-2      ATGAGATCTATGAACCTTGTTGATTCATGGGGTCAAGCTTGTTTAGTTATCAATCAATCT    60
            ************************************************************

SlG2        TTACCTTACAATTCGTTTAATGGATTGATGAAAATCAATTCGAAAAATCGAAAAATTTTG    120
slg2-1      TTACCTTACAATTCGTTTAATGGATTGATGAAAATCAATTCGAAAAATCGAAAAATTTTG    120
slg2-2      TTACCTTACAATTCGTTTAATGGATTGATGAAAATCAATTCGAAAAATCGAAAAATTTTG    120
            ************************************************************

SlG2        AAACAGAGTTTATCTTATAGAACATTTTCATCTGTAACTGTTTCAGCTATTGCTACCAAT    180
slg2-1      AAACAGAGTTTATCTTATAGAACATTTTCATCTGTAACTGTTTCAGCTATTGCTACCAAT    180
slg2-2      AAACAGAGTTTATCTTATAGAACATTTTCATCTGTAACTGTTTCAGCTATTGCTACCAAT    180
            ************************************************************

SlG2        GAGAAAGTTGTTATGGAAAAAGAAGAATTTAATTTCAAGGTTTACGTAGCTGAAAAGGCG    240
slg2-1      GAGAAAGTTGTTATGGAAAAAGAAGAATTTAATTTCAAGGTTTACGTAGCTGAAAAGGCG    240
slg2-2      GAGAAAGTTGTTATGGAAAAAGAAGAATTTAATTTCAAGGTTTACGTAGCTGAAAAGGCG    240
            ************************************************************

SlG2        ATTTGTGTAAATAAAGCTTTGGATGAGGCTATAATGGTAAAAGACCCACCTAAGATCCAT    300
slg2-1      ATTTGTGTAAATAAAGCTTTGGATGAGGCTATAATGGTAAAAGACCCACCTAAGATCCAT    300
slg2-2      ATTTGTGTAAATAAAGCTTTGGATGAGGCTATAATGGTAAAAGACCCACCTAAGATCCAT    300
            ************************************************************

SlG2        GAAGCAATGCGTTATTCGCTTCTCGCCGGCGGGAAGAGAGTCCGGCCGATGCTCTGTCTT    360
slg2-1      GAAGCAATGCGTTATTCGCTTCTCGCCGGCGGGAAGAGAGTCCGGCCGATGCTCTGTCTT    360
slg2-2      GAAGCAATGCGTTATTCGCTTCTCGCCGGCGGGAAGAGAGTCCGGCCGATGCTCTGTCTT    360
            ************************************************************

SlG2        GCTGCCTGTGAACTTGTTGGGGGGAAACCAAGGGAATGCTATGGCGGCTGCTTGTGCTGTT    420
slg2-1      GCTGCCTGTGAACTTGTTGGGGGGAAACCAAGGGAATGCTATGGCGGCTGCTTGTGCTGTT    420
slg2-2      GCTGCCTGTGAACTTGTTGGGGGGAAACCAAGGGAATGCTATGGCGGCTGCTTGTGCTGTT    420
            ************************************************************
                                                  SlG2 CRISPR Geno F

SlG2        GAGATGATACATACTATGTCTCTAATTCATGATGATTTGCCTTGTATGGATGACGACGAT    480
slg2-1      GAGATGATACATACTATGTCTCTAATTCATGATGATTTGCCTTGTATGGATGACGACGAT    480
slg2-2      GAGATGATACATACTATGTCTCTAATTCATGATGATTTGCCTTGTATGGATGACGACGAT    480
            ************************************************************

SlG2        CTCCGCCGTGGGAAGCCGACGAATCATAAAGTGTACGGTGAGGATGTGGCGGTCCTCGCC    540
slg2-1      CTCCGCCGTGGGAAGCCGACGAATCATAAAGTGTACGGTGAGGATGTGGCGGTCCTCGCC    540
slg2-2      CTCCGCCGTGGGAAGCCGACGAATCATAAAGTGTACGGTGAGGATGTGGCGGTCCTCGCC    540
            ************************************************************

SlG2        GGAGATGCGCTACTTGCTTTCGCATTCGAGTACCTCGCTACCGCTACAACCGGAGTTTCT    600
slg2-1      GGAGATGCGCTACTTGCTTTCGCATTCGAGTACCTCGCTACCGCTACAACCGGAGTTTCT    600
slg2-2      GGAGATGCGCTACTTGCTTTCGCATTCGAGTACCTCGCTACCGCTACAACCGGAGTTTCT    600
            ************************************************************

SlG2        CCGTCGAGGATCCTCGTTGCTGTCGCCGAATTGGCGAAATCTGTTGGAACGGAAGGGTTA    660
slg2-1      CCGTCGAGGATCCTCGTTGCTGTCGCCGAATTGGCGAAATCTGTTGGAACGGAAGGGTTA    660
slg2-2      CCGTCGAGGATCCTCGTTGCTGTCGCCGAATTGGCGAAATCTGTTGGAACGGAAGGGTTA    660
            ************************************************************
```

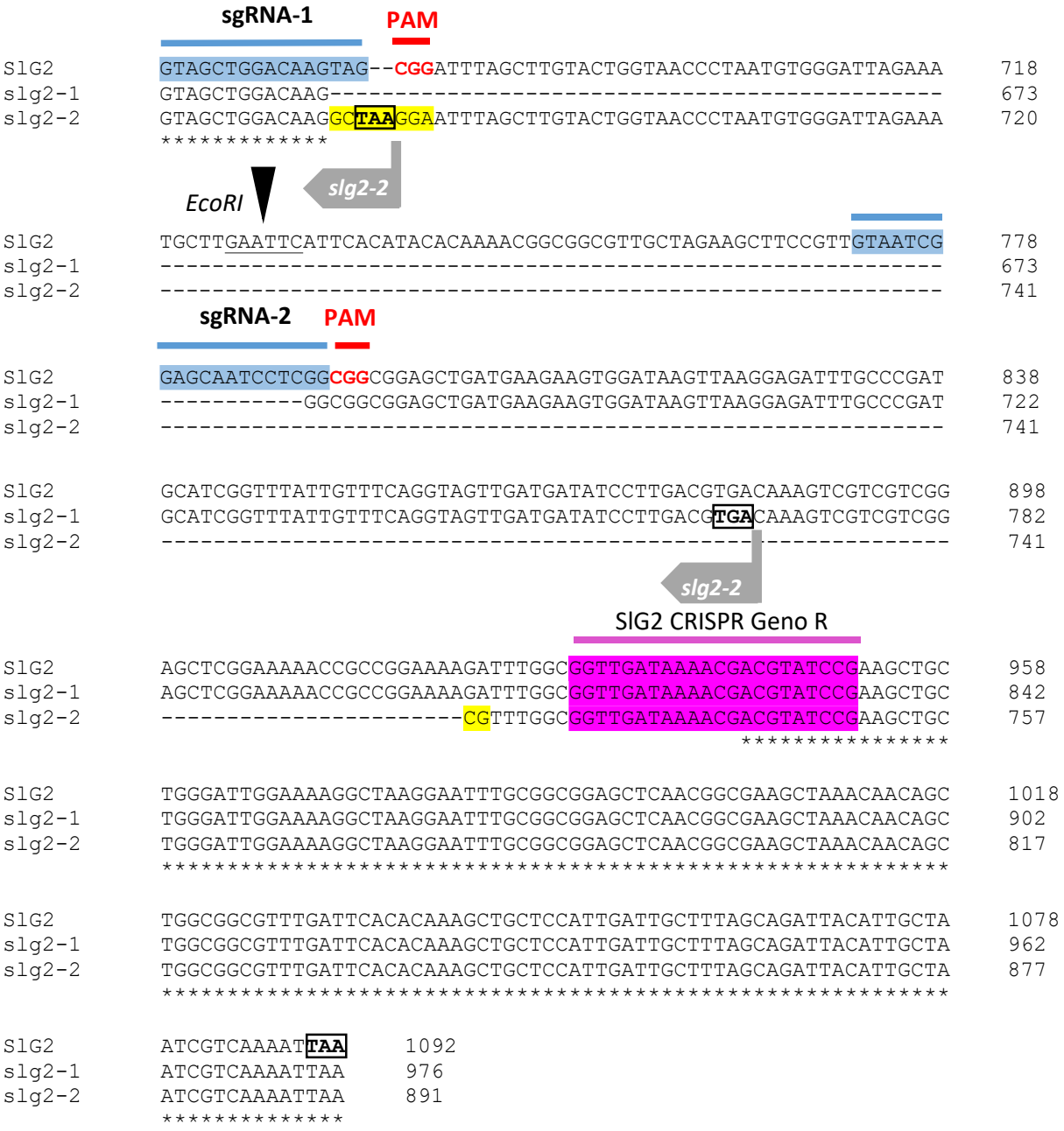

Figure S2. DNA sequence alignment of *SlG2* CRISPR mutants. Alignment was performed using *Clustal Omega* (https://www.ebi.ac.uk/Tools/msa/clustalo/) with default settings. The sequence encoding the predicted plastid-targeting peptide is boxed in green. Designed single-guide RNAs (sgRNA) and genotyping oligonucleotides are highlighted in blue and purple, respectively. The designed sgRNAs encompass an *EcoRI*restriction site (underlined in black). Protospacer adjacent motifs (PAM) are highlighted in red. Translation stop codons are boxed and marked in bold. Sequences changes due to CRISPR-Cas9 are depicted in yellow. Numbers at the end of each sequence indicate DNA sequence length.

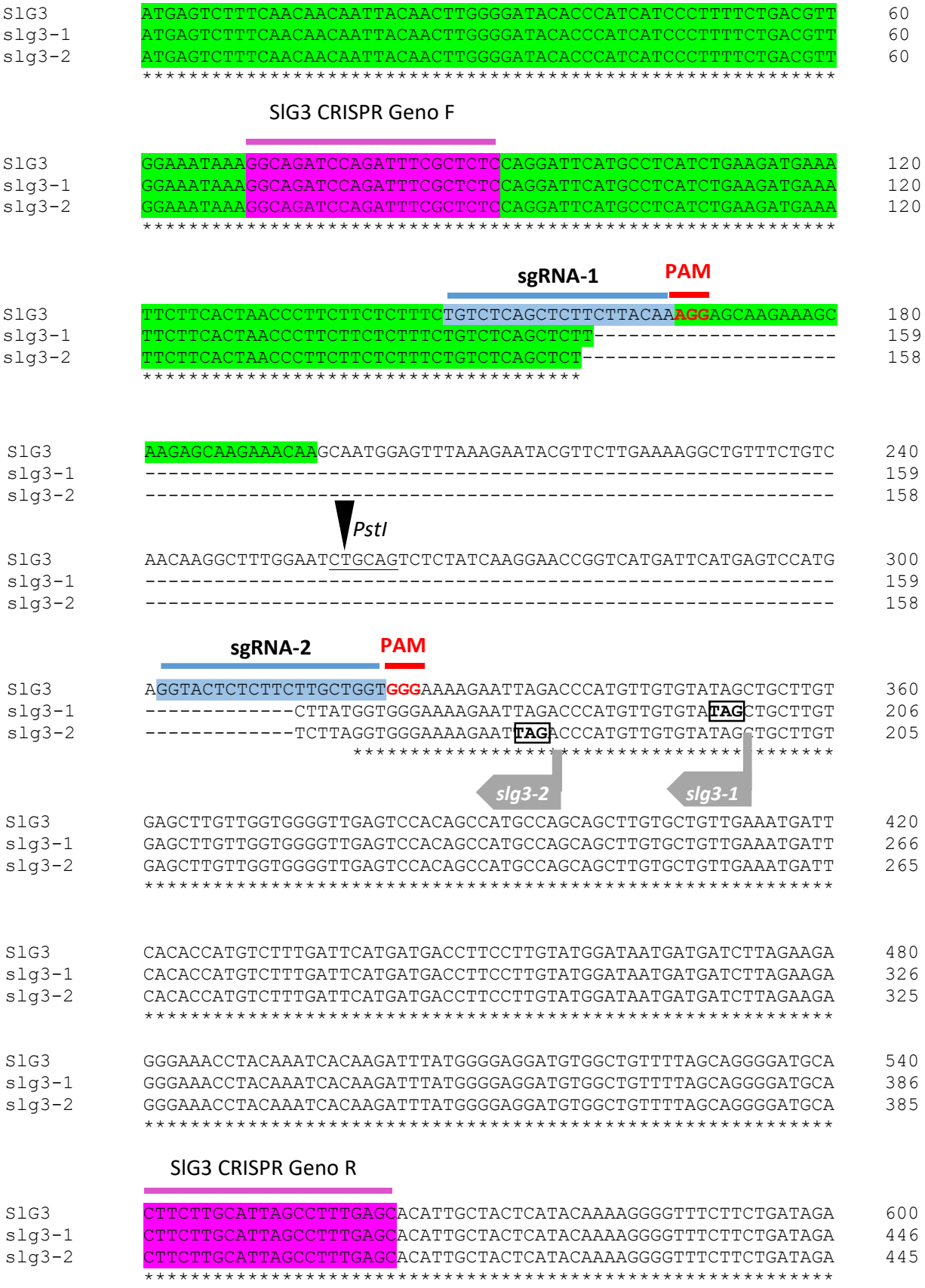
SlG3 ATGAGTCTTTCAACAACAATTACAACTTGGGGATACACCCATCATCCCTTTTCTGACGTT 60
slg3-1 ATGAGTCTTTCAACAACAATTACAACTTGGGGATACACCCATCATCCCTTTTCTGACGTT 60
slg3-2 ATGAGTCTTTCAACAACAATTACAACTTGGGGATACACCCATCATCCCTTTTCTGACGTT 60
SlG3 CRISPR Geno F
SlG3 GGAAATAAAGGCAGATCCAGATTTCGCTCTCCAGGATTCATGCCTCATCTGAAGATGAAA 120
slg3-1 GGAAATAAAGGCAGATCCAGATTTCGCTCTCCAGGATTCATGCCTCATCTGAAGATGAAA 120
slg3-2 GGAAATAAAGGCAGATCCAGATTTCGCTCTCCAGGATTCATGCCTCATCTGAAGATGAAA 120
sgRNA-1
PAM
SlG3 TTCTTCACTAACCCTTCTTCTCTTTCTGTCTCAGCTCTTCTTACAAAGGAGCAAGAAAGC 180
slg3-1 TTCTTCACTAACCCTTCTTCTCTTTCTGTCTCAGCTCTT---------- 159
slg3-2 TTCTTCACTAACCCTTCTTCTCTTTCTGTCTCAGCTCT---------- 158
SlG3 AAGAGCAAGAAACAAGCAATGGAGTTTAAAGAATACGTTCTTGAAAAGGCTGTTTCTGTC 240
slg3-1 ---------- 159
slg3-2 ---------- 158
PstI
SlG3 AACAAGGCTTTGGAATCTGCAGTCTCTATCAAGGAACCGGTCATGATTCATGAGTCCATG 300
slg3-1 ---------- 159
slg3-2 ---------- 158
sgRNA-2
PAM
SlG3 AGGTACTCTCTTCTTGCTGGTGGGAAAAGAATTAGACCCATGTTGTGTATAGCTGCTTGT 360
slg3-1 ----------CTTATGGTGGGAAAAGAATTAGACCCATGTTGTGTATAGCTGCTTGT 206
slg3-2 ----------TCTTAGGTGGGAAAAGAATTAGACCCATGTTGTGTATAGCTGCTTGT 205
slg3-2
slg3-1
SlG3 GAGCTTGTTGGTGGGGTTGAGTCCACAGCCATGCCAGCAGCTTGTGCTGTTGAAATGATT 420
slg3-1 GAGCTTGTTGGTGGGGTTGAGTCCACAGCCATGCCAGCAGCTTGTGCTGTTGAAATGATT 266
slg3-2 GAGCTTGTTGGTGGGGTTGAGTCCACAGCCATGCCAGCAGCTTGTGCTGTTGAAATGATT 265
SlG3 CACACCATGTCTTTGATTCATGATGACCTTCCTTGTATGGATAATGATGATCTTAGAAGA 480
slg3-1 CACACCATGTCTTTGATTCATGATGACCTTCCTTGTATGGATAATGATGATCTTAGAAGA 326
slg3-2 CACACCATGTCTTTGATTCATGATGACCTTCCTTGTATGGATAATGATGATCTTAGAAGA 325
SlG3 GGGAAACCTACAAATCACAAGATTTATGGGGAGGATGTGGCTGTTTTAGCAGGGGATGCA 540
slg3-1 GGGAAACCTACAAATCACAAGATTTATGGGGAGGATGTGGCTGTTTTAGCAGGGGATGCA 386
slg3-2 GGGAAACCTACAAATCACAAGATTTATGGGGAGGATGTGGCTGTTTTAGCAGGGGATGCA 385
SlG3 CRISPR Geno R
SlG3 CTTCTTGCATTAGCCTTTGAGCACATTGCTACTCATACAAAAGGGGTTTCTTCTGATAGA 600
slg3-1 CTTCTTGCATTAGCCTTTGAGCACATTGCTACTCATACAAAAGGGGTTTCTTCTGATAGA 446
slg3-2 CTTCTTGCATTAGCCTTTGAGCACATTGCTACTCATACAAAAGGGGTTTCTTCTGATAGA 445

```
SlG3        ATTGTGAGGGTGATTGGTGAGTTGGCGAAGTGTATTGGGGCAGAGGGACTTGTAGCTGGT    660
slg3-1      ATTGTGAGGGTGATTGGTGAGTTGGCGAAGTGTATTGGGGCAGAGGGACTTGTAGCTGGT    506
slg3-2      ATTGTGAGGGTGATTGGTGAGTTGGCGAAGTGTATTGGGGCAGAGGGACTTGTAGCTGGT    505
            ************************************************************

SlG3        CAGGTTGTAGATATAATTTCAGAAGGCATTTCTGATGTTGATTTGAAGCATTTAGAGTTC    720
slg3-1      CAGGTTGTAGATATAATTTCAGAAGGCATTTCTGATGTTGATTTGAAGCATTTAGAGTTC    566
slg3-2      CAGGTTGTAGATATAATTTCAGAAGGCATTTCTGATGTTGATTTGAAGCATTTAGAGTTC    565
            ************************************************************

SlG3        ATTCATCTGCACAAGACTGCAGCTTTGTTAGAAGGGTCAGTGGTGCTAGGGGCTATATTA    780
slg3-1      ATTCATCTGCACAAGACTGCAGCTTTGTTAGAAGGGTCAGTGGTGCTAGGGGCTATATTA    626
slg3-2      ATTCATCTGCACAAGACTGCAGCTTTGTTAGAAGGGTCAGTGGTGCTAGGGGCTATATTA    625
            ************************************************************

SlG3        GGAGGTGCACCAGATGAAGATGTGGAAAAGCTAAGAAAATTTGCAAGATGTATTGGTTTG    840
slg3-1      GGAGGTGCACCAGATGAAGATGTGGAAAAGCTAAGAAAATTTGCAAGATGTATTGGTTTG    686
slg3-2      GGAGGTGCACCAGATGAAGATGTGGAAAAGCTAAGAAAATTTGCAAGATGTATTGGTTTG    685
            ************************************************************

SlG3        TTATTTCAAGTTGTGGATGATATTCTTGATGTCACAAAGTCTTCTCAGCAATTGGGGAAA    900
slg3-1      TTATTTCAAGTTGTGGATGATATTCTTGATGTCACAAAGTCTTCTCAGCAATTGGGGAAA    746
slg3-2      TTATTTCAAGTTGTGGATGATATTCTTGATGTCACAAAGTCTTCTCAGCAATTGGGGAAA    745
            ************************************************************

SlG3        ACAGCTGGGAAGGACTTGGTTGCTGATAAGGTAACTTATCCCAAACTGATAGGTATTGAG    960
slg3-1      ACAGCTGGGAAGGACTTGGTTGCTGATAAGGTAACTTATCCCAAACTGATAGGTATTGAG    806
slg3-2      ACAGCTGGGAAGGACTTGGTTGCTGATAAGGTAACTTATCCCAAACTGATAGGTATTGAG    805
            ************************************************************

SlG3        AAATCTAGGGAGTTTGCTGAGGAGTTAAACAAAGAAGCGAAAGCTCAGCTTGTTGGATTT   1020
slg3-1      AAATCTAGGGAGTTTGCTGAGGAGTTAAACAAAGAAGCGAAAGCTCAGCTTGTTGGATTT    866
slg3-2      AAATCTAGGGAGTTTGCTGAGGAGTTAAACAAAGAAGCGAAAGCTCAGCTTGTTGGATTT    865
            ************************************************************

SlG3        GATCAAGAGAAAGCAGCTCCATTGTTTGCTCTTGCAAATTATATTGCTTACAGAGAGAAT   1080
slg3-1      GATCAAGAGAAAGCAGCTCCATTGTTTGCTCTTGCAAATTATATTGCTTACAGAGAGAAT    926
slg3-2      GATCAAGAGAAAGCAGCTCCATTGTTTGCTCTTGCAAATTATATTGCTTACAGAGAGAAT    925
            ************************************************************

SlG3        TAA1083
slg3-1      TAA 929
slg3-2      TAA 928
            ***
```

Figure S3. DNA sequence alignment of *SlG2* CRISPR mutants. Alignment was performed using *Clustal Omega* (https://www.ebi.ac.uk/Tools/msa/clustalo/) with default settings. The sequence encoding the predicted plastid-targeting peptide is boxed in green. Designed single-guide RNAs (sgRNA) and genotyping oligonucleotides are highlighted in blue and purple, respectively. The designed sgRNAs encompass an *EcoRI* restriction site (underlined in black). Protospacer adjacent motifs (PAM) are highlighted in red. Translation stop codons are boxed and marked in bold. Sequences changes due to CRISPR-Cas9 are depicted in yellow. Numbers at the end of each sequence indicate DNA sequence length.

A

SlG2 MRSMNLVDSWGQACLVINQSLPYNSFNGLMKINSKNRKILKQSLSYRTFSSVTVSAIATNEKVVMEKEEFNFKVYVAEKA 80
slg2-1 MRSMNLVDSWGQACLVINQSLPYNSFNGLMKINSKNRKILKQSLSYRTFSSVTVSAIATNEKVVMEKEEFNFKVYVAEKA 80
slg2-2 MRSMNLVDSWGQACLVINQSLPYNSFNGLMKINSKNRKILKQSLSYRTFSSVTVSAIATNEKVVMEKEEFNFKVYVAEKA 80
Cxxx
FARM
SlG2 ICVNKALDEAIMVKDPPKIHEAMRYSLLAGGKRVRPMLCLAACELVGGNQGNAMAAACAVEMIHTMSLIHDDLPCMDDDD 160
slg2-1 ICVNKALDEAIMVKDPPKIHEAMRYSLLAGGKRVRPMLCLAACELVGGNQGNAMAAACAVEMIHTMSLIHDDLPCMDDDD 160
slg2-2 ICVNKALDEAIMVKDPPKIHEAMRYSLLAGGKRVRPMLCLAACELVGGNQGNAMAAACAVEMIHTMSLIHDDLPCMDDDD 160
sgRNA-1
SlG2 LRRGKPTNHKVYGEDVAVLAGDALLAFAFEYLATATTGVSPSRILVAVAELAKSVGTEGLVAGQVADLACTGNPNVGLEM 240
slg2-1 LRRGKPTNHKVYGEDVAVLAGDALLAFAFEYLATATTGVSPSRILVAVAELAKSVGTEGLVAGQGRRS*---------- 228
slg2-2 LRRGKPTNHKVYGEDVAVLAGDALLAFAFEYLATATTGVSPSRILVAVAELAKSVGTEGLVAGQG*---------- 225
sgRNA-2
SARM
SlG2 LEFIHIHKTAALLEASVVIGAILGGGADEEVDKLRRFARCIGLLFQVVDDILDVTKSSSELGKTAGKDLAVDKTTYPKLL 320
slg2-1 ---------- 228
slg2-2 ---------- 225
SlG2 GLEKAKEFAAELNGEAKQQLAAFDSHKAAPLIALADYIANRQN* 363
slg2-1 ---------- 228
slg2-2 ---------- 225

.

Figure S4. Protein alignments of WT and mutant SlG2 (A) and SlG3 (B) sequences. *Clustal Omega* (https://www.ebi.ac.uk/Tools/msa/clustalo/) with default settings was used for the alignment. The predicted targeting peptide, the region of the designed sgRNAs and the catalytic motifs FARM and SARM are boxed in green, blue and black, respectively. The protein-protein interaction CxxxC motifs (x = any hydrophobic residue) are highlighted in pink. Numbers at the end of each sequence indicate protein length

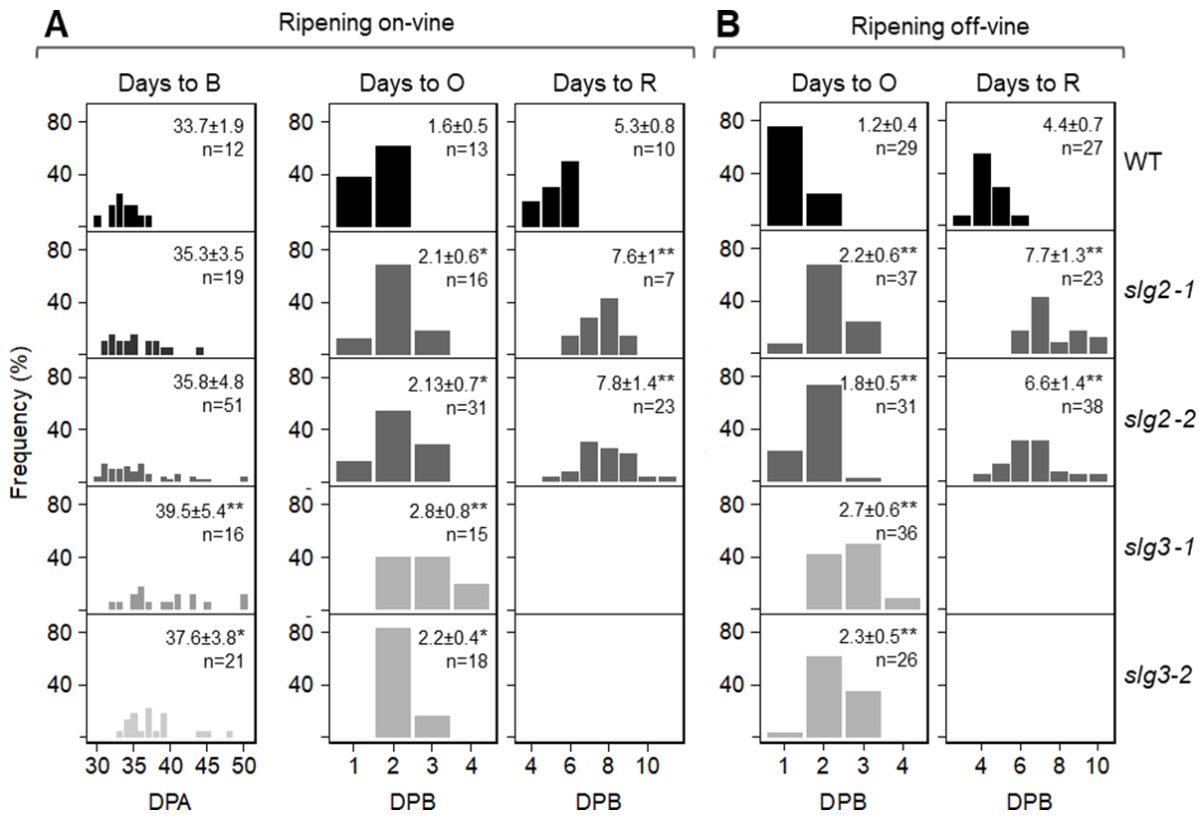

Figure S5. Fruit ripening initiation and progression in WT and mutant plants. Histograms represent the number of days to reach Breaker (B), Orange (O) and Red (R) fruit stages represented as days post-anthesis (DPA) or days post-breaker (DPB). On-vine **(A)** and off-vine **(B)** measurements are shown. For on-vine measurements, flowers were marked in anthesis and followed *in planta*. For off-vine measurements fruits were harvested at the B stage. The mean±SD values and the sample size (n) are shown in each histogram. Asterisks indicate statistically significant differences among means relative to WT samples (one-way ANOVA followed by Dunnett's multiple comparisons test, *p<0.05, **p<0.01).

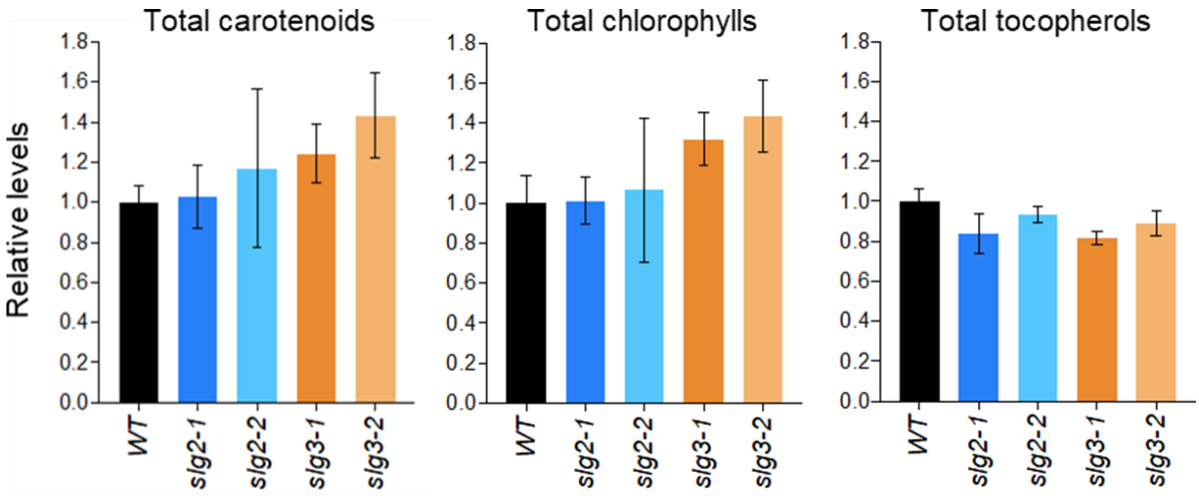

Figure S6. Relative levels of plastidial isoprenoids in mature green fruits from WT and mutant lines. Values correspond to the mean±SD of at least three independent biological replicates (n=3) relative to WT levels. No statistically significant differences among means were found (one-way ANOVA).

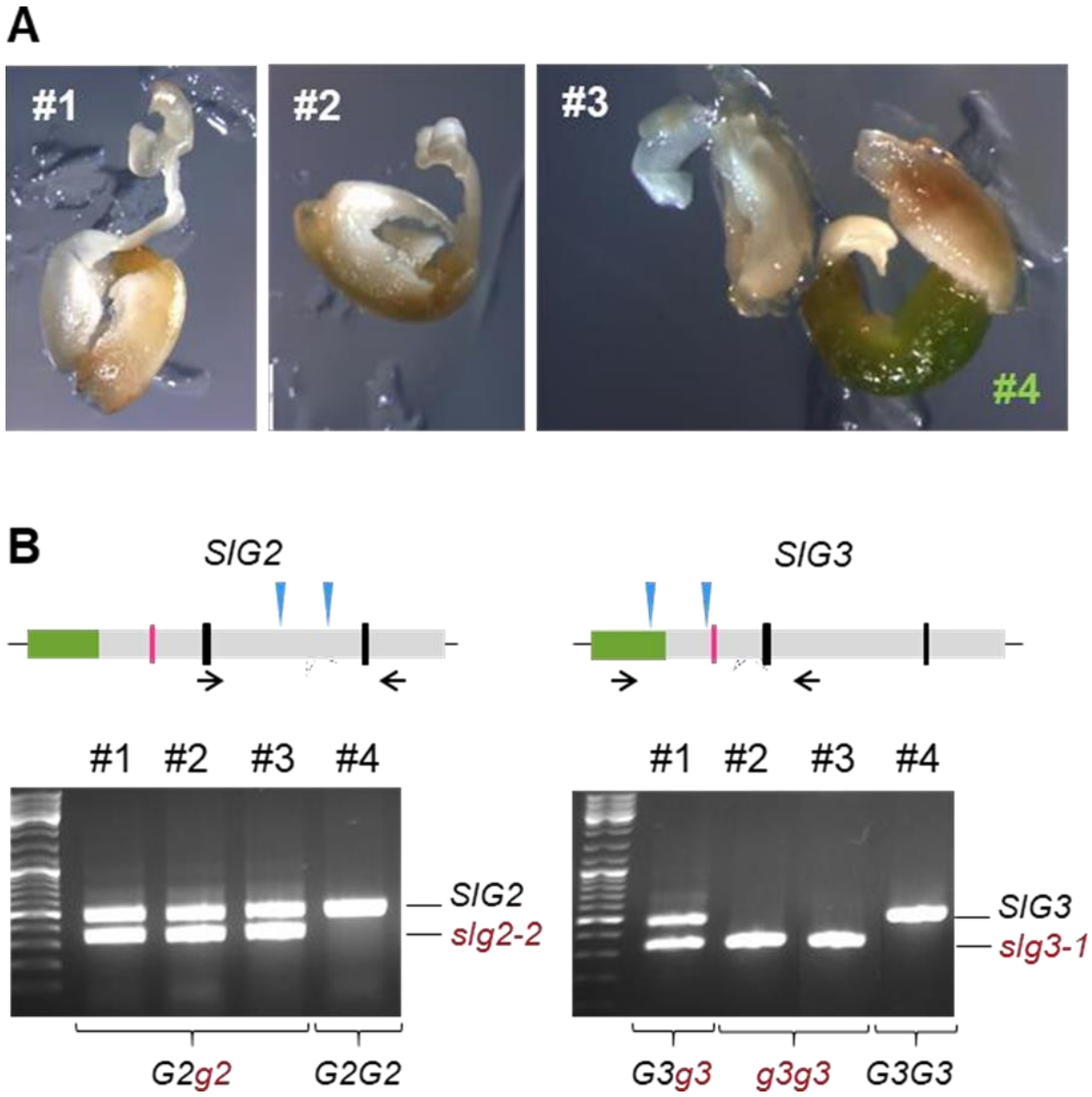

Figure S7. PCR-based genotyping of non-germinating F2 seeds from the cross of *slg2-2* and *slg3-1* mutant plants. (A) Non-germinating seeds were manually open to show the phenotype of their embryos. Only seed #4 showed a green embryo. **(B)** Scheme representing the *SlG2* and *SlG3* genes and the genotyping results. Blue arrowheads indicate the position of the designed sgRNAs to generate deletions, and black arrows represent primer pairs used for PCR-based genotyping. Gel pictures show the PCR amplification products from samples of the embryos shown in (A). The position of amplicons from WT and mutant genes (in black and red, respectively) is indicated.

Table S1. Primers used in this work.

Use	#	Name	Sequence (5'-3')[1]
Cloning	1	SlG2-attB1-F	**GGGGACAAGTTTGTACAAAAAAGCAGGCTGG**ATGAGATCTATGAACCTTGTTGATTC
	2	SlG2-attB2-R	**GGGGACCACTTTGTACAAGAAAGCTGGGTG**ATTTTGACGATTAGCAATGTAATCTG
	3	SlG3-attB1-F	**GGGGACAAGTTTGTACAAAAAAGCAGGCTGG**ATGAGTCTTTCAACAACAATTACAAC
	4	SlG3-attB2-R	**GGGGACCACTTTGTACAAGAAAGCTGGGTG**ATTCTCTCTGTAAGCAATATAATTTG
	5	SlPSY1-attB1-F	**GGGGACAAGTTTGTACAAAAAAGCAGGCT**ATGTCTGTTGCCTTGTTATGGGTTG
	6	SlPSY1-attB2-R	**GGGGACCACTTTGTACAAGAAAGCTGGGT**TTCTTTGAAGAGAGGCAGTTTTTG
	7	SlPSY2-attB1-F	**GGGGACAAGTTTGTACAAAAAAGCAGGCT**ATGTCTGTTGCTTTGTTGTGGGTTG
	8	SlPSY2-attB2-R	**GGGGACCACTTTGTACAAGAAAGCTGGGT**GTGTCTTTGCTAGTGGGGAAGAAG
	9	AtPRK-attB1-F	**GGGGACAAGTTTGTACAAAAAAGCAGGCT**ATGGCTGTCTCAACTATCTAC
	10	AtPRK-attB2-R	**GGGGACCACTTTGTACAAGAAAGCTGGGT**CGGCTTTAGCTTCTGCACGAGC
	11	SlG2stop-attB2-R	**GGGGACCACTTTGTACAAGAAAGCTGGGTG**TTAATTTTGACGATTAGCAATG
	12	SlG3stop-attB2-R	**GGGGACCACTTTGTACAAGAAAGCTGGGTG**TTAATTCTCTCTGTAAGCAATATAATTTG
RT-qPCR	13	SlG1-qPCR-F	GGCCTTTGAACATGTGGCTACC
	14	SlG1-qPCR-R	ACTCGCCAAGTCCACAATTTGC
	15	SlG2-qPCR-F	AAAGTCATCGTCGGAGCTCG
	16	SlG2-qPCR-R	GTTTAGCTTCGCCGTTGAGC
	17	SlG3-qPCR-F	AGGAGGTGCACCAGATGAAG
	18	SlG3-qPCR-R	TCAGCAACCAAGTCCTTCCC
	19	SlEXP-qPCR-F	GCTAAGAACGCTGGACCTAA
	20	SlEXP-qPCR-R	TGGGTGTGCCTTTCTGAATG
	21	SlACT-qPCR-F	CCTTCCACATGCCATTCTCC
	22	SlACT-qPCR-R	CCACGCTCGGTCAGGATCT
	23	SlE8-qPCR-F	AGCTGCAAGTTGGAGAGACACG
	24	SlE8-qPCR-R	CCGCATGGAGTTGGAAATTC
	25	SlACS2-qPCR-F	CGTTTGAATGTCAAGAGCCAGG
	26	SlACS2-qPCR-F	TCGCGAGCGCAATATCAAC
sgRNAs for CRISPR-Cas9 gene impairment	27	SlG2-sgRNA-1 F	ATTGGTTAGTAGCTGGACAAGTAG
	28	SlG2-sgRNA-1 R	AAACCTACTTGTCCAGCTACTAAC
	29	SlG2-sgRNA-2 F	ATTGGTAATCGGAGCAATCCTCGG
	30	SlG2-sgRNA-2 R	AAACCCGAGGATTGCTCCGATTAC
	31	SlG3-sgRNA-1 F	ATTGTGTCTCAGCTCTTCTTACAA
	32	SlG3-sgRNA-1 R	AAACTTGTAAGAAGAGCTGAGACA
	33	SlG3-sgRNA-2 F	ATTGGGTACTCTCTTCTTGCTGGT
	34	SlG3-sgRNA-2 R	AAACACCAGCAAGAAGAGAGTACC
CRISPR plants genotyping	35	SlG2 CRISPR Geno F	GCCTTGTATGGATGACGACGATC
	36	SlG2 CRISPR Geno R	CGGATACGTCGTTTTATCAACC
	37	SlG3 CRISPR Geno F	GGCAGATCCAGATTTCGCTCTC
	38	SlG3 CRISPR Geno R	GCTCAAAGGCTAATGCAAGAAG
	39	Cas9 F	TCCCTCATCAGATCCACCTC
	40	Cas9 R	CTGAAACGTGAGCCTTCTGG
	41	NTP II F	GAAGGGGATAGAAGGCGA
	42	NTP II R	AGATGGATTGCACGCAGG

[1]Gateway recombination sites in bold

Table S2. Constructs and cloning details.

Use	Construct	Template	Primers	Sequence cloned	Cloning method	Entry plasmid	Destiny plasmid
Co-immunoprecipitation assays	*SlG2-HA*	Tomato flower cDNA	1 +2	$SlG2_{1-1089}$	Gateway	pDONR207	pGWB414
	SlG3-HA	Tomato flower cDNA	3 + 4	$SlG3_{1-1080}$	Gateway	pDONR207	pGWB414
	SlPSY1-HA	Tomato fruit cDNA	5 + 6	$SlPSY1_{1-1236}$	Gateway	pDONR207	pGWB414
	SlPSY2-HA	Tomato leaf cDNA	7 + 8	$SlPSY2_{1-1314}$	Gateway	pDONR207	pGWB414
	SlG2-Myc	Tomato flower cDNA	1 +2	$SlG2_{1-1089}$	Gateway	pDONR207	pGWB420
	SlG3-Myc	Tomato flower cDNA	3 + 4	$SlG3_{1-1080}$	Gateway	pDONR207	pGWB420
	AtPRK-Myc	Arabidopsis seedling cDNA	9 +10	$AtPRK_{1-1556}$	Gateway	pDONR207	pGWB417
CRISPR-Cas9 gene impairment	*pEN-SlG2(sg1)*	-	27 +28	$SlG2_{657-677}$	*BbsI* / T4 ligase	pENC1.1	-
	pEN-SlG2(sg2)	-	29 +30	$SlG2_{770-790}$	*BbsI* / T4 ligase	pENC1.1	-
	pDE-SlG2(1+2)	*pEN-SlG2(sg1) + (sg2)*	-	$SlG2_{657-677}$ + $SlG2_{770-790}$	(*sg1*)*MluI* + *Bsu36I* / T4 ligase (sg2)Gateway	*pEN-SlG2(sg1) and (sg2)*	pDE-Cas9
	pEN-SlG3(1)	-	31 + 32	$SlG3_{147-167}$	*BbsI* / T4 ligase	pENC1.1	-
	pEN-SlG3(2)	-	33 + 34	$SlG3_{302-322}$	*BbsI* / T4 ligase	pENC1.1	-
	pDE-SlG3(1+2)	*pEN-SlG3(sg1) + (sg2)*	-	$SlG3_{147-167}$ + $SlG3_{302-322}$	(*sg1*)*MluI* + *Bsu36I* / T4 ligase (sg2)Gateway	*pEN-SlG3(sg1) and (sg2)*	pDE-Cas9
E. coli complementation assays	*pB-SlG2*	WT genomic DNA	1 + 11	$SlG2_{1-1092}$	*SmaI* / T4 ligase	-	pBSK+
	pB-slg2-1	*slg2-1* genomic DNA	1 + 11	$SlG2_{1-976}$	*SmaI* / T4 ligase	-	pBSK+
	pB-slg2-2	*slg2-2* genomic DNA	1 + 11	$SlG2_{1-891}$	*SmaI* / T4 ligase	-	pBSK+
	pB-SlG3	WT genomic DNA	3 +12	$SlG3_{1-1083}$	*SmaI* / T4 ligase	-	pBSK+
	pB-slg3-1	*slg3-1* genomic DNA	3 +12	$SlG3_{1-929}$	*SmaI* / T4 ligase	-	pBSK+
	pB-slg3-2	*slg3-2* genomic DNA	3 +12	$SlG3_{1-928}$	*SmaI* / T4 ligase	-	pBSK+

[1]Constructs reported in Ruiz-Sola et al. (2016b).

Table S3. Levels of GGPP-derived metabolites detected by HPLC. Individual and total carotenoids, chlorophylls and tocopherols in leaf and fruit samples from WT and mutant plants are expressed as µg/mg of dry weight.
MG represents mature green fruits, and B+10 indicates red ripe fruits. NQ, not quantified.
Asterisks indicate statistically significant differences relative to WT samples (one-way ANOVA analysis followed by Dunnett's multiple comparisons test, *p<0.05, **p<0.01).

		CAROTENOIDS							CHLOROPHYLLS			TOCOPHEROLS		
		Phytoene	Lycopene	β-carotene	Lutein	Violaxanthin	Neoxanthin	Total carotenoids	Chlorophyll a	Chlorophyll b	Total chlorophylls	Alpha-tocopherol	Gamma-tocopherol	Total tocopherols
Young leaves	WT	-	-	0.315 ± 0.031	1.255 ± 0.037	0.421 ± 0.012	0.197 ± 0.008	2.187 ± 0.072	1.557 ± 0.045	0.684 ± 0.021	2.241 ± 0.065	0.153 ± 0.005	0.008 ± 0.001	0.162 ± 0.006
	slg2-1	-	-	0.206 ± 0.050*	1.152 ± 0.037	0.383 ± 0.006	0.180 ± 0.009	1.920 ± 0.091	1.451 ± 0.037	0.641 ± 0.017	2.092 ± 0.053	0.148 ± 0.008	0.010 ± 0.000	0.159 ± 0.008
	slg2-2	-	-	0.176 ± 0.088**	1.169 ± 0.183	0.375 ± 0.041	0.182 ± 0.031	1.943 ± 0.361	1.435 ± 0.248	0.630 ± 0.112	2.065 ± 0.359	0.153 ± 0.022	0.011 ± 0.002	0.167 ± 0.023
	slg3-1	-	-	0.208 ± 0.023*	1.008 ± 0.067*	0.218 ± 0.046**	0.144 ± 0.011**	1.578 ± 0.064**	1.188 ± 0.068**	0.487 ± 0.038**	1.674 ± 0.105**	0.132 ± 0.009	0.012 ± 0.003*	0.145 ± 0.011
	slg3-2	-	-	0.165 ± 0.042**	0.934 ± 0.099**	0.198 ± 0.030**	0.133 ± 0.022**	1.430 ± 0.179**	1.094 ± 0.170**	0.445 ± 0.085**	1.539 ± 0.254**	0.127 ± 0.006*	0.010 ± 0.001	0.137 ± 0.005*
Mature leaves	WT	-	-	0.703 ± 0.065	1.812 ± 0.137	0.323 ± 0.039	0.286 ± 0.018	3.159 ± 0.255	2.215 ± 0.235	1.059 ± 0.066	3.274 ± 0.239	0.596 ± 0.080	0.015 ± 0.004	0.611 ± 0.081
	slg2-1	-	-	0.663 ± 0.057	1.592 ± 0.022	0.288 ± 0.051	0.243 ± 0.017	2.814 ± 0.129	1.890 ± 0.133	0.945 ± 0.052	2.835 ± 0.185	0.893 ± 0.220	0.050 ± 0.013**	0.944 ± 0.229
	slg2-2	-	-	0.683 ± 0.036	1.999 ± 0.163	0.340 ± 0.023	0.332 ± 0.023	3.395 ± 0.166	2.326 ± 0.133	1.222 ± 0.064	3.547 ± 0.196	0.671 ± 0.237	0.043 ± 0.016*	0.713 ± 0.253
	slg3-1	-	-	0.606 ± 0.039	1.790 ± 0.237	0.317 ± 0.015	0.277 ± 0.037	3.030 ± 0.327	2.099 ± 0.228	1.057 ± 0.121	3.156 ± 0.348	0.447 ± 0.068	0.029 ± 0.006	0.477 ± 0.074
	slg3-2	-	-	0.519 ± 0.008**	1.668 ± 0.111	0.328 ± 0.009	0.260 ± 0.020	2.814 ± 0.133	1.919 ± 0.094	0.964 ± 0.054	2.883 ± 0.148	0.436 ± 0.096	0.037 ± 0.010	0.473 ± 0.105
MG fruits	WT	-	-	0.008 ± 0.001	0.007 ± 0.001	NQ	NQ	0.014 ± 0.001	0.020 ± 0.004	0.007 ± 0.000	0.027 ± 0.004	0.083 ± 0.004	0.009 ± 0.003	0.092 ± 0.006
	slg2-1	-	-	0.007 ± 0.002	0.007 ± 0.001	NQ	NQ	0.015 ± 0.002	0.020 ± 0.003	0.007 ± 0.001	0.027 ± 0.003	0.069 ± 0.007*	0.008 ± 0.002	0.077 ± 0.009*
	slg2-2	-	-	0.009 ± 0.004	0.008 ± 0.002	NQ	NQ	0.017 ± 0.006	0.021 ± 0.008	0.007 ± 0.002	0.029 ± 0.010	0.075 ± 0.007	0.011 ± 0.004	0.086 ± 0.004
	slg3-1	-	-	0.009 ± 0.001	0.009 ± 0.001	NQ	NQ	0.018 ± 0.002	0.026 ± 0.002	0.010 ± 0.001	0.036 ± 0.004	0.069 ± 0.002*	0.006± 0.001	0.075 ± 0.003*
	slg3-2	-	-	0.010 ± 0.002	0.010 ± 0.002	NQ	NQ	0.020 ± 0.003	0.028 ± 0.003	0.011 ± 0.002*	0.039 ± 0.005	0.077 ± 0.006	0.005± 0.001	0.082 ± 0.006
B+10 fruits	WT	0.066 ± 0.014	0.769 ± 0.071	0.009 ± 0.004	0.002 ± 0.001	-	-	0.869 ± 0.086	-	-	-	0.032 ± 0.001	0.009 ± 0.004	0.041 ± 0.003
	slg2-1	0.045 ± 0.013	0.374 ± 0.040**	0.011 ± 0.000	0.003 ± 0.001	-	-	0.471 ± 0.041**	-	-	-	0.046 ± 0.008	0.008 ± 0.002	0.053 ± 0.010
	slg2-2	0.046 ± 0.001	0.372 ± 0.047**	0.011 ± 0.000	0.002 ± 0.001	-	-	0.443 ± 0.056**	-	-	-	0.036 ± 0.008	0.009 ± 0.001	0.045 ± 0.007
	slg3-1	0.020 ± 0.003**	0.246 ± 0.070**	0.015 ± 0.002	0.003 ± 0.001	-	-	0.293 ± 0.070**	-	-	-	0.066 ± 0.016**	0.010 ± 0.002	0.076 ± 0.018*
	slg3-2	0.027 ± 0.001**	0.272 ± 0.036**	0.014 ± 0.003	0.003 ± 0.001	-	-	0.325 ± 0.040**	-	-	-	0.055 ± 0.012	0.012 ± 0.005	0.066 ± 0.017

Table S4. Relative levels of metabolites detected by GC-MS in samples from WT and mutant young leaves.
Data are presented as means ± SE for six biological replicates normalized to the mean level of the WT plants. Bold numbers denote significant differences ($p < 0.05$) to the WT plants.

	WT	***slg2-1***	***slg2-2***	***slg3-1***	***slg3-2***
Lactate	1±0.1	0.98±0.1	0.97±0.08	1.06±0.16	**1.44±0.11**
Alanine	1±0.08	1.03±0.11	**1.4±0.08**	**2.49±0.39**	**2.2±0.26**
Pyruvate	1±0.1	0.86±0.11	0.98±0.11	0.97±0.15	0.81±0.1
Valine	1±0.11	1.12±0.27	1.35±0.25	**3.28±0.44**	**2.86±0.27**
Glycerol	1±0.12	0.95±0.2	**2.28±0.18**	**1.88±0.18**	1.48±0.27
Isoleucine	1±0.07	1.68±0.16	**1.85±0.19**	**4.53±0.36**	**3.18±0.35**
Glycine	1±0.13	0.85±0.2	**1.56±0.19**	**2.16±0.22**	**1.49±0.16**
Phosphoric acid	1±0.14	**1.68±0.27**	**1.46±0.12**	**2.09±0.11**	**2.08±0.13**
Proline	1±0.06	**0.69±0.03**	1.09±0.09	0.87±0.14	**0.78±0.07**
Urea	1±0.08	**0.73±0.08**	0.96±0.04	**1.3±0.04**	1.08±0.04
GABA	1±0.1	0.91±0.08	**2.18±0.35**	**2.04±0.12**	**1.49±0.18**
Glycerate	1±0.1	**1.65±0.28**	**2.7±0.31**	**1.81±0.12**	**1.74±0.25**
Serine	1±0.08	1.34±0.2	**1.75±0.19**	**1.8±0.14**	**1.76±0.18**
Succinate	1±0.14	1.15±0.14	1.4±0.24	**1.11±0.13**	**1.07±0.15**
Threonine	1±0.05	0.78±0.1	1.16±0.1	**1.8±0.05**	**1.57±0.1**
Fumarate	1±0.12	1.01±0.16	**1.75±0.26**	1.26±0.15	1.39±0.13
Nicotinate	1±0.12	0.89±0.11	0.92±0.12	1.19±0.13	1.05±0.1
beta-Alanine	1±0.02	1.11±0.14	**1.41±0.11**	**2.64±0.13**	**2.12±0.16**
Homoserine	1±0.07	1.12±0.1	**1.61±0.14**	**3.11±0.19**	**2.72±0.24**
Malate	1±0.12	1.72±0.44	1.14±0.14	**0.41±0.08**	0.73±0.13
4-OH-Proline	1±0.06	**0.67±0.03**	1±0.05	0.95±0.1	0.84±0.09
Aspartate	1±0.09	1.01±0.12	**1.55±0.09**	**1.33±0.07**	**1.48±0.06**
Methionine	1±0.07	0.9±0.12	**1.73±0.26**	**2.32±0.16**	**1.88±0.23**
Ornithine	1±0.06	0.85±0.19	1.39±0.18	**4.44±0.47**	**3.36±0.68**
Glutamine	1±0.07	**0.29±0.04**	**0.76±0.05**	**1.54±0.07**	1.4±0.45
Xylose	1±0.23	**1.88±0.24**	0.66±0.05	0.98±0.15	1.29±0.24
Glutamate	1±0.06	1.07±0.07	1.09±0.04	**1.47±0.05**	**1.41±0.06**
Putrescine	1±0.07	**0.44±0.08**	**0.51±0.07**	**0.64±0.09**	**0.48±0.1**
2-oxo-glutarate	1±0.08	0.84±0.09	0.87±0.09	**0.74±0.04**	**0.68±0.07**
Phenylalanine	1±0.1	**2.15±0.43**	**2.28±0.36**	**6.24±0.83**	**4.94±0.45**
Asparagine	1±0.22	0.52±0.15	1.63±0.19	**6.11±0.65**	**3.34±0.4**
Calystegine A3	1±0.15	**0.25±0.02**	**0.35±0.05**	**0.49±0.05**	**0.49±0.02**
Calystegine B2	1±0.16	**0.43±0.08**	0.78±0.1	**0.62±0.04**	0.72±0.05
Glycerol-3-P	1±0.08	**0.96±0.07**	1.44±0.07	**1.02±0.03**	1.15±0.07
Quinate	1±0.22	**2.66±1.26**	1.26±0.12	**0.37±0.03**	0.55±0.07
Fructose	1±0.3	**0.95±0.61**	0.63±0.16	**0.12±0.03**	0.13±0.05
Galactose	1±0.11	**1.02±0.2**	1.99±0.24	**1.26±0.13**	1.03±0.13
Glucose	1±0.24	**1.64±0.79**	1.27±0.19	**0.36±0.08**	0.28±0.08
Citrate	1±0.14	**1.9±0.35**	2.06±0.32	**1.77±0.33**	2.68±0.63
Lysine	1±0.05	**1.37±0.09**	2.11±0.26	**5.17±0.42**	3.83±0.37

	WT	***slg2-1***	***slg2-2***	***slg3-1***	***slg3-2***
1-4-lactone-Galactonate	1±0.08	1.04±0.12	1.11±0.04	**1.34±0.07**	1.22±0.09
Dehydroacorbate	1±0.25	1.47±0.44	1.85±0.58	1.24±0.24	1.17±0.22
Galactonate	1±0.09	1.2±0.15	**1.68±0.15**	**2.09±0.17**	**1.86±0.14**
Gluconate	1±0.08	1.21±0.14	**1.65±0.14**	**2.05±0.16**	**1.85±0.14**
Tyramine	1±0.09	**0.51±0.02**	**0.44±0.04**	**0.23±0.01**	**0.33±0.02**
Ascorbate	1±0.16	**0.51±0.11**	**0.54±0.08**	**0.34±0.1**	**0.4±0.13**
myo-Inositol	1±0.04	0.99±0.09	0.92±0.06	**0.49±0.06**	**0.62±0.04**
Tyrosine	1±0.06	**1.93±0.29**	**2.37±0.33**	**5.61±0.58**	**4.8±0.4**
Histidine	1±0.23	1.92±0.79	**3.1±0.67**	**16.24±1.49**	**9.8±1.62**
cis-Caffeate	1±0.12	**1.85±0.33**	**2.51±0.45**	**2.03±0.34**	**1.85±0.22**
trans-Caffeate	1±0.14	1.59±0.27	**2.38±0.25**	1.44±0.16	1.4±0.12
myo-Inositol-1-P	1±0.1	1.43±0.21	**1.93±0.14**	**1.73±0.15**	**1.52±0.11**
Tryptophan	1±0.08	**1.51±0.17**	**1.94±0.26**	**4.11±0.38**	**3.11±0.22**
Sucrose	1±0.18	1.1±0.21	**0.32±0.18**	**0.11±0.07**	**0.13±0.05**
Maltose	1±0.15	**2.88±0.77**	**2.23±0.26**	1.17±0.07	1.06±0.08
Trehalose	1±0.03	1.08±0.06	**1.26±0.07**	1.16±0.07	1.04±0.05
3-Caffeoyl-cis-quinate	1±0.16	**2.08±0.25**	**1.9±0.33**	**1.7±0.27**	**1.78±0.21**
3-Caffeoyl-trans-quinate	1±0.14	**2.46±0.64**	**2.25±0.29**	1.32±0.23	1.47±0.16
Raffinose	1±0.13	**0.6±0.05**	**0.47±0.05**	**0.5±0.06**	**0.59±0.06**
AMP	1±0.07	1.11±0.1	**1.44±0.11**	1.13±0.05	1.15±0.13

Table S5. Relative levels of metabolites detected by GC-MS in samples from WT and mutant B+10 fruit. Data are presented as means ± SE for six biological replicates normalized to the mean level of the WT plants. Bold numbers denote significant differences ($p < 0.05$) to the WT plants

	WT	***slg2-1***	***slg2-2***	***slg3-1***	***slg3-2***
Alanine	1±0.21	**0.23±0.05**	**0.16±0.01**	**0.18±0.03**	**0.12±0.01**
Pyruvate	1±0.05	**1.29±0.12**	**1.33±0.13**	**1.41±0.11**	**1.33±0.06**
Valine	1±0.28	**0.15±0.04**	**0.26±0.07**	**0.2±0.05**	**0.24±0.08**
Glycerol	1±0.23	1.3±0.14	0.86±0.25	1±0.14	0.67±0.17
Isoleucine	1±0.35	0.23±0.05	0.62±0.21	0.7±0.26	0.57±0.14
Glycine	1±0.23	**0.21±0.05**	**0.28±0.06**	**0.27±0.07**	**0.16±0.02**
Proline	1±0.2	0.79±0.1	0.63±0.18	0.73±0.18	**0.38±0.07**
Urea	1±0.29	1.06±0.21	0.67±0.07	0.76±0.15	0.75±0.11
GABA	1±0.19	**0.34±0.04**	**0.36±0.1**	**0.52±0.03**	**0.55±0.07**
Glycerate	1±0.29	0.65±0.09	0.66±0.09	0.5±0.05	0.54±0.06
Serine	1±0.36	**0.08±0.02**	**0.28±0.12**	**0.17±0.06**	**0.19±0.06**
Threonine	1±0.4	**0.06±0.01**	0.37±0.16	0.21±0.07	0.23±0.07
Fumarate	1±0.2	0.99±0.1	0.81±0.09	0.84±0.08	0.74±0.04
Nicotinate	1±0.17	0.7±0.07	0.95±0.17	0.83±0.18	0.74±0.15
beta-Alanine	1±0.34	**0.1±0.01**	0.38±0.15	0.26±0.09	0.28±0.1
Homoserine	1±0.31	**0.26±0.02**	0.58±0.12	0.55±0.1	0.64±0.07
Erythritol	1±0.23	0.59±0.05	0.71±0.14	0.53±0.07	0.52±0.06
Malate	1±0.16	0.72±0.08	1.16±0.24	1.39±0.2	1.79±0.34
OH-Proline	1±0.2	**0.45±0.03**	0.82±0.26	0.61±0.15	**0.47±0.1**
Methionine	1±0.29	**0.14±0.01**	0.72±0.25	0.77±0.23	0.81±0.21
Glutamine	1±0.34	**0.06±0**	0.65±0.27	0.4±0.16	0.4±0.14
Xylose	1±0.06	**0.61±0.04**	0.82±0.07	0.98±0.08	1.09±0.1
Putrescine	1±0.18	0.72±0.04	0.8±0.04	1.56±0.22	1.14±0.16
2-oxo-Glutarate	1±0.2	0.76±0.12	0.88±0.27	0.83±0.12	0.83±0.14
Phenylalanine	1±0.34	**0.16±0.02**	0.52±0.15	0.53±0.21	0.34±0.08
Asparagine	1±0.33	**0.06±0.01**	0.67±0.26	0.59±0.24	0.47±0.15
Calystegine A3	1±0.24	0.76±0.25	**0.39±0.07**	**0.38±0.07**	0.49±0.02
Calystegine B2	1±0.2	1.47±0.38	0.53±0.1	0.71±0.13	0.48±0.15
Ornithine	1±0.35	**0.18±0.01**	0.74±0.27	0.61±0.18	0.73±0.18
Gycerol-3-P	1±0.19	1.01±0.09	1.37±0.07	0.9±0.1	0.87±0.09
Lysine	1±0.02	0.91±0.09	1.72±0.36	1.62±0.27	1.71±0.28
DHAsc	1±0.17	1.23±0.1	0.9±0.13	1.03±0.1	0.97±0.05
Galacturonate	1±0.3	**6.1±1.21**	**7.02±2.85**	**2.73±0.76**	**7.35±1.64**
Tyrosine	1±0.2	**0.22±0.07**	**0.51±0.1**	**0.28±0.1**	**0.24±0.07**
Adenine	1±0.08	0.89±0.1	0.99±0.15	1.03±0.1	1.06±0.1
Glucose-6-P	1±0.19	**1.76±0.27**	1.23±0.29	1.44±0.32	1.66±0.4
Tryptophan	1±0.34	**0.22±0.05**	0.85±0.23	0.7±0.24	1±0.29
Maltose	1±0.56	1.38±0.48	1.18±0.47	0.88±0.4	0.55±0.15
Trehalose	1±0.57	1.99±0.61	1.35±0.51	0.95±0.39	0.67±0.18

	WT	***slg2-1***	***slg2-2***	***slg3-1***	***slg3-2***
Trehalose	1±0.57	1.99±0.61	1.35±0.51	0.95±0.39	0.67±0.18
Isomaltose	1±0.57	1.43±0.56	1.2±0.41	0.58±0.22	0.4±0.07
cis-3 caffeoyl-Quinate	1±0.24	**2.38±0.3**	1.78±0.42	1.8±0.33	1.69±0.28
trans-3 caffeoyl-Quinate	1±0.14	**2.48±0.4**	1.59±0.49	**2.18±0.51**	**1.65±0.16**
Raffinose	1±0.1	**4.83±0.64**	**3.11±1.33**	**2.09±0.24**	**1.96±0.12**
AMP	1±0.26	**2.51±0.41**	5.74±3.87	2.82±0.96	2.6±0.87
Aspartate	1±0.1	**3.61±0.22**	**13.13±2.76**	**12.52±3.99**	**9.86±1.97**
Glutamate	1±0.24	**0.04±0**	**0.25±0.09**	**0.18±0.06**	**0.15±0.04**
Fructose	1±0.36	1.48±0.18	1.2±0.27	1.3±0.31	1.17±0.24
Glucose	1±0.31	**1.84±0.1**	1.08±0.28	1.44±0.3	1.43±0.31
Citrate	1±0.1	0.98±0.1	1.33±0.23	**2.34±0.6**	**1.73±0.18**
myo-Inositol	1±0.14	**1.46±0.07**	1.28±0.12	1.06±0.07	0.87±0.02
Sucrose	1±0.11	**1.48±0.18**	0.98±0.09	**1.59±0.26**	1.27±0.17

Chapter II

Tomato geranylgeranyl diphosphate synthase isoform 1 specifically interacts with phytoene synthase isoform 3 to produce strigolactones in tomato roots.

Tomato geranylgeranyl diphosphate synthase isoform 1 specifically interacts with phytoene synthase isoform 3 to produce strigolactones in tomato roots.

Miguel Ezquerro[1,2], Changseng Li[3], Julia Pérez-Pérez[1], Yanting Wang[3], M. Pilar López-Gresa[1], M. Purificación Lisón-Parraga[1], Harro J. Bouwmeester[3], Manuel Rodríguez-Concepción[1]

1, Institute for Plant Molecular and Cell Biology (IBMCP), CSIC-Universitat Politècnica de València, 46022 Valencia, Spain

2, Centre for Research in Agricultural Genomics (CRAG) CSIC-IRTA-UAB-UB, Campus UAB Bellaterra, 08193 Barcelona, Spain

3, Swammerdam Institute for Life Sciences, University of Amsterdam, Science Park 904, 1098 XH Amsterdam, the Netherlands

*The second Chapter of this manuscript is a research article planned for publication.

NOTE: The experiments included in this thesis Chapter were co-designed and performed by the PhD candidate under the supervision of the PhD director and H.J.B. The contribution of the rest of the authors to the results shown here was the following: CL provided technical support in sample collection, RNA extraction and SLs measurements; JPP, MPLG and MPLP helped with P.syringae infection and GC-MS volatiles quantification. Y.W helped with GCN construction; The candidate and the PhD director wrote the manuscript.

Tomato geranylgeranyl diphosphate synthase isoform 1 specifically interacts with phytoene synthase isoform 3 to produce strigolactones in tomato roots.

Abstract

Carotenoids have roles as photoprotectants in photosynthetic tissues, pigments in flowers and fruit and precursors of hormones such as abscisic acid (ABA) and strigolactones (SL) in roots and other plant tissues. Carotenoids are produced in plastids from geranylgeranyl diphosphate (GGPP), a common precursor of other isoprenoids. The conversion of GGPP into phytoene, catalyzed by phytoene synthase (PSY), is the first and main rate-determining step of the carotenoid pathway. Channeling of GGPP into the carotenoid pathway is facilitated by direct interaction of GGPP synthase and PSY enzymes in several species, including tomato (*Solanum lycopersicum*). The tomato genome harbors 3 genes encoding plastid-targeted GGPP synthases (herein referred as SlG1 to 3) and other 3 genes encoding PSY isoforms (PSY1 to 3). SlG3 is a housekeeping isoform assisted by SlG2 for peak demands of GGPP in both leaves and fruit. SlG2, but not SlG3, was found to interact with PSY1 (which mainly functions in fruit) and PSY2 (the main isoform in photosynthetic tissues). The function of SlG1 remains virtually unknown, but its low expression levels and its preferential accumulation in roots suggest a restricted or specialized role. PSY3, which shows a very similar expression profile to SlG1, is involved in root SL production. In this work we generated tomato edited lines defective in SlG1 and showed that they have a wild-type phenotype in leaves and fruit in terms of isoprenoid accumulation and physiological parameters related to photosynthesis and development. Consistently, gene co-expression analyses showed very little connection with genes for plastidial isoprenoid synthesis in leaves and fruit but strong correlation with *PSY3* and other genes involved in the production carotenoids and SL (but not ABA) in roots. Co-immunoprecipitation analyses demonstrated that SlG1 (but not SlG2 or SlG3) interacts with PSY3 (but not with PSY1 or PSY2). Quantification of SL levels in tomato roots from mutants defective in different isoforms of these two enzymes confirmed a role of SlG1 in SL production. This role, however, appears to be restricted to roots as the SlG1-defective plants do not have the shoot phenotypes displayed by SL-deficient mutants.

1 Introduction

Isoprenoids are one of the most diverse family of compounds in all living organisms, but plants display the highest functional and structural variety (Bouvier et al., 2005). Despite this wide diversity, only two molecules arise as the universal building blocks for the biosynthesis of all isoprenoids, isopentenyl diphosphate (IPP) and its allylic isomer dimethylallyl diphosphate (DMAPP). Both five-carbon (C5) isoprenoid-building molecules are produced in plants by the mevalonic acid (MVA) pathway in the cytosol and the methylerythritol 4-phosphate (MEP) pathway in plastids (Pulido et al., 2012; Tholl, 2015). Condensation of one or more molecules of IPP to one molecule of DMAPP produces C10 geranyl diphosphate (GPP), C15 farnesyl diphosphate (FPP) and C20 geranylgeranyl diphosphate (GGPP), that are the precursors for most downstream isoprenoid compounds in different cell compartments (Ruiz-Sola & Rodríguez-Concepción, 2012; Zhou & Pichersky, 2020). In the cytosol, FPP is used to synthesize C15 sesquiterpenes and C30 triterpenes required for defensive responses, membrane structure and prenylation of proteins (Thulasiram & Poulter, 2006). In the plastids, GPP is used to make C10 monoterpenes (mostly volatile compounds related to aroma and plant-pathogen interactions) (Chen et al., 2015; Degenhardt et al., 2009) and GGPP is the precursor of gibberellins (GAs) and several photosynthesis-related isoprenoids such as carotenoids, tocopherols, chlorophylls, plastoquinone and phylloquinones (Barja & Rodriguez-Concepcion, 2021). However, GGPP is also used to produce C20 diterpenes in the cytosol, and both FPP and GGPP are produced in mitochondria from imported MVA-derived IPP and DMAPP for ubiquinone and C20 diterpenoid biosynthesis (Barja & Rodriguez-Concepcion, 2021; Thulasiram & Poulter, 2006).

C40 carotenoids are GGPP-derived plastidial isoprenoids that function as precursors of vitamin A and health-promoting phytonutrients in the human diet and have a great industrial interest as natural pigments (Rodriguez-Concepcion et al., 2018; Ruiz-Sola & Rodríguez-Concepción, 2012). In plants, carotenoids act as photoprotectors in leaves, as pigments in some flower and fruit species and as precursors of apocarotenoids, including bioactive compounds such the hormones abscisic acid (ABA) and strigolactones (SLs) (Al-Babili & Bouwmeester, 2015; Rodriguez-Concepcion et al., 2018). Despite their biological and economic relevance, the factors that integrate and coordinate carotenoid biosynthesis with plant metabolism and development remain little known. In this context understanding how GGPP is channeled to the production of carotenoids for particular functions in diverse tissues, developmental stages and environmental conditions remains a pivotal question.

The first committed and main flux-controlling step of the carotenoid biosynthesis pathway in plants is the condensation of two molecules of GGPP into phytoene catalyzed by phytoene synthase (PSY). Next, phytoene is desaturated and isomerized to lycopene, and the ends of the linear lycopene chain are cyclized to form β-carotene (with two β rings) or α-carotene (with one β and one ε ring). Oxidation of the rings gives rise to xanthophylls such as violaxanthin and neoxanthin (from β-carotene) or lutein (from α-carotene) (Figure 1) (Rodriguez-Concepcion et al., 2018). In the model plant *Arabidopsis thaliana* PSY is encoded by one gene and the resulting protein directly interacts with the main GGPPS synthase (GGPPS) isoform in plastids (AtG11), likely facilitating the channeling of GGPP to the production of carotenoids (Camagna et al., 2019; Ruiz-Sola et al., 2016a; Ruiz-Sola et al., 2016b).

A more complex scenario is found in tomato (*Solanum lycopersicum*). The extra roles associated to carotenoids in this species compared to Arabidopsis *(e.g.* flower and fruit pigmentation and root mycorrhization) together with genome duplication events have resulted in small gene families encoding PSY but also GGPPS. In the case of PSY, tomato has an isoform with a primary role for pigmentation of flowers and ripe fruit (PSY1, Solyc03g031860), another mainly producing carotenoids for photosynthesis and photoprotection in leaves (PSY2, Solyc02g081330) and a third one proposed to function in roots for SL and apocarotenoid biosynthesis (PSY3, Solyc01g005940) (Bramley et al., 1992; Fraser et al., 1994; Stauder et al., 2018). From the three plastid-targeted GGPPS isoforms identified in tomato, herein referred to as SlG1 (Solyc11g011240), SlG2 (Solyc04g079960) and SlG3 (Solyc02g085700) (Barja et al., 2021; Zhou & Pichersky, 2020), only SlG2 and SlG3 have been studied in detail. They both produce GGPP for carotenoid synthesis in leaves and fruits, with SlG3 being the main housekeeping isoform and SlG2 acting as a helper enzyme to meet peak demands of GGPP precursors in both organs. SlG2 can be co-immunoprecipitated with both PSY1 and PSY3, but SlG3 cannot (Barja et al. 2021). Although SlG1 is also an active plastid-targeted GGPPS enzyme (Barja et al., 2021; Zhou & Pichersky, 2020), it cannot complement the loss of both SlG2 and SlG3 activities in double mutants, who show an embryo-lethal phenotype like that reported for AtG11-defective Arabidopsis mutants (Ruiz-Sola et al., 2016a; Ruiz-Sola et al., 2016b; Barja et al. 2021). Indeed, *SlG1* transcripts are much less abundant than those for *SlG2* or *SlG3* in most plant tissues (Barja et al., 2021; Zhou & Pichersky, 2020). In leaves, *SlG1* expression is upregulated following spider mite feeding, wounding and elicitor treatments and it correlates with the production of defense-related diterpenoid volatiles (Ament et al., 2006). However, other gene expression data suggest that *SlG1* might also function in roots during mycorrhization (Stauder et al., 2018; Barja et al. 2021).

Under nitrogen and/or phosphate starvation, the roots from several plant species (including tomato) exudate small quantities of carotenoid-derived SL to promote recognition and colonization of arbuscular mycorrhizal (AM) fungi (Matthys et al., 2016; Stauder et al., 2018; Yoneyama et al., 2008; Zhang et al., 2014). These symbiotic AM fungi help the plant by providing water and mineral nutrients in poor soils, on exchange of carbon products biosynthesized by the plant (Bouwmeester et al., 2007; Yoneyama et al., 2008). Carotenoid metabolism is in turn stimulated in AM roots, which produce high amounts of pigments such as mycorrhadicins and other apocarotenoids that modulate the establishment of the AM symbiosis and rhizospheric interactions, including blumenols, zaxinone and anchorene (Baslam et al., 2013; Fester et al., 2002; Moreno et al., 2021; Stauder et al., 2018). A coordinated role has been proposed for *SlG1* and *PSY3* in SL and AM-associated apocarotenoid biosynthesis in roots, mainly based on expression data (Barja et al., 2021; Stauder et al., 2018). *SlG1* and *PSY3* are indeed the most highly up-regulated genes encoding GGPPS and PSY isoforms when roots are mycorrhized. However, *SlG2* and *PSY1* also show increased transcript levels in mycorrhized roots compared to non-mycorrhized controls (Barja et al., 2021; Stauder et al., 2018). This, together with the observation that the basal expression levels of *SlG1* and *PSY3* in roots is lower than that of *SlG2* and *PSY1* (Barja et al., 2021; Fantini et al. 2013), suggest that several isoforms might be providing precursors for carotenoids and derived compounds in roots. To experimentally test this hypothesis and better understand the biological role of SlG1 in tomato, we created CRISPR-Cas9-edited lines defective in SlG1. Here we report their generation and characterization and demonstrate the existence of a highly specific SlG1-PSY3 interaction to produce SL in roots.

.

2 Results and discussion

2.1 Generation of CRISPR lines defective in SlG1

The approach followed to create *SlG1*-defective mutants by CRISPR-Cas9 was very similar to the one followed to generate *slg2* and slg*3* mutants (Barja et al., 2021). Briefly, we designed two single guide RNAs (sgRNA) (see Table S1 and S2 for primer and construct details) with CRISPR-P 2.0 (Liu et al., 2017) to create a small deletion that would disrupt the intronless *SlG1* gen (Figure 1). After transformation of tomato MicroTom plants and genotyping, two independent mutant alleles without Cas9 were selected and named *slg1-1* and *slg1-2* (Figure 1B).

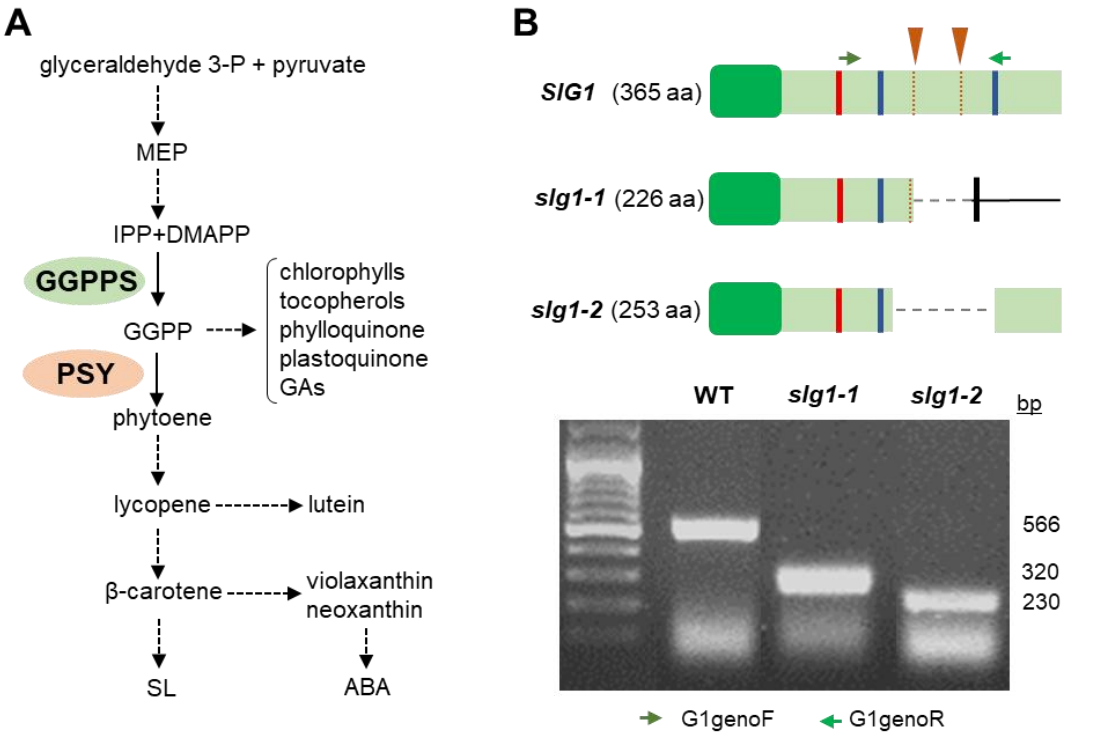

Figure 1. Carotenoid pathway and tomato mutants. (A) Carotenoid biosynthesis pathway. Dashed arrows represent multiple steps. The reactions catalyzed by geranylgeranyl diphosphate synthase (GGPPS) and phytoene synthase (PSY) are marked. (B) Scheme representing the wild-type SlG1 protein and the mutant versions generated in the corresponding CRISPR-Cas9-generated alleles (see Figure S1–S2 for further details). Green boxes represent plastid transit peptides. The regions targeted by the designed sgRNAs are indicated with orange arrowheads and dotted lines. Red and blue bars mark the position of conserved domains required for GGPPS activity (protein-protein interaction domains and Asp-rich domains, respectively). Deletions are shown with a dashed line. Green arrows represent the position of primers for PCR-based genotyping. The agarose gel shows the PCR genotyping products using these primers.

The *slg1-1* allele has a deletion that causes a frameshift and a premature translation stop codon (Figure 1B and Figures S1-S2). The resulting protein lacks the C-terminal region containing the second Asp-rich motif (SARM, essential for prenyl-transferase function) and it is smaller than the wild-type (WT) enzyme (226 aa instead of 365 aa). A longer deletion in the *slg1-2* allele maintains the open reading frame and produces a 253 aa chimeric protein that lacks a fragment of the WT enzyme containing the SARM (Figure 1B and Figures S1-S2). Similar mutations lacking the C-terminal part of the protein and the SARM were previously shown to result in complete loss of GGPPS activity in *slg2* mutants (Barja et al., 2021). Therefore, we considered these two alleles as knock-out mutants and selected them for the rest of experiments.

2.2 Loss of SlG1 does not impair the production of photosynthesis-related isoprenoids in tomato leaves.

SlG1 is expressed at low levels in all tomato plant tissues compared to *SlG2* and *SlG3* (Figure S3), but it is induced in leaves after herbivore attack, wounding and elicitor treatments (Ament et al., 2006). To investigate possible roles of SlG1 in leaves, we first analyzed the levels of GGPP-derived plastidial isoprenoids under normal growth conditions (Figure 2). Lines lacking SlG2 (*slg2-1*) or SlG3 (*slg3-1*) were also grown together with SlG1-defective mutants and WT controls for comparison. At the visual level, young and mature leaves of *slg1-1* and *slg1-2* alleles were very similar to those from *slg2* and WT plants (Figure 2A). By contrast, young emerging leaves from *slg3* plants showed a paler green color as previously reported (Barja et al., 2021). The color phenotype of young leaves correlated with their photosynthetic pigment (carotenoids and chlorophylls) content (Figure 2B) and their photosynthetic activity estimated as effective quantum yield of photosystem II (ϕPSII)

(Figure 2C), which were only reduced in the *slg3* mutant. Tocopherol levels, by contrast, were similar in all the lines, although a trend towards lower levels was detected in young leaves of the *slg3* mutant, as previously reported (Barja et al., 2021). The described results are in agreement with our previous conclusion that *SlG3* is the main isoform in suppling GGPP for photosynthesis-related isoprenoids in leaves under normal growth conditions (Barja et al., 2021). A role for SlG2 in providing extra GGPP to support the production of these isoprenoids when needed, e.g., during deetiolation, was proposed in part based on gene expression data (Barja et al., 2021). Unlike *SlG2*, however, *SlG1* is poorly co-expressed with isoprenoid biosynthetic genes in leaves and it is not induced

during seedling deetiolation (Barja et al., 2021), supporting the conclusion that SlG1 does not substantially contribute to GGPP production in chloroplasts.

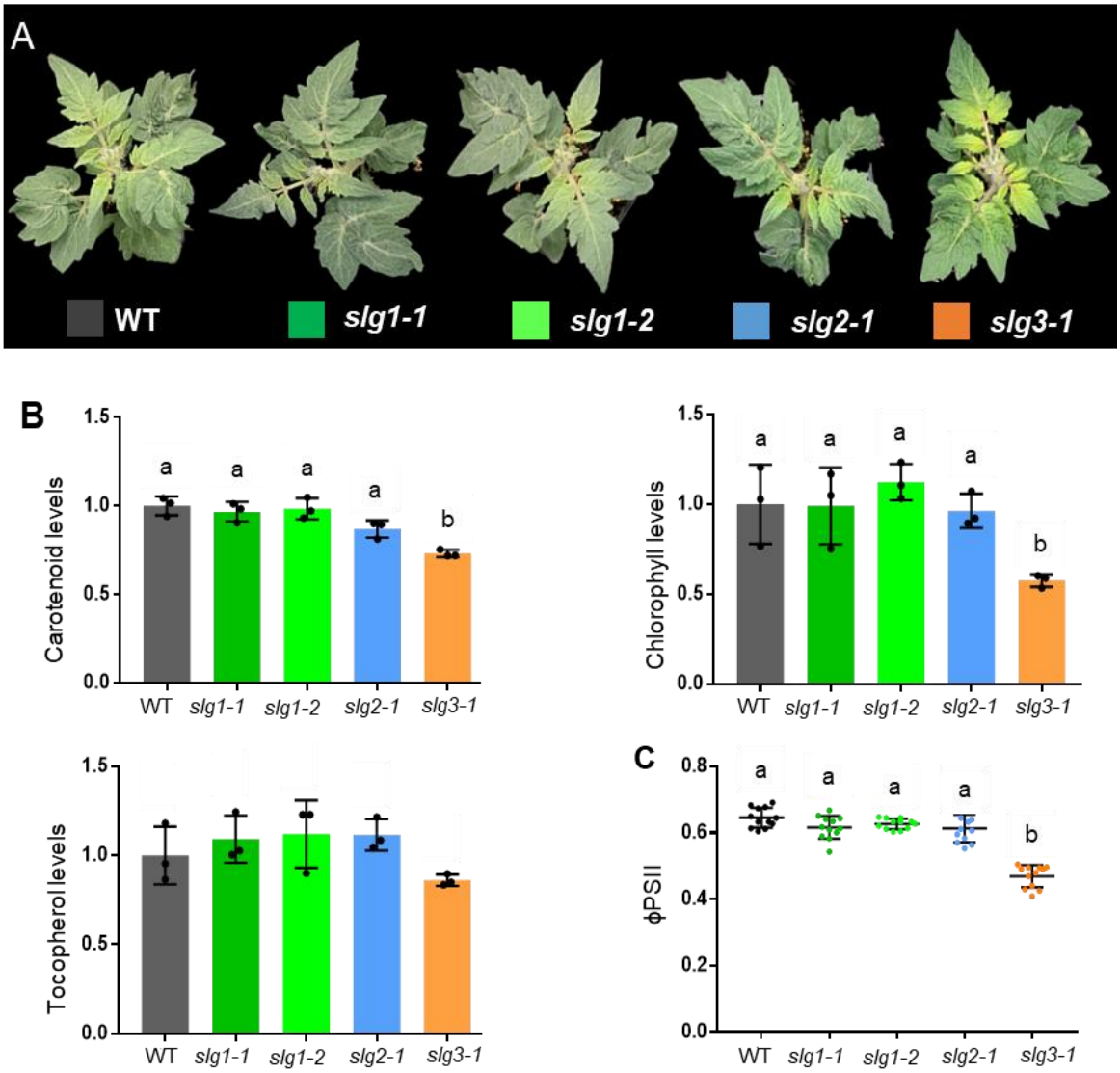

Figure 2. SlG1 does not contribute to GGPP-derived isoprenoid biosynthesis in tomato leaves. (A) Representative images of 4-week-old plants of WT and GGPPS-defective mutants. (B) Carotenoid, chlorophyll and tocopherol levels in young leaves from 4-week-old WT and mutant plants. Values are represented relative to WT levels and they correspond to mean and SD of n≥3 independent biological replicates. **(C)** Effective quantum yield of photosystem II (ϕPSII) in young leaves like those used in (B). Individual values (colored dots) and well as mean and SD are shown, and they correspond to four different areas from leaves of three different plants. In all plots, letters represent statistically significant differences ($P < 0.05$) among means according to post hoc Tukey's tests run when one way ANOVA detected different means.

2.3 SlG1 is not required for monoterpene synthesis in leaves.

Leaves are mainly photosynthetic organs but they also contain cell types lacking chloroplasts. In particular, tomato leaves contain large amounts of glandular trichomes formed by non-photosynthetic cells that produce very large amounts of volatile organic compounds (VOCs), including many of isoprenoid origin (Schuurink and Tissier, 2020). *SlG1* but also *SlG2* and *SlG3* are expressed in leaf trichomes (Zhou & Pichersky, 2020). The main groups of isoprenoid VOCs are MVA-derived sesquiterpenes (made from C15 FPP), MEP derived monoterpenes (made from C10 GPP or nerolidol diphosphate, NPP) and diterpenes (made from GGPP). A role for SlG1 in the production of GGPP-derived diterpene VOCs was investigated following the observation that *SlG1* expression was induced by treatments that stimulated the production of such VOCs (Ament et al., 2006). Our data mining of the database Genevestigator found that *SlG1* expression is also upregulated in leaves after infection with the bacterium *Pseudomonas syringae pv. tomato* DC3000, whereas *SlG2* and *SlG3* transcript levels remained unchanged (Figure S4). The most prominent isoprenoid VOCs produced upon *P. syringae* infection are monoterpenes such as linalool, limonene and α-terpineol (Lopez-Gresa et al., 2017; Zhou & Pichersky, 2020). While α-terpineol derives from NPP produced by the NPP synthase NDPS1/CPT1 (Solyc08g005680), linalool and limonene are produced from GPP synthesized by homodimeric GPP synthases such as tomato GPPS (Solyc08g023470) or heterodimeric enzymes formed by a GGPPS subunit and the small subunit type I (SSU-I) protein (Solyc07g064660) (Figure 3A). Similar to *SlG1*, tomato *NDPS1*, *GPPS* and *SSU-I* genes are induced in *P. syringae*-infected leaves, with *SlG1, SSU-I* and *NDPS1* showing the strongest upregulation (Figure S4). Because SlG1/SSU-I heterodimers have been shown to mainly produce GPP (Zhou & Pichersky, 2020) and SlG2/SSU-I heterodimers have been found to produce GPP for monoterpene biosynthesis in tomato fruit (Hivert et al., 2020)., we hypothesized that SlG1 might participate in the production of monoterpenes in leaves. To test this hypothesis, we infected WT and GGPPS-defective tomato plants with *P. syringae pv. tomato* DC3000 and quantified the levels of several monoterpenes (and a sesquiterpene as a control) before and 24 h after the infection (Figure 3). Strikingly, bacterial infection did not cause significant changes of monoterpene or sesquiterpene levels in WT plants or any of the mutants tested (Figure 3A) despite a clear upregulation of *SlG1* expression was observed (Figure 3B).

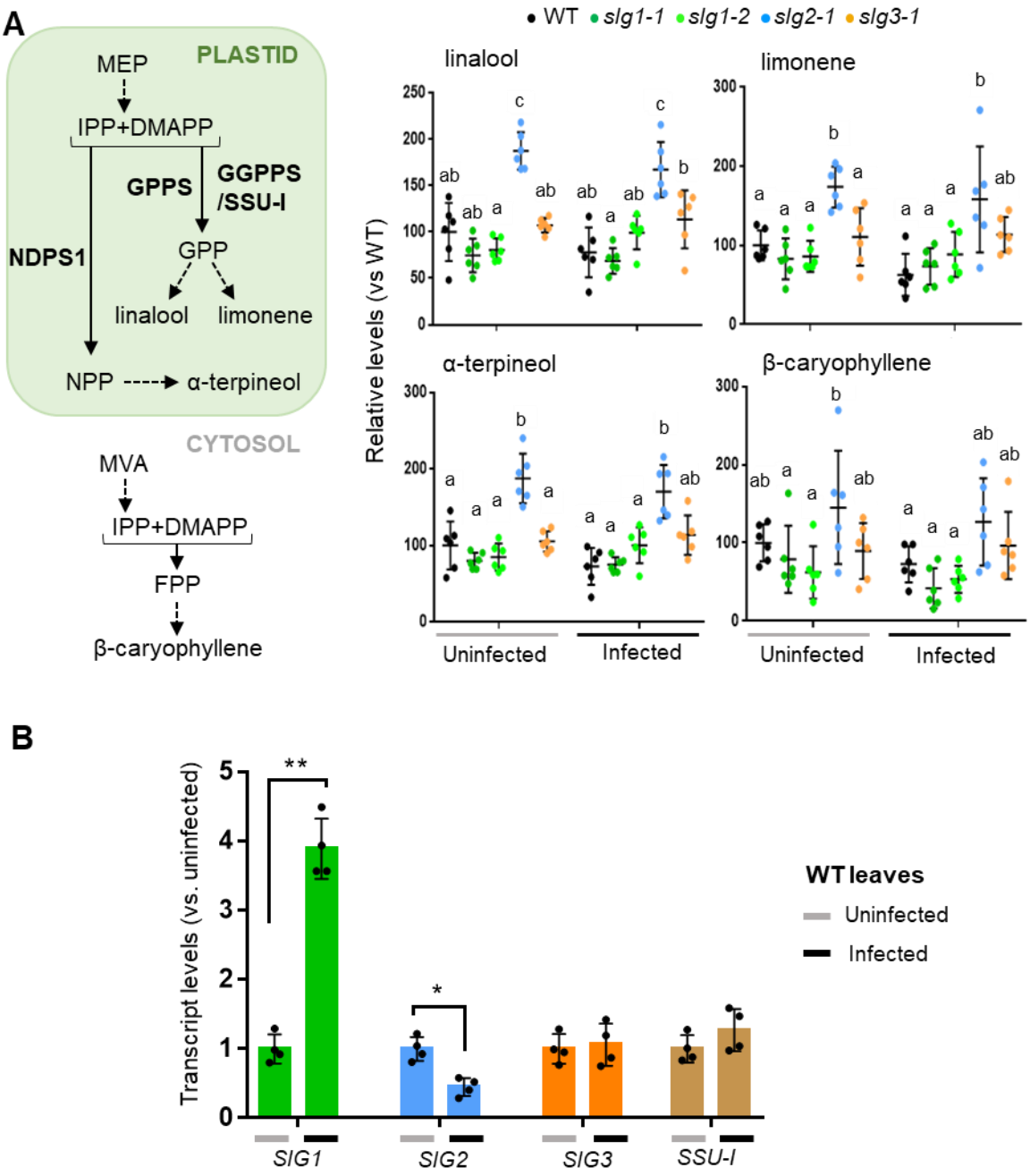

Figure 3. SlG1 is not required for monoterpene production in leaves. MicroTom WT and edited plants were infected with Pseudomonas syringae pv. tomato DC3000 and samples were collected 24 h later. (A) Levels of representative VOCs in infected and uninfected leaves of WT and GGPPS-defective mutants. Data are represented relative to the levels in uninfected WT samples (100%) and correspond to the mean ± SD of n=6 biological replicates. Letters represent statistically significant differences (one-way ANOVA followed by Tukey's multiple comparisons test, $P < 0.05$). A schematic representation of the VOC biosynthesis pathway is shown in the left side. **(B)** RT-qPCR expression data of the indicated genes in WT leaves. Expression levels are shown relative to uninfected samples and they correspond to the mean ± SD of n=4 independent biological replicates. Asterisks indicate statistically significant differences among means between uninfected and infected samples (t-test: *, $P < 0.05$; **, $P < 0.01$).

Unlike that deduced from Genevestigator RNA-seq data (Figure S4), in our experiment we did not detect any changes in the levels of *SSU-I* transcripts (Figure 3B). This differential expression profile might be a consequence of different genetic backgrounds used in the experiments.

In agreement with this hypothesis, *SSU-I* transcript levels are very low in cultivated tomatoes (*S. lycopersicum*) but are abundant in the fruits of wild relatives (*S. pimpinellifolium* and *S. cheesmaniae*), which produce substantially more monoterpenes (Hivert et al., 2020). Whereas MicroTom has been broadly used for infection experiments with some bacteria and fungi (Costa et al., 2021; Deganello et al., 2014; Nakahara et al., 2016), previous experiments using *P. syringae pv. tomato* DC3000 found no wilt symptoms or bacterial growth eight days after infection (Takahashi et al., 2005), strongly suggesting that *P. syringae pv. tomato* DC3000 is just an opportunistic MicroTom pathogen. All these data together suggest that tomato MicroTom is not a proper cultivar to investigate the molecular and metabolic changes triggered by *P. syringae pv. tomato* DC3000 infection, including the production of monoterpenes. In any case, the similar levels of monoterpenes found in non-infected leaves of WT and SlG1-defective alleles argues against a role of SlG1 in the production of these plastidial isoprenoids in leaves.

Surprisingly, *slg2* mutants contained increased basal levels of all VOCs analyzed, that did not change after the bacterial infection (Figure 3A). This result suggests that impairment of SlG2 activity somehow causes the accumulation or higher production of these VOCs, which are derived from IPP and DMAPP from different origins: the MVA pathway (via FPP) and the MEP pathway (via NPP or GPP). However, the levels of leaf isoprenoid products made from MEP-derived GGPP (carotenoids, chlorophylls, tocopherols) were similar to those in WT controls (Figure 2B) (Barja et al., 2021).

We speculate that SlG2 might have a specialized role in trichomes (the VOC-producing cells in the leaf) and its loss of function in the *slg2* mutant might cause a metabolic imbalance or a defense response that cannot be rescued by SlG1 or SlG3 and eventually leads to VOC overproduction.

2.4 SlG1 is dispensable for carotenoid biosynthesis in fruit.

Carotenoids are synthesized at very high rates during tomato fruit ripening, contributing together with the degradation of chlorophylls to progressively change the fruit color from green at the mature green (MG) stage to orange (O) and eventually red at the ripe (R) stage. The first visual symptoms of color change define the breaker (B) stage. *SlG1* is expressed at low levels during fruit ripening (Figure S3), when GGPP produced by SlG3

and upregulated levels of SlG2 support carotenoid overproduction (Barja et al., 2021). Reduced activity of SlG2 and SlG3 results in lower levels of lycopene (the main carotenoid accumulated during ripening) in ripe fruit collected at 10 days after the B stage (B+10) but only SlG3-defective lines showed significantly decreased levels of total carotenoids at this stage and none of the mutants showed differences with the WT in MG fruit (Barja et al., 2021). When we measured carotenoid levels in B+3 fruits (*i.e.,* between O and R stages), WT levels of total carotenoids were found in *slg1* or *slg2* lines, whereas *slg3* fruits showed significantly lower levels (Figure 4A). In particular, phytoene and lycopene levels were strongly reduced in *slg3* fruits, whereas β-carotene levels were similar to those of WT controls (Figure 4A).

The absence of significant differences in carotenoid levels among WT, *slg1* and *slg2* fruit at the B+3 stage (Figure 4A) suggests that SlG3 is the main GGPP provider in the early stages of fruit ripening. As ripening advances, up-regulation of SlG2 contributes with extra GGPP. The WT phenotype of SlG1-deficient mutant fruits together with the lack of gene expression changes during ripening support the conclusion that this isoform has a null or minor contribution to GGPP production in fruit.

Lower levels of the carotenoid-derived hormone ABA were measured in the fruit pericarp of tomato mutants lacking SlG2 and particularly SlG3, eventually contributing to a delay in ripening (Barja et al., 2021). Consistently, the number of days that B fruits needed to reach the O stage in the plant was higher in *slg2* and *slg3* lines compared to WT controls (Figure 4B). ABA has also been shown to promote fruit growth (McQuinn et al., 2020; Zhang et al., 2009; Ezquerro et al. 2022). Reduced ABA contents in *slg2* and *slg3* fruit pericarp (Barja et al., 2021) actually correlate with a reduced fruit volume of ripe fruit, although it was only statistically significant for *slg3* fruit and it did not affect fruit weight (Figure 4B). Again, *slg1* fruits were undistinguishable from WT controls (Figure 4B).

The observation that losing SlG1 activity does not impact any of the fruit phenotypes tested strongly supports the conclusion that this isoform is dispensable for the production of GGPP for carotenoids and related metabolites during fruit ripening.

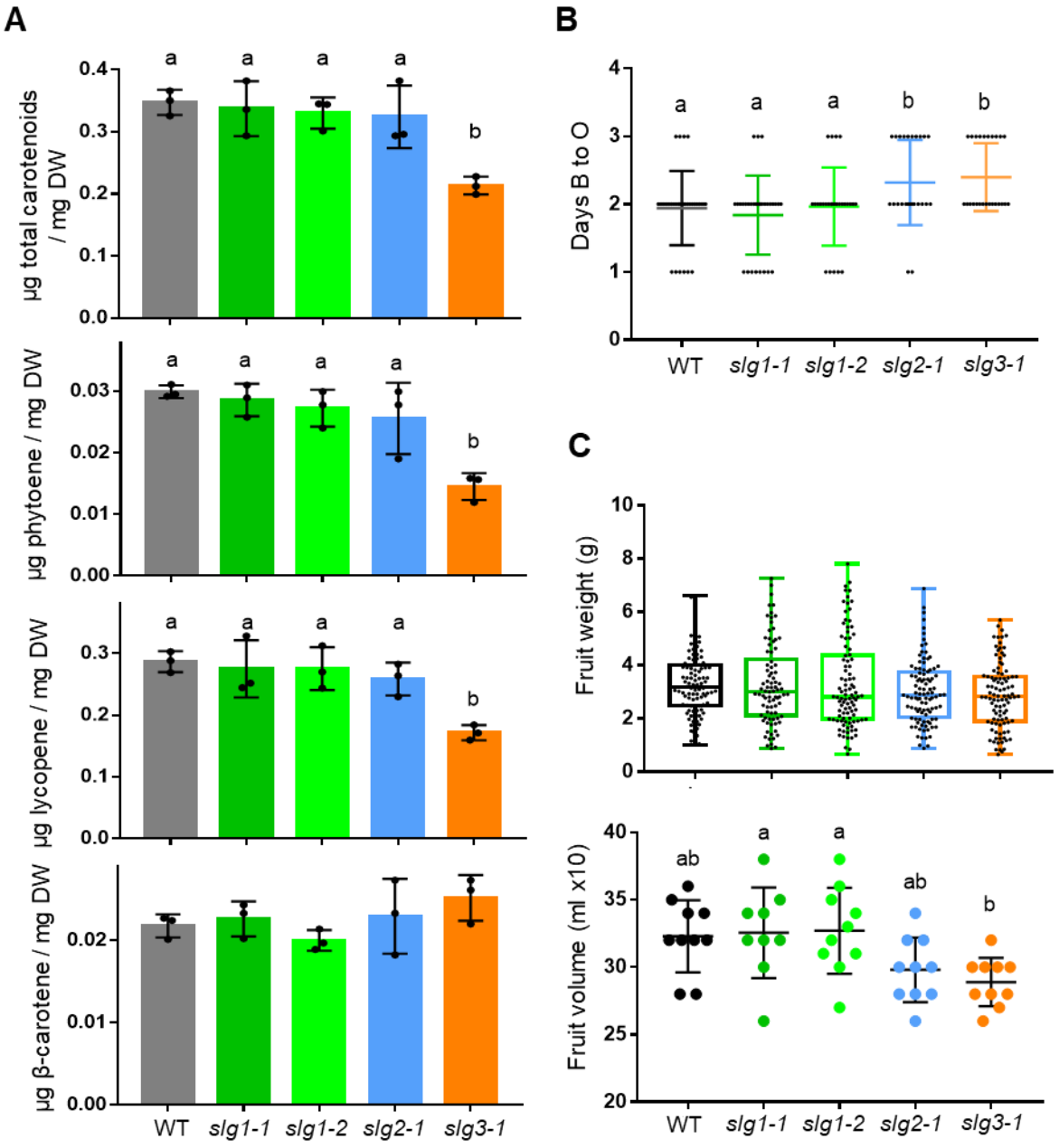

Figure 4. SlG1 is dispensable for carotenoid biosynthesis in fruits. (A) Levels of total and individual carotenoids (phytoene, lycopene and β-carotene) in tomato fruits collected from the plant 3 days after the breaker stage (B+3) fruits. Values represent mean and SD of n=3 independent biological replicates**. (B)** Fruit ripening rate estimated as the number of days from B to O stages in the plant. Black dots indicate individual values and colored lines represent the mean and the SD. **(C)** Weight and volume of fully ripe (R) fruits of the indicated genotypes. In the weight boxplot, the lower and upper boundary of the boxes indicate the 25th and 75th percentile, respectively; the line inside the boxes represents the median; dots mark individual data values; and whiskers above and below the boxes indicate the maximum and minimum values. In the volume dotplot, central line represents the mean and whiskers represent SD. In all cases, letters represent statistically significant differences ($P < 0.05$) among means according to post hoc Tukey's tests run when one way ANOVA detected different means.

2.5 Gene co-expression analyses suggest a major role of SlG1 in roots.

In our previous work we demonstrated that *SlG2* and, to a lower extent, *SlG3* expression were highly connected to plastidial isoprenoid biosynthetic genes in leaf tissue. In fruits, *SlG3* had a higher connection than *SlG2* to genes from these metabolic pathways (Barja et al., 2021). What was clear is that correlation of *SlG1* with other plastidial isoprenoid genes was very poor in leaves as well as in fruits. Other gene expression data suggested that *SlG1* might function in roots to produce SL or/and AM-related apocarotenoids (Stauder et al., 2018; Barja et al. 2021). To provide further evidence for this hypothesis, we performed a gene co-expression network (GCN) analysis in roots. We used publicly available data for plant comparative genomics (PLAZA 4.0 Phytozome) to look for tomato homologues of genes for plastidial isoprenoid biosynthesis and related pathways. We obtained the expression data of such tomato homologs from recently published tomato RNA-seq data in root tissue (Wang et al., 2021) and calculated their expression correlation with *SlG1*, *SlG2* and *SlG3* expression using pairwise Pearson correlations as previously reported (Wang et al., 2022). Results are shown in Figure 5 and correlations and gene details are listed in Table S3. Opposite to that observed in leaf tissue, *SlG2* is the isoform that shows a lower correlation with other isoprenoid biosynthetic genes (Figure 5). *SlG3* shows a medium connectivity to many of the selected genes, probably because it is the isoform providing GGPP for housekeeping functions (Barja et al., 2021). *SlG1* showed the highest correlation ratios with most of the genes involved in SL and apocarotenoid biosynthesis, including those from the MEP pathway (Figure 5). By contrast, *SlG1* showed limited connectivity with genes converting carotenoids into ABA (Figure 5). Unexpectedly, connectivity was very high with GA biosynthetic genes. GAs are GGPP-derived phytohormones that, among many other roles in the regulation of plant development, promote elongation of shoot and root tissues (Tanimoto, 2005; Ubeda-Tomás et al., 2008). They appear to act together with SLs during root mycorrhization (Nouri et al., 2021; Ruiz-Lozano et al., 2016), promoting root growth to help establishment of AM symbiosis. The results suggest that SlG1 might be involved in the production of GGPP in roots for the production of hormones such as GAs and SLs (via carotenoids). Most interestingly, they also suggest that coordinated gene expression might be key to channel SlG1-derived root carotenoids to the production of SLs but not ABA.

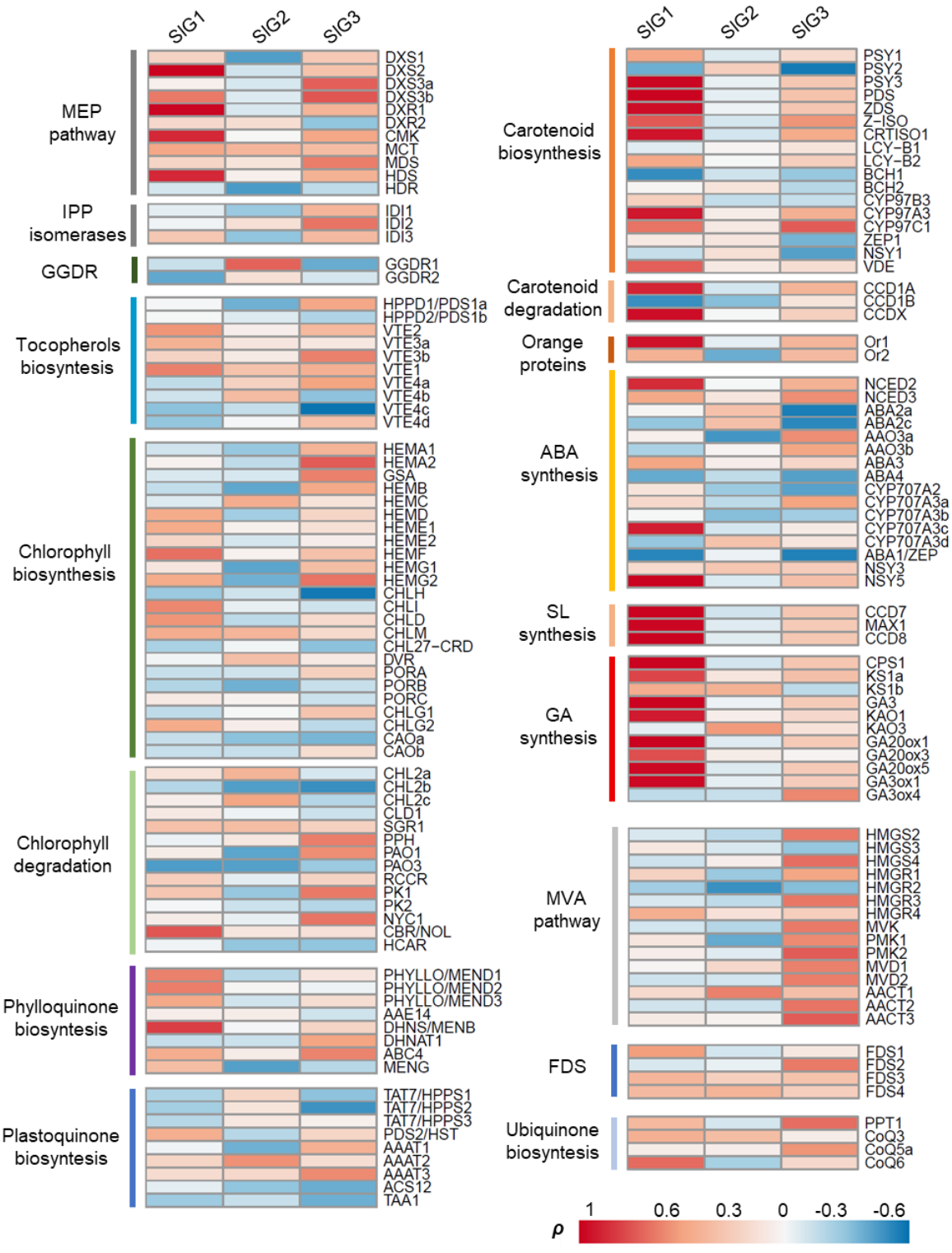

Figure 5. Gene co-expression network analysis of tomato *GGPPS* genes in roots. Heatmap represents pairwise Pearson correlations (ρ) between the expression of genes encoding GGPPS isoforms and those for the indicated enzymes from pathways upstream and downstream of GGPP. Gene details, abbreviations, accessions, and data correlations are listed in Table S3.

2.6 SlG1 specifically interacts with PSY3

Gene expression data, including our GCN analysis (Figure 5), supports the conclusion that *SlG1* might function in coordination with *PSY3* to produce SL and likely other AM-associated apocarotenoids (but not ABA) in roots (Barja et al., 2021; Stauder et al., 2018). GGPPS proteins have been shown to physically interact to PSY enzymes in different plant systems (Fraser et al., 2000; Ruiz-Sola et al., 2016b; Wang et al., 2018; Camagna et al., 2019; Barja et al., 2021). In tomato, co-immunoprecipitation experiments in *Nicotiana benthamiana* leaves showed direct interaction of SlG2 with PSY1 and PSY2, while no interaction with these PSY isoforms was found for SlG3 despite the protein was shown to homodimerize and heterodimerize with SlG2 using the same experimental design (Barja et al., 2021). To complete the tomato GGPPS-PSY interaction map including SlG1, we performed co-immunoprecipitation assays *in planta* using Myc-tagged GGPPS and HA-tagged PSY proteins (Figure 6). Tagged proteins were transiently expressed in *N. benthamiana* leaves by agroinfiltration and then protein extracts were used to confirm the presence of the recombinant enzymes (Figure 6A) and for co-immunoprecipitation with anti-Myc antibodies followed by immunoblot analysis with both anti-Myc and anti-HA antibodies (Figure 6B). A Myc-tagged phosphoribulokinase protein from Arabidopsis (PRK-Myc) was used as a negative control (Barja et al., 2021). Additionally, a SlG1-HA construct used together with SlG1-Myc confirmed that SlG1 forms homodimers and that the Myc-tagged version worked to co-immunoprecipitate protein partners (Figure S5). When combined with PSY isoforms, SlG1 was found to only co-immunoprecipitate with PSY3, whereas SlG2 and SlG3 were unable to interact with this particular isoform (Figure 6B).

It has been stated that PSY enzymes cannot access freely diffusible plastidial GGPP, probably because their specific plastid location attached to membranes (Camagna et al., 2019), making interaction among GGPPS and PSY enzymes necessary for GGPP channeling into the carotenoid pathway. Strikingly, the tomato housekeeping isoform SlG3 is unable to directly interact with any of the PSY isoforms present in tomato (Figure 6B) (Barja et al., 2021). However, there are several possibilities for an indirect interaction of SlG3 with PSY enzymes (Barja & Rodriguez-Concepcion, 2021). Heterodimerization of SlG2 and SlG3 might allow interaction of SlG3 with PSY1 or PSY2 via the SlG2 monomer (Barja et al., 2021), whereas heterodimerization of SlG1 and SlG3 might allow interaction with PSY3 via the SlG1 monomer (Figure 6B). Another possibility to deliver GGPP to PSY enzymes could be interaction with the small subunit type II (SSU-II) protein (Solyc09g008920), a catalytically inactive polypeptide shown to interact with different GGPPS enzymes to improve their GGPP production (Wang et al., 2018; Zhou et al.,

2017; Zhou & Pichersky, 2020) but also to stimulate interaction with PSY enzymes (Wang et al., 2018). While the described interactions potentially allow any of the three tomato GGPPS isoforms to form a complex with any of the PSY isoforms, it is expected that direct interactions (SlG1-PSY3, SlG2-PSY1 and SlG2-PSY2) would be most efficient to convert GGPP into phytoene. In the case of SlG1 and PSY3, this interaction is strengthened by the coordinated expression profiles of the corresponding genes in roots upon phosphate starvation and mycorrhization with AM fungi (Figure 5) (Barja et al., 2021; Stauder et al., 2018) and strongly supports the conclusion that both isoforms share the same functional role(s).

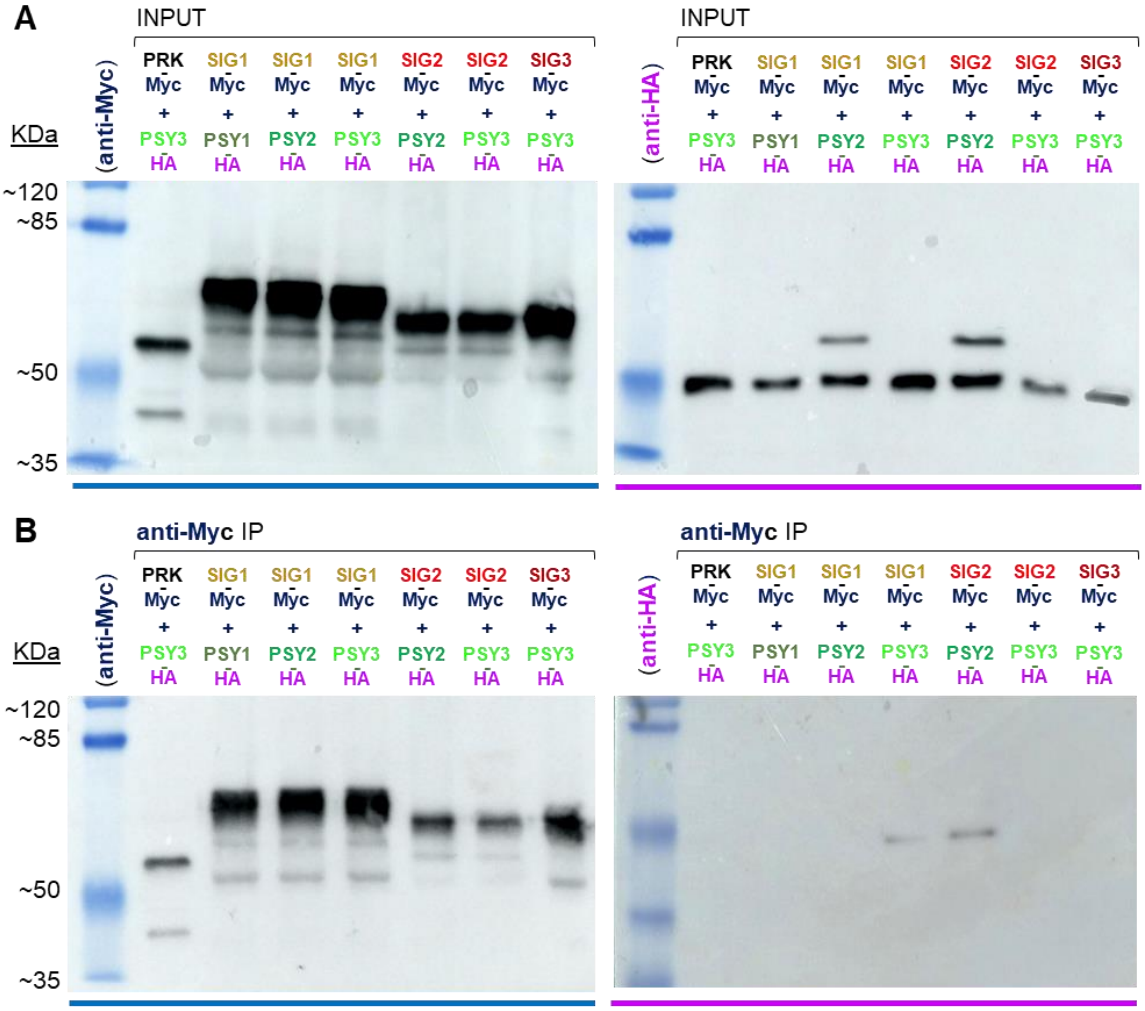

Figure 6. SlG1 specifically interacts with PSY3 *in planta*. *N. benthamiana* leaves were co-agroinfiltrated with constructs encoding the indicated proteins tagged with C-terminal Myc or HA epitopes. (A) Immunoblot analysis of crude extracts (INPUT) with anti-Myc (dark blue) and anti-HA (purple) antibodies to confirm successful protein production. (B) Immunoblot analysis of extracts after immunoprecipitation (IP) with anti-Myc. The same samples were used for immunodetection with anti-Myc (to confirm successful IP) or anti-HA (to identify co-immunoprecipitated partners). Predicted protein molecular weights (KDa): PRK-Myc, 52.1; SlG1-Myc, 56.9; SlG2-Myc, 55.3; SlG3-Myc, 55.5; PSY1-HA, 50.7; PSY2-HA, 51.0; PSY3-HA, 50.2.

2.7 SL synthesis is impaired in *slg1* and *psy1* mutants

To experimentally confirm the role of the different GGPPS and PSY isoforms for the production of carotenoid precursors for SL or/and ABA biosynthesis in roots, we analyzed the levels of these metabolites in WT plants and mutant lines defective in GGPPS and PSY isoforms. In the latter case, only CRISPR-Cas9 lines lacking PSY1 (*psy1-2*) and PSY2 (*psy2-1*) were used (Ezquerro et al., 2022), as PSY3-defective lines are not available yet. As a control, we also used a tomato mutant with a defective activity of the SL biosynthetic enzyme carotenoid-cleavage dioxygenase 7 (CCD7, Solyc01g090660) (Vogel et al., 2010). We grew the plants in half-strength Hoagland solution either containing normal phosphate (NP) or without phosphate (-P) to induce SL synthesis and measured carotenoid and ABA levels in root tissues and SL levels in root exudates (Figure 7). Carotenoid levels measured in roots were very low in all genotypes both under NP and -P conditions (Figure 7A). Only *ccd7* mutants showed statistically significant changes between conditions, as carotenoid levels increased under phosphate starvation (Figure 7A). However, the low levels of these metabolites in roots and the limited resolution of the HPLC-DAD technique used for their quantification compared to the MS-based methods used for ABA and SL measurements make it difficult to draw meaningful conclusions.

Next, we measured the levels of the carotenoid-derived phytohormone ABA in the same samples used for carotenoid quantification. Consistent with our GCN data showing no correlation of ABA biosynthetic genes with any of the tomato genes for GGPPS isoforms (Figure 5), none of the GGPPS-defective mutants presented statistically significant differences in root ABA levels in either NP or -P conditions compared to WT controls (Figure 7B). Interestingly, ABA levels were higher in *psy1-2* and *psy2-1* mutant roots from plants grown under NP or –P conditions (Figure 7B). Analysis of gene expression levels by qRT-PCR showed that loss of PSY1 or PSY2 activities did not substantially increased the expression of any remaining PSY-encoding gene or any GGPPS-encoding gene in roots (Figure 8). We therefore conclude that other genes involved in ABA synthesis might be upregulated in *psy1* and *psy2* roots. Alternatively, loss of PSY1 or PSY2 in roots might cause a metabolic imbalance that cannot be rescued by the remaining PSY isoforms and eventually leads to ABA overproduction.

The levels of several SLs were next measured in root exudates from plants grown under phosphate starvation for seven days (Figure 7C). All SL measured (except for oxo-orobanchol who also present a trend towards lower levels) were significantly reduced in both *slg1* mutant alleles compared to WT controls, confirming a major role for the SlG1 isoform in producing GGPP precursors for these carotenoid-derived hormones.

Exudates from *slg2-1* and *slg3-1* roots contained WT levels of SLs (Figure 7C). However, the observation that none of the two null *slg1* mutant alleles showed a complete absence of SLs suggest that SlG2 or/and SlG3 can also contribute to SL production, at least when SlG1 activity is absent. Because a role for PSY3 in root SL production has been demonstrated in the legume *Medicago truncatula* and suggested in tomato (Stauder et al., 2018), we expected WT levels of SLs in mutants defective in PSY1 and PSY2, which harbor a functional PSY3 enzyme. However, *psy1-2* mutants presented very similar reduction in SL levels to that detected in *slg1* mutants, suggesting that PSY1 may also have a role on SL synthesis in tomato roots (Figure 7C). In agreement, *PSY1* basal expression levels in roots are higher than those of *PSY3* (Barja et al., 2021; Fantini et al. 2013) and they increase in mycorrhized roots compared to non-mycorrhized controls (Figure 8) (Barja et al., 2021; Stauder et al., 2018). Strikingly, PSY1-defective roots failed to upregulate SlG1 expression under phosphate starvation (Figure 8), suggesting that this might be the main cause of the low SL levels produced by the *psy1-2* mutant (Figure 7C). This results also reinforces the conclusion that SlG1 has a central role for SL production in roots. Furthermore, upregulation of *PSY3* expression under phosphate starvation was also reduced (but not impaired) in *psy1-2* roots, similar to that observed in SlG1-defective roots (Figure 8). This result suggests that SLs might feed-forward promote *PSY3* expression. Alternatively, the absence of SlG1 (in *slg1* mutants) or the failure to upregulate its levels under phosphate starvation (in *psy1* mutants) might be the reason why *PSY3* expression also becomes less responsive to phosphate starvation, As SlG1 and PSY3 isoforms physically interact (Figure 6), it is not surprising that their transcription is coordinated. In any case, the data strongly support a central role for SlG1 and PSY3 in root SL.

2.8 SL reduction in *slg1* and *psy1* roots does not affect aerial plant architecture

SLs are plant phytohormones that regulate developmental processes in roots, shoots and leaves. They promote root hair elongation and primary root growth and inhibit adventitious root formation (Al-Babili & Bouwmeester, 2015; Bouwmeester et al., 2007; Matthys et al., 2016). In shoots, they promote secondary growth and inhibit auxiliary bud branching (Gomez-Roldan et al., 2008; Ruyter-Spira et al., 2013), and in leaves they promote leaf senescence together with other plant hormones (Ueda & Kusaba, 2015; Yamada & Umehara, 2015). While increased branching is one of the most conspicuous phenotypes derived from reduced SL levels, a visual inspection could not detect any obvious branching phenotype in greenhouse-grown plants of any of our CRISPR-Cas9-edited lines.

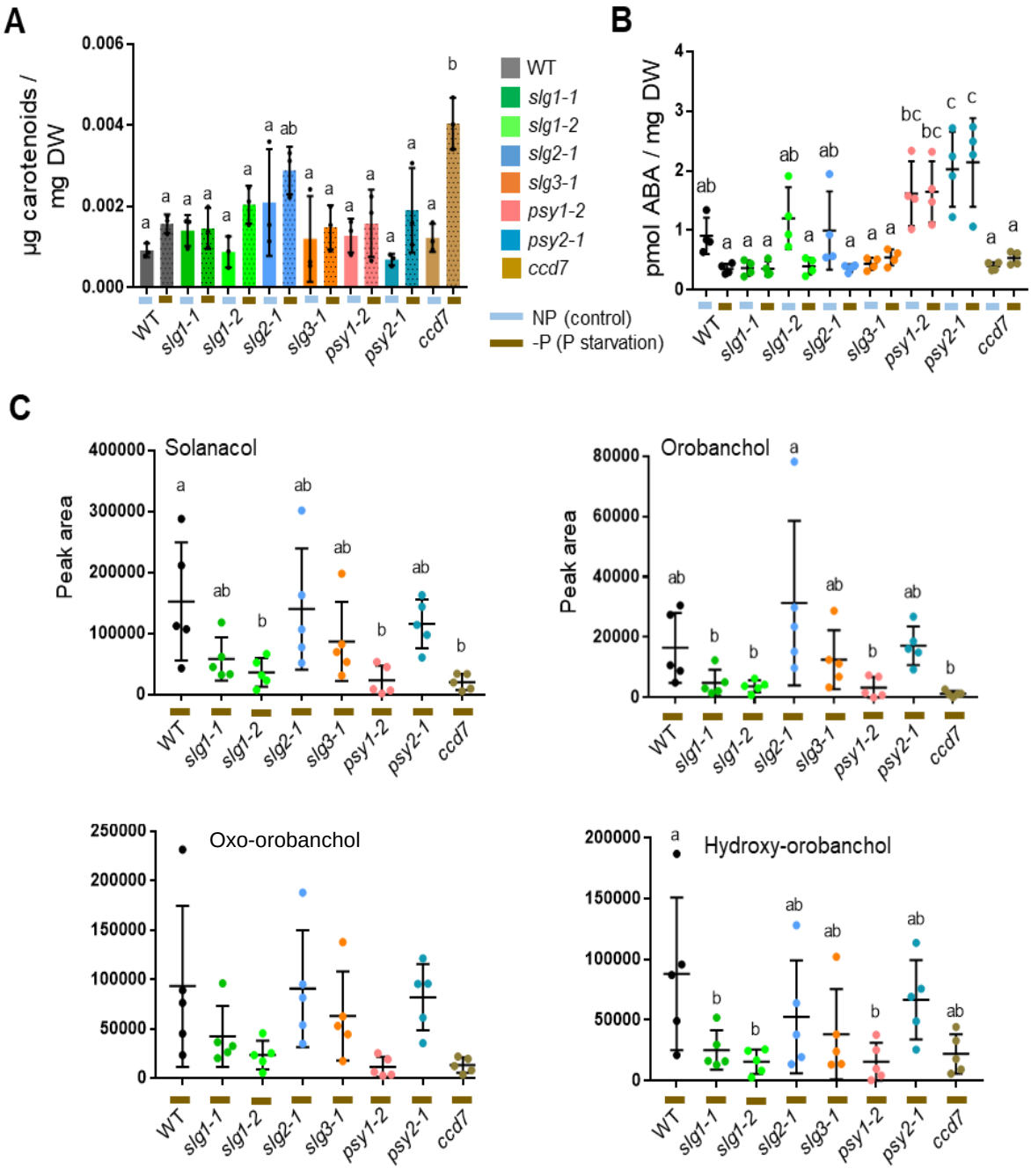

Figure 7. SlG1 is involved in root SL production. Plants of the indicated genotypes were grown in half-strength Hoagland solution with normal phosphate (NP) or under phosphate starvation (-P) conditions. Samples of root tissues or exudates were collected for metabolite analyses. (A) Carotenoid levels in root tissues. Values correspond to the mean and SD of n≥3 independent biological replicates. **(B)** ABA levels in root tissues. Values correspond to mean and SD of n≥4 independent biological replicates. **(C)** Levels of individual SLs in root exudates. Values represent the mean and SD of n≥5 independent biological replicates. In dotplots, inner line is the mean and whiskers represent SD. In all cases, letters represent statistically significant differences ($p<0.05$) among means according to posthoc Tukey's tests run when one-way ANOVA detected different means.

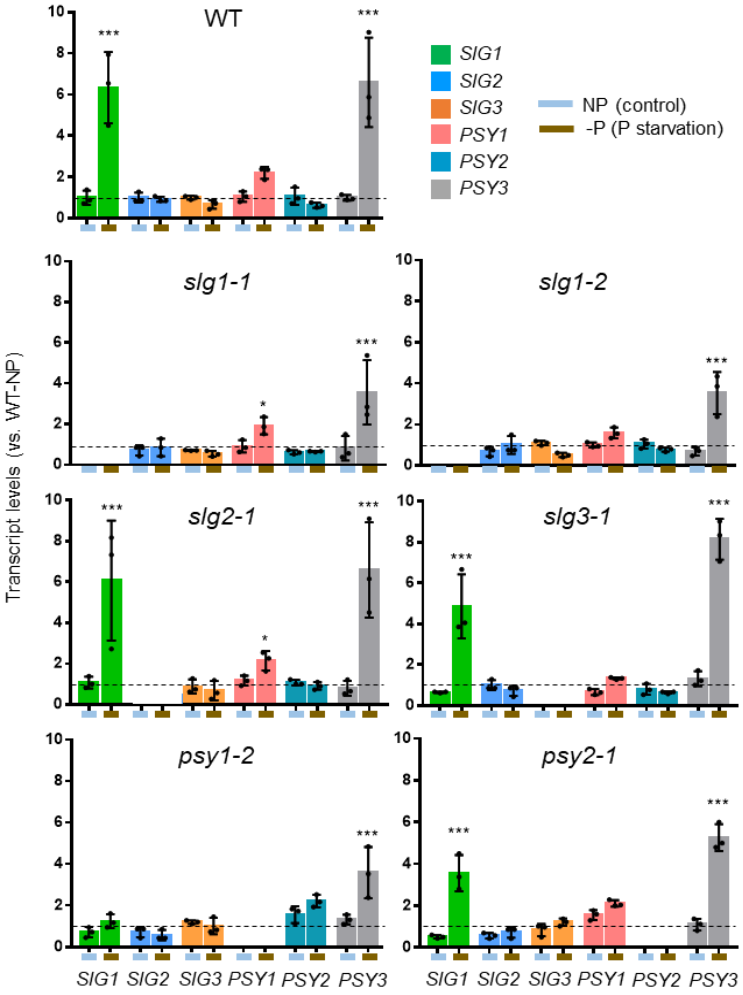

Figure 8. Expression profiles of genes encoding GGPPS and PSY paralogues in roots. RNA samples from roots collected from the plants described in Figure 7 were used for RT-qPCR experiments. Transcript levels were normalized using the tomato *ACT4* gene and they are shown relative to those in control (NP) WT samples (dotted line). The scale is the same in all plots to facilitate comparisons. Mean and SD of n=3 independent biological replicates are shown. Asterisks indicate statistically significant differences between conditions (NP vs –P) for each gene in each genotype according to one-way ANOVA with Dunnett's multiple comparisons test: *, $P < 0.05$; **, $P < 0.01$; ***, $P < 0.001$).

To obtain quantitative data, we measured several phenotypic parameters related with SL-regulated plant growth in these lines grown together with WT controls and SL-deficient *ccd7* mutant plants (Vogel et al., 2010). Measurements were performed on fifteen plants per genotype grown under NP for four weeks and then transferred to -P for two more weeks to promote SL synthesis (Ruyter-Spira et al., 2013) (Figure 9). Dry root weight was reduced in SL-deficient *slg1-1*, *slg1-2*, *psy1-2* and *cdd7* mutants compared to WT controls and mutants with normal SL production, i.e., *slg2-1*, *slg3-1* and *psy2-1* plants (Figure 9A). These data confirm that SLs have a role on promoting root growth (Al-Babili & Bouwmeester, 2015; Ruyter-Spira et al., 2013). Next, we measured the height of the plants and observed that *ccd7* plants were smaller than WT plants (Figure 9B). Surprisingly, the SL-deficient mutants (*slg1-1*, *slg1-2* and *psy1-2*) showed a very similar size when compared to WT plants, whereas *slg2-1* and *slg3-1*, which produced normal levels of SLs in roots, were smaller (Figure 9B). Plant height is the result of

multiple inputs, including hormone levels. Maybe reduced GGPP levels in *slg2* and *slg3* shoots reduce the production of GAs, which are stem elongation promoters (Livne et al., 2015; Yamaguchi, 2008). SL-synthesis mutants typically present smaller plants with increased number of lateral branches (Gomez-Roldan et al., 2008; Yamada et al., 2014). Indeed, *ccd7* plants not only were smaller (Figure 9B) but they presented higher number of lateral branches compared to WT controls in our experimental conditions (Figure 9C). Consistent with our preliminar visual observations, none of the mutants defective in GGPPS or PSY isoforms showed a branching phenotype (Figure 9C). The results indicate that only *ccd7* plants present phenotypes related to SL deficiency in the whole plant, probably because the impairment in CCD7 enzyme activity affects SL production in all plant tissues. By contrast, loss of SlG1 in the whole plant appears to only affect SL production in roots, impacting root growth but not shoot or branching. The similar phenotypes of *slg1-1*, *slg1-2* and *psy1-2* plants further support the conclusion that the reduced SL production by PSY1-defective roots is due to a block in *SlG1* upregulation rather than caused by decreased PSY1 activity. It is commonly believed that SLs are synthetized in plant roots and later transported to aerial parts, where they are able to regulate plant growth and shoot branching (Al-Babili & Bouwmeester, 2015; Gomez-Roldan et al., 2008; Ruyter-Spira et al., 2013). Nevertheless, grafting studies in tomato and pea have shown that the SL biosynthetic machinery is active in stems and can produce SLs that are later transported by the xylem to shoots and leaves (Beveridge et al., 2009; Visentin et al., 2016; Xie et al., 2010). As the expression levels of *SlG1* in aerial parts under normal conditions are very low (about 40-fold lower than *SlG2* and 50-fold lower than *SlG3*) (Figure S3) (Barja et al., 2021; Stauder et al., 2018), we propose that SlG1 is exclusively involved in providing GGPP for SL synthesis in roots. In shoots, much higher levels of carotenoids (derived from GGPP made by SlG2 and/or SlG3) may supply enough precursors to produce SLs supporting normal growth and development.

In summary, the only clear phenotype of the tomato *slg1* mutant is a reduction of SL levels exclusively in roots. SLs released by plant roots to the soil are well-known signaling molecules for colonization by AM fungi but also for germination of parasitic plants (López-Ráez et al., 2009; Yoneyama et al., 2008, 2010). The particular characteristics of the *slg1* mutant could make it immune to the negative effects associated to infection by parasitic plants without altering normal shoot growth and metabolism, including photosynthesis and fruit ripening.

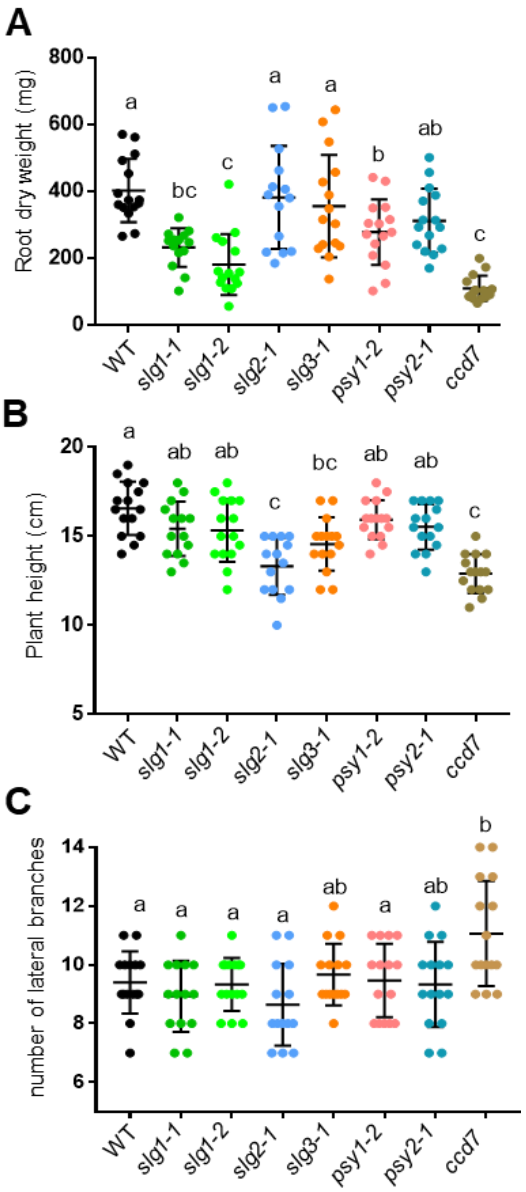

Figure 9. Defective SL synthesis in *slg1* plants does not impact shoot growth or branching. Measurements were performed using plants of the indicated genotypes grown under NP for 4 weeks and then transferred to -P for 2 more week to promote SL synthesis. (A) Weight of entire roots after freeze-drying. (B) Plant height from the root-stem transition to the apical meristem bud. (C) Number of lateral branches arising from the main stem. In all plots, dots indicate individual values, whiskers indicate mean and SD, and letters represent statistically significant differences ($P < 0.05$) among means according to posthoc Tukey's tests run when one-way ANOVA detected different means.

3 Materials and methods

3.1 Plant material, sample collection and phenotypical analyses.

Tomato (Solanum lycopersicum var. MicroTom) plants were used for most experiments. Seeds were surface-sterilized by a 30 min water wash followed by a 15 min incubation in 10 ml of 40% bleach with 10 µl of Tween-20. After three consecutive 10 min washes with sterile milli-Q water, seeds were germinated on plates with solid 0.5x Murashige and Skoog (MS) medium containing 1% agar (without vitamins or sucrose). The medium was supplemented with kanamycin (100 µg/ml) when required to select transgenic plants. Plates were incubated in a climate-controlled growth chamber (Ibercex) at 26°C with a photoperiod of 14 h of white light (photon flux density of 50 µmol m-2 s-1) and 10 h of darkness. After 10-14 days, seedlings were transferred to soil and grown under standard greenhouse conditions (14 h light at 25 ± 1 °C and 10 h dark at 22 ± 1 °C). Those plants used for root metabolic analysis were grown in a greenhouse with the same conditions but in a mixture of sand and clay pebbles (1:1) instead of soil for easier root collection. *N.benthamiana* plants that were used for co-immunoprecipitation experiments were grown in the greenhouse under long day conditions at 24°C for 21 days.

Total tomato roots were manually cleaned and collected from plants grown in mixture of sand and clay pebbles (1:1). Young leaf samples were collected from 4-week-old plants and correspond to growing leaflets from the fifth and sixth true leaves. Tomato fruit pericarp samples for isoprenoid quantification were collected at breaker + 3 (B+3). Roots, leaflets and pericarp samples were frozen in liquid nitrogen immediately after collection, freeze-dried and stored at -80 °C. For counting the days fruits needed to change from breaker (B, when the first symptoms of chlorophyll degradation and carotenoid accumulation became visually obvious) to orange (Or) stage, thirty fruits (n=30) from each genotype on vine were visually followed every day and annotated. For fruit weight determination, 100 fully ripe individual fruits from each genotype were collected and weighted one by one using a precision scale (Kern). Fruit volume was estimated in 10 pools of 10 fruits each by measuring the displaced water volume in a graduated cylinder. For the analysis of phenotypical traits influenced by SL synthesis, fifteen 6-week-old plants were used, grown 4 weeks under half strength Hoagland solution and the last 2 weeks under half strength Hoagland solution without PO_4^{-3}.

3.2 Generation of constructs and tomato transformation

For co-immunoprecipitation experiments, full-length cDNAs encoding SlG1 and SlPSY3 proteins without their stop codons were amplified from root cDNA using the Phusion High-fidelity DNA polymerase (ThermoFisher). Next, the amplicons were introduced via BP clonase into pDONR207 entry plasmid using Gateway (GW) technology (Invitrogen). Full-length sequences were then subcloned through an LR reaction into pGWB414 and pGWB420 plasmids as previously reported (Barja et al., 2021). For CRISPR-Cas9-mediated disruption of *SlGGPP1*, two single guide RNAs (sgRNA) (Figure S1-2) were designed using the online tool CRISPR-P 2.0 (Liu et al., 2017). Cloning of the CRISPR-Cas9 constructs was carried out as previously described (Barja et al., 2021) using primers listed in Table S1. As a result, a single final binary plasmid harboring the Cas9 sequence, the NPTII gene providing kanamycin resistance, and the sgRNAs to disrupt SlGGPPS1 was obtained and named pDE-Cas9-SlG1 (Table S2). All constructs were confirmed by restriction mapping and DNA sequencing. Agrobacterium tumefaciens GV3101 strain was used to stably transform tomato MicroTom cotyledons with pDE-Cas9-SlG1 as described (Ezquerro et al., 2022). *In vitro* regenerated T1 lines were identified based on kanamycin resistance (100 µg/ml) PCR genotyping and sequencing (Table S1). Homozygous T2 lines lacking Cas9 were obtained after segregation and stable T3 offspring was used for next experiments.

3.3 Gene co-expression network (GCN) analyses

The data set used for Gene co-expression network construction was described in Wang et al., 2021 and is publicly available in https://dataview.ncbi.nlm.nih.gov/ object/ PRJNA 679261? reviewer=vs5lk 0a94j04c2rgieta1lrlro. It is composed by tomato root samples grown in normal and -P conditions. Pairwise pearson correlation coefficients (PCC) were calculated between every two genes using *SlG1*, *SlG2* and *SlG3* as baits and isoprenoid biosynthetic genes as preys (https://bioinformatics.psb.ugent.be/plaza/) as previously described (Wang et al., 2022). Figures were constructed using R software (https://www.r-project.org/).

3.4 Photosynthetic parameters

Chlorophyll a fluorescence measurements were carried out Chlorophyll fluorescence measurements were carried out with a Handy FluorCam (Photon Systems Instruments). ϕPSII was measure at 30 PAR with an actinic light of 3 µmol m^{-2} s^{-1}.

3.5 *P.syringae* infection of tomato plants

Pseudomonas syringae *pv. tomato DC3000* (Pst) strain were used for tomato infection as previously reported (López-Gresa et al., 2018). Briefly, bacteria were grown during 48 h at 28°C in LB agar medium with rifampicin (10 mg/mL) and kanamicin (0.5 mg/mL). When colonies appeared, they were transferred to King's B liquid medium supplemented with antibiotics and grown overnight at 28°C with shaking. Next, bacteria were centrifugated at 3000 g for 15 minutes and resuspended in 10mM $MgCl_2$ to a final optical density of 0.1 for further infection. Inoculation with bacteria was carried out in 4-week-old MicroTom plants without flowers by immersion. Plants were dipped into the bacterial suspension containing 0.05% Silwet L-77 for 30 seconds and left 24 hours for further sample collection.

3.6 Co-immunoprecipitation assays

Co-immunoprecipitation experiments were carried out as described previously (Barja & Rodríguez-Concepción, 2020; Barja et al., 2021). Constructs encoding new and previously Myc- and HA-tagged tomato GGPPS and PSY proteins (Table S2) (Barja et al., 2021) were transformed into *A. tumefaciens* GV3101 strains. A plasmid containing the Arabidopsis phosphoribulokinase protein with a Myc tag (pGWB417_PRK-Myc) was used as negative control. Agroinflintration of *N.benthamiana* leaves, sample collection, protein extraction and immunoprecipitation of proteins was performed as previously described (Barja et al., 2021). The presence of Myc- and HA-tagged proteins in input and Co-IP samples were detected by immunoblot analyses using 1:2000-diluted αMyc (Sigma) and 1:1000-diluted αHA (Roche) as primary antibodies. Horseradish peroxidase (HRP)-conjugated secondary antibodies against mouse and rat IgGs, respectively were used in a 1:10000 dilution. Amersham ECL Prime Western Blotting Detection Kit (GE Healthcare) was used for detection and the signal was visualized using the Amersham ImageQuant 800 Western blot imaging system.

3.7 RNA extraction and RT-qPCR analyses

Total RNA from freeze-dried leaves and roots was extracted using TriPure isolation reagent (Sigma) combined with a Qiagen RNeasy mini spin column kit following manufacturer's instructions. RNA was quantified using a NanoDropTM 8000 spectrophotometer (ThermoFisher Scientific). ThermoFisher First Strand cDNA synthesis kit using oligo(dT) primer was used to reverse transcribe 1000 ng of RNA into 20 µL of cDNA, which was subsequently diluted 10-fold with mili-Q water and stored at -

20 °C for further analysis. Relative mRNA abundance was evaluated via Real-Time Quantitative Polymerase Chain Reaction (RT-qPCR) in a reaction volume of 10 µL containing 5 µL of SYBR Green Master Mix (Thermo Fisher Scientific), 0.3 µM of each specific forward and reverse primer (Table S1) and 2 µL of cDNA. Transcript abundance was evaluated via real-time quantitative PCR (RT-qPCR) in a reaction volume of 10 µl containing 2 µl of the cDNA dilution, 5 µl of SYBR Green Master Mix (Thermo Fisher Scientific), and 0.3 µM of each specific forward and reverse primer (Table S1). The RT-qPCR was carried out on a QuantStudio 3 Real-Time PCR System (Thermo Fisher Scientific) using three independent biological samples and three technical replicates of each sample. Normalized transcript abundance was calculated as previously described (Simon, 2003) using tomato *ACT4* (Solyc04g011500) as endogenous reference gene.

3.8 GC-MS analysis of volatile organic compounds

For the analysis of leaf volatile compounds, 150 mg of frozen tomato leaf powder was weighted and added into a 15 ml glass vial and mixed with 1 mL of a saturated $CaCl_2$ solution and 100 µL of 750 mM EDTA (pH 7.5). The vial was sealed and sonicated for 5 min and volatile compounds extraction was performed by Head Space Solid-Phase Microextraction (HS-SPME) as previously reported (López-Gresa et al., 2017, 2018) Volatile organic compounds (VOCs) were analyzed in an Agilent 6890N (Santa Clara, CA, USA) gas chromatograph coupled to an Agilent 5975B Inert XL electronic impact (EI) mass detector with an ionization energy of 70 eV and a source temperature of 230°C. Then, chromatograms were acquired and processed using the Enhanced ChemStation software (Agilent). Final identification of VOCs was performed using commercial standards. (Sigma-Aldrich) as reported previously (López-Gresa et al., 2018).

3.9 Isoprenoid identification and quantification

Carotenoids, chlorophylls and tocopherols were extracted as described (Barja et al., 2021; Ezquerro et al., 2022) with some modifications. 25 mg of freeze-dried root tissue and 8 mg of freeze-dried leaves were mixed in 2 ml Eppendorf tubes with 375 µl of methanol as extraction solvent, 25 µl of a 10 % (w/v) solution of canthaxanthin (Sigma) in chloroform as internal control, and three 2 mm glass beads. For fruit pericarp tissue (20 mg of freeze-dried tissue) extraction, powder was mixed in 2 ml Eppendorf tubes with 1 ml of 2:1:1 hexane:acetone:methanol as extraction solvent, 25 µl of the canthaxanthin solution, and glass beads. Following extraction steps were performed as

described (Barja et al., 2021; Ezquerro et al., 2022). Extracted pigments were resuspended in 200 µl of acetone by using an ultrasound bath and filtered with 0.2 µm filters into amber-colored 2 ml glass vials. Separation and quantification of individual carotenoids and chlorophylls was performed as described (Barja et al., 2021).

3.10 ABA extraction and quantification

For ABA quantification in tomato roots, 20 mg of freeze-dried powder was mixed using 1 ml of 10% MeOH in water (containing internal ABA standard) by shaking in a TissueLyser II (Quiagen) at 27 Hz for 3 minutes. Next, samples were placed in a rotator for 1 hour at 4°C. Extracts were then centrifuge at 14000 x g at 4°C for 15 minutes. Around 800 µl of the liquid phase was recover in 1,5 ml Eppendorf for further steps. Eluted liquid was run through an Oasis HLB (reverse phase) column, as described (Flokova et al., 2014). The dry residues were dissolved in 1 ml of pure MeOH and after, dried under a nitrogen flow in a fume hood for 40 minutes. The eluate was dissolved in 5% acetonitrile and ABA was detected using a reverse phase UHPLC chromatography. The gradient used contains 5 to 50% acetronitrile with 0.05% acetic acid, at a flow speed of 400 µL/min over 21 min. Quantification of ABA was perform with a Q-Exactive mass spectrometer (Orbitrap detector; ThermoFisher Scientific) in conjunction with internal standards (deuterium-labelled hormone at 1pmol/µl), calibration curves and the TraceFinder 4.1 SP1 software.

3.11 Strigolactones extraction and measurement

Tomato seedlings growing in a mixture of sand and clay pebbles (1:1) were twice a week supplied with half-strength Hoagland solution for 28 days. After 28 days, plants were divided in two groups and one was supplied with half-strength Hoagland solution for 7 days, and the other group was brought under phosphorus (P) deficiency (by using half-strength Hoagland solutions without phosphate (PO_4^{-3})) to induce SL synthesis and further release into the soil. 100 ml of sterile mili-Q water was used to wash the roots and collect SLs-rich root exudates. SLs were concentrated with C18 columns (Grace, C18-fast/5000 mg) as previously described (Zhang et al., 2014, 2018) and next analysed by LC-MS/MS as previously reported (Zhang et al., 2018).

4 Acknowledgments

We greatly thank We thank Mª Rosa Rodriguez-Goberna for technical help with HPLC analyses, Kristýna Floková for the help in ABA measurements, Ernesto Llamas for providing the pGWB417_AtPRK construct, and Albert Ferrer and Laura Gutiérrez for the pDE-Cas9 (with kanamycin resistance) plasmid. This work was funded by grants from Spanish MCIN/AEI/10.13039/501100011033 and European NextGeneration EU/PRTR and PRIMA programs to MR-C (PID2020-115810GB-I00 and UToPIQ-PCI2021-121941). MR-C is also supported by CSIC (202040E299) and Generalitat Valenciana (PROMETEU/2021/056). ME received a predoctoral fellowship from MCIN/AEI (BES-2017-080652) and an EMBO Scientific Exchange Grant (9315). No conflict of interest is declared.

5 References

Ahrazem, O., Argandoña, J., Fiore, A., Aguado, C., Luján, R., Rubio-Moraga, Á., Marro, M., Araujo-Andrade, C., Loza-Alvarez, P., Diretto, G., & Gómez-Gómez, L. (2018). Transcriptome analysis in tissue sectors with contrasting crocins accumulation provides novel insights into apocarotenoid biosynthesis and regulation during chromoplast biogenesis. *Scientific Reports*, 8(1): 2843-2861

Ahrazem, O., Diretto, G., Argandoña Picazo, J., Fiore, A., Rubio-Moraga, Á., Rial, C., Varela, R. M., Macías, F. A., Castillo, R., Romano, E., & Gómez-Gómez, L. (2019). The specialized roles in carotenogenesis and apocarotenogenesis of the phytoene synthase gene family in saffron. *Frontiers in Plant Science*,10: 249-270

Al-Babili, S., & Bouwmeester, H. J. (2015). Strigolactones, a novel carotenoid-derived plant hormone. *Annual Review of Plant Biology*, *66*, 161–186.

Ament, K., van Schie, C. C., Bouwmeester, H. J., Haring, M. A., & Schuurink, R. C. (2006). Induction of a leaf specific geranylgeranyl pyrophosphate synthase and emission of (E,E)-4,8,12-trimethyltrideca-1,3,7,11-tetraene in tomato are dependent on both jasmonic acid and salicylic acid signaling pathways. *Planta*, *224*(5), 1197–1208.

Arango, J., Wüst, F., Beyer, P., & Welsch, R. (2010). Characterization of phytoene synthases from cassava and their involvement in abiotic stress-mediated responses. *Planta*, *232*(5), 1251–1262.

Banerjee, A., Wu, Y., Banerjee, R., Li, Y., Yan, H., & Sharkey, T. D. (2013). Feedback inhibition of deoxy-D-xylulose-5-phosphate synthase regulates the methylerythritol 4-phosphate pathway. *Journal of Biological Chemistry*, *288*(23), 16926.

Bari, V. K., Nassar, J. A., Kheredin, S. M., Gal-On, A., Ron, M., Britt, A., Steele, D., Yoder, J., & Aly, R. (2019). CRISPR/Cas9-mediated mutagenesis of CAROTENOID CLEAVAGE DIOXYGENASE 8 in tomato provides resistance against the parasitic weed *Phelipanche aegyptiaca*. *Scientific Reports*, (9) (11438).

Barja, M. V., Ezquerro, M., Beretta, S., Diretto, G., Florez-Sarasa, I., Feixes, E., Fiore, A., Karlova, R., Fernie, A. R., Beekwilder, J., & Rodríguez-Concepción, M. (2021). Several geranylgeranyl diphosphate synthase isoforms supply metabolic substrates for carotenoid biosynthesis in tomato. *New Phytologist*, *231*(1), 255–272.

Barja, M. V., & Rodriguez-Concepcion, M. (2021). Plant geranylgeranyl diphosphate synthases: every (gene) family has a story. *aBIOTECH, Springer*, 2(3), 289-298.

Baslam, M., Esteban, R., García-Plazaola, J. I., & Goicoechea, N. (2013). Effectiveness of arbuscular mycorrhizal fungi (AMF) for inducing the accumulation of major carotenoids, chlorophylls and tocopherol in green and red leaf lettuces. *Applied Microbiology and Biotechnology*, 97(7), 3119–3128.

Beveridge, C. A., Dun, E. A., & Rameau, C. (2009). Pea has its tendrils in branching discoveries spanning a century from auxin to strigolactones. *Plant Physiology*, *151*(3), 985–990.

Bouvier, F., Rahier, A., & Camara, B. (2005). Biogenesis, molecular regulation and function of plant isoprenoids. *Progress in Lipid Research,* 4(6), 357-429.

Bouwmeester, H. J., Roux, C., Lopez-Raez, J. A., & Bécard, G. (2007). Rhizosphere communication of plants, parasitic plants and AM fungi. *Trends in Plant Science*, 12(5), 224–230.

Bramley, P., Teulieres, C., Blain, I., Bird, C., Schuch, W., & Holloway, R. (1992). Biochemical characterization of transgenic tomato plants in which carotenoid synthesis has been inhibited through the expression of antisense RNA to pTOM5. *The Plant Journal,* 92(1).

Camagna, M., Grundmann, A., Bar, C., Koschmieder, J., Beyer, P., & Welsch, R. (2019). Enzyme fusion removes competition for geranylgeranyl diphosphate in carotenogenesis. *Plant Physiology*, 179(3), 1013–1027.

Chen, Q., Fan, D., & Wang, G. (2015). Heteromeric geranyl(geranyl) diphosphate synthase is involved in monoterpene biosynthesis in arabidopsis flowers. *Molecular Plant*, 8(9), 1434–1437.

Costa, J. L., Paschoal, D., da Silva, E. M., Silva, J. S., do Carmo, R. M., Carrera, E., López-Díaz, I., Rossi, M. L., Freschi, L., Mieczkowski, P., Peres, L. E. P., Teixeira, P. J. P. L., & Figueira, A. (2021). *Moniliophthora perniciosa*, the causal agent of witches' broom disease of cacao, interferes with cytokinin metabolism during infection of Micro-Tom tomato and promotes symptom development. *New Phytologist*, 231(1), 365–381.

Deganello, J., Leal, G. A., Rossi, M. L., Peres, L. E. P., & Figueira, A. (2014). Interaction of moniliophthora perniciosa biotypes with micro-tom tomato: A model system to investigate the witches' broom disease of theobroma cacao. *Plant Pathology*, *63*(6), 1251–1263.

Degenhardt, J., Köllner, T. G., & Gershenzon, J. (2009). Monoterpene and sesquiterpene synthases and the origin of terpene skeletal diversity in plants. *Phytochemistry*, 70 (15), 1621–1637.

Diretto, G., Frusciante, S., Fabbri, C., Schauer, N., Busta, L., Wang, Z., Matas, A. J., Fiore, A., K.C. Rose, J., Fernie, A. R., Jetter, R., Mattei, B., Giovannoni, J., & Giuliano, G. (2020). Manipulation of β-carotene levels in tomato fruits results in increased ABA content and extended shelf life. *Plant Biotechnology Journal*, 18(5), 1185–1199.

Ezquerro, M., Burbano, E., & Rodríguez-Concepción,M. (2022) Overlapping and specialized roles of tomato phytoene synthase isoforms PSY1 and PSY2 in carotenoid and ABA production. *bioRxiv.*

Fantini, E., Falcone, G., Frusciante, S., Giliberto, L., & Giuliano, G. (2013). Dissection of tomato lycopene biosynthesis through virus-induced gene silencing. *Plant Physiology*, 163(2), 986–998.

Fester, T., Schmidt, D., Lohse, S., Walter, M. H., Giuliano, G., Bramley, P. M., Fraser, P. D., Hause, B., & Strack, D. (2002). Stimulation of carotenoid metabolism in arbuscular mycorrhizal roots. *Planta,* 216(1), 148–154.

Floková, K., Tarkowská, D., Miersch, O., Strnad, M., Wasternack, C., & Novák, O. (2014). UHPLC–MS/MS based target profiling of stress-induced phytohormones. *Phytochemistry*, 105, 147-157.

Fornalé, S., Shi, X., Chai, C., Encina, A., Irar, S., Capellades, M., Fuguet, E., Torres, J. L., Rovira, P., Puigdomènech, P., Rigau, J., Grotewold, E., Gray, J., & Caparrós-Ruiz, D. (2010). ZmMYB31 directly represses maize lignin genes and redirects the phenylpropanoid metabolic flux. *Plant Journal*, 64(4), 633–644.

Fraser, P. D., Kiano, J. W., Truesdale, M. R., Schuch, W., & Bramley, P. M. (1999). Phytoene synthase-2 enzyme activity in tomato does not contribute to carotenoid synthesis in ripening fruit. *Plant Molecular Biology*, 40, 687–698.

Fraser, P. D., Truesdale, M. R., Bird, C. R., Schuch, W., & Bramley, P. M. (1994). Carotenoid Biosynthesis during Tomato Fruit Development' Evidence for Tissue-Specific Gene Expression. *Plant Physiology*, 105(1), 405-413.

Fujisawa, M., Nakano, T., Shima, Y., & Ito, Y. (2013). A large-scale identification of direct targets of the tomato MADS box transcription factor RIPENING INHIBITOR reveals the regulation of fruit ripening. *Plant Cell*, 25(2), 371–386.

Gomez-Roldan, V., Fermas, S., Brewer, P. B., Puech-Pagès, V., Dun, E. A., Pillot, J. P., Letisse, F., Matusova, R., Danoun, S., Portais, J. C., Bouwmeester, H., Bécard, G., Beveridge, C. A., Rameau, C., & Rochange, S. F. (2008). Strigolactone inhibition of shoot branching. *Nature*, 455(7210), 189–194.

Groot, S. P. C., & Karssen, C. M. (1992). Dormancy and Germination of Abscisic Acid-Deficient Tomato Seeds' Studies with the sitiens Mutant. *Plant Physiology*, 99(3), 952-958

Hernandez-Espinoza, L. H., & Barrios-Masias, F. H. (2020). Physiological and anatomical changes in tomato roots in response to low water stress. *Scientia Horticulturae*, 265, 109208.

Hivert, G., Davidovich-Rikanati, R., Bar, E., Sitrit, Y., Schaffer, A., Dudareva, N., & Lewinsohn, E. (2020). Prenyltransferases catalyzing geranyldiphosphate formation in tomato fruit. *Plant Science*, 296, 110504

Ilahy, R., Tlili, I., Siddiqui, M. W., Hdider, C., & Lenucci, M. S. (2019). Inside and beyond color: Comparative overview of functional quality of tomato and watermelon fruits. *Frontiers in Plant Science* 10, 769-780

Jang, S. J., Jeong, H. B., Jung, A., Kang, M. Y., Kim, S., Ha, S. H., Kwon, J. K., & Kang, B. C. (2020). Phytoene synthase 2 can compensate for the absence of PSY1 in the control of color in Capsicum fruit. *Journal of Experimental Botany*, 71(12), 3417–3427.

Kovacs, K., Zhang, L., Linforth, R. S. T., Whittaker, B., Hayes, C. J., & Fray, R. G. (2007). Redirection of carotenoid metabolism for the efficient production of taxadiene [taxa-4(5),11(12)-diene] in transgenic tomato fruit. *Transgenic Research*, 16(1), 121–126.

Kuromori, T., Seo, M., & Shinozaki, K. (2018). ABA Transport and Plant Water Stress Responses. *Trends in Plant Science* 23(6), 513–522.

Li, F., Vallabhaneni, R., Yu, J., Rocheford, T., & Wurtzel, E. T. (2008). The maize phytoene synthase gene family: Overlapping roles for carotenogenesis in endosperm, photomorphogenesis, and thermal stress tolerance. *Plant Physiology*, 147(3), 1334–1346.

Li, Y., Lu, Y., Li, L., Chu, Z., Zhang, H., Li, H., Fernie, A. R., & Ouyang, B. (2019). Impairment of hormone pathways results in a general disturbance of fruit primary metabolism in tomato. *Food Chemistry*, 274, 170–179.

Liu, H., Ding, Y., Zhou, Y., Jin, W., Xie, K., & Chen, L. L. (2017). CRISPR-P 2.0: An Improved CRISPR-Cas9 Tool for Genome Editing in Plants. *Molecular Plant* 10(3), 530–532

Livne, S., Lor, V. S., Nir, I., Eliaz, N., Aharoni, A., Olszewski, N. E., Eshed, Y., & Weiss, D. (2015). Uncovering DELLA-independent gibberellin responses by characterizing new tomato procera mutants. *Plant Cell*, 27(6), 1579–1594.

López-Gresa, M. P., Lisón, P., Campos, L., Rodrigo, I., Rambla, J. L., Granell, A., Conejero, V., & Bellés, J. M. (2017). A non-targeted metabolomics approach unravels the VOCs associated with the tomato immune response against Pseudomonas syringae. *Frontiers in Plant Science*, 8, 1188-1199.

López-Gresa, M. P., Payá, C., Ozáez, M., Rodrigo, I., Conejero, V., Klee, H., Bellés, J. M., & Lisón, P. (2018). A new role for green leaf volatile esters in tomato stomatal defense against pseudomonas syringe pv. Tomato. *Frontiers in Plant Science*, 9, 1855-1869.

López-Ráez, J. A., Matusova, R., Cardoso, C., Jamil, M., Charnikhova, T., Kohlen, W., Carolien, R. S., Verstappen, F., & Bouwmeester, H. (2009). Strigolactones: Ecological significance and use as a target for parasitic plant control. *Pest Management Science* 65(5), 471–477.

Matthys, C., Walton, A., Struk, S., Stes, E., Boyer, F. D., Gevaert, K., & Goormachtig, S. (2016). The Whats, the Wheres and the Hows of strigolactone action in the roots. *Planta* 243(6), 1327–1337.

McQuinn, R. P., Gapper, N. E., Gray, A. G., Zhong, S., Tohge, T., Fei, Z., Fernie, A. R., & Giovannoni, J. J. (2020). Manipulation of ZDS in tomato exposes carotenoid- and ABA-specific effects on fruit development and ripening. *Plant Biotechnology Journal*, 18(11), 2210–2224.

Moreno, J. C., Mi, J., Alagoz, Y., & Al-Babili, S. (2021). Plant apocarotenoids: from retrograde signaling to interspecific communication. *The Plant Journal*, 105(2), 351–375.

Mou, W., Li, D., Bu, J., Jiang, Y., Khan, Z. U., Luo, Z., Mao, L., & Ying, T. (2016). Comprehensive analysis of ABA effects on ethylene biosynthesis and signaling during tomato fruit ripening. *PLoS ONE*, 11(4).

Nakahara, H., Mori, T., Sadakari, N., Matsusaki, H., & Matsuzoe, N. (2016). Biological control of the bacterial wilt of the tomato “Micro-Tom” by phenotypic conversion mutants of ralstonia solanacearum. *Environmental Control in Biology*, 54(3), 139–145.

Nitsch, L., Kohlen, W., Oplaat, C., Charnikhova, T., Cristescu, S., Michieli, P., Wolters-Arts, M., Bouwmeester, H., Mariani, C., Vriezen, W. H., & Rieu, I. (2012). ABA-deficiency results in reduced plant and fruit size in tomato. *Journal of Plant Physiology*, 169(9), 878–883.

Nouri, E., Surve, R., Bapaume, L., Stumpe, M., Chen, M., Zhang, Y., Ruyter-Spira, C., Bouwmeester, H., Glauser, G., Bruisson, S., & Reinhardt, D. (2021). Phosphate Suppression of Arbuscular Mycorrhizal Symbiosis Involves Gibberellic Acid Signaling. *Plant and Cell Physiology*, 62(6), 959–970.

Pokhilko, A., Bou-Torrent, J., Pulido, P., Rodríguez-Concepción, M., & Ebenhöh, O. (2015). Mathematical modelling of the diurnal regulation of the MEP pathway in Arabidopsis. *New Phytologist*, 206(3), 1075–1085.

Pombo MA, Zheng Y, Fernandez-Pozo N, Dunham DM, Fei Z, Martin GB. (2014) Transcriptomic analysis reveals tomato genes whose expression is induced specifically during effector-triggered immunity and identifies the Epk1 protein kinase which is required for the host response to three bacterial effector proteins. *Genome Biology*, 15(10), 492.

Pulido, P., Perello, C., & Rodriguez-Concepcion, M. (2012). New Insights into Plant Isoprenoid Metabolism. *Molecular Plant*, 5(5), 964–967.

Rodriguez-Concepcion, M., Avalos, J., Bonet, M. L., Boronat, A., Gomez-Gomez, L., Hornero-Mendez, D., Limon, M. C., Meléndez-Martínez, A. J., Olmedilla-Alonso, B., Palou, A., Ribot, J., Rodrigo, M. J., Zacarias, L., & Zhu, C. (2018). A global perspective on carotenoids: Metabolism, biotechnology, and benefits for nutrition and health. *Progress in Lipid Research* 70, 62–93.

Rodríguez-Concepción, M., & Welsch, R. (2020). *Plant and Food Carotenoids Methods and Protocols Methods in Molecular Biology,* 2083.

Rosli HG, Zheng Y, Pombo MA, Zhong S, Bombarely A, Fei Z, Collmer A, Martin GB. (2013). Transcriptomics-based screen for genes induced by flagellin and repressed by pathogen effectors identifies a cell wall-associated kinase involved in plant immunity. *Genome Biology*, 20(14), 139.

Ruiz-Lozano, J. M., Aroca, R., Zamarreño, Á. M., Molina, S., Andreo-Jiménez, B., Porcel, R., García-Mina, J. M., Ruyter-Spira, C., & López-Ráez, J. A. (2016). Arbuscular mycorrhizal symbiosis induces strigolactone biosynthesis under drought and improves drought tolerance in lettuce and tomato. *Plant Cell and Environment*, 39(2), 441–452.

Ruiz-Sola, M. Á., Barja, M. V., Manzano, D., Llorente, B., Schipper, B., Beekwilder, J., & Rodriguez-Concepcion, M. (2016a). A single arabidopsis gene encodes two differentially targeted geranylgeranyl diphosphate synthase isoforms. *Plant Physiology*, 172(3), 1393–1402.

Ruiz-Sola, M. Á., Coman, D., Beck, G., Barja, M. V., Colinas, M., Graf, A., Welsch, R., Rütimann, P., Bühlmann, P., Bigler, L., Gruissem, W., Rodríguez-Concepción, M., & Vranová, E. (2016b). Arabidopsis GERANYLGERANYL DIPHOSPHATE SYNTHASE 11 is a hub isozyme required for the production of most photosynthesis-related isoprenoids. *New Phytologist*, 209(1), 252-64

Ruiz-Sola, M. Á., & Rodríguez-Concepción, M. (2012). Carotenoid Biosynthesis in Arabidopsis: A Colorful Pathway. *The Arabidopsis Book*, 10, e0158.

Ruyter-Spira, C., Al-Babili, S., van der Krol, S., & Bouwmeester, H. (2013). The biology of strigolactones. *Trends in Plant Science* 18(2), 72–83.

Schilmiller, A. L., Schauvinhold, I., Larson, M., Xu, R., Charbonneau, A. L., Schmidt, A., Wilkerson, C., Last, R. L., & Pichersky, E. (2013). Monoterpenes in the glandular trichomes of tomato are synthesized from a neryl diphosphate precursor rather than geranyl diphosphate. *Proceedings of the National Academy of Sciences*, 106(26), 10865-10870.

Schuurink R, Tissier A. (2020). Glandular trichomes: micro-organs with model status*? New Phytologist*, 225(6), 2251-2266.

Serrani, J. C., Sanjuán, R., Ruiz-Rivero, O., Fos, M., & García-Martínez, J. L. (2007). Gibberellin regulation of fruit set and growth in tomato. *Plant Physiology*, 145(1), 246–257.

Shih, P. M. (2018). Towards a sustainable bio-based economy: Redirecting primary metabolism to new products with plant synthetic biology. *Plant Science*, 273, 84–91.

Shwartz, I., Levy, M., Ori, N., & Bar, M. (2016). Hormones in tomato leaf development. *Developmental Biology*, 419(1), 132–142.

Simon, P. (2003). Q-Gene: Processing quantitative real-time RT-PCR data. *Bioinformatics*, 19(11), 1439–1440.

Stauder, R., Welsch, R., Camagna, M., Kohlen, W., Balcke, G. U., Tissier, A., & Walter, M. H. (2018). Strigolactone levels in dicot roots are determined by an ancestral symbiosis-regulated clade of the PHYTOENE SYNTHASE gene family. *Frontiers in Plant Science*, 9, 255-271.

Szkopińska, A., & Płochocka, D. *(*2005). Farnesyl diphosphate synthase; regulation of product specificity*. Acta Biochimica Polonica*, 52(1), 45-55

Takahashi, H., Shimizu, A., Arie, T., Rosmalawati, S., Fukushima, S., Kikuchi, M., Hikichi, Y., Kanda, A., Takahashi, A., Kiba, A., Ohnishi, K., Ichinose, Y., Taguchi, F., Yasuda, C., Kodama, M., Egusa, M., Masuta, C., Sawada, H., Shibata, D., & Watanabe, Y. (2005). Catalog of Micro-Tom tomato responses to common fungal, bacterial, and viral pathogens. *Journal of General Plant Pathology*, 71(1), 8–22.

Tanimoto, E. (2005). Regulation of root growth by plant hormones - Roles for auxin and gibberellin. *Critical Reviews in Plant Sciences* 24(4), 249–265.

Tholl, D. (2015). Biosynthesis and Biological Functions of Terpenoids in Plants. *Advances in biochemical engineering/biotechnology* 148, 63–106.

Thulasiram, H. v., & Poulter, C. D. (2006). Farnesyl diphosphate synthase: The art of compromise between substrate selectivity and stereoselectivity. *Journal of the American Chemical Society*, 128(49), 15819–15823.

Torres-Montilla, S., & Rodriguez-Concepcion, M. (2021). Making extra room for carotenoids in plant cells: new opportunities for biofortification. *Progress in Lipid Research*, 84, 101128.

Ubeda-Tomás, S., Swarup, R., Coates, J., Swarup, K., Laplaze, L., Beemster, G. T. S., Hedden, P., Bhalerao, R., & Bennett, M. J. (2008). Root growth in Arabidopsis requires gibberellin/DELLA signalling in the endodermis. *Nature Cell Biology*, 10(5), 625–628.

Ueda, H., & Kusaba, M. (2015). Strigolactone regulates leaf senescence in concert with ethylene in arabidopsis. *Plant Physiology*, 169(1), 138–147.

Visentin, I., Vitali, M., Ferrero, M., Zhang, Y., Ruyter-Spira, C., Novák, O., Strnad, M., Lovisolo, C., Schubert, A., & Cardinale, F. (2016). Low levels of strigolactones in roots as a component of the systemic signal of drought stress in tomato. *New Phytologist*, 212(4), 954–963.

Vogel, J. T., Walter, M. H., Giavalisco, P., Lytovchenko, A., Kohlen, W., Charnikhova, T., Simkin, A. J., Goulet, C., Strack, D., Bouwmeester, H. J., Fernie, A. R., & Klee, H. J. (2010). SlCCD7 controls strigolactone biosynthesis, shoot branching and mycorrhiza-induced apocarotenoid formation in tomato. *The Plant Journal*, 61(2), 300–311.

Walter, M. H., Stauder, R., & Tissier, A. (2015). Evolution of root-specific carotenoid precursor pathways for apocarotenoid signal biogenesis. *Plant Science* 233, 1–10.

Wang, F., Park, Y.-L., & Gutensohn, M. (2021). Glandular Trichome-Derived Mono- and Sesquiterpenes of Tomato Have Contrasting Roles in the Interaction with the Potato Aphid Macrosiphum euphorbiae. *Journal of Chemical Ecology*, 47(2), 204-214.

Wang, Q., Huang, X. Q., Cao, T. J., Zhuang, Z., Wang, R., & Lu, S. (2018). Heteromeric Geranylgeranyl Diphosphate Synthase Contributes to Carotenoid Biosynthesis in Ripening Fruits of Red Pepper (Capsicum annuum var. conoides). *Journal of Agricultural and Food Chemistry*, 66(44), 11691–11700.

Wang, R., Angenent, G. C., Seymour, G., & de Maagd, R. A. (2020). Revisiting the Role of Master Regulators in Tomato Ripening. *Trends in Plant Science* 25(3), 291–301.

Wang, Y., Duran, H. G. S., van Haarst, J. C., Schijlen, E. G., Ruyter-Spira, C., Medema, M. H., Dong, L., & Bouwmeester, H. J. (2021). The role of strigolactones in P deficiency induced transcriptional changes in tomato roots. *BMC plant biology*, 21(1), 1-21.

Wang, Y., Durairaj, J., Duran, H. G. S, van Velzen, R., Flokova, K., Liao, C. Y., Chojnacka, A., MacFarlane, S., Schranz, M. E., Medema, M. H., van Dijk, A. D. J., Dong, L., & Bouwmeester, H. J. (2022). The tomato cytochrome P450 CYP712G1 catalyses the double oxidation of orobanchol en route to the rhizosphere signalling strigolactone, solanacol. *New Phytologist* 235(5), 1884-1899.

Welsch, R., Wüst, F., Bär, C., Al-Babili, S., & Beyer, P. (2008). A third phytoene synthase is devoted to abiotic stress-induced abscisic acid formation in rice and defines functional diversification of phytoene synthase genes. *Plant Physiology*, 147(1), 367–380.

Xie, X., Yoneyama, K., & Yoneyama, K. (2010). The strigolactone story. *Annual Review of Phytopathology*, 48, 93–117.

Yamada, Y., Furusawa, S., Nagasaka, S., Shimomura, K., Yamaguchi, S., & Umehara, M. (2014). Strigolactone signaling regulates rice leaf senescence in response to a phosphate deficiency. *Planta*, 240(2), 399–408.

Yamada, Y., & Umehara, M. (2015). Possible roles of strigolactones during leaf senescence. *Plants* 4(3), 664–677.

Yamaguchi, S. (2008). Gibberellin metabolism and its regulation. In *Annual Review of Plant Biology*, 59, 225–251.

Yang Y, Wang M, Yin L, Onac E, Zhou F, Peng S, Xia J, Shi K, Yu Q, Zhou H. (2015). RNA-seq analysis reveals the role of red light in resistance against Pseudomonas syringae pv. tomato DC3000 in tomato plants. *BMC Genomics*. 25(16), 120-134.

Yoneyama, K., Awad, A. A., Xie, X., Yoneyama, K., & Takeuchi, Y. (2010). Strigolactones as germination stimulants for root parasitic plants. *Plant and Cell Physiology*, 51(7), 1095–1103.

Yoneyama, K., Xie, X., Sekimoto, H., Takeuchi, Y., Ogasawara, S., Akiyama, K., Hayashi, H., & Yoneyama, K. (2008). Strigolactones, host recognition signals for root parasitic plants and arbuscular mycorrhizal fungi, from Fabaceae plants. *New Phytologist*, 179(2), 484–494.

Zhang, M., Yuan, B., & Leng, P. (2009). The role of ABA in triggering ethylene biosynthesis and ripening of tomato fruit. *Journal of Experimental Botany*, 60(6), 1579–1588.

Zhang, Y., Cheng, X., Wang, Y., Díez-Simón, C., Flokova, K., Bimbo, A., Bouwmeester, H. J., & Ruyter-Spira, C. (2018). The tomato MAX1 homolog, SlMAX1, is involved in the biosynthesis of tomato strigolactones from carlactone. *New Phytologist*, 219(1), 297–309.

Zhang, Y., van Dijk, A. D. J., Scaffidi, A., Flematti, G. R., Hofmann, M., Charnikhova, T., Verstappen, F., Hepworth, J., van der Krol, S., Leyser, O., Smith, S. M., Zwanenburg, B., Al-Babili, S., Ruyter-Spira, C., & Bouwmeester, H. J. (2014). Rice cytochrome P450 MAX1 homologs catalyze distinct steps in strigolactone biosynthesis. *Nature Chemical Biology*, 10(12), 1028–1033.

Zhou, F., & Pichersky, E. (2020). The complete functional characterisation of the terpene synthase family in tomato. *New Phytologist*, 226(5), 1341–1360.

6 Supplemental information

```
GGPPS1        ATGGCATTTTTAGCTACCATTTCTGGCCTTGACAATCTGTTCCTTTCTAATACCCCAAAC 60
GGPPS1g1-1    ATGGCATTTTTAGCTACCATTTCTGGCCTTGACAATCTGTTCCTTTCTAATACCCCAAAC 60
GGPPS1g1-2    ATGGCATTTTTAGCTACCATTTCTGGCCTTGACAATCTGTTCCTTTCTAATACCCCAAAC 60
              ************************************************************

GGPPS1        AATAACTTTGCTTTCAGTAGAAAACTCCCACCAAGCCAATCTTACAGTTTCCTTCACAAG 120
GGPPS1g1-1    AATAACTTTGCTTTCAGTAGAAAACTCCCACCAAGCCAATCTTACAGTTTCCTTCACAAG 120
GGPPS1g1-2    AATAACTTTGCTTTCAGTAGAAAACTCCCACCAAGCCAATCTTACAGTTTCCTTCACAAG 120
              ************************************************************

GGPPS1        AAAATACACGCTAGCGATGTTGCGAACTCGTTCCAAACTTTTCAAGTCAAGGAACGAGAT 180
GGPPS1g1-1    AAAATACACGCTAGCGATGTTGCGAACTCGTTCCAAACTTTTCAAGTCAAGGAACGAGAT 180
GGPPS1g1-2    AAAATACACGCTAGCGATGTTGCGAACTCGTTCCAAACTTTTCAAGTCAAGGAACGAGAT 180
              ************************************************************

GGPPS1        GTTTCATCCAAGGCAGAGAAATTCATCTTGCCTGAGTTTGAGTTTCAAGAATACATGGTA 240
GGPPS1g1-1    GTTTCATCCAAGGCAGAGAAATTCATCTTGCCTGAGTTTGAGTTTCAAGAATACATGGTA 240
GGPPS1g1-2    GTTTCATCCAAGGCAGAGAAATTCATCTTGCCTGAGTTTGAGTTTCAAGAATACATGGTA 240
              ************************************************************

GGPPS1        ACGAAGGCAATCAAGGTAAACAAAGCACTAGATGAAGCAATACCAATGCAAGAGCCTATA 300
GGPPS1g1-1    ACGAAGGCAATCAAGGTAAACAAAGCACTAGATGAAGCAATACCAATGCAAGAGCCTATA 300
GGPPS1g1-2    ACGAAGGCAATCAAGGTAAACAAAGCACTAGATGAAGCAATACCAATGCAAGAGCCTATA 300
              ************************************************************

GGPPS1        AAAGTTCATGAAGCCATGAGGTACTCACTTCTAGCTGGAGGAAAACGTGTCCGGCCGATC 360
GGPPS1g1-1    AAAGTTCATGAAGCCATGAGGTACTCACTTCTAGCTGGAGGAAAACGTGTCCGGCCGATC 360
GGPPS1g1-2    AAAGTTCATGAAGCCATGAGGTACTCACTTCTAGCTGGAGGAAAACGTGTCCGGCCGATC 360
              ************************************************************

GGPPS1        CTCTGCATGGCTTCTTGTGAAGTTGTAGGAGGGGATGAATCCTTAGCTATACCTGCAGCT 420
GGPPS1g1-1    CTCTGCATGGCTTCTTGTGAAGTTGTAGGAGGGGATGAATCCTTAGCTATACCTGCAGCT 420
GGPPS1g1-2    CTCTGCATGGCTTCTTGTGAAGTTGTAGGAGGGGATGAATCCTTAGCTATACCTGCAGCT 420
              ************************************************************
                    G1 Geno F
GGPPS1        TGCGCAGTTGAGATGATCCATACCATGTCACTCGTCCATGATGATCTTCCCTGCATGGAC 480
GGPPS1g1-1    TGCGCAGTTGAGATGATCCATACCATGTCACTCGTCCATGATGATCTTCCCTGCATGGAC 480
GGPPS1g1-2    TGCGCAGTTGAGATGATCCATACCATGTCACTCGTCCATGATGATCTTCCCTGCATGGAC 480
              ************************************************************

GGPPS1        AACGATGATCTACGTCGTGGCAAGCCCACGAACCATAAGGTTTTTGGAGAAAACACTGCA 540
GGPPS1g1-1    AACGATGATCTACGTCGTGGCAAGCCCACGAACCATAAGGTTTTTGGAGAAAACACTGCA 540
GGPPS1g1-2    AACGATGATCTACGTCGTGGCAAGCCCACGAACCATAAGGTTTTTGGAGAAAACACTGCA 540
              ************************************************************
                PAM
GGPPS1        GAAGGGCTCGTGGCAGGGCAAATTGTGGACTTGGCGAGTGAAGGAAAACAAGTTAGCCTA 720
GGPPS1g1-1    GAAGGGCTCGTGGCAGG------------------------------------------ 677
GGPPS1g1-2     ------------------------------------------------------------ 541

                                sgRNA-2        PAM
GGPPS1        ACTGAACTGGAGTACATTCACCACCATAAGACGGCGAAGCTTTTGGAGGCTGCTGTGGTT 780
GGPPS1g1-1     ------------------------------------------------------------ 677
GGPPS1g1-2     ------------------------------------------------------------ 541
```

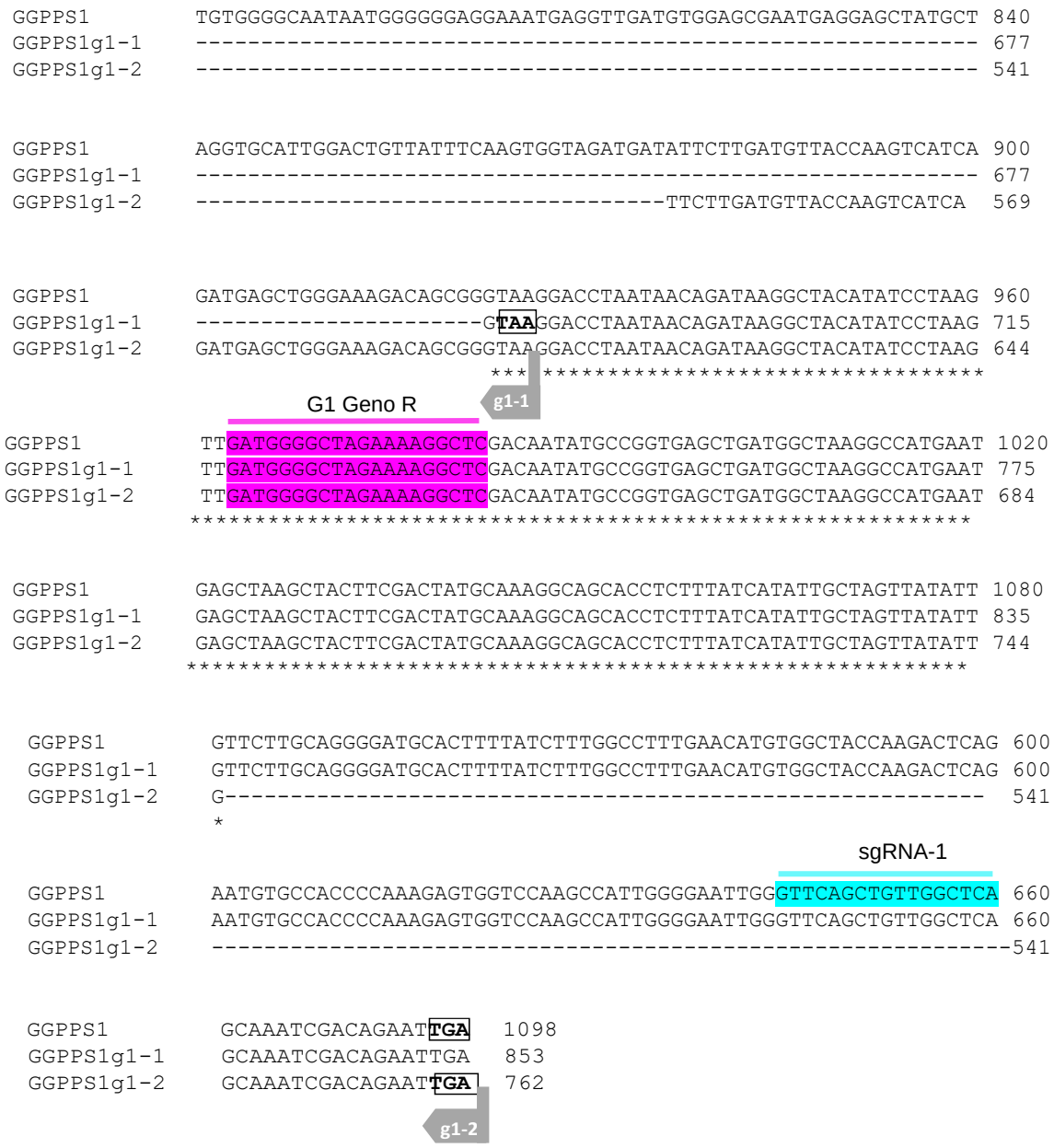

Figure S1. DNA sequence alignment of SlG1 CRISPR mutants. Alignment was performed using Clustal Omega (https://www.ebi.ac.uk/Tools/msa/clustalo/) with default settings. The sequence encoding the predicted plastid-targeting peptide is boxed in green. Designed single-guide RNAs (sgRNA) are highlighted in blue and genotyping oligonucleotides are highlighted in purple. Protospacer adjacent motifs (PAM) are highlighted in red. Translation stop codons are boxed and marked in bold. Numbers at the end of each sequence indicate DNA sequence length.

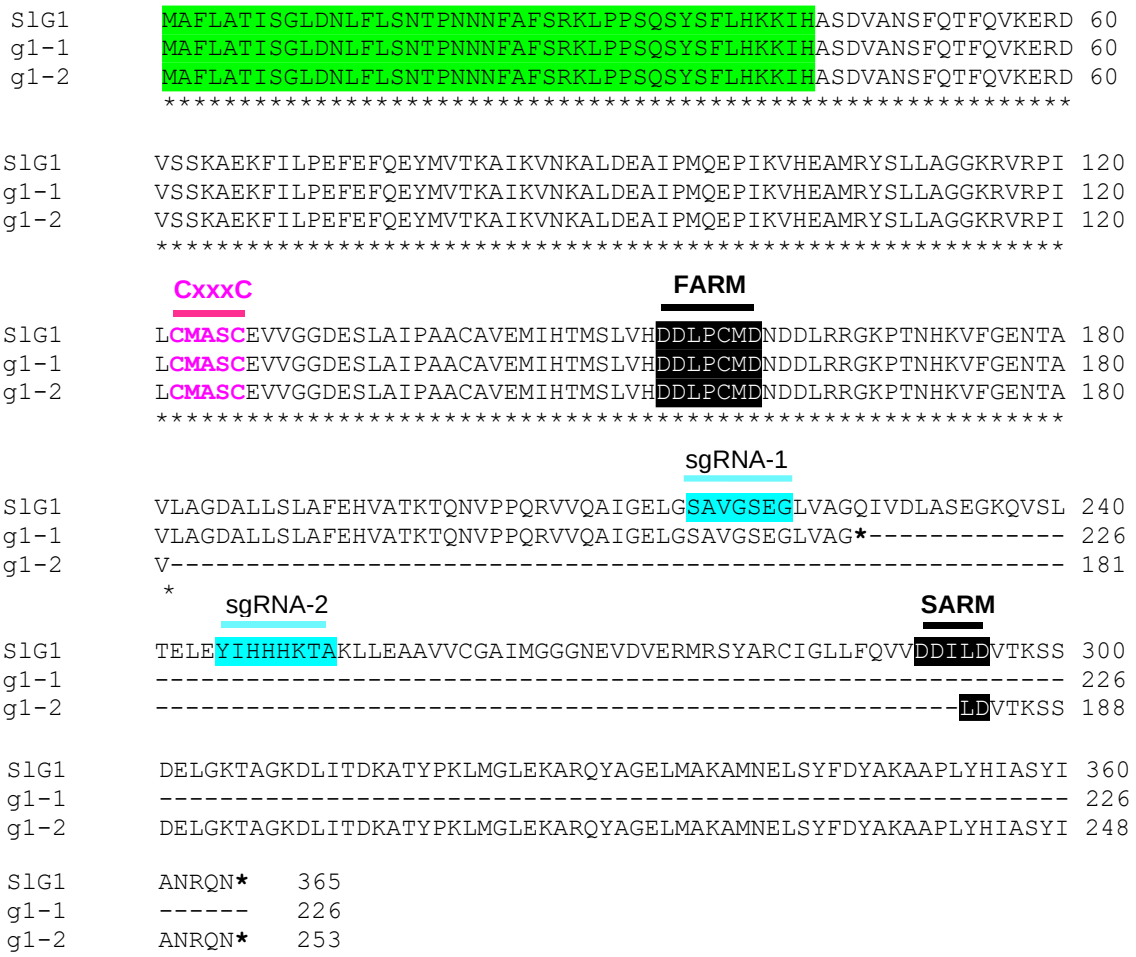

Figure S2. Protein alignments of SlG1 wild-type sequences with the selected CRISPR mutants. Multiple sequence alignment was performed using *Clustal Omega* (https://www.ebi.ac.uk/Tools/msa/clustalo/) with default settings**.** The predicted targeting peptides, the region of the designed sgRNAs and the catalytic motifs FARM (first aspartate-rich motif) and SARM (second-aspartate rich motif) are boxed in green, blue and black, respectively. The protein-protein interaction CxxxC (x = any hydrophobic residue) motifs are highlighted in pink. Numbers at the end of each sequence indicate protein length.

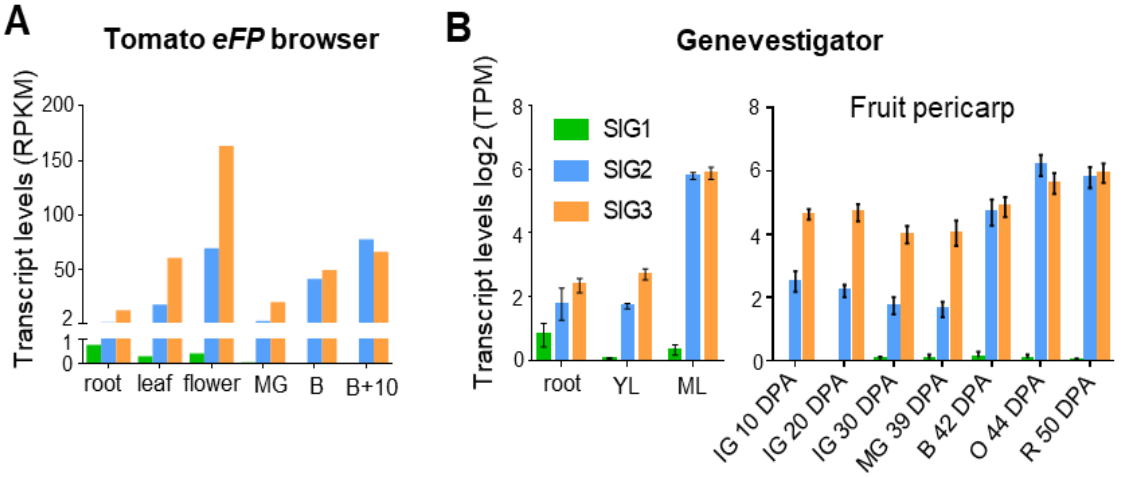

Figure S3. *SlG1, SlG2 and SlG3* transcript levels in different tissues and developmental stages. (A) RNAseq data retrieved from the *Tomato eFP Browser* database (http://bar.utoronto.ca/efp_tomato/cgi-bin/efpWeb.cgi). Levels are represented as RPKM (Reads per Kilobase of transcript per Million mapped reads). **(B)** RNAseq data obtained from Genevestigator (https://genevestigator.com). Levels are represented as log2 TPM (Transcripts Per Million mapped reads). Abbreviations: DPA, days post-anthesis; IG, immature green; MG, mature green; B, breaker; O, orange, R, red. YL, young leaves; ML, mature leaves.

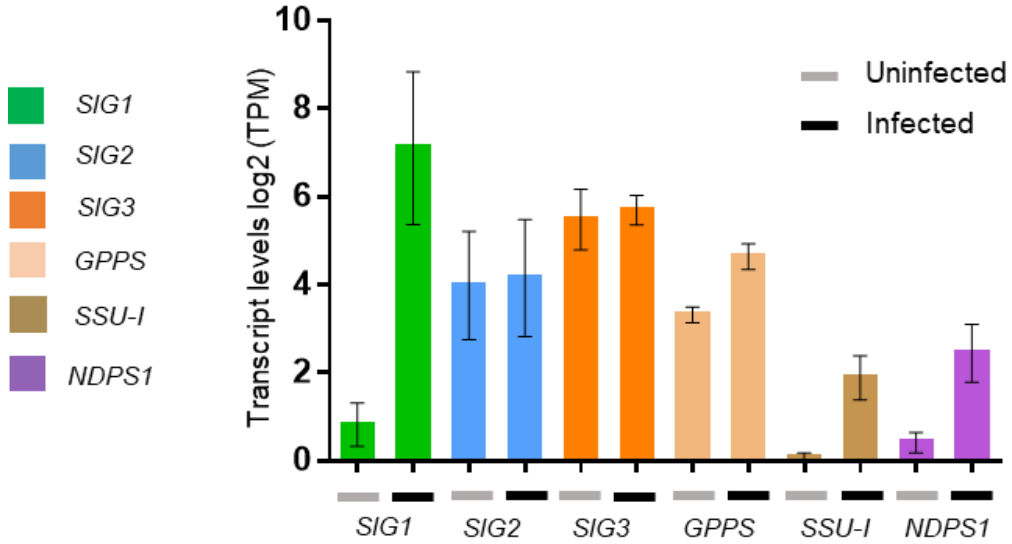

Figure S4. Expression levels of *SlGGPPS, SlGPPS, SlSSUI and SlNPS1* in leaves after *Pseudomonas syringae* infection. RNAseq data obtained from Genevestigator (https://genevestigator.com) of three different tomato infection experiments with *P.syringae pv. tomato* DC3000. Two different tomato cultivars were used, Ailsa Craig (Yang et al. 2016) and Rio Grande (Rosli et al., 2013; Pombo et al., 2014). Samples were collected at 9 (Ailsa Craig) or 6 (Rio Grande) hours post infection, respectively. Plots show the transcript levels of the indicated genes in leaves of both cultivars during P. *P.syringae pv. tomato* DC3000 infection and are shown as log2 TPM (Transcripts per Million mapped reads).

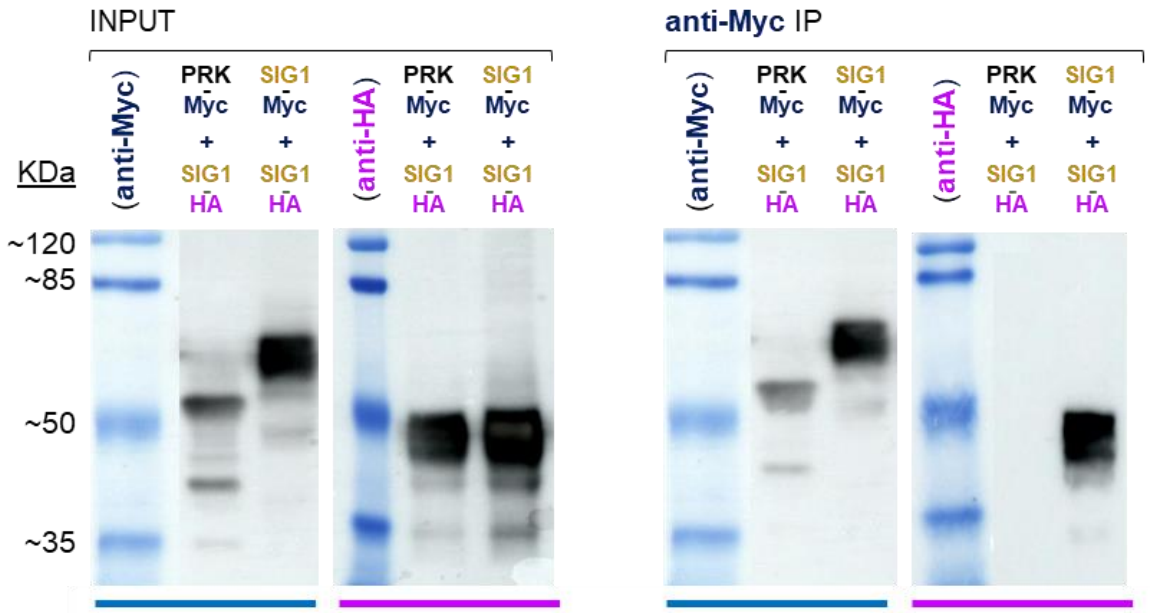

Figure S5. SlG1-Myc is able to specifically bind to protein partners. *N. benthamiana* leaves were co-agroinfiltrated with constructs encoding the indicated proteins tagged with C-terminal Myc or HA epitopes. Immunoblot analysis of crude extracts (INPUT) with anti-Myc (dark blue) and anti-HA (purple) antibodies was carried out to confirm successful protein production. The same samples were used for immunoprecipitation (IP) with anti-Myc followed by immunodetection with anti-Myc (to confirm successful IP) or anti-HA (to identify co-immunoprecipitated partners). Predicted protein molecular weights (KDa): PRK-Myc, 52.1; SlG1-Myc, 56.9; SlG1-HA 47.8.

Table S1. List of primers used in this work

Use	#	Name	Sequence (5'-3')[1]
Cloning	1	SlG1-attB1-F	**GGGGACAAGTTTGTACAAAAAAGCAGGCTGG**ATGGCATTTTTAGCTACCATTTCTG
	2	SlG1-attB2-R	**GGGGACCACTTTGTACAAGAAAGCTGGGTG**ATTCTGTCGATTTGCAATATAACTAGC
	3	SlPSY3-attB1-F	**GGGGACAAGTTTGTACAAAAAAGCAGGCTGG**ATGTGTCCAGCAACACTTTCTTATT
	4	SlPSY3-attB2-R	**GGGGACCACTTTGTACAAGAAAGCTGGGTG**TTGAATGGCTAAACTAGGCAAAGATAAAG
	5	AtPRK-attB1-F	**GGGGACAAGTTTGTACAAAAAAGCAGGCT**ATGGCTGTCTCAACTATCTAC
	6	AtPRK-attB2-R	**GGGGACCACTTTGTACAAGAAAGCTGGGT**CGGCTTTAGCTTCTGCACGAGC
RT-qPCR	7	SlPSY1-qPCR-F	ACAGGCAGGTCTATCCGATG
	8	SlPSY1-qPCR-R	ACGCCTTTCTCTGCCTCATC
	9	SlPSY2-qPCR-F	CAGGGCTCTCCGATGAAGAC
	10	SlPSY2-qPCR-R	CACCGGCCATCTACTAGCAG
	11	SlPSY3-qPCR-F	TTGGATGCAATAGAGGAGAATG
	12	SlPSY3-qPCR-R	ATTGAATGGCTAAACTAGGCAAAG
	13	SlG1-qPCR-F	GGCCTTTGAACATGTGGCTACC
	14	SlG1-qPCR-R	ACTCGCCAAGTCCACAATTTGC
	15	SlG2-qPCR-F	AAAGTCATCGTCGGAGCTCG
	16	SlG2-qPCR-R	GTTTAGCTTCGCCGTTGAGC
	17	SlG3-qPCR-F	AGGAGGTGCACCAGATGAAG
	18	SlG3-qPCR-R	TCAGCAACCAAGTCCTTCCC
	19	SlACT4-qPCR-F	CCTTCCACATGCCATTCTCC
	20	SlACT4-qPCR-R	CCACGCTCGGTCAGGATCT
	21	SlSSUI-qPCR F	GGACAGCTAGAAGGCCAATATC
	22	SlSSUI-qPCR R	GCTCCACATGCATGAATTTCC
sgRNAs for CRISPR-Cas9 gene impairment	23	SlG1-sgRNA-1 F	ATTGGTTCAGCTGTTGGCTCAGAA
	24	SlG1-sgRNA-1 R	AAACTTCTGAGCCAACAGCTGAAC
	25	SlG1-sgRNA-2 F	ATTGGTACATTCACCACCATAAGA
	26	SlG1-sgRNA-2 R	AAACTCTTATGGTGGTGAATGTAC
CRISPR plants genotyping	27	SlG1 Geno F	GCTTGCGCAGTTGAGATGATCC
	28	SlG1 Geno R	GGTCCTTACCCGCTGTCTTTCC
	29	Cas9 F	TCCCTCATCAGATCCACCTC
	30	Cas9 R	CTGAAACGTGAGCCTTCTGG
	31	NTP II F	GAAGGGGATAGAAGGCGA
	32	NTP II R	AGATGGATTGCACGCAGG

[1]Gateway recombination sites in bold

Table S2. Constructs and cloning details.

Use	Construct	Template	Primers[1]	Sequence cloned[2]	Cloning method	Entry plasmid	Destiny plasmid
Co-immunoprecipitation assays	*SlG1-HA*	Tomato root cDNA	1+2	$SlG1_{1-1098}$	Gateway	pDONR207	pGWB414
	SlPSY1-HA	Tomato fruit cDNA		$SlPSY1_{1-1236}$	Gateway	pDONR207	pGWB414
	SlPSY2-HA	Tomato leaf cDNA		$SlPSY2_{1-1314}$	Gateway	pDONR207	pGWB414
	SlPSY3-HA	Tomato root cDNA	3+4	$SlPSY3_{1-1186}$	Gateway	pDONR207	pGWB414
	SlG1-Myc	Tomato root cDNA	1+2	$SlG1_{1-1098}$	Gateway	pDONR207	pGWB420
	SlG2-Myc	Tomato flower cDNA		$SlG2_{1-1089}$	Gateway	pDONR207	pGWB420
	SlG3-Myc	Tomato flower cDNA		$SlG3_{1-1080}$	Gateway	pDONR207	pGWB420
	AtPRK-Myc	Arabidopsis seedling cDNA	5+6	$AtPRK_{1-1556}$	Gateway	pDONR207	pGWB417
CRISPR-Cas9 gene impairment	*pEN-SlG1(sg1)*	-	23+24	$SlG1_{644-664}$	*BbsI* / T4 ligase	pENC1.1	-
	pEN-SlG1(sg2)	-	25+26	$SlG1_{732-752}$	*BbsI* / T4 ligase	pENC1.1	-
	pDE-SlG1(1+2)	*pEN-SlG1(sg1) + (sg2)*	-	$SlG2_{644-664}$ + $SlG2_{732-752}$	(*sg1*)*MluI* + *Bsu36I* / T4 ligase (sg2)Gateway	*pEN-SlG1(sg1) + (sg2)*	pDE-Cas9

[1]Constructs without primers reported in Barja et al.(2021)

[2]Numbers indicate the first and last nucleotide positions cloned from the coding sequence of the indicated gene.

Table S3. Co-expression of tomato GGPPS paralogs (guide genes) with isoprenoid-related genes (query genes) in root tissue. Significant pairwise Pearson correlations between guide and query genes (≥0.55) are highlighted in red (when positive) or green (when negative). Arabidopsis genes were used as queries to search for tomato homologs in PLAZA 4 (https://bioinformatics.psb.ugent.be/plaza/versions/plaza_v4_dicots/). Genes are organized by pathways.

			GGPPS1	GGPPS2	GGPPS3
Pathway/Family	Name	SOL Tomato gene	Solyc11g011240	Solyc04g079960	Solyc02g085700
MEP	DXS1	Solyc01g067890	0,227817285	-0,432217062	0,28528147
MEP	DXS2	Solyc11g010850	0,997036917	-0,103686573	0,326655343
MEP	DXS3a	Solyc01g028900	0,055742093	-0,087928801	0,718940454
MEP	DXS3b	Solyc08g066950	0,639972045	-0,070017463	0,741305712
MEP	DXR1	Solyc03g114340	0,983938259	-0,082546381	0,410076944
MEP	DXR2	Solyc06g060860	0,199524053	0,166352456	-0,292225453
MEP	CMK	Solyc01g009010	0,884968181	0,014512289	0,480860925
MEP	MCT	Solyc01g102820	0,488415714	0,40006911	0,364206591
MEP	MDS	Solyc08g081570	0,213003447	0,122519655	0,623933883
MEP	HDS	Solyc11g069380	0,882686457	0,057137735	0,423279789
MEP	HDR	Solyc01g109300	-0,092325695	-0,444207896	-0,15767962
IDI	IDI1	Solyc08g075390	-0,053766114	-0,27002078	0,408431113
IDI	IDI2	Solyc05g055760	-0,01368272	0,152778807	0,657783139
IDI	IDI3	Solyc04g056390	0,29426506	-0,292380737	0,371964203
GGDR	GGDR1	Solyc01g088310	-0,130952114	0,708765564	-0,384847304
GGDR	GGDR2	Solyc03g115980	-0,396270784	0,152964101	-0,09490842
Tocopherols	HPPD1/PDS1a	Solyc05g041200	-0,003258982	-0,363823003	0,48259298
Tocopherols	HPPD2/PDS1b	Solyc07g045050	0,002860197	-0,071459139	-0,200460026
Tocopherols	VTE2	Solyc07g017770	0,553561893	0,064150277	0,381503736
Tocopherols	VTE3a	Solyc03g005230	0,424721351	0,110779221	0,105863188
Tocopherols	VTE3b	Solyc09g065730	0,228218686	0,081748204	0,610840864
Tocopherols	VTE1	Solyc08g068570	0,616813434	0,325744429	0,431115249
Tocopherols	VTE4a	Solyc08g076360	-0,151515162	0,236492581	0,506975932
Tocopherols	VTE4b	Solyc04g063230	-0,110780823	0,36361524	-0,302450315
Tocopherols	VTE4c	Solyc08g077240	-0,303071631	-0,145364926	-0,583830612
Tocopherols	VTE4d	Solyc03g116150	-0,290047454	-0,003146301	0,334972422
Chlorophyll synthesis	HEMA1	Solyc04g076870	-0,105259917	-0,274261136	0,419202338
Chlorophyll synthesis	HEMA2	Solyc01g106390	0,040718913	-0,159382416	0,72009636
Chlorophyll synthesis	HEMA3	Solyc01g089840	#N/D	#N/D	#N/D
Chlorophyll synthesis	GSA	Solyc04g009200	-0,082894254	-0,089319358	0,612747431
Chlorophyll synthesis	HEMB	Solyc08g069030	-0,151430238	-0,405537832	0,478103613
Chlorophyll synthesis	HEMC	Solyc07g066470	-0,071151521	0,459018759	0,129818671
Chlorophyll synthesis	HEMD	Solyc04g079320	0,469479524	-0,246514255	0,214036299
Chlorophyll synthesis	HEME1	Solyc10g007320	0,465700714	0,057792204	0,15566927
Chlorophyll synthesis	HEME2	Solyc06g048730	0,211799103	-0,094178477	0,065673668
Chlorophyll synthesis	HEMF	Solyc10g005110	0,665308945	0,044622375	0,339341703
Chlorophyll synthesis	HEMG1	Solyc01g079090	0,117133036	-0,407554853	0,350194089
Chlorophyll synthesis	HEMG2	Solyc03g005080	0,467537798	-0,369333515	0,659054874
Chlorophyll synthesis	CHLH	Solyc04g015750	-0,26701238	-0,110482093	-0,566896786
Chlorophyll synthesis	CHLI	Solyc10g008740	0,594459595	-0,038296053	-0,114544313
Chlorophyll synthesis	CHLD	Solyc04g015490	0,556081009	-0,167039536	0,183230703
Chlorophyll synthesis	CHLM	Solyc03g118240	0,458485616	0,400565799	0,182033019
Chlorophyll synthesis	CHL27-CRD	Solyc10g077040	-0,223630138	-0,00816874	-0,307798293
Chlorophyll synthesis	DVR	Solyc01g067290	-0,010768598	0,348905198	0,097673629
Chlorophyll synthesis	PORA	Solyc12g013710	-0,134290208	-0,112528933	0,241062199
Chlorophyll synthesis	PORB	Solyc07g054210	-0,196642498	-0,364421753	-0,136536604
Chlorophyll synthesis	PORC	Solyc10g006900	0,099037913	0,045790641	-0,121562843
Chlorophyll synthesis	CHLG1	Solyc05g024190	-0,162371852	0,001311095	0,31995561
Chlorophyll synthesis	CHLG2	Solyc09g014760	0,467429605	0,065746944	-0,1716427
Chlorophyll synthesis	CAOa	Solyc06g060310	-0,140415216	-0,307867459	-0,346880611
Chlorophyll synthesis	CAOb	Solyc11g012850	-0,134284865	-0,135540982	0,160700206

			GGPPS1	GGPPS2	GGPPS3
Pathway/Family	Name	SOL Tomato gene	Solyc11g011240	Solyc04g079960	Solyc02g085700
Chlorophyll degradation	CHL1	Solyc09g065620	#N/D	#N/D	#N/D
Chlorophyll degradation	CHL2a	Solyc06g053980	0,135263552	0,414254359	-0,090432445
Chlorophyll degradation	CHL2b	Solyc09g082600	-0,189527461	-0,431145721	-0,485581871
Chlorophyll degradation	CHL2c	Solyc12g005300	0,063207593	0,494543447	-0,189462652
Chlorophyll degradation	CLD1	Solyc02g070490	0,097418732	-0,019030447	-0,121496138
Chlorophyll degradation	SGR1	Solyc08g080090	0,334525535	0,351924964	0,239984752
Chlorophyll degradation	SGR2	Solyc12g056480	#N/D	#N/D	#N/D
Chlorophyll degradation	SGR3	Solyc04g063240	#N/D	#N/D	#N/D
Chlorophyll degradation	PPH	Solyc01g088090	-0,02570926	0,102250436	0,624178482
Chlorophyll degradation	PAO1	Solyc11g066440	0,075470096	-0,407248086	0,574465029
Chlorophyll degradation	PAO2	Solyc04g040160	#N/D	#N/D	#N/D
Chlorophyll degradation	PAO3	Solyc12g096550	-0,441818414	-0,426715473	-0,264975363
Chlorophyll degradation	RCCR	Solyc03g044470	0,252496332	-0,050336257	0,221137805
Chlorophyll degradation	PK1	Solyc03g071720	0,306310405	-0,274536284	0,638200534
Chlorophyll degradation	PK2	Solyc09g018510	-0,002769879	-0,124326081	-0,192384004
Chlorophyll degradation	NYC1	Solyc07g024000	0,079814353	-0,037916608	0,65448831
Chlorophyll degradation	CBR/NOL	Solyc05g032660	0,747124715	0,111886245	0,146036329
Chlorophyll degradation	HCAR	Solyc09g091100	-0,0128925	-0,289975445	-0,294073066
Phyllooquinone	ICS1/MENF	Solyc06g071030	#N/D	#N/D	#N/D
Phyllooquinone	PHYLLO/MEND1	Solyc04g005190	0,610474528	-0,184506979	0,118924512
Phyllooquinone	PHYLLO/MEND2	Solyc04g005200	0,622287417	0,021210242	-0,02088809
Phyllooquinone	PHYLLO/MEND3	Solyc04g005180	0,475484562	-0,108459214	0,163378551
Phyllooquinone	AAE14	Solyc02g069920	0,06366328	0,073537116	-0,109614114
Phyllooquinone	DHNS/MENB	Solyc05g005180	0,811508543	-0,001651354	0,216802597
Phyllooquinone	DHNAT1	Solyc02g078410	-0,143053242	-0,125034472	0,501479632
Phyllooquinone	DHNAT2	Solyc03g006440	#N/D	#N/D	#N/D
Phyllooquinone	DHNAT3	Solyc03g006450	#N/D	#N/D	#N/D
Phyllooquinone	ABC4	Solyc01g105460	0,45668733	0,076177322	0,606850632
Phyllooquinone	MENG	Solyc12g019010	0,355667655	-0,429933867	-0,182348
Plastoquinone	TAT7/HPPS1	Solyc10g007110	-0,211383766	0,21345445	-0,302773187
Plastoquinone	TAT7/HPPS2	Solyc12g088000	-0,23856167	0,12907316	-0,477127228
Plastoquinone	TAT7/HPPS3	Solyc12g096240	-0,183757802	0,101931181	0,050024062
Plastoquinone	PDS2/HST	Solyc03g051810	0,449387501	-0,187413559	0,21955408
Plastoquinone	AAAT1	Solyc07g053720	-0,015951791	-0,366235433	0,43220791
Plastoquinone	AAAT2	Solyc10g008200	0,217492085	0,566893925	0,166994149
Plastoquinone	AAAT3	Solyc07g053710	0,17507915	0,196294288	0,588052247
Plastoquinone	ACS12	Solyc03g007070	-0,050853036	-0,291718623	-0,376091867
Plastoquinone	TAA1	Solyc05g031600	-0,259243414	-0,139275642	-0,375694205
Carotenoids	PSY1	Solyc03g031860	0,48436295	-0,068458482	0,183689089
Carotenoids	PSY2	Solyc02g081330	-0,372992877	0,255376259	-0,563151392
Carotenoids	PSY3	Solyc01g005940	0,9887403	-0,031173898	0,291125507
Carotenoids	PDS	Solyc03g123760	0,993379539	-0,045712605	0,322656275
Carotenoids	ZDS	Solyc01g097810	0,960459119	-0,021713467	0,302818591
Carotenoids	Z-ISO	Solyc12g098710	0,738619978	-0,091519099	0,551931703
Carotenoids	CRTISO1	Solyc10g081650	0,943765101	-0,100731764	0,464601885
Carotenoids	CRTISO2	Solyc05g010180	#N/D	#N/D	#N/D
Carotenoids	LCY-B1	Solyc04g040190	-0,060826955	0,034921071	0,126715816
Carotenoids	LCY-B2 (CYC-B)	Solyc10g079480	0,47083548	0,004718384	0,258287127
Carotenoids	LCY-E	Solyc12g008980	#N/D	#N/D	#N/D
Carotenoids	BCH1	Solyc06g036260	-0,494401783	-0,110140751	-0,278124838
Carotenoids	BCH2	Solyc03g007960	0,022206108	0,123623457	-0,182607406
Carotenoids	CYP97B3	Solyc05g016330	0,247342197	-0,15114203	-0,143317243
Carotenoids	CYP97A3	Solyc04g051190	0,934087572	0,079186798	0,433488572
Carotenoids	CYP97C1	Solyc10g083790	0,656435414	0,092000116	0,720760803
Carotenoids	ZEP1	Solyc06g060880	0,092497037	0,119284103	-0,356821625
Carotenoids	NSY1	Solyc02g089050	-0,141068334	0,150647962	-0,429764058
Carotenoids	VDE	Solyc04g050930	0,710345593	0,09745212	0,163692149

			GGPPS1	GGPPS2	GGPPS3
Pathway/Family	Name	SOL Tomato gene	Solyc11g011240	Solyc04g079960	Solyc02g085700
Carotenoid degradation	CCD1A	Solyc01g087250	0,897385096	-0,097410517	0,413828304
Carotenoid degradation	CCD1B	Solyc01g087260	-0,486507306	-0,319343808	0,12600825
Carotenoid degradation	CCDX	Solyc08g066720	0,962831828	0,005214157	0,244918912
Carotenoid degradation	CCD4A	Solyc08g075480	#N/D	#N/D	#N/D
Carotenoid degradation	CCD4B	Solyc08g075490	#N/D	#N/D	#N/D
Orange	Or1	Solyc03g093830	0,956695311	-0,047672533	0,407062323
Orange	Or2	Solyc09g010110	0,429020461	-0,375775452	0,375550783
ABA	NCED2	Solyc08g016720	0,877409595	0,007780788	0,427354139
ABA	NCED3	Solyc07g056570	0,471895819	0,112222671	0,570947911
ABA	NCED6	Solyc05g053530	#N/D	#N/D	#N/D
ABA	ABA2a	Solyc04g071940	0,028984238	0,338164225	-0,549218342
ABA	ABA2b	Solyc04g071960	#N/D	#N/D	#N/D
ABA	ABA2c	Solyc10g085380	-0,288588412	0,346337388	-0,511417212
ABA	ABA2d	Solyc11g018600	#N/D	#N/D	#N/D
ABA	AAO3a	Solyc11g065920	0,053296522	-0,464463544	0,571416643
ABA	AAO3b	Solyc11g065930	-0,22308611	0,03808593	0,499516268
ABA	ABA3	Solyc07g066480	0,498915173	0,063687929	0,200693733
ABA	ABA4	Solyc02g063170	-0,388641886	-0,152190581	-0,427829713
ABA	CYP707A1	Solyc04g078900	#N/D	#N/D	#N/D
ABA	CYP707A2	Solyc08g075320	0,121000641	-0,263589633	-0,418754624
ABA	CYP707A3a	Solyc01g108210	0,191959425	-0,166036381	0,502077133
ABA	CYP707A3b	Solyc08g005610	0,005129081	-0,321170606	-0,244657287
ABA	CYP707A3c	Solyc04g071150	0,911640177	-0,093816362	0,087467239
ABA	CYP707A3d	Solyc04g080650	-0,279642404	0,32164075	0,116087837
ABA	ABA1/ZEP	Solyc02g090890	-0,51934943	-0,030013217	-0,538058819
ABA	NSY3	Solyc02g086050	0,185788857	0,303292174	0,269656709
ABA	NSY5	Solyc06g074240	0,992272356	-0,075441014	0,340861095
SLs	MAX3 (CCD7)	Solyc01g090660	0,992904154	-0,106902828	0,300371981
SLs	MAX1	Solyc08g062950	0,986086882	-0,065425469	0,276445814
SLs	MAX4 (CCD8)	Solyc08g066650	0,996596827	-0,059714661	0,297058985
Giberellins	CPS1	Solyc06g084240	0,997400089	-0,102023381	0,306665528
Giberellins	CPS2	Solyc08g005710	#N/D	#N/D	#N/D
Giberellins	CPS3	Solyc09g065230	#N/D	#N/D	#N/D
Giberellins	KS1a	Solyc07g066670	0,797763542	0,116676707	0,341005665
Giberellins	KS1b	Solyc08g005720	0,45802595	0,427222273	-0,164064737
Giberellins	GA3	Solyc04g083160	0,99177426	-0,02644603	0,273361971
Giberellins	KAO1	Solyc01g080900	0,925218611	0,063463248	0,195364444
Giberellins	KAO2	Solyc08g007050	#N/D	#N/D	#N/D
Giberellins	KAO3	Solyc12g006460	-0,043884958	0,538148128	0,135522157
Giberellins	KAO4	Solyc10g007860	#N/D	#N/D	#N/D
Giberellins	GA20ox1	Solyc03g006880	0,990700671	-0,061266037	0,279604246
Giberellins	GA20ox2	Solyc09g009110	#N/D	#N/D	#N/D
Giberellins	GA20ox3	Solyc11g072310	0,764067607	0,079907645	0,030099693
Giberellins	GA20ox4	Solyc06g035530	#N/D	#N/D	#N/D
Giberellins	GA20ox5	Solyc01g093980	0,979136723	-0,070374827	0,274557014
Giberellins	GA20ox6	Solyc06g050110	#N/D	#N/D	#N/D
Giberellins	GA20ox7	Solyc11g013360	#N/D	#N/D	#N/D
Giberellins	GA3ox1	Solyc06g066820	0,97438317	-0,042467304	0,262767095
Giberellins	GA3ox2	Solyc03g119910	#N/D	#N/D	#N/D
Giberellins	GA3ox3	Solyc00g007180	#N/D	#N/D	#N/D
Giberellins	GA3ox4	Solyc01g058250	-0,158328167	-0,133515069	0,596201491
Giberellins	GA3ox5	Solyc05g052740	#N/D	#N/D	#N/D

			GGPPS1	GGPPS2	GGPPS3
Pathway/Family	Name	SOL Tomato gene	Solyc11g011240	Solyc04g079960	Solyc02g085700
MVA pathway	HMGS1	Solyc08g080160	#N/D	#N/D	#N/D
MVA pathway	HMGS2	Solyc08g007790	-0,082203011	-0,171648603	0,636394447
MVA pathway	HMGS3	Solyc12g056450	0,108375307	-0,083799696	-0,282527204
MVA pathway	HMGS4	Solyc08g080170	-0,119184485	0,064018582	0,67219755
MVA pathway	HMGR1	Solyc03g032020	0,233838251	-0,269895899	0,493862077
MVA pathway	HMGR2	Solyc02g082260	-0,243850449	-0,482597207	-0,321043725
MVA pathway	HMGR3	Solyc02g038740	-0,08065974	-0,159039759	0,64130647
MVA pathway	HMGR4	Solyc03g032010	0,448026273	0,140362687	0,252487654
MVA pathway	MVK	Solyc01g098840	-0,101188848	-0,192849616	0,63006538
MVA pathway	PMK1	Solyc08g076140	0,118637298	-0,392787149	0,587969204
MVA pathway	PMK2	Solyc06g066310	0,063436412	-0,060619985	0,729922806
MVA pathway	MVD1	Solyc04g009650	0,028841528	0,197760815	0,612150651
MVA pathway	MVD2	Solyc11g007020	-0,120558081	-0,097527905	0,629381981
MVA pathway	AACT1	Solyc05g017760	0,185899173	0,615360485	0,347271304
MVA pathway	AACT2	Solyc07g045350	-0,108831687	-0,122710038	0,650776949
MVA pathway	AACT3	Solyc04g015100	0,088470241	0,04828122	0,728496447
FDS	FDS1	Solyc10g005840	0,523849783	-0,102281461	0,102421253
FDS	FDS2	Solyc12g015860	-0,079504135	-0,031898035	0,637541783
FDS	FDS3	Solyc10g005810	0,4018755	0,248462877	0,32880738
FDS	FDS4	Solyc10g005820	0,375810018	0,419812374	0,253962811
Ubiquinone	PPT1	Solyc03g114300	0,388805365	-0,095730347	0,673083897
Ubiquinone	CoQ3	Solyc07g055850	0,43200067	0,35963032	0,07331323
Ubiquinone	CoQ5a	Solyc01g081470	0,074871819	0,06013107	0,559041736
Ubiquinone	CoQ6	Solyc09g091570	0,68029036	-0,227989585	0,196851133

Chapter III

Overlapping and specialized roles of tomato phytoene synthase isoforms PSY1 and PSY2 in carotenoid and ABA production

Overlapping and specialized roles of tomato phytoene synthase isoforms PSY1 and PSY2 in carotenoid and ABA production

Miguel EZQUERRO[1,2], Esteban BURBANO[1], Manuel RODRIGUEZ-CONCEPCION[1]

1, Institute for Plant Molecular and Cell Biology (IBMCP), CSIC-Universitat Politècnica de València, 46022 Valencia, Spain

2, Centre for Research in Agricultural Genomics (CRAG) CSIC-IRTA-UAB-UB, Campus UAB Bellaterra, 08193 Barcelona, Spain

The results presented in this Chapter are available at bioRxiv (Ezquerro et al., 2022 doi 10.1101/2022.08.11.503628) and are under review in *Plant Physiology* (manuscript number PP2022-RA-01075).

Note: The experiments included in this Chapter were co-designed and performed by the PhD candidate under the supervision of the PhD director. EB helped providing support to the PhD candidate with sample and picture collection.

Overlapping and specialized roles of tomato phytoene synthase isoforms PSY1 and PSY2 in carotenoid and ABA production

Abstract

Carotenoids are plastidial isoprenoids required for photosynthesis and production of hormones such as abscisic acid (ABA) in all plants. In tomato (*Solanum lycopersicum*), carotenoids also provide color to flowers and ripe fruit. Phytoene synthase (PSY) catalyzes the first and main flux-controlling step of the carotenoid pathway. Three PSY isoforms are present in tomato, PSY1 to 3. Mutants have shown that PSY1 is the isoform providing carotenoids for fruit pigmentation but it is dispensable in photosynthetic tissues. No mutants are available for PSY2 or PSY3, but their expression profiles suggest a main role for PSY2 in leaves and PSY3 in roots. To further investigate isoform specialization with genetic tools, we created tomato edited lines defective in PSY1 and PSY2 in the MicroTom background. The albino phenotype of lines lacking both PSY1 and PSY2 confirmed that PSY3 does not contribute to carotenoid biosynthesis in shoot tissues. Our work further shows that carotenoid production in tomato shoots relies on both PSY1 and PSY2 but with different contributions in different tissues. PSY2 is the main isoform for carotenoid biosynthesis in leaf chloroplasts, but the supporting role of PSY1 is particularly important under high light. PSY2 also contributes to the production of carotenoids in flower petals and, to a lower extent, fruit chromoplasts. Most interestingly, our results demonstrate that fruit growth and ripening is controlled by ABA produced in the pericarp from PSY1-derived precursors whereas PSY2 provides precursors for ABA synthesis in seeds to control germination.

1 Introduction

Carotenoids are a group of isoprenoid molecules synthetized by all photosynthetic organisms and some non-photosynthetic bacteria and fungi (Rodriguez-Concepcion et al., 2018; Sun et al., 2018). Carotenoids are essential micronutrients in our diet as precursors of retinoids such as vitamin A. Their characteristic colors in the range of yellow to orange and red also make them economically relevant as natural pigments in the chemical, pharma and agrofood industry. In plants, carotenoids are essential for photosynthesis (by contributing to the assembly of the photosynthetic apparatus and by participating in light harvesting) and for photoprotection (by dissipating the excess of light energy as heat and by scavenging free radicals). They also provide color to some non-photosynthetic tissues such as flower petals and ripe fruit to attract animals for pollination and seed dispersal. Besides, carotenoids are precursors of the phytohormones abscisic acid (ABA) and strigolactones (SL) and other biologically active signals involved in plastid-to-nucleus communication (e.g., beta-cyclocitral) and environmental interactions (e.g., apocarotenoids modulating root mycorrhization), among other processes (Moreno et al., 2021; Sun et al., 2018).

Carotenoids in plants are produced in plastids from geranylgeranyl diphosphate (GGPP) produced by the methylerythritol 4-phosphate (MEP) pathway (Figure 1). GGPP is also used to produce other essential isoprenoids in the plastid, including plastoquinone, phylloquinone, tocopherols and chlorophylls (Rodriguez-Concepcion et al., 2018). The first committed step of carotenoid biosynthesis is the condensation of two GGPP molecules to produce phytoene (Figure 1A). This step is catalyzed by phytoene synthase (PSY), the main flux-controlling enzyme of the carotenoid pathway (Cao et al., 2019; Zhou et al., 2022). Several desaturation and isomerization steps convert uncolored phytoene into red lycopene. From lycopene, carotenoid synthesis branches out depending on the type of cyclization of the ends of the lycopene carbon chain. The production of two β rings at the two ends of the chain produces β-carotene (β,β branch) while the production of one β ring and one ε ring produces α-carotene (β,ε branch). Oxygenation of the rings of carotenes produces xanthophylls such as violaxanthin and neoxanthin (β,β branch) or lutein (β,ε branch) (Figure 1).

Tomato (*Solanum lycopersicum*) is a very well-suited model system to study carotenoid biosynthesis. Like all plants, tomato produces carotenoids for photosynthesis and photoprotection in chloroplasts and uses them as precursors to produce ABA and SLs in photosynthetic and non-photosynthetic tissues. But unlike Arabidopsis (*Arabidopsis thaliana*) and other plant models, tomato accumulates high levels of carotenoids in

specialized plastids named chromoplasts, which are present in flower petals and ripe fruit. Also different from Arabidopsis, which only has a single PSY (At5g17230), the tomato genome harbors three PSY-encoding genes: *PSY1* (Solyc03g031860), *PSY2* (Solyc02g081330), and *PSY3* (Solyc01g005940) (Giorio et al., 2008; Stauder et al., 2018). While PSY1 and PSY2 are similar proteins that share conserved sequences and have a common origin (Cao et al., 2019; Giorio et al., 2008), PSY3 belongs to a different widespread clade restricted to dicots (Stauder et al., 2018). Tomato lines defective in PSY1 have been reported as *yellow-flesh* (*r*) mutants (Fray and Grierson 1993; Kachanovsky et al., 2012; Kang et al., 2014; Karniel et al., 2022), silenced lines (Bird et al., 1991; Bramley et al., 1992.; Fantini et al., 2013; Fraser et al., 1999) and CRISPR-Cas9-edited lines (D'Ambrosio et al., 2018), but lines impaired in PSY2 or PSY3 have not been described yet. Based on gene expression data and phenotypic features of PSY1-defective lines, it was proposed that PSY3 function might be restricted to roots whereas PSY1 and PSY2 differentially support carotenogenesis in shoot tissues: PSY1 for pigmentation in chromoplasts and PSY2 for photosynthesis in chloroplasts (Fraser et al., 1999; Giorio et al., 2008; Hirschberg 2001; Stauder et al., 2018). However, other sources of evidence suggest that isoform specialization is not complete. For example, the low but statistically significant upregulation of *PSY1* during seedling de-etiolation (when carotenoids are essential for the proper assembly of the photosynthetic apparatus and for photoprotection) and the high levels of *PSY2* transcripts in flower petals (where accumulation of xanthophylls is responsible for their characteristic yellow color) allows to hypothesize that both isoforms might participate in carotenoid biosynthesis in chloroplasts and chromoplasts (Barja et al., 2021; Giorio et al., 2008). To genetically test this hypothesis, we created tomato edited lines defective in PSY1 and PSY2 in the same tomato background (MicroTom, a widely used accession in molecular biology labs all over the world) and compared their physiological and metabolic phenotypes. The albino phenotype of lines defective in both PSY1 and PSY2 confirmed that PSY3 does not contribute to carotenoid biosynthesis in shoot tissues. Our work further confirmed that PSY2 is the main isoform supporting chloroplast carotenoid biosynthesis but uncovered a supporting role for PSY1 under conditions requiring an extra supply of carotenoids such as high light exposure. PSY1 was confirmed to be the main isoform in charge of phytoene production for carotenoid pigments in the chromoplasts of flower petals and fruit pericarp. Most interestingly, lower carotenoid levels resulted in a preferential reduction of ABA levels in the fruit pericarp but not in the seeds of the *psy1* mutant, whereas loss of PSY2 caused a major reduction of ABA in seeds. This differential ABA decrease in *psy1* and *psy2* mutants allowed to establish a specific contribution of pericarp ABA to fruit growth and ripening and seed ABA to seed germination.

2 Results

2.1 Loss of both PSY1 and PSY2 causes an albino-lethal phenotype

To generate plants defective in PSY1 or/and PSY2 in the MicroTom background, we designed one single guide RNA (sgRNA) annealing on the start of the first translated exon for each gene using the online tool CRISPR-P 2.0 (Liu et al., 2017). Two independent alleles with premature translation stop codons were selected for each gene and named *psy1-1, psy1-2*, *psy2-1* and *psy2-2* (Figure 1B and Figure S1-S3). For subsequent experiments we selected homozygous lines of each allele without the Cas9-encoding transgene. In the case of *psy1-1* and *psy1-2* alleles, we observed paler yellow flowers and pale orange fruits (Figure S4), which are previously described phenotypes of *r* tomato lines, hence confirming that both were true PSY1-defective mutants. No distinctive phenotype was observed in the case of *psy2-1* and *psy2-2* lines. Analysis of transcript levels in fruits by RT-qPCR showed that loss of one of the isoforms did not influence the expression of the remaining genes (Figure S4). To assess the impact of simultaneous disruption of PSY1 and PSY2, we crossed lines defective in PSY1 (*psy1-2*, as female) and PSY2 (*psy2-1*, as male). Double heterozygous F_1 plants with normal yellow flowers and red fruits were obtained and allowed to self-pollinate. Among the segregating F_2 population we found several albino seedlings with a Mendelian proportion (1/16) consistent with this phenotype being the result of the loss of both PSY1 and PSY2 in double mutant individuals (Figure 1C). The rest of the seedlings of the F_2 population displayed a normal green phenotype indistinguishable from the MicroTom wild-type (WT). PCR-based genotyping of several individuals (Figure S5) confirmed that green seedlings showed at least one WT copy of either *PSY1* or *PSY2* whereas all albino seedlings were double homozygous mutants. These results indicate that both PSY1 and PSY2 (but not PSY3) are essential for the production of carotenoids supporting seedling establishment and photosynthetic shoot development. Consistently, *PSY3* transcripts are hardly detectable in shoot tissues whereas *PSY1* and *PSY2* transcripts are abundant in all tissues of the tomato plant (Barja et al., 2021; Giorio et al., 2008; Stauder et al. 2018) (Figure S6).

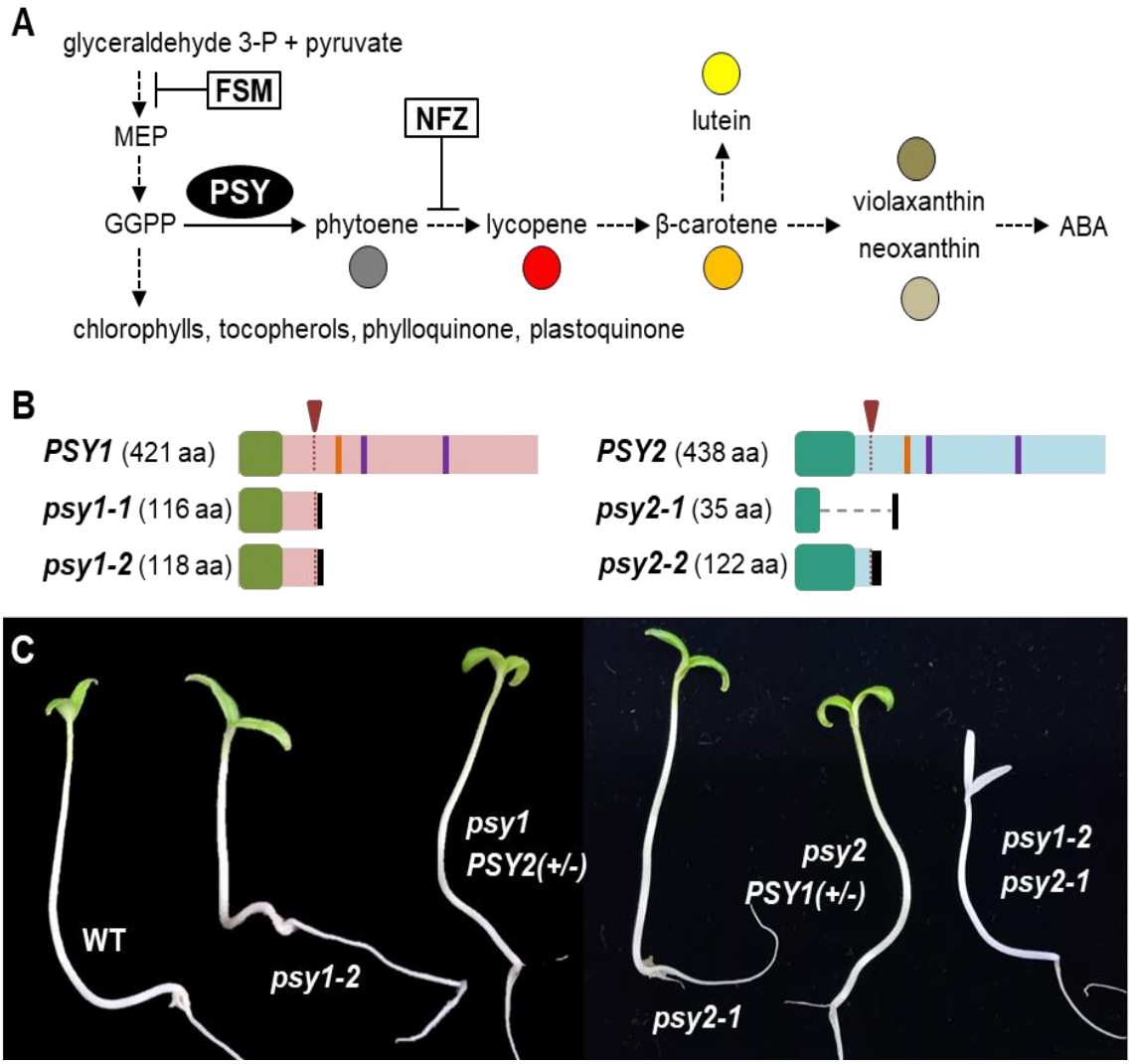

Figure 1. Carotenoid pathway and tomato mutants. (A) Carotenoid biosynthesis pathway. Dashed arrows represent multiple steps. The reaction catalyzed by phytoene synthase (PSY) is marked, and steps interrupted by inhibitors fosmidomycin (FSM) and norflurazon (NFZ) are indicated. Each individual carotenoid is represented by the indicated color (circle) in the corresponding plots representing their levels. **(B)** Scheme representing the wild-type PSY1 and PSY2 proteins and the mutant versions generated in the corresponding CRISPR-Cas9-generated alleles (see Figure S1–S3 for further details). The region targeted by the designed sgRNAs is indicated with an arrowhead and a dotted line. Orange and purple bars mark the position of conserved domains required for PSY activity (hydrophobic flap and Asp-rich domains, respectively). Green boxes represent plastid transit peptides. Black boxes represent the protein sequence resulting after a frame-shift in the mutants. The large deletion generated in the *psy2-1* allele is shown with a dashed line. **(C)** Representative seven-day-old seedlings of the indicated genotypes resulting from a cross of *psy1-2* and *psy2-1* mutants.

.

2.2 PSY2 is supported by PSY1 to produce carotenoids for photoprotection in leaves

To test whether carotenoid levels were reduced in leaves of single *psy1* and *psy2* mutant lines, we collected young emerging leaves from plants grown for 18 days under long-day conditions in the greenhouse and used them for HPLC analysis of carotenoids and chlorophylls (Figure 2). Despite WT and mutant plants were phenotypically identical (Figure 2A), a slight reduction in carotenoid levels was detected in mutant leaves compared to WT controls (Figure 2B). Chlorophylls were not as reduced as carotenoids (Figure 2B). These results suggest that both PSY1 and PSY2 can produce carotenoids in chloroplasts under normal growth conditions, as the loss of one of the isoforms can be similarly rescued by the activity of the remaining isoform. Most interestingly, photosynthetic performance was only significantly reduced in *psy2* mutant alleles, as estimated from effective quantum yield of photosystem II (ΦPSII) measurements (Figure 2C).

The main role of carotenoids in photosynthetic organs such as leaves is photoprotection against photooxidative damage associated to intense light. In particular, carotenoids can dissipate the excess of light energy as heat through a process known as non-photochemical quenching (NPQ). Consistent with this essential function of leaf carotenoids, when 10-day-old tomato plants grown under normal light (NL) conditions (50 µmol photons m^{-2} s^{-1}) were transferred to high light (HL) conditions (300 µmol photons m^{-2} s^{-1}) for 5 days, expression of genes encoding PSY1 and PSY2 and concomitant production of carotenoids were up-regulated compared to control plants leaves from NL or HL samples (Figure 3A), whereas chlorophylls remained virtually transferred for the same time to NL (Figure 3). *PSY3* transcripts were undetectable in unchanged (Figure 3B). The increase in carotenoid levels associated to HL exposure of WT plants was significantly repressed in *psy2* mutants and attenuated in *psy1* mutants (Figure 3B). The potential photosynthetic capacity estimated from the measurement of the maximum quantum yield of photosystem II (Fv/Fm) was reduced in leaves from the two *psy2* alleles under normal conditions (Figure 3C), similar to that observed for ΦPSII (Figure 2C). Upon transfer from NL to HL, Fv/Fm progressively decreased in both WT and PSY-defective mutants, but the drop was stronger in *psy1* mutants and highest in *psy2* alleles (Figure 3C). NPQ was also reduced in HL-exposed *psy1* and *psy2* mutants compared to WT controls, with *psy2* plants showing lower values than *psy1* alleles (Figure 3D). These results suggest a main role for PSY2 and a supporting role for PSY1 in supplying phytoene when enhanced carotenoid synthesis is needed for photoprotection.

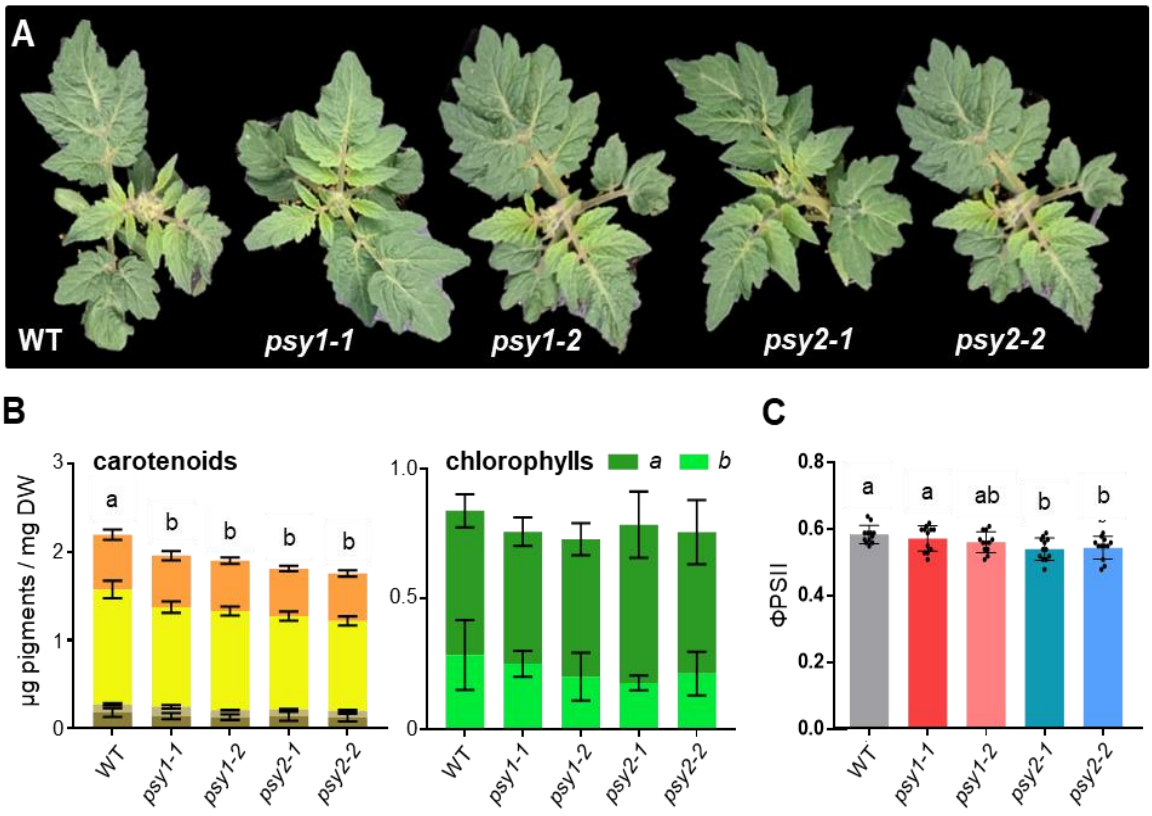

Figure 2. Tomato mutants defective in PSY1 or PSY2 show lower carotenoid levels under normal growth conditions. (A) Representative images of 4-week-old plants of the indicated lines. **(B)** Total levels of carotenoids and chlorophylls in young leaves of WT and mutant plants like those shown in (A). In the carotenoid plot, colors correspond to the species shown in Figure 1A. Mean and SD of n≥3 independent biological replicates are shown. DW, dried weight. **(C)** Effective quantum yield of photosystem II (ϕPSII) in young leaves like those used in (B). Individual values (black dots) and well as mean and SD are shown, and they correspond to four different leaf areas from three different plants. In (B) and (C), bar letters represent statistically significant differences ($P < 0.05$) among means according to post hoc Tukey's tests run when one way ANOVA detected different means.

2.3 PSY1 is supported by PSY2 to produce carotenoids for flower and fruit pigmentation

Besides their essential role in chloroplasts, carotenoids accumulate in specialized plastids named chromoplasts that provide distinctive yellow, orange and red colors to non-photosynthetic tissues such as flower petals and ripe fruit. In tomato, carotenoids (mainly conjugated xanthophylls) are responsible for the yellow color of flower petals (Figure 4) (Ariizumi et al., 2014). As previously reported for PSY1-defective lines (Bird et al., 1991; Bramley et al., 1992; Fraser et al., 1999), *psy1-1* and *psy1-2* alleles showed flowers of a paler yellow color than the WT (Figure 4A and Figure S4).

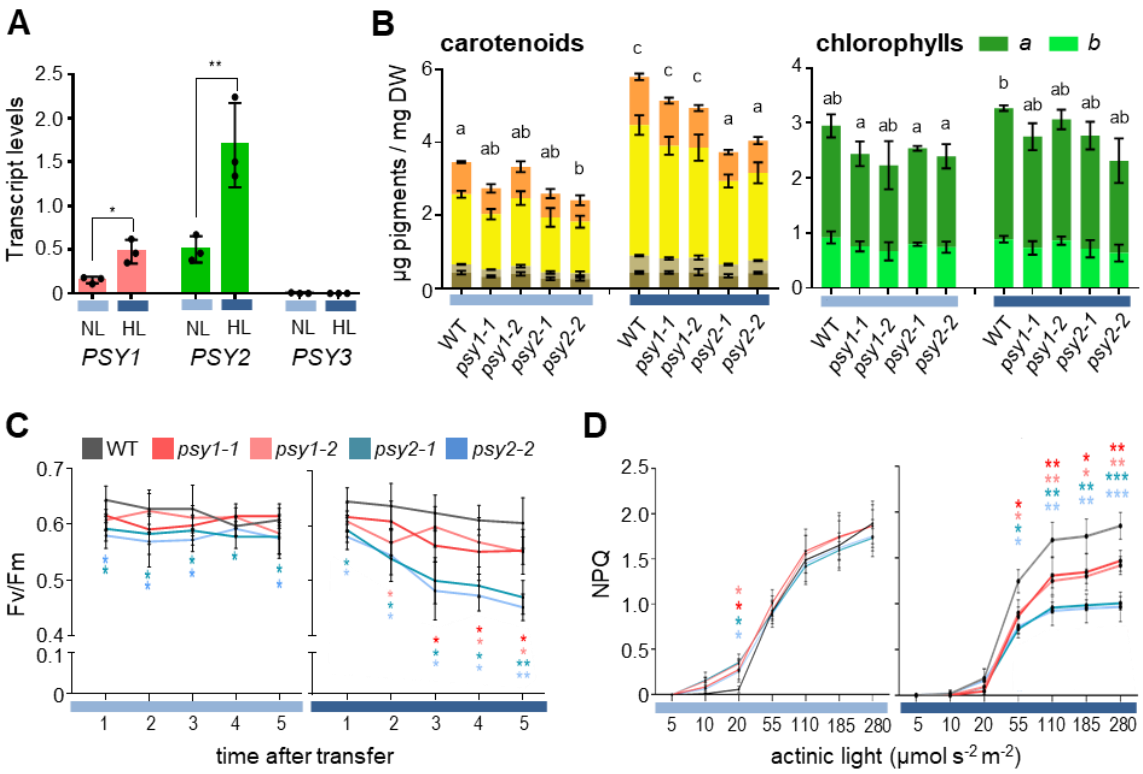

Figure 3. PSY2 is the main isoform required for photoprotection. Tomato WT and mutant seedlings germinated and grown under normal light conditions were left for 5 more days under the same light conditions (NL; pale blue) or transferred to high light (HL; dark blue) for the same time. **(A)** RT-qPCR analysis of *PSY1, PSY2* and *PSY3* transcript levels in WT seedlings at the end of the experiment normalized using the *ACT4* gene. Data correspond to mean and SD of n=3 independent biological replicates. Asterisks indicate statistically significant differences between means relative to NL conditions (*t*-test). **(B)** Total carotenoid and chlorophyll levels in WT and mutant seedlings exposed to either NL or HL. In the carotenoid plot, colors correspond to the species shown in Figure 1A. Mean and SD of n=3 independent biological replicates are shown. Bar letters represent statistically significant differences ($P < 0.05$) among means according to post hoc Tukey's tests run when one way ANOVA detected different means. **(C)** Maximum quantum yield of photosystem II (Fv/Fm) during the indicated treatments. **(D)** Non-photochemical quenching (NPQ) values at the indicated times of exposure to either NL or HL upon increasing actinic light. In (C) and (D), values represent the mean and SD of four different leaf areas from three different seedlings and asterisks indicate statistically significant differences among means in each differential time point (one way ANOVA followed by Tukey's test). *, $P < 0.05$; **, $P < 0.01$, *** $P < 0.001$).

HPLC analysis of free and conjugated xanthophyll content showed a reduction of about 50% in PSY1-defective compared to WT corollas (Figure 4B). While the absence of *PSY3* transcripts in flowers (Figure S6) suggests that PSY2 feeds the production of the carotenoids detected in PSY1-defective fruit, a reduction of PSY2 activity in *psy1-2* mutants with the *psy2-1* mutation in heterozygosis, herein referred to as *psy1 PSY2(+/-)*, resulted in only a marginal reduction in carotenoid levels compared to *psy1-2* flowers (Figure 4B). Both *psy2-1* and *psy2-2* mutant alleles showed normal-looking flowers

(Figure 4A) with a virtually WT carotenoid profile (Figure 4B), but carotenoid levels were slightly reduced in flowers of *psy2 PSY1(+/-)* plants with only one *PSY1* gene copy in a *psy2-1* background (Figure 4B). We therefore conclude that an excess of PSY1 activity ensures enough carotenoid production in tomato flower corollas.

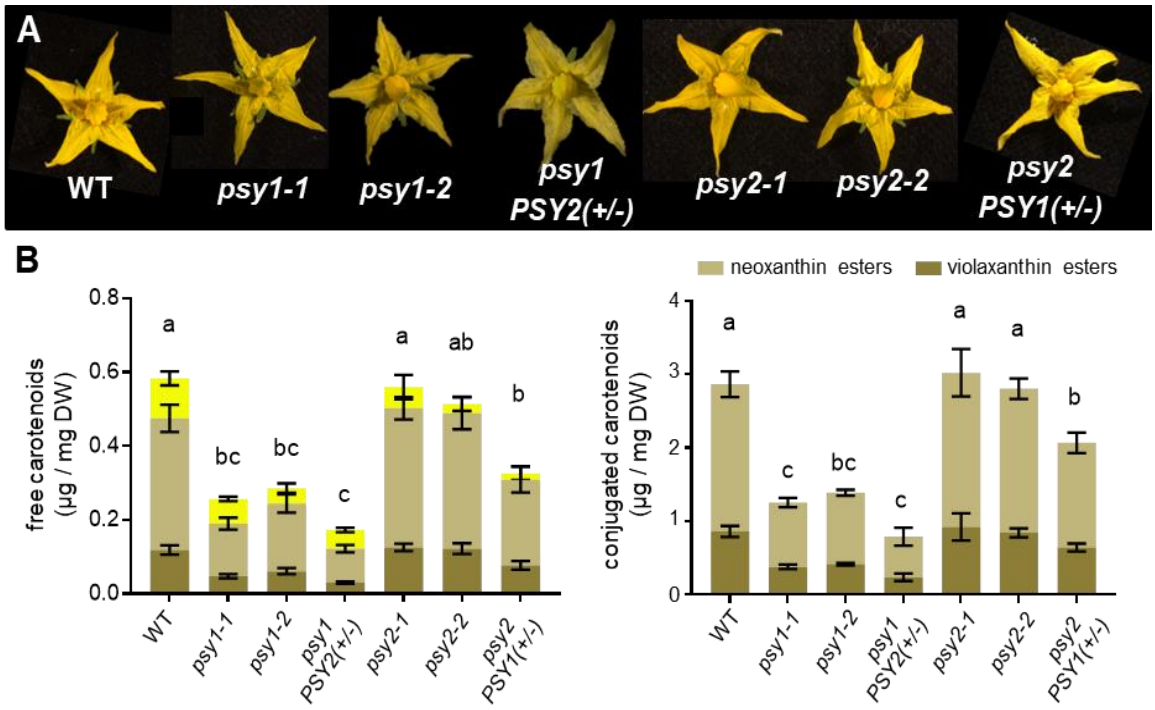

Figure 4. PSY1 is the main isoform contributing to carotenoid biosynthesis in petal chromoplasts. (A) Representative images of anthesis (fully open) flowers of the indicated lines. **(B)** Total levels of free and conjugated carotenoids in petals. In the free carotenoid plot, colors correspond to the species shown in Figure 1A. Mean and SD of n=3 independent biological replicates are shown. Bar letters represent statistically significant differences ($P < 0.05$) among means according to one way ANOVA followed by post hoc Tukey's tests.

The most characteristic phenotype of PSY1-defective tomato lines is the yellow color of the ripe fruit (Bird et al. 1991; D'Ambrosio et al., 2018; Fraser et al., 1999; Fray & Grierson, 1993; Gupta et al., 2022; Kachanovsky et al., 2012; Kang et al., 2014; Karniel et al., 2022). Tomato fruit ripening is a carotenoid-demanding process as great amounts of lycopene and, to a lower extent, β-carotene are produced to provide the characteristic red and orange color to the ripe fruit flesh: the pericarp (Figure 5).

Besides carotenoid synthesis, ripening also involves degradation of chlorophylls after the fruit reaches its final size at the mature green (MG) stage, which changes the fruit color from the breaker (B) stage (Figure 5A). Previous reports have shown that loss of PSY1 activity does not impact carotenoid levels at the MG stage but it results in a drastic reduction in pericarp carotenoid levels in ripe fruit, which show a yellowish color due to

flavonoid compounds such as naringenin chalcone (D'Ambrosio et al., 2018; Fraser et al., 1999; Fray & Grierson, 1993; Kachanovsky et al., 2012; Kang et al., 2014). Consistently, our edited lines with reduced PSY1 levels showed WT carotenoid and chlorophyll levels in the pericarp of MG fruit (Figure 5B). Also as expected, analysis of pericarp carotenoid contents at six days after the B stage (B+6) showed extremely low (but still detectable) levels of carotenoids (lutein and β-carotene) in PSY1-defective fruit (Figure 5C). To investigate the contribution of PSY2 to the residual carotenoid contents of B+6 (i.e. ripe) fruit with a complete loss of PSY1, we compared the carotenoid profile of *psy1-2* and *psy1 PSY2(+/-)* fruit. A reduction in total carotenoids was observed in *psy1-2 PSY2(+/-)* relative to *psy1-2* fruit (Figure 5C) but it was only statistically significant for β-carotene. In agreement with the conclusion that PSY1 is by far the main contributor to carotenoid production in the pericarp of ripe fruit, complete loss of PSY2 in single *psy2-1* mutant fruit had no impact in carotenoid levels compared to WT fruit whereas a statistically significant reduction of pigment contents was found when PSY1 activity was genetically reduced in *psy2 PSY1(+/-)* fruit (Figure 5C).

After the B stage, our *psy1-2* and *psy1 PSY2(+/-)* fruits acquired a distinctive yellowish color but PSY2-defective *psy2-1* and *psy2 PSY1(+/-)* fruits were undistinguishable from WT fruits (Figure 5A). Color analysis using TomatoAnalyzer showed that color changes in *psy2-1* and *psy2-2* fruits occurred at a similar rate as in WT controls (Figure 6A). To test whether mutant fruit showed other ripening-associated phenotypes besides color, the expression of ripening marker genes such as *E8* (Solyc09g089580) and *ACS2* (Solyc01g095080) was quantified by RT-qPCR (Barja et al., 2021). As shown in Figure 6B, the expression profile of these genes was very similar in WT and *psy2-1* fruit during ripening. By contrast, the peak of *E8* and *ACS2* expression observed at the B stage was significantly reduced in *psy1-2* fruit (Figure 6B).

2.4 PSY1 and PSY2 are major contributors to ABA synthesis in tomato fruit pericarp and seeds, respectively

ABA is a carotenoid-derived phytohormone (Figure 1A) which, besides regulating plant adaptation to abiotic stress conditions and promoting seed dormancy, appears to regulate fruit growth and development in tomato (Leng et al., 2014; Nambara & Marion-Poll, 2005; Zhang et al., 2009).

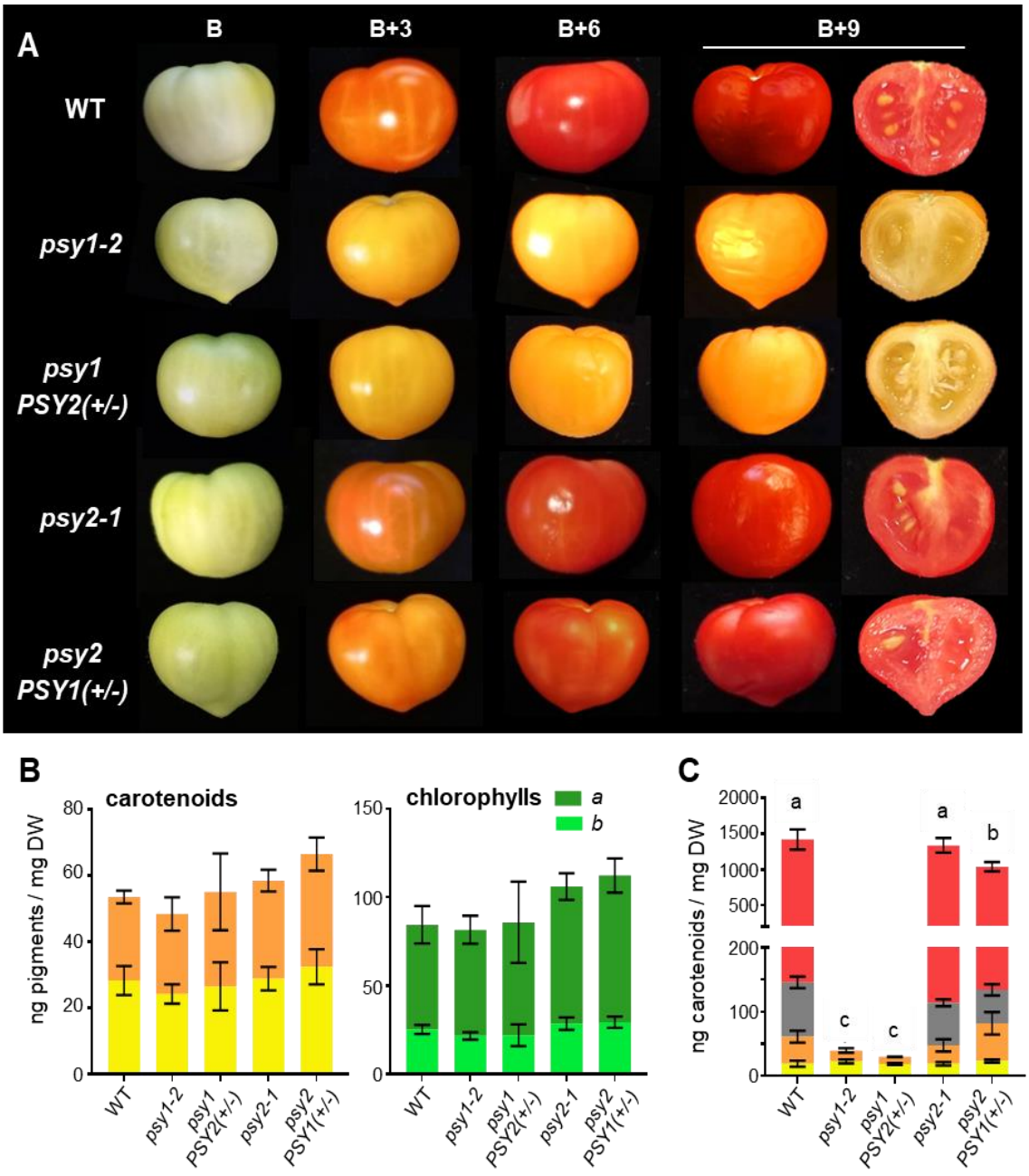

Figure 5. PSY1 is the main isoform contributing to carotenoid biosynthesis in fruit pericarp chromoplasts. **(A)** Representative images of WT and mutant fruit collected at the breaker (B) stage and left to ripe off-vine in a controlled environment chamber for the indicated times (in days). **(B)** Total carotenoid and chlorophyll levels in WT and mutant in the pericarp of fruit collected from the plants at the MG stage. **(C)** Total carotenoid levels in WT and mutant in the pericarp of fruit collected from the plants at the B+6 stage. In the carotenoid plots, colors correspond to the species shown in Figure 1A. In all the plots, mean and SD of n=3 independent biological replicates are shown. Bar letters represent statistically significant differences ($P < 0.05$) among means according to post hoc Tukey's tests run when one way ANOVA detected different means

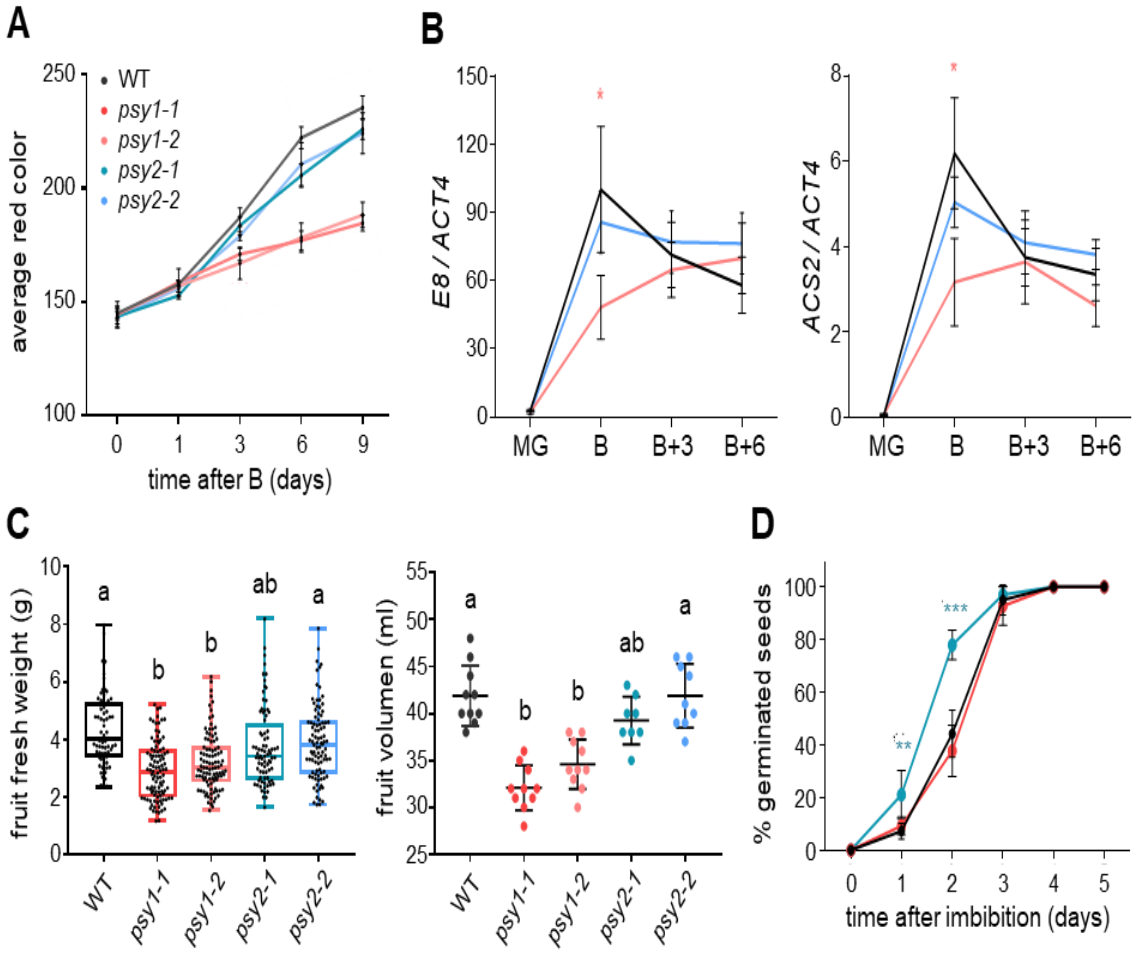

Figure 6. Fruit development and seed germination are differentially impacted in mutants defective in PSY1 or PSY2. (A) Average red color quantification (arbitrary units) of fruit collected at the B stage and left to ripe off-vine in chambers for the indicated times. Values represent the mean and SD of n=3 different fruits for each time point. **(B)** RT-qPCR analysis of *E8* and *ACS2* transcript levels in WT and mutant fruit collected from the plant at the indicated stage. Data correspond to mean and SD of n=3 independent biological replicates. Asterisks indicate statistically significant differences relative to the WT (*t*-test, $P < 0.05$). **(C)** Weight and volume of fully ripe fruits of the indicated genotypes. In the boxplot, the lower and upper boundary of the boxes indicate the 25th and 75th percentile, respectively; the line inside the boxes represents the median; dots mark individual data values; and whiskers above and below the boxes indicate the maximum and minimum values. In the dot plots, central line represents the mean and whiskers represent SD. Different letters represent statistically significant differences (one way ANOVA followed by Tukey's multiple comparisons test, $P < 0.05$). **(D)** Kinetics of germination of WT and mutant seeds after imbibition. Error bars indicate SD of n=6 biological replicates with 25 seeds each. Asterisks indicate statistically significant differences among means relative to WT samples (*t*-test: **, $P < 0.01$, *** $P < 0.001$).

Indeed, reduced hormone levels in mutants defective in ABA biosynthetic genes such as *notabilis* (*NOT/NCED*), *sitiens* (*SIT/AAO3*), and *flacca* (*FLC/ABA3*) are associated to slower ripening but also to reduced fruit size and accelerated seed germination (De Castro & Hilhorst 2006; Galpaz et al., 2008; Groot & Karssen, 1992; McQuinn et al., 2020; Nitsch et al., 2012). ABA levels in pericarp and seeds peak around the B stage, preceding the burst of ethylene biosynthesis that regulates many aspects of the ripening process in a climacteric fruit such as tomato (Berry & Bewley 1992; De Castro & Hilhorst 2006; Diretto et al., 2020; Zhang et al., 2009). Quantification of ABA in pericarp and seed samples from WT and mutant fruit at the B stage showed decreased levels of the hormone in the pericarp of *psy1-2* fruit and the seeds of *psy2-1* samples (Figure 7). Consistent with the decrease in pericarp ABA levels, fruits lacking PSY1 not only showed a reduced peak of ripening-related gene expression (Figure 6B) but also lower fruit weight and volume compared to WT and PSY2-defective fruits (Figure 6C). We also analyzed the germination (root emergence) of WT and mutant seeds freshly collected from ripe fruits. Accordingly to the reduced levels of ABA in the seeds of PSY2-defective mutants (Figure 7), *psy2-1* seeds showed an accelerated germination compared to WT and *psy1-2* seeds (Figure 6D).

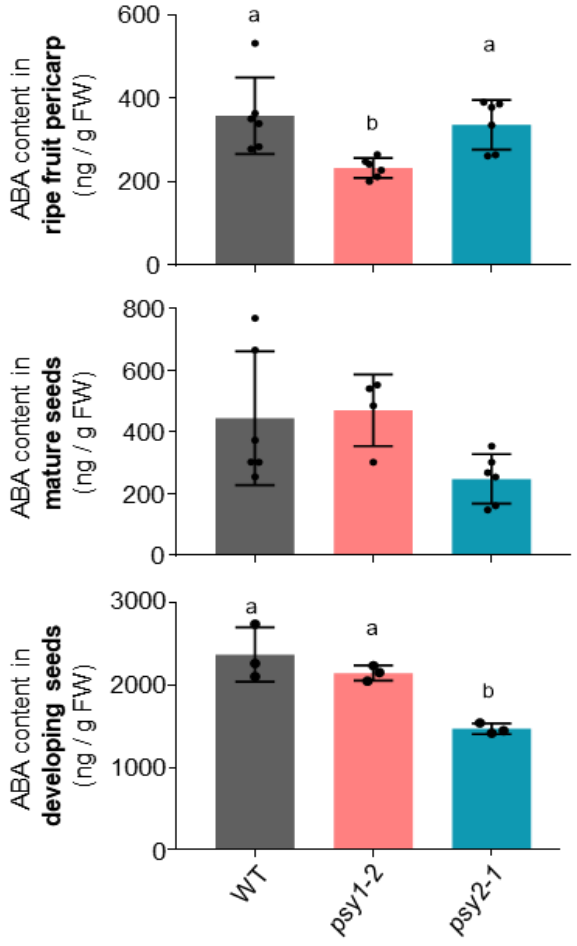

Figure 7. ABA levels are different in fruit pericarp and seed samples from mutants defective in PSY1 or PSY2. Pericarp and mature seed samples were collected from ripe (B+6) fruit, whereas developing seeds were collected from immature fruits. Values correspond to the mean and SD of samples collected from n≥3 independent fruits. Different letters represent statistically significant differences among means (one way ANOVA followed by Tukey's multiple comparisons test, $P < 0.05$).

The described data suggest that PSY1 might be most important for ABA production in the pericarp and PSY2 in seeds. This conclusion is only partially consistent with transcript abundance profiles during fruit pericarp and seed development (Figure S6-S8). In the pericarp, *PSY1* is expressed at higher levels than *PSY2* from early stages of fruit development, and the differences become much more dramatic after the MG stage (Figure S6 and S7). In developing seeds, both genes are expressed at similar levels (Figure S6 and S8) and yet ABA contents are reduced in the *psy2-1* mutant but not in the *psy1-1* line when compared to the WT (Figure 7). As fruits ripe, *PSY1* expression increases and *PSY2* expression decreases in mature seeds (Figure S6 and S8), which similar to developing seeds only show reduced ABA levels when PSY2 activity is removed (Figure 7). To provide further evidence on the role of specific PSY isoforms in the production of ABA involved in the control of seed dormancy, we blocked carotenoid production in all the tissues of MG fruits of WT and mutant fruits using specific inhibitors (Figure 8). Specifically, we used the MEP pathway inhibitor fosmidomycin (FSM) and the phytoene desaturase inhibitor norflurazon (NFZ) (Figure 1A). WT, *psy1-2* and *psy2-1* fruits were collected from the plant at the MG stage and injected with one of the inhibitors or a mock solution (water). After twelve days, WT and *psy2-1* fruits treated with either FSM or NFZ showed a yellow color identical to that of *psy1-2* fruit treated with mock or inhibitor solutions (Figure 8A), confirming that both FSM and NFZ successfully inhibited carotenoid production, at least in the pericarp. At this point, seeds were collected from the detached fruits, dried overnight, and immediately used for germination assays (Figure 8B). In the case of WT and *psy1-2* seeds, germination was accelerated by the treatment with either FSM or NFZ, suggesting an inhibitor-mediated blockage of carotenoid and hence downstream ABA production in seeds. By contrast, inhibitor treatment had no effect on the germination rate of *psy2-1* seeds (Figure 8B).

These results support the conclusion that seed dormancy is independent of the ABA content of the fruit pericarp or developing seeds but it is regulated by ABA produced in mature seeds from PSY2-derived carotenoids.

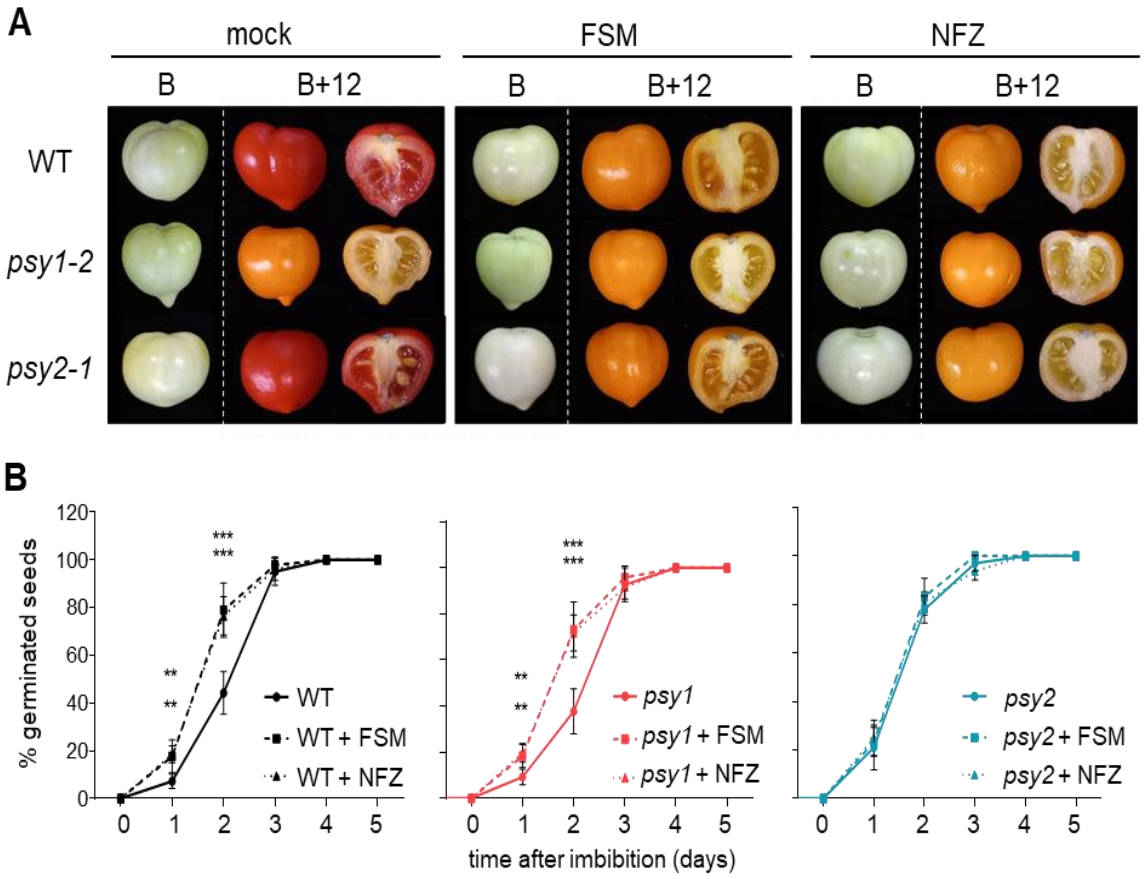

Figure 8. Germination of tomato seeds is regulated by ABA produced in mature seeds from PSY2-derived carotenoids. (A) Representative images of WT and mutant fruits treated with fosmidomycin (FSM), norflurazon (NFZ) or a mock solution at the MG stage and then allowed to ripe off-vine. **(B)** Kinetics of germination of fresh seeds collected from fruits as those shown in (A) at the B+12 stage. Error bars indicate SD of n=6 biological replicates with 25 seeds each. Asterisks indicate statistically significant differences among means relative to WT samples (*t*-test: **, $P < 0.01$, *** $P < 0.001$).

3 Discussion

PSY catalyzes the first committed and main rate-determining step of the carotenoid pathway. In most plants, several PSY isoforms control the production for carotenoids in different tissues and in response to developmental or environmental cues that require an enhanced production of these photoprotective pigments (Zhou et al., 2022). The presence of three PSY isoforms in tomato has been known for a long time, but genetic evidence on their physiological roles was only available for PSY1. Removal of PSY1 activity in mutants or silenced lines leads to strongly reduced levels of carotenoid pigments in ripe fruit and, to a lower extent, in corollas but unchanged carotenoid levels in green tissues, which led to conclude that PSY1 is mainly involved in carotenoid biosynthesis in chromoplasts (Bird et al. 1991; Bramley et al., 1992.; D'Ambrosio et al., 2018; Fantini et al., 2013; Fraser et al., 1999; Giorio et al., 2008; Kang et al., 2014).

3.1 PSY1 supports PSY2 in the production of photoprotective carotenoids in leaves and PSY1, PSY2 defective mutants are albino lethal.

Compared to *PSY1*, *PSY2* expression is higher in leaves and increases more strongly during seedling deetiolation, supporting the conclusion that PSY2 might be the main isoform producing phytoene for carotenoids involved in photosynthesis and photoprotection (Barja et al., 2021; Bartley & Scolnik, 1993; Fraser et al., 1999; Gupta et al., 2022) (Figure S6). *PSY3* expression levels are very low in all the tissues compared to *PSY1* and *PSY2* (Giorio et al., 2008; Stauder et al., 2018) (Figure S6). Similar to most members of the PSY3 clade, tomato *PSY3* expression is highest in roots, where it is induced during arbuscular mycorrhizal (AM) fungi colonization (Barja et al., 2021; Stauder et al., 2018; Walter et al., 2015). Based on these expression data, it was concluded that PSY3 might have a main role in roots, supplying phytoene to produce carotenoids and derived SLs and apocarotenoid molecules essential for the establishment of the AM symbiosis (Baslam et al., 2013; Fester et al., 2002; Ruiz-Lozano et al., 2016; Stauder et al., 2018). This work aimed to genetically test the hypothesis that besides the main role of PSY1 for carotenoid production in flowers and fruit (chromoplasts), PSY2 in green tissues (chloroplasts) and PSY3 in roots (leucoplasts), tomato PSY isoforms might also provide extra phytoene when a sudden requirement of carotenoid production could not be met by the isoform normally operating in a particular tissue. The generation of lines defective in PSY1 and/or PSY2 reported here provided strong genetic support to correctly frame this conclusion and it went a step beyond by unveiling a role for particular PSY isoforms in tissue-specific ABA production.

Complete loss of PSY activity in Arabidopsis results in albino seedlings (Pokhilko et al., 2015). In *Nicotiana benthamiana* (a closer relative to tomato), several genes encode PSY1, PSY2 and PSY3 homologues, but the virus-induced silencing of only those for PSY1 and PSY2 results in leaf bleaching, lower carotenoid levels and reduced photosynthetic parameters such as ΦPSII, Fv/Fm and NPQ (Wang et al., 2021). Similarly, we observed a seedling-lethal albino phenotype in tomato lines lacking PSY1 and PSY2 but retaining a functional PSY3 gene (Figure 1C). This result demonstrates that PSY3 is unable to produce enough phytoene to support photosynthetic shoot development when PSY1 and PSY2 activities are missing. Indirectly, the result also provides genetic evidence supporting a root-restricted role for tomato PSY3. In the shoot, both PSY1 and PSY2 appear to provide precursors for carotenoid biosynthesis in chloroplasts under normal growth conditions (Figure 2). However, the lower up-regulation of *PSY1* expression compared to *PSY2* in response to HL (Figure 3A) together with the reduced impact of the loss of PSY1 function on carotenoid levels and photosynthetic performance (Figure 2 and 3) supports the model of a predominant role for PSY2 and a supporting contribution of PSY1 to carotenoid biosynthesis in tomato chloroplasts for photoprotection.

3.2 PSY1 is supported by PSY2 to produce carotenoids for flower pigmentation and to a lower extent in fruit flesh.

Besides chloroplasts, tomato plants accumulate very high levels of carotenoids in the chromoplasts that develop in flower corollas and ripening fruit pericarp. Loss of PSY1 had a much stronger impact than removing PSY2 on total carotenoid levels of both tissues. However, the effect in flowers (Figure 4) was much less dramatic than in fruit (Figure 5). Despite *PSY2* is highly expressed in petals (Giorio et al., 2007) (Figure S6) and PSY2 catalytic activity appears to be higher than that of PSY1 (Cao et al., 2019), complete absence of PSY2 had no effect of petal carotenoids (Figure 4). By contrast, a 50% decrease compared to the WT was observed in PSY1-defective corollas (Figure 4), suggesting that PSY2 only produces phytoene for carotenoid synthesis in flower chromoplasts when PSY1 activity is missing. A similar conclusion was deduced for PSY2 during fruit ripening (Gupta et al., 2022; Karniel et al., 2022). In fruit pericarp tissues, carotenoid levels were unaffected in mutants defective in PSY1 and PSY2 until the onset of ripening (Figure 5), supporting our conclusion that loss of one of the two isoforms can be rescued by the remaining isoform in chloroplasts. As chloroplasts differentiate into chromoplasts, however, the contribution of PSY1 to the production of pericarp carotenoids becomes much more predominant, mainly supported by a dramatic up-

regulation of gene expression (Cao et al., 2019; Giorio et al., 2007) (Figure S4 and S6). Without PSY1, ripe fruit accumulate a very small amount of carotenoid pigments (Figure 5C). These carotenoids (mainly lutein and β-carotene) might be remnants of the carotenoids present in MG fruits. However, PSY activity has been measured in chromoplasts of PSY1-defective fruit (Fraser et al., 1999), and a PSY2-dependent increase in carotenoid synthesis was observed during ripening of PSY1-lacking fruit treated with different inhibitors (Gupta et al., 2022; Karniel et al., 2022). A role for PSY2 in the production of β-carotene in pericarp chromoplasts during ripening can also be deduced from the reduced accumulation of this carotenoid in *psy1 PSY2(+/-)* compared to *psy1-2* fruit (Figure 5C). A similar role distribution has been recently described in pepper (*Capsicum annuum*), where PSY1 is the isoform supporting the bulk of pericarp carotenoid biosynthesis during fruit ripening and PSY2 is mainly associated to chloroplast-containing tissues (leaves, stems) but it also contributes to produce carotenoids in fruit chromoplasts (Jang et al., 2020; Wei et al., 2021). It has been proposed that recruitment of primary (i.e. photosynthetic) carotenoids as secondary metabolites for flower and fruit pigmentation likely required duplication and further subfunctionalization of genes encoding rate-controlling steps, including PSY (Galpaz et al., 2006; Giorio et al., 2008). In tomato, the duplicated pathway might have been originally employed for flower pigmentation and later for fruit pigmentation, explaining why all tomato species have yellow flowers but only some develop fruit chromoplasts (Galpaz et al., 2006; Giorio et al., 2008).

3.3 PSY1 and PSY2 are major contributors to ABA synthesis in tomato fruit pericarp and seeds, respectively.

Besides providing strong genetic evidence supporting long-standing models on the subfunctionalization of tomato PSY1 and PSY2 isoforms to feed the carotenoid pathway in particular tissues, our results have unveiled isoform-specific roles in ABA-regulated processes in tomato fruit and seeds. Genetic and pharmacological interference with carotenoid biosynthesis was previously shown to impact ABA-regulated characters such as fruit size, the onset of fruit ripening and seed dormancy (Diretto et al., 2020; Galpaz et al., 2008; McQuinn et al., 2020; Zhang et al., 2009). Also, pharmacological approaches had provided evidence suggesting (but not demonstrating) that PSY2 might be involved in the production of ABA in tomato fruits (Gupta et al., 2022), most particularly in seeds (Rodriguez-Concepcion et al. 2001). Here we showed that in the absence of PSY1, PSY2-derived carotenoids sustain the production of about 2/3 of the ABA measured in the pericarp of tomato B fruit (Figure 7). The 1/3 reduction was sufficient to trigger

phenotypes associated to low ABA levels in *psy1* fruit, including an attenuated expression of ethylene-associated ripening gene (Figure 6B) and a lower fruit weight and volume (Figure 6C), suggesting that a threshold of ABA is required to support normal fruit growth and ripening. Alternatively, PSY1-derived carotenoids might be responsible for the production of ABA in specific tissues or cell compartments causing the observed phenotypes. A differential channeling of phytoene produced by either PSY1 or PSY2 to produce carotenoids for specific ABA pools is supported by the seed germination experiments. When PSY2 is not present, PSY1 still produces about 2/3 of the ABA measured in developing and mature seeds (Figure 7) but this relatively high amount of remaining ABA is not enough to prevent a germination delay phenotype in the *psy2* mutant (Figure 6D). Furthermore, complete block of carotenoid (and hence downstream) ABA production in MG fruit with inhibitors did not exacerbate the seed dormancy phenotype of the *psy2* mutant (Figure 8B). These results strongly suggest that only PSY2-derived carotenoids produced after the MG stage are used to generate the ABA that regulates dormancy in tomato seeds. Following an initial phase of tissue differentiation, tomato seed development proceeds as fruit expand with a second phase that includes the accumulation of nutrient reserves and the acquisition of germination and desiccation tolerance (De Castro & Hilhorst 2006) (Figure S8). When fruits reach their final size at the MG stage, seeds achieve show full germinability. Later, as fruit start to ripe, ABA production peaks and mature seeds dry and acquire their dormancy (De Castro & Hilhorst 2006). This transient accumulation of ABA is mainly supplied by the embryo (Berry & Bewley 1992). Our results confirm that ABA produced by PSY2 in seeds during ripening regulates seed dormancy (Figure 8). Strikingly, the contribution of PSY2 to produce this ABA could not be predicted based on available expression data. Thus, *PSY2* expression is higher in developing seeds but then it drops from the MG stage in embryonic and other tissues of mature seeds (Figure S8). While a *PSY2*-like profile is observed for the *NOT/NCED* gene (Solyc07g056570), which encodes the first enzyme specific for ABA biosynthesis (Figure S8), downstream genes of the pathway such as *SIT/AAO3* (Solyc01g009230) and *FLC/ABA3* (Solyc07g066480) are more highly expressed in mature seeds (including embryos) (Figure S8). Although *PSY1* expression is also higher in mature seeds, little to no expression was found in embryos. These results clearly illustrate the challenges of deducing function based only on gene expression profiles.

A question arising from our data is how interference with PSY activity is specifically translated into changes in the production of ABA (Figure 1A and Figure S8). A possible scenario would be the existence of metabolons channeling GGPP to ABA in cells from

the pericarp or the seed. GGPP required to produce pericarp carotenoids and ABA during fruit ripening is mainly supplied by the GGPPS isoform SlG3 with a supporting contribution of SlG2 (Barja et al., 2021). While SlG2 can interact with both PSY1 and PSY2, no interaction was reported for SlG3 in transient co-expression assays in *N. benthamiana* leaves (Barja et al., 2021). It is possible that interaction of SlG3 with particular PSY isoforms requires specific partners only found in tomato pericarp (to interact with PSY1) or seed (to interact with PSY2) tissues. In agreement with the existence of metabolons or any other kind of metabolic channeling, the extremely low PSY2 activity present in the pericarp of *psy1* fruit appears to be more directly involved in the production of the β-carotene instead of lutein (Figure 5C), i.e. it might be preferentially acting to produce carotenoids that could then be used as precursors for ABA synthesis (Figure 1A). However, the channeling of specific pools of carotenoids all the way to ABA is harder to fit in a metabolon-dependent model due to the large number of reactions and the diversity of subcellular localizations reported for the enzymes involved, which include several cytosolic steps following the cleavage of β-carotene-derived xanthophyll precursors (Nambara & Marion-Poll, 2005) (Figure 1A and Figure S8). Alternatively, expression of specific isoforms in particular tissue microdomains controlling fruit ripening (directly or indirectly through ethylene), pericarp growth, or seed dormancy might explain why only PSY1-derived ABA appears to contribute to fruit ripening and only PSY2-derived ABA influences seed germination.

3.4 Concluding remarks

In summary, we show that both PSY1 and PSY2 support carotenoid production in tomato shoots with diverging contributions in different tissues: PSY2 > PSY1 in leaves (i.e. chloroplasts), PSY1 > PSY2 in corollas, and PSY1 >> PSY2 in fruit pericarp tissues. Furthermore, we demonstrate a differential contribution to the production of ABA of PSY1 in the pericarp (to regulate fruit growth and ripening) and PSY2 in the seeds (to control dormancy). Further work should determine the mechanism by which the production of phytoene by given PSY isoforms is eventually channeled to produce ABA is particular locations for specific functions.

4 Materials and methods

4.1 Plant material, treatments and sample collection.

Tomato (*Solanum lycopersicum* var. MicroTom) plants were used for all the experiments. Seeds were surface-sterilized by a 30 min water wash followed by a 15 min incubation in 10 ml of 40% bleach with 10 µl of Tween-20. After three consecutive 10 min washes with sterile milli-Q water, seeds were germinated on plates with solid 0.5x Murashige and Skoog (MS) medium containing 1% agar (without vitamins or sucrose). The medium was supplemented with kanamycin (100 µg/ml) when required to select transgenic plants. Plates were incubated in a climate-controlled growth chamber (Ibercex) at 26°C with a photoperiod of 14 h of white light (photon flux density of 50 µmol m^{-2} s^{-1}) and 10 h of darkness. After 10-14 days, seedlings were transferred to soil and grown under standard greenhouse conditions (14 h light at 25 ± 1 °C and 10 h dark at 22 ± 1 °C). Young leaves were collected from 4-week-old plants and they correspond to growing leaflets from the fourth and fifth true leaves. Petal samples were collected from anthesis flowers. Fruit pericarp samples were collected at different stages, including mature green (MG, about 30 days post-anthesis), breaker (B, 2-3 days later, when the first symptoms of chlorophyll degradation and carotenoid accumulation became visually obvious), and several days after breaker. After collection, samples were immediately frozen in liquid nitrogen and stored at -80°C. For fruit weight determination, 100 fully ripe individual fruits from each genotype were collected and weighted one by one using a precision scale (Kern). Fruit volume was estimated in 10 pools of 10 fruits each by measuring the displaced water volume in a graduated cylinder. For inhibitor treatments, MG fruits were collected from the plant and measured to estimate their volume. Then, a Hamilton syringe was used to inject 2-5 µl of sterile water or inhibitor solution into the fruit. The exact volume of fosmidomycin (FSM, Sigma) or norflurazon (NFZ, Zorial, Syngenta) solution to inject was calculated based on the fruit volume so the final concentration in the fruits was 200 µM FSM or 50 µM NFZ. After injection, fruits were kept in a climate-controlled growth chamber at 26°C for 12 days and then seeds were collected and immediately used for germination assays on 0.5x MS plates. Germination was scored based on root protrusion.

4.2 Generation of CRISPR-Cas9 mutants and tomato transformation.

For CRISPR-Cas9-mediated disruption of *PSY1* and *PSY2*, one single guide RNA (sgRNA) was designed for each gene using the online tool CRISPR-P 2.0 (Liu et al.,

2017). Cloning of the CRISPR-Cas9 constructs was carried out as previously described (Barja et al., 2021) using primers listed in Table S1. As a result, a single final binary plasmid harboring the Cas9 sequence, the *NPTII* gene providing kanamycin resistance, and the sgRNAs to disrupt *PSY1* and *PSY2* was obtained and named pDE-PSY1,2 (Table S2). All constructs were confirmed by restriction mapping and DNA sequencing. *Agrobacterium tumefaciens* GV3101 strain was used to stably transform tomato MicroTom cotyledons with pDE-PSY1,2 as described (Barja et al., 2021). *In vitro* regenerated lines showing kanamycin (100 µg/ml) resistance were used for PCR amplification and sequencing of the genomic sequences. Following further segregation and PCR-based genotyping using specific primers (Table S1), stable homozygous lines lacking the Cas9-encoding transgene were obtained and named *psy1-1, psy1-2, psy2-1* and *psy2-2.* For the generation of double double mutants lacking both PSY1 and PSY2, *psy1-2* and *psy2-1* homozygous plants were crossed and the segregating F2 offspring was used for PCR-based genotyping of individual plants.

4.3 Photosynthetic parameters.

Tomato seedlings were germinated and grown for ten days under white light with a fluorescence photon flux density of 50 µmol m^{-2} s^{-1} (referred to as normal light, NL) and then either left under NL or transferred to a chamber with a more intense light of 300 µmol m^{-2} s^{-1} (referred to as high light, HL) for five more days. Chlorophyll fluorescence measurements were carried out with a Handy FluorCam (Photon Systems Instruments). Fv/Fm was measured in seedlings incubated in the dark for 30 min to allow full relaxation of photosystems. ϕPSII was measure at 30 PAR with an actinic light of 3 µmol m^{-2} s^{-1}. For NPQ measurements, the following steps of actinic irradiance were used: 0, 5, 10, 20, 55, 110, 185 and 280 µmol photons m^{-2} s^{-1}.

4.4 RNA extraction and RT-qPCR analyses.

Total RNA was extracted from tomato freeze-dried tissue using the PureLink RNA MINI extraction kit (Ambion). RNA was quantified using a NanoDropTM 8000 spectrophotometer (ThermoFischer Scientific) and checked for integrity by agarose gel electrophoresis. The Transcriptor First Strand cDNA Synthesis Kit (Nzytech) was used to reverse transcribe 1 µg of extracted RNA and the generated cDNA volume (20 µl) was subsequently diluted 5-fold with mili-Q water and stored at -20 °C for further analysis. Transcript abundance was evaluated via real-time quantitative PCR (RT-qPCR) in a reaction volume of 10 µl containing 2 µl of the cDNA dilution, 5 µl of SYBR Green Master Mix (Thermo Fisher Scientific), and 0.3 µM of each specific forward and reverse primer

(Table S1). The RT-qPCR was carried out on a QuantStudio 3 Real-Time PCR System (Thermo Fisher Scientific) using three independent biological samples and three technical replicates of each sample. Normalized transcript abundance was calculated as previously described (Simon, 2003) using tomato *ACT4* (Solyc04g011500) as endogenous reference gene.

4.5 Pigment quantification.

Carotenoids and chlorophylls were extracted as described (Barja et al., 2021) with some modifications. Freeze-dried material from leaves (8 mg) were mixed with 375 µl of methanol as extraction solvent, 25 µl of a 10 % (w/v) solution of canthaxanthin (Sigma) in chloroform as internal control, and glass beads. Following steps were performed as described (Barja et al., 2021). Freeze-dried flower petals and fruit pericarp tissue (20 mg) were mixed in 2 ml Epperdorf tubes with 1 ml of 2:1:1 hexane:acetone:methanol as extraction solvent, 25 µl of the canthaxanthin solution, and glass beads. After vortexing the samples, 100 µl of milli-Q water were added to the mix. Then, samples were shaken for 1 min in a TissueLyser II (Qiagen) and then centrifuged at 4ºC for 5 min at maximum speed in a tabletop microfuge. The organic phase was transferred to a 1.5 ml tube and the rest was re-extracted with 1 ml of 2:1:1 hexane:acetone:methanol. The organic phases from the two rounds of extraction were mixed in the same tube and evaporated using a SpeedVac. Extracted pigments were resuspended in 200 µl of acetone by using an ultrasound bath and filtered with 0.2 µm filters into amber-colored 2 ml glass vials. Separation and quantification of individual carotenoids and chlorophylls was performed as described (Barja et al., 2021). Fruit pigmentation (Average Red Color) was measured in three different tomato fruit samples of each genotype using the default settings of the TomatoAnalyzer 4.0 software (https://vanderknaaplab.uga.edu/tomato_analyzer.html).

4.6 Determination of ABA levels

For ABA extraction, 100 mg of frozen pericarp tissue or seeds were ground with a mortar and pestle and resuspended in a solution of 80% (v/v) methanol and 1% (v/v) acetic acid with deuterium-labelled ABA as internal standard. After shaking for 1 h at 4°C, the extract was centrifuged at maximum speed in a table top microfuge and the supertnatant was collected and dried in a SpeedVac. The dry residue was dissolved in 1% (v/v) acetic acid and run through a reverse phase column (Oasis HLB) as described (Seo et al., 2011). The eluate was dissolved in 5% (v/v) acetonitrile and 1% (v/v) acetic acid and used for UHPLC chromatography with a reverse phase 2.6 µg Accucore RP-MS column of 100

mm length x 2.1 mm i.d. (ThermoFisher Scientific). The mobile phase was 5 to 50% (v/v) acetronitrile gradient containing 0.05% (v/v) acetic acid at 400 µl/min over 21 min. Quantification of ABA was performed with a Q-Exactive mass spectrometer equipped with an Orbitrap detector (ThermoFisher Scientific) by targeted Selected Ion 100 Monitoring (SIM). The concentrations of ABA in the extracts were determined using embedded calibration curves and the TraceFinder 4.1 SP1 software.

5 Acknowledgments

We thank Mª Rosa Rodriguez-Goberna for technical help with HPLC analyses and Tsuyoshi Nakagawa (Shimane University, Japan) for the Gateway vectors. We also thank members of our laboratory for helpful discussions. This work was funded by grants from Spanish MCIN/AEI/10.13039/501100011033 and European NextGeneration EU/PRTR and PRIMA programs to MR-C (PID2020-115810GB-I00 and UToPIQ-PCI2021-121941). MR-C is also supported by CSIC (202040E299) and Generalitat Valenciana (PROMETEU/2021/056). ME and EB received predoctoral fellowships from MCIN/AEI (BES-2017-080652) and Colombia's Doctorado Exterior program (10852908329), respectively. No conflict of interest is declared.

6 References

Ariizumi, T., Kishimoto, S., Kakami, R., Maoka, T., Hirakawa, H., Suzuki, Y., Ozeki, Y., Shirasawa, K., Bernillon, S., Okabe, Y., Moing, A., Asamizu, E., Rothan, C., Ohmiya, A., & Ezura, H. (2014). Identification of the carotenoid modifying gene PALE YELLOW PETAL 1 as an essential factor in xanthophyll esterification and yellow flower pigmentation in tomato (Solanum lycopersicum). *Plant Journal*, *79*(3), 453–465.

Barja, M. V., Ezquerro, M., Beretta, S., Diretto, G., Florez-Sarasa, I., Feixes, E., Fiore, A., Karlova, R., Fernie, A. R., Beekwilder, J., & Rodríguez-Concepción, M. (2021). Several geranylgeranyl diphosphate synthase isoforms supply metabolic substrates for carotenoid biosynthesis in tomato. *New Phytologist*, 231(1), 255–272.

Bartley, G. E., & Scolnik, P. A. (1993). cDNA cloning, expression during development, and genome mapping of PSY2, a second tomato gene encoding phytoene synthase. *Journal of Biological Chemistry*, 268(34), 25718–25721.

Baslam, M., Esteban, R., García-Plazaola, J. I., & Goicoechea, N. (2013). Effectiveness of arbuscular mycorrhizal fungi (AMF) for inducing the accumulation of major carotenoids, chlorophylls and tocopherol in green and red leaf lettuces. *Applied Microbiology and Biotechnology*, *97*(7), 3119–3128.

Berry, T, & Bewley. J.D. (1992) A Role for the Surrounding Fruit Tissues in Preventing the Germination of Tomato (Lycopersicon esculentum) Seeds: A Consideration of the Osmotic Environment and Abscisic Acid. *Plant Physiology* 100(2), 951-957.

Bird, C. R., Ray, J. A., Fletcher, J. D., Boniwell, J. M., Bird, A. S., Teulieres, C., Blain I., Bramley, P., & Schuch, W. (1991). Using Antisense RNA to Study Gene Function: Inhibition of Carotenoid Biosynthesis in Transgenic Tomatoes. *Nature Biotechnology 9*, 635–639.

Bramley, P., Teulieres, C., Blain, I., Bird, C., Schuch, W., & Holloway, R. (1992). Biochemical characterization of transgenic tomato plants in which carotenoid synthesis has been inhibited through the expression of antisense RNA to pTOM5. In *The Plant Journal* 992(1).

Cao, H., Luo, H., Yuan, H., Eissa, M. A., Thannhauser, T. W., Welsch, R., Hao, Y. J., Cheng, L., & Li, L. (2019). A neighboring aromatic-aromatic amino acid combination governs activity divergence between tomato phytoene synthases. *Plant Physiology*, 180(4), 1988–2003.

D'Ambrosio, C., Stigliani, A. L., & Giorio, G. (2018). CRISPR/Cas9 editing of carotenoid genes in tomato. *Transgenic Research*, *27*(4), 367–378.

De Castro, R.D. & Hilhorst, H.W.M. (2006). Hormonal control of seed development in GA- and ABA-deficient tomato (*Lycopersicon esculentum* Mill. cv. Moneymaker) mutants. *Plant Science* 170, 462–70.

Diretto, G., Frusciante, S., Fabbri, C., Schauer, N., Busta, L., Wang, Z., Matas, A. J., Fiore, A., K.C. Rose, J., Fernie, A. R., Jetter, R., Mattei, B., Giovannoni, J., & Giuliano, G. (2020). Manipulation of β-carotene levels in tomato fruits results in increased ABA content and extended shelf life. *Plant Biotechnology Journal*, 18(5), 1185–1199.

Fantini, E., Falcone, G., Frusciante, S., Giliberto, L., & Giuliano, G. (2013). Dissection of tomato lycopene biosynthesis through virus-induced gene silencing. *Plant Physiology*, 163(2), 986–998.

Fester, T., Schmidt, D., Lohse, S., Walter, M. H., Giuliano, G., Bramley, P. M., Fraser, P. D., Hause, B., & Strack, D. (2002). Stimulation of carotenoid metabolism in arbuscular mycorrhizal roots. *Planta*, *216*(1), 148–154.

Fraser, P. D., Kiano, J. W., Truesdale, M. R., Schuch, W., & Bramley, P. M. (1999). Phytoene synthase-2 enzyme activity in tomato does not contribute to carotenoid synthesis in ripening fruit. *Plant Molecular Biology*, 40, 687–698

Fray, R. G., & Grierson, D. (1993). Identification and genetic analysis of normal and mutant phytoene synthase genes of tomato by sequencing, complementation and co-suppression.*Plant Molecular Biology*, 22, 589–602.

Galpaz, N., Ronen, G., Khalfa, Z., Zamir, D., & Hirschberg, J. (2006). A chromoplast-specific carotenoid biosynthesis pathway is revealed by cloning of the tomato white-flower locus. *Plant Cell*, 18(8), 1947–1960.

Galpaz, N., Wang, Q., Menda, N., Zamir, D., & Hirschberg, J. (2008). Abscisic acid deficiency in the tomato mutant high-pigment 3 leading to increased plastid number and higher fruit lycopene content. *Plant Journal*, *53*(5), 717–730.

Giorio, G., Stigliani, A. L., & D'Ambrosio, C. (2008). Phytoene synthase genes in tomato (Solanum lycopersicum L.) - New data on the structures, the deduced amino acid sequences and the expression patterns. *FEBS Journal*, *275*(3), 527–535.

Groot, S. P. C., & Karssen, C. M. (1992). Dormancy and Germination of Abscisic Acid-Deficient Tomato Seeds' Studies with the sitiens Mutant. In *Plant Physiol*ogy 99(3), 952-958.

Gupta, P., Rodriguez-Franco, M., Bodanapu, R., Sreelakshmi, Y., & Sharma, R. (2022). Phytoene synthase 2 in tomato fruits remains functional and contributes to abscisic acid formation. *Plant Science*, 316.

Hirschberg J. (2001). Carotenoid biosynthesis in flowering plants. *Current Opinion in Plant Biology*, 4(3):210-8.

Jang, S. J., Jeong, H. B., Jung, A., Kang, M. Y., Kim, S., Ha, S. H., Kwon, J. K., & Kang, B. C. (2020). Phytoene synthase 2 can compensate for the absence of PSY1 in the control of color in Capsicum fruit. *Journal of Experimental Botany*, 71(12), 3417–3427.

Kachanovsky, D. E., Filler, S., Isaacson, T., & Hirschberg, J. (2012). Epistasis in tomato color mutations involves regulation of phytoene synthase 1 expression by cis-carotenoids. *Proceedings of the National Academy of Sciences of the United States of America*, 109(46), 19021–19026.

Kang, B., Gu, Q., Tian, P., Xiao, L., Cao, H., & Yang, W. (2014). A chimeric transcript containing Psy1 and a potential mRNA is associated with yellow flesh color in tomato accession PI 114490. *Planta*, 240(5), 1011–1021.

Karniel, U., Adler Berke, N., Mann, V., & Hirschberg, J. (2022). Perturbations in the Carotenoid Biosynthesis Pathway in Tomato Fruit Reactivate the Leaf-Specific Phytoene Synthase 2. *Frontiers in Plant Science*, 13.

Leng, P., Yuan, B., Guo, Y., & Chen, P. (2014). The role of abscisic acid in fruit ripening and responses to abiotic stress. *Journal of Experimental Botany,* 65(16), 4577–4588.

Liu, H., Ding, Y., Zhou, Y., Jin, W., Xie, K., & Chen, L. L. (2017). CRISPR-P 2.0: An Improved CRISPR-Cas9 Tool for Genome Editing in Plants. *Molecular Plant* 10(3), 530–532.

McQuinn, R. P., Gapper, N. E., Gray, A. G., Zhong, S., Tohge, T., Fei, Z., Fernie, A. R., & Giovannoni, J. J. (2020). Manipulation of ZDS in tomato exposes carotenoid- and ABA-specific effects on fruit development and ripening. *Plant Biotechnology Journal*, 18(11), 2210–2224.

Moreno, J. C., Mi, J., Alagoz, Y., & Al-Babili, S. (2021). Plant apocarotenoids: from retrograde signaling to interspecific communication. *Plant Journal*, 105(2), 351–375.

Nambara, E., & Marion-Poll, A. (2005). Abscisic acid biosynthesis and catabolism. In *Annual Review of Plant Biology*, 56, 165–185.

Nitsch, L., Kohlen, W., Oplaat, C., Charnikhova, T., Cristescu, S., Michieli, P., Wolters-Arts, M., Bouwmeester, H., Mariani, C., Vriezen, W. H., & Rieu, I. (2012). ABA-deficiency results in reduced plant and fruit size in tomato. *Journal of Plant Physiology*, 169(9), 878–883.

Pokhilko, A., Bou-Torrent, J., Pulido, P., Rodríguez-Concepción, M., & Ebenhöh, O. (2015). Mathematical modelling of the diurnal regulation of the MEP pathway in Arabidopsis. *New Phytologist*, 206(3), 1075–1085.

Rodríguez-Concepción M, Ahumada I, Diez-Juez E, Sauret-Güeto S, Lois LM, Gallego F, Carretero-Paulet L, Campos N, Boronat A. (2001) 1-Deoxy-D-xylulose 5-phosphate reductoisomerase and plastid isoprenoid biosynthesis during tomato fruit ripening. *Plant Journal*, 27(3), 213-22

Rodríguez-Concepción, M., Avalos, J., Bonet, M. L., Boronat, A., Gomez-Gomez, L., Hornero-Mendez, D., Limon, M. C., Meléndez-Martínez, A. J., Olmedilla-Alonso, B., Palou, A., Ribot, J., Rodrigo, M. J., Zacarias, L., & Zhu, C. (2018). A global perspective on carotenoids: Metabolism, biotechnology, and benefits for nutrition and health. *Progress in Lipid Research* 70, 62–93.

Ruiz-Lozano, J. M., Aroca, R., Zamarreño, Á. M., Molina, S., Andreo-Jiménez, B., Porcel, R., García-Mina, J. M., Ruyter-Spira, C., & López-Ráez, J. A. (2016). Arbuscular mycorrhizal symbiosis induces strigolactone biosynthesis under drought and improves drought tolerance in lettuce and tomato. *Plant Cell and Environment*, 39(2), 441–452.

Seo, M., Jikumaru, Y. & Kamiya Y. (2011). Profiling of Hormones and Related Metabolites in Seed Dormancy and Germination Studies. *Methods in Molecular Biology* 773, 99–111.

Simon, P. (2003). Q-Gene: Processing quantitative real-time RT-PCR data. *Bioinformatics*, 19(11), 1439–1440.

Stauder, R., Welsch, R., Camagna, M., Kohlen, W., Balcke, G. U., Tissier, A., & Walter, M. H. (2018). Strigolactone levels in dicot roots are determined by an ancestral symbiosis-regulated clade of the PHYTOENE SYNTHASE gene family. *Frontiers in Plant Science*, *9*.

Sun, T., Yuan, H., Cao, H., Yazdani, M., Tadmor, Y., & Li, L. (2018). Carotenoid Metabolism in Plants: The Role of Plastids. *Molecular Plant*, 11(1), 58–74.

Walter, M. H., Stauder, R., & Tissier, A. (2015). Evolution of root-specific carotenoid precursor pathways for apocarotenoid signal biogenesis. *Plant Science*, 233, 1–10.

Wang, Z., Zhang, L., Dong, C., Guo, J., Jin, L., Wei, P., Li, F., Zhang, X., & Wang, R. (2021). Characterization and functional analysis of phytoene synthase gene family in tobacco. *BMC Plant Biology*, 21(1) 34-50.

Wei, X., Meng, C., Yuan, Y., Nath, U. K., Zhao, Y., Wang, Z., Yang, S., Li, L., Niu, L., Yao, Q., Wei, F., & Zhang, X. (2021). CaPSY1 gene plays likely the key role in carotenoid metabolism of pepper (Capsicum annuum) at ripening. *Functional Plant Biology*, 48(2), 141–155.

Zhang, M., Yuan, B., & Leng, P. (2009). The role of ABA in triggering ethylene biosynthesis and ripening of tomato fruit. *Journal of Experimental Botany*, 60(6), 1579–1588.

Zhou, X., Rao, S., Wrightstone, E., Sun, T., Lui, A. C. W., Welsch, R., & Li, L. (2022). Phytoene Synthase: The Key Rate-Limiting Enzyme of Carotenoid Biosynthesis in Plants. In *Frontiers in Plant Science,* 13.

7 Supplemental information

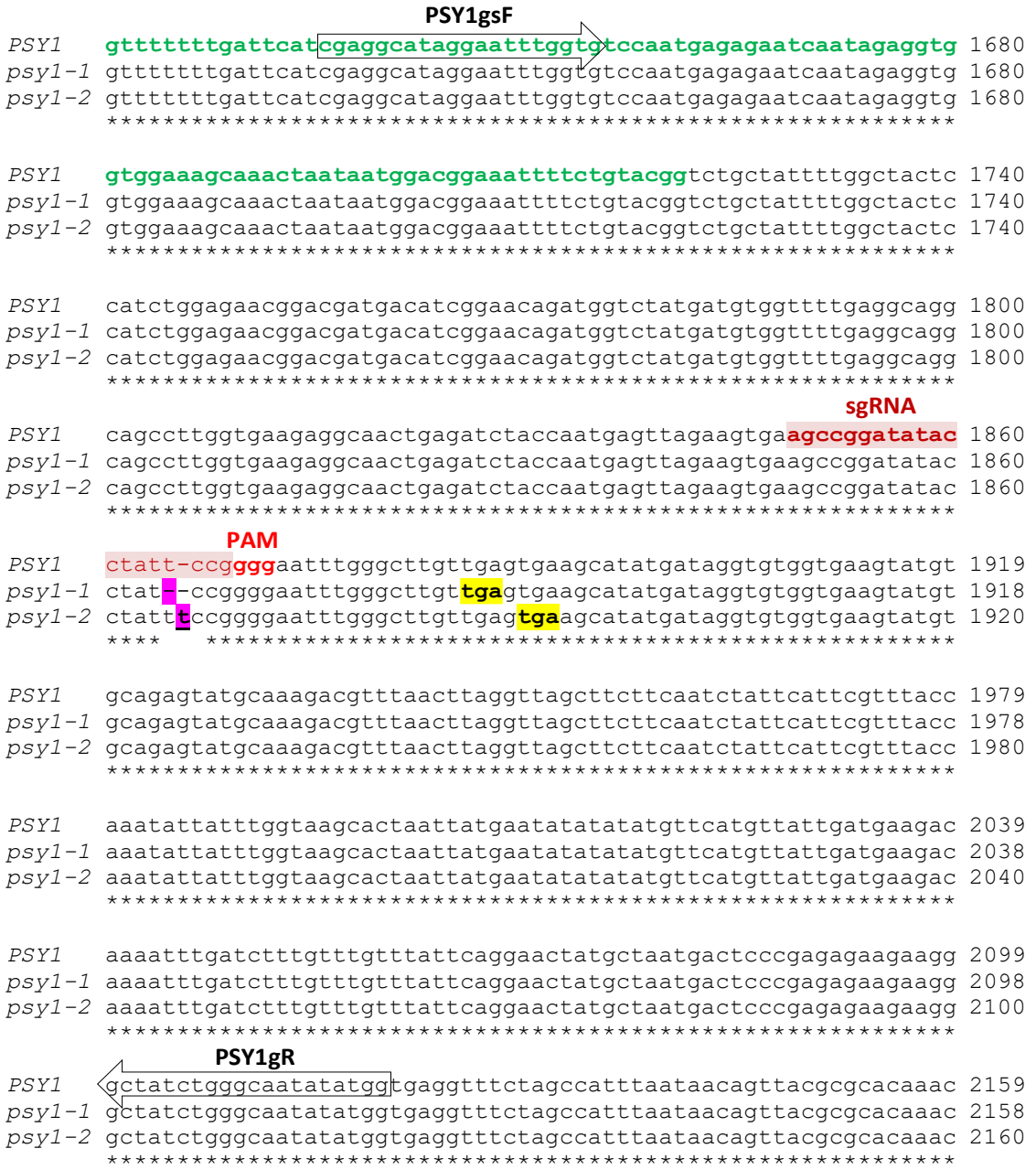

Figure S1. DNA sequence alignment of *PSY1* sequences from WT and CRISPR mutants. Alignment was performed using Clustal Omega with default settings (https://www.ebi.ac.uk/Tools/msa/clustalo/). The WT sequence encoding the plastid targeting sequence is marked in green and the designed single-guide RNA (sgRNA) sequence and protospacer adjacent motif (PAM) in red. The position of genotyping primers is highlighted as arrows. Mutations are boxed in pink and translation stop codons are boxed in yellow.

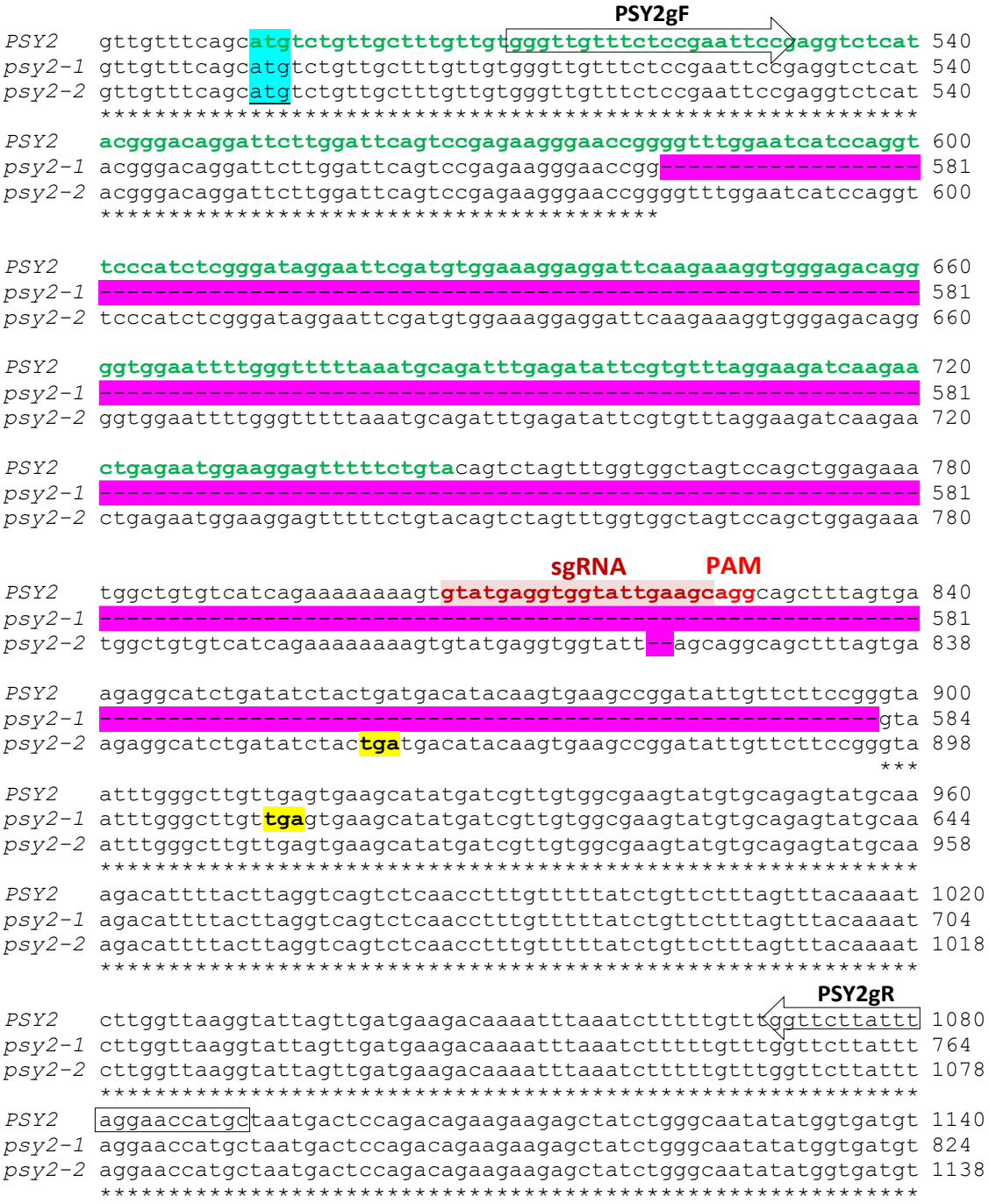

Figure S2. DNA sequence alignment of *PSY2* sequences from WT and CRISPR mutants. Alignment was performed using Clustal Omega with default settings (https://www.ebi.ac.uk/Tools/msa/clustalo/). The WT sequence encoding the plastid targeting sequence is marked in green and the designed single-guide RNA (sgRNA) sequence and protospacer adjacent motif (PAM) in red. The position of genotyping primers is highlighted as arrows. Mutations are boxed in pink and translation start and stop codons are boxed in blue and yellow, respectively.

```
PSY1        MSVALLWVVSPCDVSNGTSFMESVREGNRFFDSSRHRNLVSNERINRGGGKQTNNGRKFS    60
psy1-1      MSVALLWVVSPCDVSNGTSFMESVREGNRFFDSSRHRNLVSNERINRGGGKQTNNGRKFS    60
psy1-2      MSVALLWVVSPCDVSNGTSFMESVREGNRFFDSSRHRNLVSNERINRGGGKQTNNGRKFS    60

PSY1        VRSAILATPSGERTMTSEQMVYDVVLRQAALVKRQLRSTNELEVKPDIPIPGNLGLLSEA    120
psy1-1      VRSAILATPSGERTMTSEQMVYDVVLRQAALVKRQLRSTNELEVKPDIPIRGIWAC*---    116
psy1-2      VRSAILATPSGERTMTSEQMVYDVVLRQAALVKRQLRSTNELEVKPDIPISGEFGLVE*-    118

PSY1        YDRCGEVCAEYAKTFNLGTMLMTPERRRAIWAIYVWCRRTDELVDGPNASYITPAALDRW    180
psy1-1      ------------------------------------------------------------    116
psy1-2      ------------------------------------------------------------    118

PSY1        ENRLEDVFNGRPFDMLDGALSDTVSNFPVDIQPFFRDMIEGMRMDLRKSRYKNFDELYLYC    240
psy1-1      ------------------------------------------------------------    116
psy1-2      ------------------------------------------------------------    118

PSY1        YYVAGTVGLMSVPIMGIAPESKATTESVYNAALALGIANQLTNILRDVGEDARRGRVYLP    300
psy1-1      ------------------------------------------------------------    116
psy1-2      ------------------------------------------------------------    118

PSY1        QDELAQAGLSDEDIFAGRVTDKWRIFMKKQIHRARKFFDEAEKGVTELSSASRFPVWASL    360
psy1-1      ------------------------------------------------------------    116
psy1-2      ------------------------------------------------------------    118

PSY1        VLYRKILDEIEANDYNNFTKRAYVSKSKKLIALPIAYAKSLVPPTKTAQR*    412
psy1-1      ----------------------------------------------------    116
psy1-2      ----------------------------------------------------    118


PSY2        MSVALLWVVSPNSEVSYGTGFLDSVREGNRGLESSRFPSRDRNSMWKGGFKKGGRQGWNF    60
psy2-1      MSVALLWVVSPNSEVSYGTGFLDSVREGNRVIWAC*----------------------    35
psy2-2      MSVALLWVVSPNSEVSYGTGFLDSVREGNRGLESSRFPSRDRNSMWKGGFKKGGRQGWNF    60

PSY2        GFLNADLRYSCLGRSRTENGRSFSVQSSLVASPAGEMAVSSEKKVYEVVLKQAALVKRHL    120
psy2-1      ------------------------------------------------------------    35
psy2-2      GFLNADLRYSCLGRSRTENGRSFSVQSSLVASPAGEMAVSSEKKVYEVVLAGSFSEEASD    120

PSY2        ISTDDIQVKPDIVLPGNLGLLSEAYDRCGEVCAEYAKTFYLGTMLMTPDRRRAIWAIYVW    180
psy2-1      ------------------------------------------------------------    35
psy2-2      IY*-------------------------------------------------------------    122

PSY2        CRRTDELVDGPNASHITPQALDRWEARLEDIFNGRPFDMLDAALSDTVSRFPVDIQPFRD    240
psy2-1      ------------------------------------------------------------    35
psy2-2      ------------------------------------------------------------    122

PSY2        MVEGMRMDLWKSRYNNFDELYLYCYYVAGTVGLMSVPIMGIAPESKATTESVYNAALALG    300
psy2-1      ------------------------------------------------------------    35
psy2-2      ------------------------------------------------------------    122

PSY2        IANQLTNILRDVGEDARRGRVYLPQDELAQAGLSDEDIFAGKVTDKWRIFMKKQIQRARK    360
psy2-1      ------------------------------------------------------------    35
psy2-2      ------------------------------------------------------------    122

PSY2        FFDEAEKGVTELSSASRWPVLASLLLYRKILDEIEANDYNNFTRRAYVSKPKKLLTLPIA    420
psy2-1      ------------------------------------------------------------    35
psy2-2      ------------------------------------------------------------    122

PSY2        YARSLVPPKSTSSPLAKT*        438
psy2-1      ------------------         35
psy2-2      ------------------         122
```

Figure S3. Protein sequence alignment of PSY1 and PSY2 sequences from WT and CRISPR mutants. Alignment was performed using Clustal Omega with default settings (https://www.ebi.ac.uk/Tools/msa/clustalo/). The WT sequences show the plastid targeting sequence marked in green and the position targeted by the designed single-guide RNA (sgRNA) sequence in red. They also show conserved domains pivotal to PSY function: hydrobofic flap (boxed in orange) and Asp-rich domains (boxed in purple). The sequence present in the different alleles as a consequence of their respective mutations is underlined. Translation stop codons are boxed in yellow.

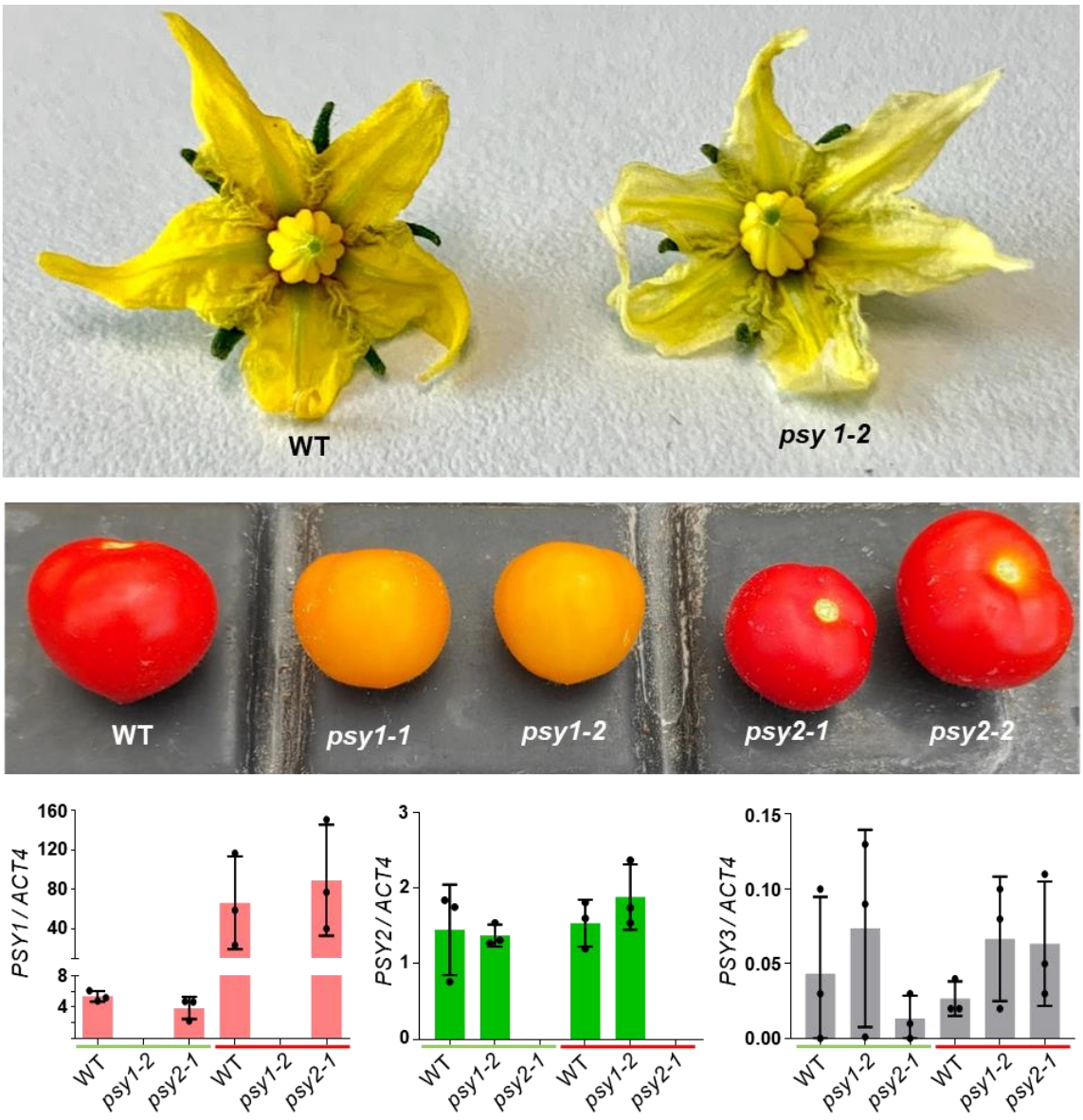

Figure S4. Representative phenotypes of tomato mutants defective in PSY1 or PSY2. The upper picture shows WT and psy1-2 flowers in anthesis. The picture below shows representative ripe fruits from the indicated genotypes. The plots show the result of RT-qPCR analysis of PSY1, PSY2 and PSY3 transcript levels in pericarp tissue from WT and mutant fruit collected from the plant at MG (green bar) and ripe (B+6, red bar) stages. Individual values after normalization with the ACT4 gene are shown together with the mean and SD of n=3 independent biological replicates.

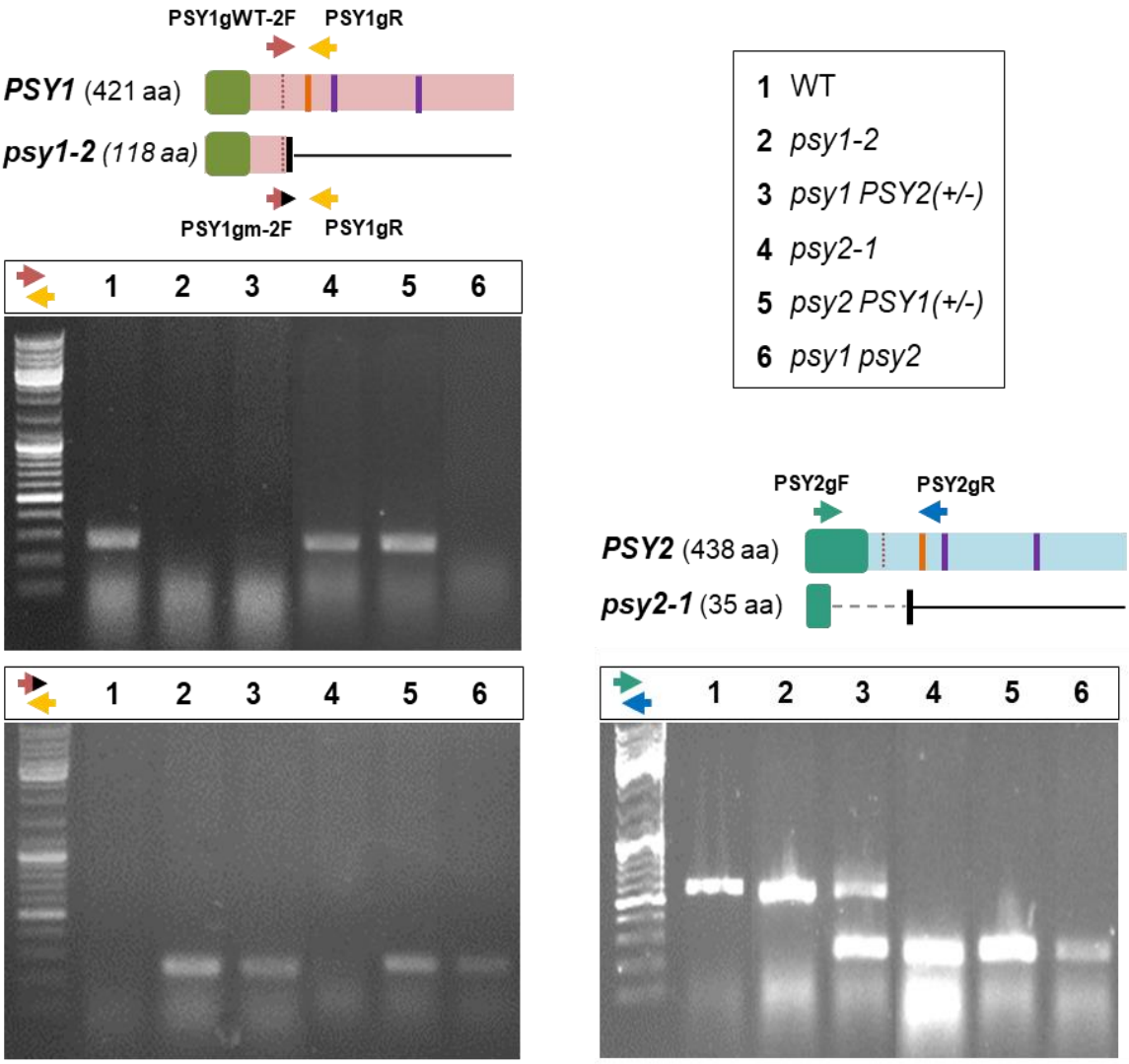

Figure S5. PCR genotyping of mutant alleles. The schemes representing the WT PSY1 and PSY2 proteins and the mutant versions generated in this work are described in Figure 1B. Arrows represent the position of primers for genotyping. Agarose gel analysis of the results for the indicated genotypes resulting from the cross of psy1-2 and psy2-1 plants are shown.

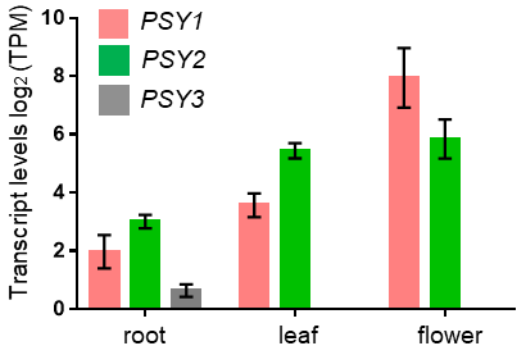

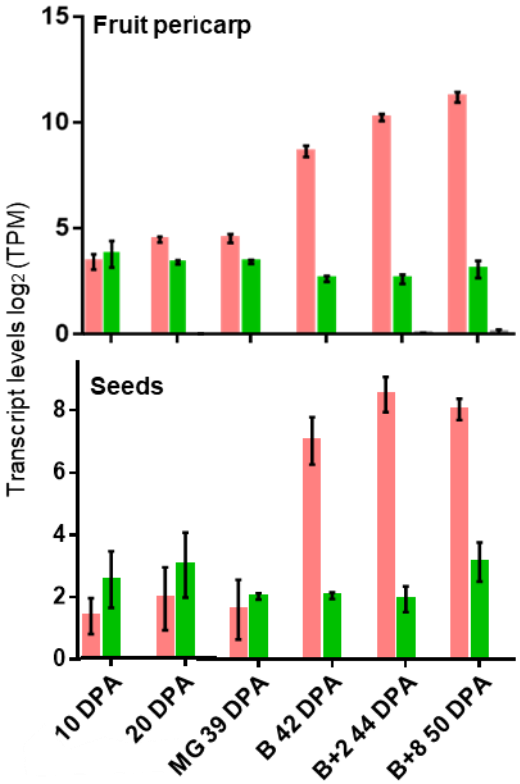

Figure S6. *PSY1*, *PSY2* and *PSY3* transcript levels in different tissues. Plots represent RNAseq data obtained from Genevestigator (https://genevestigator.com). Transcript levels are represented as log2 TPM (transcripts per million mapped reads). DPA, days post-anthesis; MG, mature green; B, breaker.

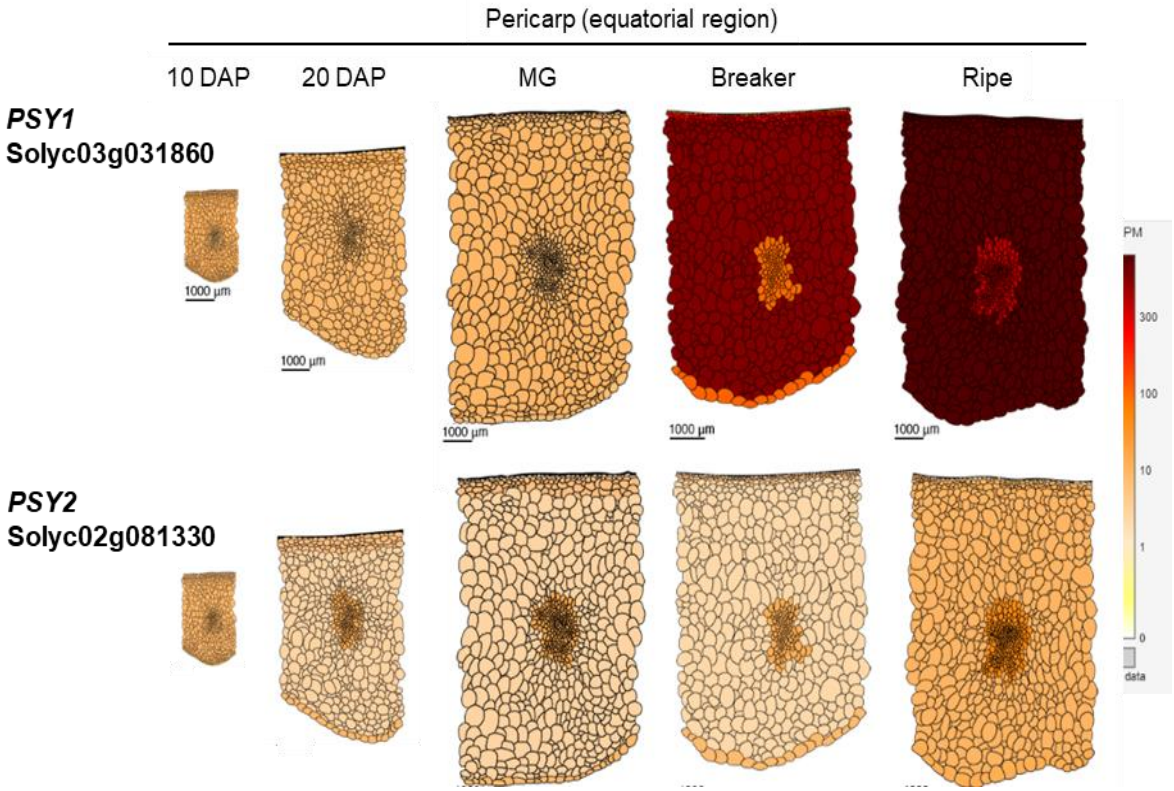

Figure S7. Expression profile of *PSY1* and *PSY2* in the fruit pericarp during development. Data were retrieved from the Tomato Expression Atlas' expression viewer (https://tea.solgenomics.net/expression_viewer/input). DPA, days post-anthesis; MG, mature green.

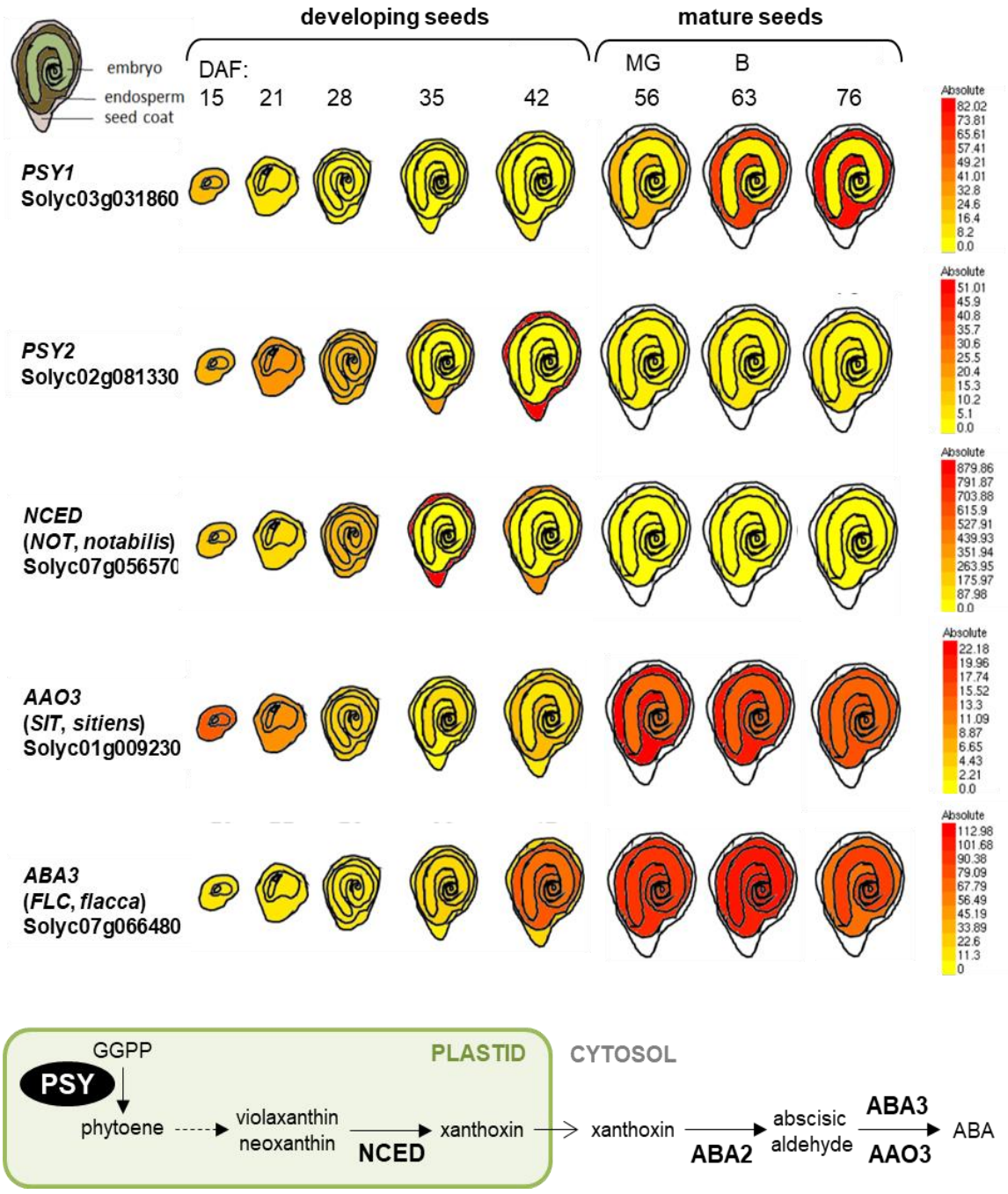

Figure S8. Expression profile of ABA biosynthetic genes in developing seeds. Data were retrieved from the Tomato eFP Browser (http://bar.utoronto.ca/efp_tomato/cgi-bin/efpWeb.cgi). DAF, days after flowering; MG, mature green; B, breaker. A schematic ABA biosynthesis pathway is also shown.

Table S1. Primers used in this work.

Use	#	Name	Sequence (5'-3')[1]
sgRNAs for CRISPR-Cas9 gene impairment	1	PSY1sgRNA-F	ATTGAGCCGGATATACCTATTCCG
	2	PSY1sgRNA-R	AAACCGGAATAGGTATATCCGGCT
	3	PSY2sgRNA-F	ATTGGTATGAGGTGGTATTGAAGC
	4	PSY2sgRNA-R	AAACGCTTCAATACCACCTCATAC
RT-qPCR	5	PSY1-qF	ACAGGCAGGTCTATCCGATG
	6	PSY1-qR	ACGCCTTTCTCTGCCTCATC
	7	PSY2-qF	CAGGGCTCTCCGATGAAGAC
	8	PSY2-qR	CACCGGCCATCTACTAGCAG
	9	PSY3-qF	TTGGATGCAATAGAGGAGAATG
	10	PSY3-qR	ATTGAATGGCTAAACTAGGCAAAG
	11	ACT4-qF	CCTTCCACATGCCATTCTCC
	12	ACT4-qR	CCACGCTCGGTCAGGATCT
CRISPR plants genotyping	13	PSY1gsF	CGAGGCATAGGAATTTGGTG
	14	PSY1gWT-1F	GTGAAGCCGGATATACCTATT
	15	PSY1gm-1F	GTGAAGCCGGATATACCTATC
	16	PSY1gWT-2F	GTGAAGCCGGATATACCTATTC
	17	PSY1gm-2F	GTGAAGCCGGATATACCTATTT
	18	PSY1gR	CCATATATTGCCCAGATAGC
	19	PSY2gF	GGGTTGTTTCTCCGAATTCCG
	20	PSY2gR	GCATGGTTCCTAAATAAGAACC
	21	Cas9F	TCCCTCATCAGATCCACCTC
	22	Cas9R	CTGAAACGTGAGCCTTCTGG
	23	NTPIIF	GAAGGGGATAGAAGGCGA
	24	NTPIIR	AGATGGATTGCACGCAGG

Table S2. CRISPR-Cas9 constructs and cloning details.

Use	Construct	Template	Primers	Sequence cloned[1]	Cloning method	Entry plasmid	Destiny plasmid
CRISPR-Cas9 gene impairment	*pEN-SlPSY1(sg1)*	-	1+2	$SlPSY1_{1849-1868}$	*BbsI* / T4 ligase	pENC1.1	-
	pEN-SlPSY2(sg1)	-	3+4	$SlPSY2_{806-825}$	*BbsI* / T4 ligase	pENC1.1	-
	pDE-SlPSY1,2(1+1)	*pEN-SlPSY1(sg1)* + *pEN-SlPSY2(sg1)*	-	$SlPSY1_{1849-1868}$ + $SlPSY2_{806-825}$	PSY1(*sg1*)*MluI* + *Bsu36I* / T4 ligase PSY2(sg1)Gateway	*pEN-SlPSY1(sg1)* + *pEN-SlPSY2(sg1)*	pDE-Cas9

[1]Numbers indicate the first and last nucleotide positions cloned from the gDNA of the indicated genes

General discussion

1 Evolution of GGPPS and PSY gene families in plants

The presence of several homolog genes in a genome typically results from duplication of genomic fragments, chromosomes, or even whole genomes (Innan & Kondrashov, 2010; Wendel et al., 2016). While ortholog genes (homolog genes in different species) display similar function across species, several paralogs (homolog genes in the same species) are only maintained in a genome if its presence involves an evolutive advantage. There are three options for a paralog gene after a duplication event: (1) to evolve towards a new function, changing its original role (what is called **neofunctionalization**), (2) to retain and share the ancestral function with other paralogs, but providing it in different cell compartments or under different environmental cues (what is called **subfunctionalization**), or (3) to inactivate through different mutations and become a pseudogene (Coman et al., 2014; Wendel et al., 2016). In plants, GGPP is a hub metabolite for the synthesis of multiple plastidial and cytosolic isoprenoids. Evolution of GGPPS homologs in photosynthetic organisms is a clear example of how neofunctionalization and subfunctionalization work (Figure 1). Several conserved domains are key for SC-PT activity, and genetic changes in those domains have given origin to SSU-I, SSU-II, GGPS, FPPS, and GGPPS enzymes, among others (Nagel et al., 2019; Wang et al., 2016; Wang & Dixon, 2009) (Figure 1). Two conserved domains are key for SC-PT catalytic activity, named first and second Asp-rich motifs (FARM and SARM, respectively). Accumulation of inactivating mutations in FARM and SARM domains resulted in SSU proteins, which are enzymatically inactive by themselves (Figure 1). SSU-I proteins lost both FARM and SARM, whereas SSU-II lost the SARM (Coman et al., 2014; Zhou & Pichersky, 2020). A third domain upstream the FARM and named CxxxC is responsible for protein-protein interaction. SSU proteins acquired a second motif upstream the SARM that allows them to heterodimerize with a more diverse range of proteins, including LSUs (Barja & Rodriguez-Concepcion, 2021). For example, heterodimerization with LSU-GGPPS members allow SSU proteins to modulate their activity in order to produce specifically GGP or enhance GGPP synthesis in a diversity of plant species (Wang et al., 2018; Zhou et al., 2017; Zhou & Pichersky, 2020). Another important motif in SC-PT enzymes is the chain-length determination motif (CLD), located upstream the FARM. The motif forms an elongation pocket in which the size of the side chains of the residues at the fourth and/or the fifth position before the FARM determine the length of the final product (e.g., GPP, FPP or GGPP) (Nagel et al., 2015; Wang et al., 2016). Changes in the CLD domain are therefore key for neofunctionalization as they generated LSU-GPPS, LSU-FPPS, or LSU-GGPPS enzymes (Figure 1). In any case,

prediction of product specificity of LSUs based only on sequence homology is still a challenge and experimental evidence is still a must to ascertain enzymatic activity and biological function.

In the case of LSU-GGPPS enzymes, a single copy gene is present in green algae, but small gene families are typically present in higher plants (Barja & Rodriguez-Concepcion, 2021; Coman et al., 2014). This evolution has been associated to subfunctionalization as new and more diverse roles were attributed to isoprenoid metabolites along the plant kingdom during evolution.

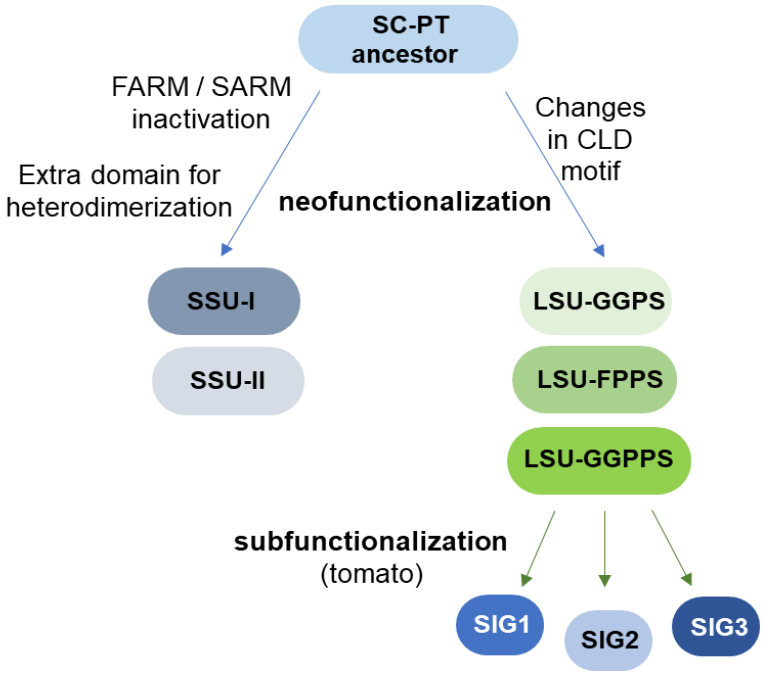

Figure 1. Simplified model for GGPPS evolution. Neofunctionalization created SSU and LSU proteins with different activities. Later on, subfunctionalization of tomato LSU-GGPPS proteins generated the current complement of three paralogs producing GGPP in plastids of different tissues, at particular developmental stages or under specific environmental cues.

PSY enzymes have also gone through a subfunctionalization process during land plant evolution (Figure 2). PSY enzymes in bacteria, algae, mosses, and monocot and dicot plants share conserved Asp-rich domains and hydrophobic flap pockets that are essential for their activity to transform GGPP into phytoene (Dibari et al., 2012; Gallagher et al., 2004; Han et al., 2015). Phylogenetical analyses initially divided PSY plant enzymes into two separate clades. From these, one clade corresponds to monocot and dicot PSY isoforms where sub-clades partially divide PSY sequences specifically into monocot or dicot groups (Han et al., 2015). The second clade contains far-related green

algae and moss PSY enzymes (Han et al., 2015; Rensing et al., 2007). More complete analyses separated plant PSY into two clades. The largest clade includes all angiosperm (monocot and dicot) PSY1 and PSY2 genes and also the monocot PSY3 sub-clade (Walter et al., 2015). The other clade contains far-related dicot PSY3 isoforms that only share around 50% homology with dicot PSY1 and PSY2 counterparts., Moss PSY isoforms are found outside these clades (Walter et al., 2015). The subfunctionalization of PSY1 and PSY2 paralogs was the result of mutations and mainly by acquiring different tissue-specific expression patterns (Walter et al., 2015). Numbering of these PSY isoforms is based on their order of discovery and does not give clues about evolutionary origin or function. PSY2, the housekeeping isoform providing carotenoids for leaf photoprotection in most species, is believed to be the presumable ancestor of specialized PSY1 isoforms by duplication (Figure 2). Several PSY1 isoforms are involved in the accumulation of high amount of carotenoids as pigments in particular tissues, such as fruit pericarp in tomato and pepper (Fanciullino et al., 2007; Fraser et al., 1999; Wei et al., 2021), seed endosperm in maize and sorghum (Li et al., 2008; Welsch et al., 2008), secondary root in carrot (Fuentes et al., 2012; Just et al., 2007) or tubers in cassava (Arango et al., 2010; Welsch et al., 2010). It is important to mention that in most of these species, PSY1 and PSY2 paralogs work in coordination to produce carotenoids for photoprotection or for pigmentation, even though their relative contributions change (Bowman et al., 2014). Monocot PSY3 isoforms are involved in the synthesis of ABA under drought or salt stress in roots (Dibari et al., 2012; Li et al., 2008; Welsch et al., 2008). By contrast, the phylogenetically distant dicot PSY3 isoforms are associated with the production of apocarotenoids such as SL (but not ABA) in roots (Stauder et al., 2018; Barja et al., 2021). Our work supports this classification as the tomato PSY3 is not involved in ABA biosynthesis but in SL production in roots (Chapter II).

The available data suggest that dicot PSY3 evolved very early, during (or before) transition from gymnosperms to angiosperms, long after the appearance of SLs, which are already produced in mosses (Walter et al., 2015). The reason why monocot (that appeared later in the evolutionary lineage) lost their dicot PSY3 ancestor remains unknown. Several groups of dicot plants such as Brassicaceae have also lost their dicot-PSY3 members (Walter et al., 2015), and Arabidopsis only maintains one PSY-encoding gene in its genome. In tomato, the presence of all three PSY types (PSY1, PSY2 and PSY3) strongly suggest an association with specialized new roles of carotenoids as pigments (in flowers and fruit) and modulators of mycorrhization (in roots) which favored the maintenance of the three genes and their subfunctionalization.

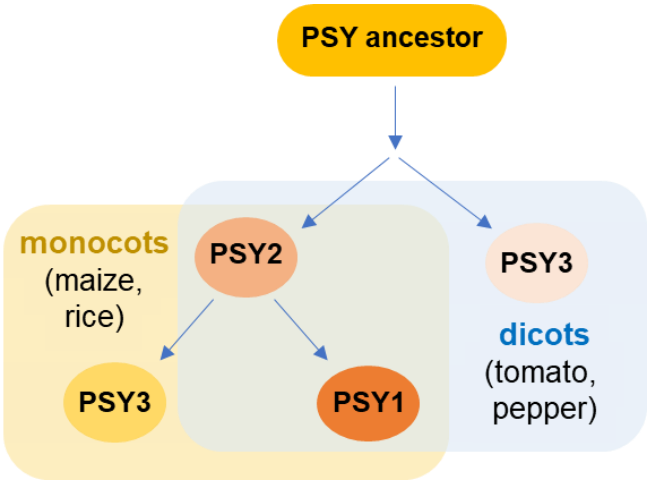

Figure 2. Simplified model for PSY evolution. Subfunctionalization from a PSY ancestor created new PSY paralogs that produce phytoene in different tissues, at particular developmental stages and/or in response to specific developmental (internal) or environmental (external) cues.

2 The GGPPS family in tomato

The knowledge regarding the GGPPS family in tomato at the start of this work was only partial and scattered. In these years, our work and that from other labs has represented a major advance in this issue. In the tomato genome there are two genes encoding homologs of SSU proteins: SSU-I (Solyc07g064660) and SSU-II (Solyc09g008920) (Zhou & Pichersky, 2020). Both proteins localize in plastids and lack catalytic activity *in vitro* in the presence of IPP and DMAPP. Regarding GGPPS-like enzymes, five putative homologs were found. From these, two lack GGPPS activity and localize in mitochondria: SlTPT1, (Solyc02g085710) and SlTPT2 (Solyc02g085720). The other three paralogs are SlG1 (Solyc11g011240), SlG2 (Solyc04g079960) and SlG3 (Solyc02g085700), the ones analyzed in detail in this thesis work. All three of them have been shown to be targeted to plastids and to produce GGPP as their main product (Barja et al., 2021; Zhou & Pichersky, 2020). The set of plastidial GGPPS enzymes present in tomato (SlG1, SlG2 and SlG3) has undergone subfunctionalization to provide GGPP in a tissue-specific manner and attending to different developmental or environmental cues (Figure 3). Throughout this doctoral thesis, genetic, biochemical, molecular, transcriptomic and metabolic approaches have allowed to unveil the roles of these three GGPPS paralogs. *SlG3* is highly and almost constitutively expressed in most tomato plant tissues, and acts as a housekeeping gene in charge of providing most of the GGPP necessary to produce photosynthesis-related isoprenoids and fruit carotenoids (Figure 3). *SlG2* is generally expressed at lower levels than *SlG3* but it is highly connected to other genes involved in

plastidial isoprenoid biosynthesis as its expression responds to peak demands of carotenoids and/or other isoprenoids, *e.g.,* during deetiolation or fruit ripening. We therefore consider SlG2 to be a support GGPPS that helps SlG3 in providing GGPP in both leaves and fruits when most needed (Figure 3). Intriguingly, both isoforms additively contribute to GGPP production in embryo/seed development, and absence of both SlG2 and SlG3 results in a lethal embryo phenotype that might be independent of the role of these enzymes in plastids, similar to that described in Arabidopsis (Ruiz-Sola et al., 2016a). Finally, our work allowed to conclusively demonstrate that SlG1 mainly functions in roots to provide precursors for SL synthesis (and likely other mycorrhization-associated apocarotenoids) (Figure 3), as suggested by a previous model based on gene expression profiles (Stauder et al., 2018). Double mutants defective in SlG1 and SlG2 or SlG3 have been generated and their analysis will provide new clues to establish possible cooperative roles of these GGPPS paralogs in different tomato tissues.

3 The PSY family in tomato

Three members form the PSY family in tomato: PSY1 (Solyc03g031860), PSY2 (Solyc02g081330), and PSY3 (Solyc01g005940) (Fraser et al., 1999; Giorio et al., 2008; Stauder et al., 2018). Some information was available at the beginning of this thesis about the roles of the different tomato PSY paralogs, particularly for PSY1 and PSY2, based on gene expression data and phenotypic features of PSY1-defective lines (Giorio et al., 2008; Kachanovsky et al., 2012; Fantini et al., 2013; Kang et al., 2014). The model of PSY subfunctionalization in tomato was that PSY1 supports carotenoid synthesis in the chromoplasts of flowers and fruits and PSY2 in leaf chloroplasts. More recently, PSY3 was proposed to have a role restricted to roots for SL and mycorrhization-associated apocarotenoid synthesis (Stauder et al., 2018).

With our genetic and metabolic approaches based on generating and characterizing edited tomato lines defective in PSY1 or PSY2, we have correctly framed the proposed roles for tomato PSY isozymes and unraveled new functions related to ABA production. PSY2 is indeed the major isoform providing phytoene for carotenoid biosynthesis in the chloroplasts of green tissues, but we found that PSY1 has an important role to sustain carotenoid production when needed for peak demands, such as after exposure to intense light. PSY1 acting as a helper isoform of PSY2 in leaves is similar to that proposed for SlG2 and SlG3 (Figure 3). Unlike that observed for GGPPS paralogs, however, the distribution of functions is swapped between PSY isoforms in chromoplast-harboring

flower petals and fruit-pericarp tissues, where PSY1 is the one in charge of providing most precursors for carotenoids required for pigmentation (Figure 3).

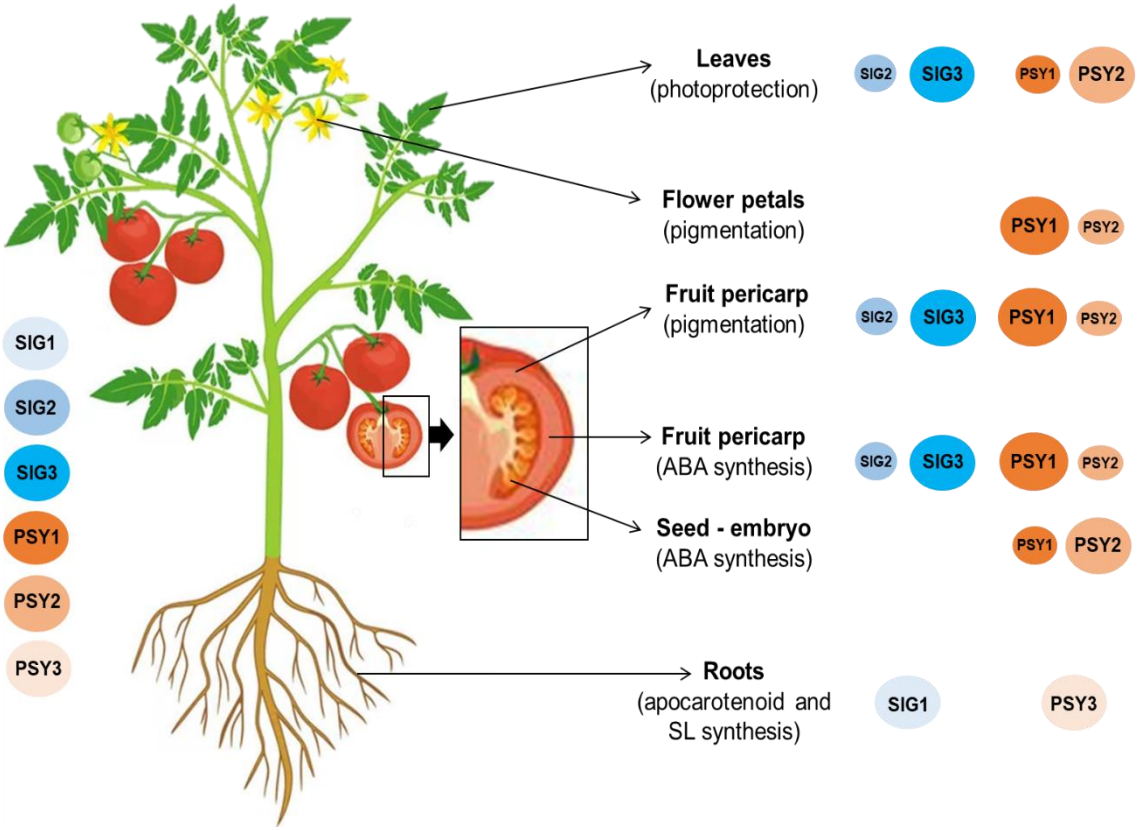

Figure 3. Proposed model for SlG1-3 and PSY1-3 functions in tomato. The size of the ellipses (proteins) represents the importance of that particular isoform for that specific function. Source of the picture: https://sp.depositphotos.com/vector-images/vue-g%C3%A9n%C3%A9rale.

Intriguingly, in flowers, where *PSY2* transcript levels are most abundant, the helper role of PSY2 only comes to light when PSY1 is absent. In tomato fruits, this role is even more difficult to see as the loss of PSY1 results in an almost complete absence of carotenoids in the pericarp of ripe tomatoes. Our work also found that PSY1 and PSY2 activities are essential to produce ABA in pericarp cells and seed embryos, respectively (Figure 3). Furthermore, we demonstrate that PSY1-derived ABA regulates fruit growth and ripening, whereas PSY2-derived ABA regulates seed dormancy and germination. The mechanisms whereby the phytoene specifically produced by PSY1 or PSY2 in different spatial locations of the same organ is channeled to the production of ABA remains unknown. The observation that double mutants lacking PSY1 and PSY2 show an albino seedling-lethal phenotype confirmed that PSY3 is unable to complement the loss of the other two paralogs and to produce photoprotective carotenoids during seedling

development. Analysis of SL production by roots of different mutants defective in individual GGPPS and PSY isoforms indirectly supported a role for PSY3 in this process, acting in close coordination with SlG1 (Figure 3). However, a role for PSY1 cannot be completely excluded. Generation and analysis of a PSY3-defective mutant would be necessary to clarify this issue.

4 The GGPPS and PSY interaction network to direct GGPP flux into the carotenoid pathway: an open question

As summarized in the Introduction section, physical interaction between GGPPS and PSY is required for efficient channeling of MEP-derived IPP and DMAPP into phytoene for downstream carotenoid and apocarotenoid (including ABA and SL) biosynthesis. This interaction has been shown in several dicot plants, including Arabidopsis, pepper and tomato (Chapter III) (Barja et al., 2021; Camagna et al., 2019; Dogbo and Camara 1987; Fraser et al., 2000; Maudinas et al. 1977; Ruiz-Sola et al., 2016b; Wang et al., 2018). Strikingly, in the monocot rice, interaction of OsGGPPS1 with PSY enzymes could not be observed. Instead, OsGGPPS1 was recruited by SSU-II to a large protein complex with GGR to channel GGPP into the chlorophyll biosynthesis pathway (Zhou et al., 2017). In this thesis, we found that tomato SlG2 is able to interact with PSY1 and PSY2, whereas SlG1 interacts exclusively with PSY3 *in planta*. Although some protein structural data are available for GGPPS and PSY, little is known about their protein-protein interaction domains, and how the sequence differences of the paralogs selectively affect GGPPS/PSY interaction. All SlG1-3 isoforms have an active protein-protein interaction domain (CxxxC) located upstream the FARM in a very similar position (Coman et al., 2014). This CxxxC domain has been proved to be active for the formation of GGPPS homo and heterodimers but it is unknown whether it could also participate in the interaction with PSY isoforms. Structural information about key sites involved in tomato PSY1 and PSY2 substrate and co-factor binding, active catalytic residues and Asp-rich regions is relatively complete (Cao et al., 2019; Giorio et al., 2008) but no information about possible protein interaction sites is available. In Arabidopsis, ClpC1 chaperones bind to the N-terminal region of PSY to deliver the enzyme to proteolytic degradation by the Clp protease complex (Welsch et al., 2018).

Strikingly, such N-terminal region is one of the less conserved region among plant and particular tomato PSY proteins (Cao et al., 2019; Giorio et al., 2008), so it is very difficult to predict which are the domains that mediate PSY interaction with other proteins.

It is surprising that SlG3, the tomato housekeeping GGPPS, does not appear to directly interact with any PSY isoform in homodimeric form. We showed that SlG3 is able to form heterodimers with SlG2, and these heterodimers could then interact with PSY1 or PSY2. It is reasonable that SlG3 and SlG1 could also form heterodimers, hence allowing access of SlG3 to PSY3 in roots. An alternative possibility involves interaction with SSU-II. Pepper SSU-II interacts with CaGGPPS1 but also with PSY (Wang et al., 2018), and rice SSU-II interacts with OsGGPPS1 to deliver it to a multiprotein complex (Zhou et al., 2017).. It is therefore possible that heterodimerization with tomato SSU-II might also deliver SlG3 (as well as SlG1 and SlG2) to PSY-containing protein complexes.

Another possibility is that interaction of SlG3 with particular PSY isoforms requires specific partners only found in some tomato tissues (*e.g.,* in flowers and fruit pericarp to interact with PSY1, leaves and seeds to interact with PSY2 or roots to interact with PSY3). Such multienzymatic complex approach, appears to be particularly important for metabolic channeling of GGPP. In tomato and pepper chromoplasts, large protein complexes containing PSY, GGPPS and other isoprenoid biosynthetic enzymes were isolated long time ago, even though specific members of these complexes were never identified (Camara et al., 1993; Fraser et al., 2000; Maudinas et al., 1977). Also, in cauliflower a large protein complex associated to membranes and containing PDS has been reported (Lopez et al., 2008). The existence of such complexes appears as an attractive explanation to the channeling of MEP-derived isoprenoid precursors produced in the plastid stroma to the carotenoid biosynthesis, that is believed to be associated to membranes (Ruiz-Sola & Rodriguez-Concepcion, 2012). However channeling of specific carotenoid pools all the way to ABA (in fruits) or SLs (in roots) are difficult to fit in a metabolon-dependent model due to the large number of reactions and the diversity of subcellular localizations reported for the enzymes involved, which include several cytosolic steps following the cleavage of β-carotene-derived precursors (Al-Babili & Bouwmeester, 2015; Nambara & Marion-Poll, 2005). In any case, double mutants defective in SlG3 and particular PSY isoforms could bring some light into how GGPP is derived specifically to carotenoid biosynthesis in tomato tissues.

In summary, the results obtained in this doctoral thesis show a finely spatio-temporal regulation of GGPPS and PSY function in tomato. Different subfunctionalized isoforms accomplish specific functions (i.e. photoprotection, mycorrhization, hormone production or petal and fruit pigmentation) hence explaining why tomato maintains small GGPPS and PSY gene families. The knowledge acquired here will be helpful to set up new agro-genetic tools that would allow the development of crops biofortified in health promoting GGPP-derived metabolites in a more sustainable way with the environment.

Conclusions

1. Gene families of three members encode plastidial GGPP synthases (SlG1-3) and phytoene synthases (PSY1-3) in tomato, showing a strong subfunctionalization.

2. SlG3 functions as the housekeeping isoform and supplies GGPP for general isoprenoid production in plastids, whereas SlG2 has a helper role when extra GGPP is needed in shoot tissues, including leaves and fruits.

3. Loss of both SlG3 and SlG2 results in an embryo lethal phenotype, indicating that SlG1 cannot complement their activities at least during embryo development.

4. SlG1 works specifically in roots, providing GGPP for the biosynthesis of strigolactones (SLs), a group of carotenoid-derived hormones.

5. Tomato mutants defective in SlG1 do not have the shoot phenotypes displayed by SL-deficient mutants, suggesting that SiG1 only provides precursors for these hormones in roots.

6. Efficient channeling of GGPP into the carotenoid pathway involves direct interaction of GGPP and phytoene synthases. SlG2 interacts with PSY1 and PSY2 (but not with PSY3), and SlG1 interacts with PSY3 (but not with PSY1 and PSY2). Strikingly, SlG3 does not interact with any PSY.

7. Loss of PSY1 and PSY2 generates an albino seedling-lethal phenotype that cannot be rescued by PSY3, an isoform closely associated to SlG1 for root SL production.

8. In the shoot, PSY2 provides carotenoid for photoprotection in chloroplasts with the help of PSY1, whereas PSY1 is the main isoform for carotenoid biosynthesis in the chromoplasts of flower and fruit pericarp tissues.

9. The production of ABA, another carotenoid-derived hormone, is differentially associated to PSY1 and PSY2 isoforms in fruit. Mutants defective in PSY1 show lower ABA levels in the fruit flesh, leading to smaller fruit and a slower ripening, whereas those lacking PSY2 have reduced ABA in seeds causing faster germination.

10. Genetic evidence (generation and analysis of mutants) is necessary to unravel specific roles acquired after subfunctionalization of enzyme isoforms that cannot be deduced from the analysis of gene expression profiles.

General references

Ahrazem O, Diretto G, Argandoña Picazo J, Fiore A, Rubio-Moraga Á, Rial C, Varela RM, Macías FA, Castillo R, Romano E & Gómez-Gómez L. (2019). The Specialized Roles in Carotenogenesis and Apocarotenogenesis of the Phytoene Synthase Gene Family in Saffron. *Frontiers in Plant Science*, 10(249).

Akhtar, T. A., Matsuba, Y., Schauvinhold, I., Yu, G., Lees, H. A., Klein, S. E., & Pichersky, E. (2013). The tomato cis–prenyltransferase gene family. The Plant Journal, 73(4), 640-652.

Al-Babili, S., & Beyer, P. (2005). Golden Rice - Five years on the road - Five years to go? *Trends in Plant Science*, 10(12), 565–573.

Al-Babili, S., & Bouwmeester, H. J. (2015). Strigolactones, a novel carotenoid-derived plant hormone. *Annual Review of Plant Biology*, 66, 161–186.

Álvarez, D., Voß, B., Maass, D., Wüst, F., Schaub, P., Beyer, P., & Welsch, R. (2016). Carotenogenesis is regulated by 5'UTR-mediated translation of phytoene synthase splice variants. *Plant Physiology,* 172(4), 2314–2326.

Ament, K., van Schie, C. C., Bouwmeester, H. J., Haring, M. A., & Schuurink, R. C. (2006). Induction of a leaf specific geranylgeranyl pyrophosphate synthase and emission of (E,E)-4,8,12-trimethyltrideca-1,3,7,11-tetraene in tomato are dependent on both jasmonic acid and salicylic acid signaling pathways. *Planta*, 224(5), 1197–1208.

Arango, J., Wüst, F., Beyer, P., & Welsch, R. (2010). Characterization of phytoene synthases from cassava and their involvement in abiotic stress-mediated responses. *Planta*, 232(5), 1251–1262.

Barja, M. V., Ezquerro, M., Beretta, S., Diretto, G., Florez-Sarasa, I., Feixes, E., Fiore, A., Karlova, R., Fernie, A. R., Beekwilder, J., & Rodríguez-Concepción, M. (2021). Several geranylgeranyl diphosphate synthase isoforms supply metabolic substrates for carotenoid biosynthesis in tomato*. New Phytologist*, 231(1), 255–272.

Barja, M. V., & Rodriguez-Concepcion, M. (2021). Plant geranylgeranyl diphosphate synthases: every (gene) family has a story*. aBIOTECH*, 2(3), 289–298.

Bartley, G. E., & Scolnik, P. A. (1993). cDNA cloning, expression during development, and genome mapping of PSY2, a second tomato gene encoding phytoene synthase. *Journal of Biological Chemistry*, 268(34), 25718–25721.

Beck, G., Coman, D., Herren, E., Ruiz-Sola, M. Á., Rodríguez-Concepción, M., Gruissem, W., & Vranová, E. (2013). Characterization of the GGPP synthase gene family in Arabidopsis thaliana. *Plant Molecular Biology*, 82(4–5), 393–416.

Bramley, P. M. (2002). Regulation of carotenoid formation during tomato fruit ripening and development. *Journal of experimental botany*, 53(377), 2107-2113.

Dogbo, O., & Camara, B. (1987). Purification of isopentenyl pyrophosphate isomerase and geranylgeranyl pyrophosphate synthase from Capsicum chromoplasts by affinity chromatography. *Biochimica et Biophysica Acta (BBA)-Lipids and Lipid Metabolism*, 920(2), 140-148.

Bouvier, F., Rahier, A., & Camara, B. (2005). Biogenesis, molecular regulation and function of plant isoprenoids. *Progress in Lipid Research* 44(6), 357–429.

Bowman, M. J., Willis, D. K., & Simon, P. W. (2014). Transcript abundance of phytoene synthase 1 and phytoene synthase 2 is associated with natural variation of storage root carotenoid pigmentation in carrot. *Journal of the American Society for Horticultural Science*, 139(1), 63-68.

Camagna, M., Grundmann, A., Bar, C., Koschmieder, J., Beyer, P., & Welsch, R. (2019). Enzyme fusion removes competition for geranylgeranyl diphosphate in carotenogenesis. *Plant Physiology*, 179(3), 1013–1027.

Camara, B. (1993). Plant phytoene synthase complex: Component enzymes, Immunology and Biogenesis. *Methods in Enzymology*, 214, 352–365.

Cao, H., Luo, H., Yuan, H., Eissa, M. A., Thannhauser, T. W., Welsch, R., Hao, Y. J., Cheng, L., & Li, L. (2019). A neighboring aromatic-aromatic amino acid combination governs activity divergence between tomato phytoene synthases. *Plant Physiology*, 180(4), 1988–2003.

Celedon, J. M., & Bohlmann, J. (2019). Oleoresin defenses in conifers: chemical diversity, terpene synthases and limitations of oleoresin defense under climate change. *New Phytologist,* 224(4), 1444–1463.

Coman, D., Altenhoff, A., Zoller, S., Gruissem, W., & Vranová, E. (2014). Distinct evolutionary strategies in the GGPPS family from plants. *Frontiers in Plant Science*, 5(230).

D'Andrea, L., & Rodriguez-Concepcion, M. (2019). Manipulation of Plastidial Protein Quality Control Components as a New Strategy to Improve Carotenoid Contents in Tomato Fruit. *Frontiers in Plant Science*, 10(1071).

Degenhardt, J., Köllner, T. G., & Gershenzon, J. (2009). Monoterpene and sesquiterpene synthases and the origin of terpene skeletal diversity in plants. *Phytochemistry* 70(15), 1621–1637.

Dhar, M. K., Koul, A., & Kaul, S. (2013). Farnesyl pyrophosphate synthase: A key enzyme in isoprenoid biosynthetic pathway and potential molecular target for drug development. *New Biotechnology*, 30(2), 114–123.

Dibari, B., Murat, F., Chosson, A., Gautier, V., Poncet, C., Lecomte, P., Mercier, I., Bergès,H., Pont, C., Blanco, A., & Salse, J. (2012). Deciphering the genomic structure, function and evolution of carotenogenesis related phytoene synthases in grasses. *BMC Genomics*, 13(1).

Duetz, W. A., Bouwmeester, H., van Beilen, J. B., & Witholt, B. (2003). Biotransformation of limonene by bacteria, fungi, yeasts, and plants. *Applied Microbiology and Biotechnology* 61(4), 269–277.

Falara, V., Akhtar, T. A., Nguyen, T. T. H., Spyropoulou, E. A., Bleeker, P. M., Schauvinhold, I., Matsuba, Y., Bonini, M. E., Schilmiller, A. L., Last, R. L., Schuurink, R. C., & Pichersky, E. (2011). The tomato terpene synthase gene family. *Plant Physiology*, 157(2), 770–789.

Fanciullino, A. L., Dhuique-Mayer, C., Luro, F., Morillon, R., & Ollitrault, P. (2007). Carotenoid biosynthetic pathway in the Citrus genus: Number of copies and phylogenetic diversity of seven genes. *Journal of Agricultural and Food Chemistry*, 55(18), 7405–7417.

Fester, T., Schmidt, D., Lohse, S., Walter, M. H., Giuliano, G., Bramley, P. M., Fraser, P. D., Hause, B., & Strack, D. (2002). Stimulation of carotenoid metabolism in arbuscular mycorrhizal roots. *Planta*, 216(1), 148–154.

Fraser, P. D., Kiano, J. W., Truesdale, M. R., Schuch, W., & Bramley, P. M. (1999). Phytoene synthase-2 enzyme activity in tomato does not contribute to carotenoid synthesis in ripening fruit. *Plant Molecular Biology*, 40, 687–698.

Fraser PD, Schuch W, Bramley PM (2000) Phytoene synthase from tomato (Lycopersicon esculentum) chloroplasts–partial purification and biochemical properties. *Planta* 211, 361–369.

Fraser, P. D., Truesdale, M. R., Bird, C. R., Schuch, W., & Bramley, P. M. (1994). Carotenoid Biosynthesis during Tomato Fruit Development Evidence for Tissue-Specific Gene Expression. *Plant Physiology*, 105(1), 405-413.

Fuentes, P., Pizarro, L., Moreno, J. C., Handford, M., Rodriguez-Concepcion, M., & Stange, C. (2012). Light-dependent changes in plastid differentiation influence carotenoid gene expression and accumulation in carrot roots. *Plant Molecular Biology*, 79(1), 47–59.

Fujisawa, M., Shima, Y., Nakagawa, H., Kitagawa, M., Kimbara, J., Nakano, T., Kasumi, T., & Ito, Y. (2014). Transcriptional regulation of fruit ripening by tomato FRUITFULL homologs and associated MADS box proteins. *Plant Cell*, 26(1), 89–101.

Gallagher, C. E., Matthews, P. D., Li, F., & Wurtzel, E. T. (2004). Gene duplication in the carotenoid biosynthetic pathway preceded evolution of the grasses. *Plant Physiology*, 135(3), 1776–1783.

García-Llatas, G., & Rodríguez-Estrada, M. T. (2011). Current and new insights on phytosterol oxides in plant sterol-enriched food. *Chemistry and Physics of Lipids*, 164(6), 607–624.

Giorio, G., Stigliani, A. L., & D'Ambrosio, C. (2008). Phytoene synthase genes in tomato (Solanum lycopersicum L.) - New data on the structures, the deduced amino acid sequences and the expression patterns. *FEBS Journal*, 275(3), 527–535.

Han, Y., Zheng, Q. S., Wei, Y. P., Chen, J., Liu, R., & Wan, H. J. (2015). In silico identification and analysis of phytoene synthase genes in plants. *Genetics and Molecular Research*, 14(3), 9412–9422.

Harel-Beja, R,. Tzuri, G,.. Portnoy,, V,.. Lotan-Pompan, M,. Lev S,. Cohen, S, Dai N,. Yeselson, L,. Meir A,. SE L, Avisar E,. Melame T,. Van Koert P,. Verbakel H,. Hofstede R, Volpin H, Oliver M, Fougedoire A, Stalh C, Fauve J, Copes B, Fei Z, Giovannoni J,. Ori N, Lewinsohn E,. Sherman A,. Burger J,. Tadmor Y,. AA S., & Katzir N. (2010). A genetic map of melon highly enriched with fruit quality QTLs and EST markers, including sugar and carotenoid metabolism genes. *Theoretical and Applied Genetics*, 121, 511–533.

Hemmerlin, A., Harwood, J. L., & Bach, T. J. (2012). A raison d'être for two distinct pathways in the early steps of plant isoprenoid biosynthesis? *Progress in Lipid Research*, 51(2), 95–148

Hivert, G., Davidovich-Rikanati, R., Bar, E., Sitrit, Y., Schaffer, A., Dudareva, N., & Lewinsohn, E. (2020). Prenyltransferases catalyzing geranyldiphosphate formation in tomato fruit. *Plant Science*, 296, 110504.

Innan, H., & Kondrashov, F. (2010). The evolution of gene duplications: Classifying and distinguishing between models. *Nature Reviews Genetics*, 11(2) 97–108.

Jang, S. J., Jeong, H. B., Jung, A., Kang, M. Y., Kim, S., Ha, S. H., Kwon, J. K., & Kang, B. C. (2020). Phytoene synthase 2 can compensate for the absence of PSY1 in the control of color in Capsicum fruit. *Journal of Experimental Botany*, 71(12), 3417–3427.

Jansen, R. M. C., Miebach, M., Kleist, E., van Henten, E. J., & Wildt, J. (2009). Release of lipoxygenase products and monoterpenes by tomato plants as an indicator of Botrytis cinerea-induced stress. *Plant Biology*, 11(6), 859–868.

Jaswir, I., Noviendri, D., Hasrini, R. F., & Octavianti, F. (2011). Carotenoids: Sources, medicinal properties and their application in food and nutraceutical industry. *Journal of Medicinal Plant Research*, 5(33), 7119–7131.

Just, B. J., Santos, C. A. F., Fonseca, M. E. N., Boiteux, L. S., Oloizia, B. B., & Simon, P. W. (2007). Carotenoid biosynthesis structural genes in carrot (Daucus carota): Isolation, sequence-characterization, single nucleotide polymorphism (SNP) markers and genome mapping. *Theoretical and Applied Genetics*, 114(4), 693–704.

Kachanovsky, D. E., Filler, S., Isaacson, T., & Hirschberg, J. (2012). Epistasis in tomato color mutations involves regulation of phytoene synthase 1 expression by cis-carotenoids. *Proceedings of the National Academy of Sciences*, 109(46), 19021–19026.

Kang, B., Gu, Q., Tian, P., Xiao, L., Cao, H., & Yang, W. (2014). A chimeric transcript containing Psy1 and a potential mRNA is associated with yellow flesh color in tomato accession PI 114490. *Planta*, 240(5), 1011–1021.

Karniel, U., Adler Berke, N., Mann, V., & Hirschberg, J. (2022). Perturbations in the Carotenoid Biosynthesis Pathway in Tomato Fruit Reactivate the Leaf-Specific Phytoene Synthase 2. Frontiers in Plant Science, 13.

Kim, O. R., Cho, M. C., Kim, B. D., & Huh, J. H. (2010). A splicing mutation in the gene encoding phytoene synthase causes orange coloration in Habanero pepper fruits. *Molecules and Cells*, 30(6), 569–574.

Kirby, J., & Keasling, J. D. (2009). Biosynthesis of plant isoprenoids: Perspectives for microbial engineering. *Annual Review of Plant Biology*, 60, 335–355.

Kumar, S. R., Rai, A., Bomzan, D. P., Kumar, K., Hemmerlin, A., Dwivedi, V., Godbole, R. C., Barvkar, V., Shanker, K., Shilpashree, H. B., Bhattacharya, A., Smitha, A. R., Hegde, N., & Nagegowda, D. A. (2020). A plastid-localized bona fide geranylgeranyl diphosphate synthase plays a necessary role in monoterpene indole alkaloid biosynthesis in Catharanthus roseus. *Plant Journal*, 103(1), 248–265.

Kuromori, T., Seo, M., & Shinozaki, K. (2018). ABA Transport and Plant Water Stress Responses. *Trends in Plant Science,* 23(6), 513–522.

Li, F., Vallabhaneni, R., Yu, J., Rocheford, T., & Wurtzel, E. T. (2008). The maize phytoene synthase gene family: Overlapping roles for carotenogenesis in endosperm, photomorphogenesis, and thermal stress tolerance. *Plant Physiology*, 147(3), 1334–1346.

Liang, P. H., Ko, T. P., & Wang, A. H. J. (2002). Structure, mechanism and function of prenyltransferases. *European Journal of Biochemistry,* 269(14), 3339–3354.

Lopez, A.B., Yang, Y., Thannhauser, T.W., and Li, L. (2008). Phytoene desaturase is present in a large protein complex in the plastid membrane. *Plant physiology*, 133, 190-198.

Llorente, B., D'Andrea, L., Ruiz-Sola, M. A., Botterweg, E., Pulido, P., Andilla, J., Loza-Alvarez, P., & Rodriguez-Concepcion, M. (2016). Tomato fruit carotenoid biosynthesis is adjusted to actual ripening progression by a light-dependent mechanism. *Plant Journal*, 85(1), 107–119.

Lu, S., Zhang, Y., Zhu, K., Yang, W., Ye, J., Chai, L., Xu, Q., & Deng, X. (2018). The citrus transcription factor CsMADS6 modulates carotenoid metabolism by directly regulating carotenogenic genes. *Plant Physiology*, 176(4), 2657–2676.

Matthys, C., Walton, A., Struk, S., Stes, E., Boyer, F. D., Gevaert, K., & Goormachtig, S. (2016). The Whats, the Wheres and the Hows of strigolactone action in the roots. *Planta* 243(6), 1327–1337.

Maudinas, B., Bucholtz, M.L., Papastephanou, C., Katiyar, S.S., Briedis, A. V., and Porter, J.W. (1977). The partial purification and properties of a phytoene synthesizing enzyme system. *Archives of Biochemistry and Biophysics,* 180, 354–362.

Moreno, J. C., Mi, J., Alagoz, Y., & Al-Babili, S. (2021). Plant apocarotenoids: from retrograde signaling to interspecific communication. *Plant Journal*, 105(2), 351–375.

Nagel, R., Bernholz, C., Vranová, E., Košuth, J., Bergau, N., Ludwig, S., Wessjohann, L., Gershenzon, J., Tissier, A., & Schmidt, A. (2015). Arabidopsis thaliana isoprenyl diphosphate synthases produce the C25 intermediate geranylfarnesyl diphosphate. *Plant Journal*, 84(5), 847–859.

Nagel, R., Schmidt, A., & Peters, R. J. (2019). Isoprenyl diphosphate synthases: the chain length determining step in terpene biosynthesis. *Planta*, 249(1), 9–20.

Nambara, E., & Marion-Poll, A. (2005). Abscisic acid biosynthesis and catabolism. *Annual Review of Plant Biology*, 56, 165–185.

Nawade, B., Shaltiel-Harpaz, L., Yahyaa, M., Bosamia, T. C., Kabaha, A., Kedoshim, R., Zohar, M., Isaacson, T., & Ibdah, M. (2020). Analysis of apocarotenoid volatiles during the development of Ficus carica fruits and characterization of carotenoid cleavage dioxygenase genes. *Plant Science*, 290, 110292.

Nouri, E., Surve, R., Bapaume, L., Stumpe, M., Chen, M., Zhang, Y., Ruyter-Spira, C., Bouwmeester, H., Glauser, G., Bruisson, S., & Reinhardt, D. (2021). Phosphate Suppression of Arbuscular Mycorrhizal Symbiosis Involves Gibberellic Acid Signaling. *Plant and Cell Physiology*, 62(6), 959–970.

Paine, J. A., Shipton, C. A., Chaggar, S., Howells, R. M., Kennedy, M. J., Vernon, G., Wright, S. Y., Hinchliffe, E., Adams, J. L., Silverstone, A. L., & Drake, R. (2005). Improving the nutritional value of Golden Rice through increased pro-vitamin A content. *Nature Biotechnology*, 23(4), 482–487.

Pasare S, Wright K, Campbell R, Morris W, Ducreux L, Chapman S, Bramley P, Fraser P, Roberts A & Taylor M. (2013). The sub-cellular localisation of the potato (Solanum tuberosum L.) carotenoid biosynthetic enzymes, CrtRb2 and PSY2. *Protoplasma* 250, 1381–1392.

Pokhilko, A., Bou-Torrent, J., Pulido, P., Rodríguez-Concepción, M., & Ebenhöh, O. (2015). Mathematical modelling of the diurnal regulation of the MEP pathway in Arabidopsis. *New Phytologist*, 206(3), 1075–1085.

Qin X, Coku A, Inoue K & Tian L. (2011). Expression, subcellular localization, and cis-regulatory structure of duplicated phytoene synthase genes in melon (Cucumis melo L.). *Planta* 234, 737–748.

Rao, A. v., & Rao, L. G. (2007). Carotenoids and human health. *Pharmacological Research*, 55(3), 207–216.

Rensing, S. A., Ick, J., Fawcett, J. A., Lang, D., Zimmer, A., van de Peer, Y., & Reski, R. (2007). An ancient genome duplication contributed to the abundance of metabolic genes in the moss Physcomitrella patens. *BMC Evolutionary Biology*, 7, 130-144.

Rodríguez-Concepción, M., Avalos, J., Bonet, M. L., Boronat, A., Gomez-Gomez, L., Hornero-Mendez, D., Limon, M. C., Meléndez-Martínez, A. J., Olmedilla-Alonso, B., Palou, A., Ribot, J., Rodrigo, M. J., Zacarias, L., & Zhu, C. (2018). A global perspective on carotenoids: Metabolism, biotechnology, and benefits for nutrition and health. *Progress in Lipid Research,* 70, 62–93.

Rodríguez-Villalón, A., Gas, E., & Rodríguez-Concepción, M. (2009). Phytoene synthase activity controls the biosynthesis of carotenoids and the supply of their metabolic precursors in dark-grown Arabidopsis seedlings. *Plant Journal,* 60(3), 424–435.

Rubio-Moraga, A., Rambla, J. L., Fernández-De-Carmen, A., Trapero-Mozos, A., Ahrazem, O., Orzáez, D., Granell, A., & Gómez-Gómez, L. (2014). New target carotenoids for CCD4 enzymes are revealed with the characterization of a novel stress-induced carotenoid cleavage dioxygenase gene from Crocus sativus. *Plant Molecular Biology*, 86(45), 555–569.

Ruiz-Lozano, J. M., Aroca, R., Zamarreño, Á. M., Molina, S., Andreo-Jiménez, B., Porcel, R., García-Mina, J. M., Ruyter-Spira, C., & López-Ráez, J. A. (2016). Arbuscular mycorrhizal symbiosis induces strigolactone biosynthesis under drought and improves drought tolerance in lettuce and tomato. *Plant Cell and Environment*, 39(2), 441–452.

Ruiz-Sola, M. Á., Barja, M. V., Manzano, D., Llorente, B., Schipper, B., Beekwilder, J., & Rodriguez-Concepcion, M. (2016a). A single arabidopsis gene encodes two differentially targeted geranylgeranyl diphosphate synthase isoforms. *Plant Physiology*, 172(3), 1393–1402.

Ruiz-Sola, M. Á., Coman, D., Beck, G., Barja, M. V., Colinas, M., Graf, A., Welsch, R., Rütimann, P., Bühlmann, P., Bigler, L., Gruissem, W., Rodríguez-Concepción, M., & Vranová, E. (2016b). Arabidopsis GERANYLGERANYL DIPHOSPHATE SYNTHASE 11 is a hub isozyme required for the production of most photosynthesis-related isoprenoids. *New Phytologist*, 209(1), 252–264.

Ruiz-Sola, M. Á., & Rodríguez-Concepción, M. (2012). Carotenoid Biosynthesis in Arabidopsis: A Colorful Pathway. *The Arabidopsis Book*, 10, e0158.

Ruyter-Spira, C., Al-Babili, S., van der Krol, S., & Bouwmeester, H. (2013). The biology of strigolactones. *Trends in Plant Science*, 18(2), 72–83.

Schuhr, C. A., Radykewicz, T., Sagner, S., Latzel, C., Zenk, M. H., Arigoni, D., Bacher, A., Rohdich, F., & Eisenreich, W. (2003). Quantitative assessment of crosstalk between the two isoprenoid biosynthesis pathways in plants by NMR spectroscopy. *Phytochemistry Reviews* 2, 3–16.

Simkin, A. J., Underwood, B. A., Auldridge, M., Loucas, H. M., Shibuya, K., Schmelz, E., Clark, D. G., & Klee, H. J. (2004). Circadian regulation of the PhCCD1 carotenoid cleavage dioxygenase controls emission of β-ionone, a fragrance volatile of petunia flowers. *Plant Physiology*, 136(3), 3504–3514.

Stauder, R., Welsch, R., Camagna, M., Kohlen, W., Balcke, G. U., Tissier, A., & Walter, M. H. (2018). Strigolactone levels in dicot roots are determined by an ancestral symbiosis-regulated clade of the PHYTOENE SYNTHASE gene family. *Frontiers in Plant Science*, 9, 255.

Sun, J. (2007). D-Limonene: Safety and Clinical Applications. *Alternative Medicine Review*, 12(3), 259-264.

Sun, T., Yuan, H., Cao, H., Yazdani, M., Tadmor, Y., & Li, L. (2018). Carotenoid Metabolism in Plants: The Role of Plastids. *Molecular Plant* 11(1), 58–74.

Takahashi, S., & Koyama, T. (2006). Structure and function of cis-prenyl chain elongating enzymes. *Chemical Record*, 6(4), 194–205.

Tanaka, A., & Tanaka, R. (2006). Chlorophyll metabolism. *Current Opinion in Plant Biology*, 9(3), 248–255.

Tholl, D. (2015). Biosynthesis and Biological Functions of Terpenoids in Plants. Biotechnology of Isoprenoids. *Advances in Biochemical Engineering/Biotechnology*, 148 ,148-163.

Thulasiram, H. v., & Poulter, C. D. (2006). Farnesyl diphosphate synthase: The art of compromise between substrate selectivity and stereoselectivity. *Journal of the American Chemical Society*, 128(49), 15819–15823.

Toledo-Ortiz, G., Huq, E., & Rodríguez-Concepción, M. (2010). Direct regulation of phytoene synthase gene expression and carotenoid biosynthesis by phytochrome-interacting factors. *Proceedings of the National Academy of Sciences*, 107(25), 11626–11631.

Torres-Montilla, S., & Rodriguez-Concepcion, M. (2021). Making extra room for carotenoids in plant cells: new opportunities for biofortification. *Progress in Lipid Research*, 84, 101128.

Vandermoten, S., Haubruge, É., & Cusson, M. (2009). New insights into short-chain prenyltransferases: Structural features, evolutionary history and potential for selective inhibition. *Cellular and Molecular Life Sciences*, 66(23), 3685–3695.

Vickers, C. E., Bongers, M., Liu, Q., Delatte, T., & Bouwmeester, H. (2014). Metabolic engineering of volatile isoprenoids in plants and microbes. *Plant, Cell and Environment*, 37(8), 1753–1775.

Vranová, E., Coman, D., & Gruissem, W. (2013). Network analysis of the MVA and MEP pathways for isoprenoid synthesis. *Annual Review of Plant Biology* 64, 665–700.

Walter, M. H., Stauder, R., & Tissier, A. (2015). Evolution of root-specific carotenoid precursor pathways for apocarotenoid signal biogenesis. *Plant Science*, 233, 1–10.

Wang, C., Chen, Q., Fan, D., Li, J., Wang, G., & Zhang, P. (2016). Structural Analyses of Short-Chain Prenyltransferases Identify an Evolutionarily Conserved GFPPS Clade in Brassicaceae Plants. *Molecular Plant*, 9(2), 195–204.

Wang, G., & Dixon, R. A. (2009). Heterodimeric geranyl(geranyl)diphosphate synthase from hop (Humulus lupulus) and the evolution of monoterpene biosynthesis. *Proceedings of the National Academy of Sciences* 106(24), 9914-9919.

Wang, G., Tian, L., Aziz, N., Broun, P., Dai, X., He, J., King, A., Zhao, P. X., & Dixon, R. A. (2008). Terpene biosynthesis in glandular trichomes of hop. *Plant Physiology*, 148(3), 1254–1266.

Wang, J., Lin, H. X., Su, P., Chen, T., Guo, J., Gao, W., & Huang, L. Q. (2019). Molecular cloning and functional characterization of multiple geranylgeranyl pyrophosphate synthases (ApGGPPS) from Andrographis paniculata. *Plant Cell Reports*, 38(1), 117–128.

Wang, Q., Huang, X. Q., Cao, T. J., Zhuang, Z., Wang, R., & Lu, S. (2018). Heteromeric Geranylgeranyl Diphosphate Synthase Contributes to Carotenoid Biosynthesis in Ripening Fruits of Red Pepper (Capsicum annuum var. conoides). *Journal of Agricultural and Food Chemistry*, 66(44), 11691–11700.

Wang, Y., & Hekimi, S. (2016). Understanding Ubiquinone. *Trends in Cell Biology*, 26(5), 367–378.

Wang, Z,. Zhang, L,. Dong, C,. Jinggong, G,. Lifeng,J,. Wei, P,. Li, F,. Zhang, X ., & Wang, R (2021). Characterization and functional analysis of phytoene synthase gene family in tobacco. *BMC Plant Biology*. 21, 32-45.

Wei, X., Meng, C., Yuan, Y., Nath, U. K., Zhao, Y., Wang, Z., Yang, S., Li, L., Niu, L., Yao, Q., Wei, F., & Zhang, X. (2021). CaPSY1 gene plays likely the key role in carotenoid metabolism of pepper (Capsicum annuum) at ripening. *Functional Plant Biology*, 48(2), 141–155.

Welsch, R., Arango, J., Bär, C., Salazar, B., Al-Babili, S., Beltrán, J., Chavarriaga, P., Ceballos, H., Tohme, J., & Beyera, P. (2010). Provitamin A accumulation in cassava (*Manihot esculenta*) roots driven by a single nucleotide polymorphism in a phytoene synthase gene. *Plant Cell*, 22(10), 3348–3356.

Welsch, R., Wüst, F., Bär, C., Al-Babili, S., & Beyer, P. (2008). A third phytoene synthase is devoted to abiotic stress-induced abscisic acid formation in rice and defines functional diversification of phytoene synthase genes. *Plant Physiology*, 147(1), 367–380.

Welsch, R,. Zhou, X,. Yuan, H,. Álvarez, D,. Sun, T,. Schlossarek, D,. Yang, Y., Shen, G,. Zhang, H,. Rodriguez-Concepcion, M., Thannhauser, TW,. & Li, L. (2018). Clp Protease and OR Directly Control the Proteostasis of Phytoene Synthase, the Crucial Enzyme for Carotenoid Biosynthesis in Arabidopsis. Molecular Plant, 11(1), 149-162

Wendel, J. F., Jackson, S. A., Meyers, B. C., & Wing, R. A. (2016). Evolution of plant genome architecture. *Genome Biology*, 17(1), 37-50.

Yang, L. E., Huang, X. Q., Lu, Q. Q., Zhu, J. Y., & Lu, S. (2016). Cloning and characterization of the geranylgeranyl diphosphate synthase (GGPS) responsible for carotenoid biosynthesis in *Pyropia umbilicalis*. *Journal of Applied Phycology*, 28(1), 671–678.

You, M. K., Lee, Y. J., Yu, J. S., & Ha, S. H. (2020). The predicted functional compartmentation of rice terpenoid metabolism by trans-prenyltransferase structural analysis, expression and localization. *International Journal of Molecular Sciences*, 21(23), 1–19.

Zhang, Y., Cheng, X., Wang, Y., Díez-Simón, C., Flokova, K., Bimbo, A., Bouwmeester, H. J., & Ruyter-Spira, C. (2018). The tomato MAX1 homolog, SlMAX1, is involved in the biosynthesis of tomato strigolactones from carlactone. *New Phytologist*, 219(1), 297–309.

Zhang J, Tao N, Xu Q, Zhou W, Cao H, Xu, J & Deng X. (2009). Functional characterization of Citrus PSY gene in Hongkong kumquat (Fortunella hindsii Swingle). *Plant Cell Reports*, 28(11), 1737-1746.

Zhou, F., & Pichersky, E. (2020). The complete functional characterisation of the terpene synthase family in tomato. *New Phytologist,* 226(5), 1341–1360.

Zhou, F., Wang, C. Y., Gutensohn, M., Jiang, L., Zhang, P., Zhang, D., Dudareva, N., & Lua, S. (2017). A recruiting protein of geranylgeranyl diphosphate synthase controls metabolic flux toward chlorophyll biosynthesis in rice. *Proceedings of the National Academy of Sciences*, 114(26), 6866–6871.

Zhou, X., Rao, S., Wrightstone, E., Sun, T., Lui, A. C. W., Welsch, R., & Li, L. (2022). Phytoene Synthase: The Key Rate-Limiting Enzyme of Carotenoid Biosynthesis in Plants. *Frontiers in Plant Science* 13, 884720.

Annex

Publication

Barja, M. V., **Ezquerro, M.,** Beretta, S., Diretto, G., Florez-Sarasa, I., Feixes, E., Fiore, A., Karlova, R., Fernie, A. R., Beekwilder, J., & Rodríguez-Concepción, M. (2021). Several geranylgeranyl diphosphate synthase isoforms supply metabolic substrates for carotenoid biosynthesis in tomato*. New Phytologist*, 231(1), 255–272.

Note: The PhD candidate is co-author of this work

New
Phytologist
July 2021
Vol. 231
No. 1
ISSN 0028-646X
www.newphytologist.com
International Journal of Plant Science
TANSLEY
INSIGHTS

Check for updates

New Phytologist

Research

Several geranylgeranyl diphosphate synthase isoforms supply metabolic substrates for carotenoid biosynthesis in tomato

M. Victoria Barja[1]*, Miguel Ezquerro[1,*], Stefano Beretta[1], Gianfranco Diretto[2], Igor Florez-Sarasa[1], Elisenda Feixes[1], Alessia Fiore[2], Rumyana Karlova[3], Alisdair R. Fernie[4], Jules Beekwilder[5] and Manuel Rodríguez-Concepción[1,6]

[1]Centre for Research in Agricultural Genomics (CRAG) CSIC-IRTA-UAB-UB, Campus UAB Bellaterra, Barcelona 08193, Spain; [2]Italian National Agency for New Technologies, Energy, and Sustainable Development, Casaccia Research Centre, Rome 00123, Italy; [3]Laboratory of Plant Physiology, Wageningen University and Research, Wageningen 6700AA, the Netherlands; [4]Max-Planck-Institut für Molekulare Pflanzenphysiologie, Potsdam-Golm 14476, Germany; [5]BU Bioscience, Wageningen University and Research, Wageningen 6700AA, the Netherlands; [6]Institute for Plant Molecular and Cell Biology (IBMCP), CSIC-Universitat Politècnica de València, València 46022, Spain

Author for correspondence:
Manuel Rodriguez-Concepcion
Email: manuelrc@ibmcp.upv.es

Received: *22 July 2020*
Accepted: *8 February 2021*

New Phytologist (2021)
doi: 10.1111/nph.17283

Key words: carotenoids, geranylgeranyl diphosphate, prenyltransferase, ripening, synthase, tomato.

Summary

- Geranylgeranyl diphosphate (GGPP) produced by GGPP synthase (GGPPS) serves as a precursor for many plastidial isoprenoids, including carotenoids. Phytoene synthase (PSY) converts GGPP into phytoene, the first committed intermediate of the carotenoid pathway.
- Here we used biochemical, molecular, and genetic tools to characterise the plastidial members of the GGPPS family in tomato (*Solanum lycopersicum*) and their interaction with PSY isoforms.
- The three tomato GGPPS isoforms found to localise in plastids (SlG1, 2 and 3) exhibit similar kinetic parameters. Gene expression analyses showed a preferential association of individual GGPPS and PSY isoforms when carotenoid biosynthesis was induced during root mycorrhization, seedling de-etiolation and fruit ripening. SlG2, but not SlG3, physically interacts with PSY proteins. By contrast, CRISPR-Cas9 mutants defective in SlG3 showed a stronger impact on carotenoid levels and derived metabolic, physiological and developmental phenotypes compared with those impaired in SlG2. Double mutants defective in both genes could not be rescued.
- Our work demonstrates that the bulk of GGPP production in tomato chloroplasts and chromoplasts relies on two cooperating GGPPS paralogues, unlike other plant species such as *Arabidopsis thaliana*, rice or pepper, which produce their essential plastidial isoprenoids using a single GGPPS isoform.

Introduction

Isoprenoids are essential biological molecules in all living organisms. In particular, plants are the main source of the enormous structural and functional variety that characterises this family of compounds (Pulido *et al.*, 2012; Tholl, 2015). The building blocks for the biosynthesis of all isoprenoids are isopentenyl diphosphate (IPP) and its double-bond isomer dimethylallyl diphosphate (DMAPP). These five-carbon (C5) universal isoprenoid units are produced in plants through the mevalonic acid (MVA) pathway in the cytosol and the methylerythritol 4-phosphate (MEP) pathway in plastids (Vranová *et al.*, 2013; Rodríguez-Concepción & Boronat, 2015). Short-chain prenyltransferases subsequently condense one or more molecules of IPP to one molecule of DMAPP giving rise to C10, C15, C20 and C25 prenyl diphosphates, known as geranyl diphosphate (GPP), farnesyl diphosphate (FPP), geranylgeranyl diphosphate (GGPP), and geranylfarnesyl diphosphate (GFPP), respectively. These molecules are the immediate precursors for downstream pathways leading to the production of the main groups of isoprenoids.

Carotenoids are one of the most studied groups of plant isoprenoids. These C40 tetraterpenes are greatly demanded by cosmetic and agro-food industries as natural red to yellow pigments and provide benefits for human health, for example as precursors of vitamin A and other biologically active molecules (Sandmann, 2015; Rodríguez-Concepción *et al.*, 2018). In plants, carotenoids have different functions. In photosynthetic tissues, they are required for the assembly of the photosynthetic apparatus, contribute to light harvesting and are essential for photoprotection by dissipating excess light energy as heat and by scavenging reactive oxygen species. They are also fundamental in growth regulation as they are the precursors of retrograde signals and phytohormones such as abscisic acid (ABA) and strigolactones. As a secondary role, carotenoids provide distinctive colours to flowers and fruits to

*These authors contributed equally to this work.

© 2021 The Authors
New Phytologist © 2021 New Phytologist Foundation

attract pollinators and seed dispersal animals (Nisar *et al.*, 2015; Yuan *et al.*, 2015). In plants, carotenoids are produced and stored in plastids, including chloroplasts and chromoplasts (Ruiz-Sola & Rodríguez-Concepción, 2012; Sun *et al.*, 2018). MEP-derived IPP and DMAPP are converted into GGPP by plastidial GGPP synthase (GGPPS) isoforms and then GGPP is transformed into phytoene by phytoene synthase (PSY) enzymes. The production of phytoene, the first committed intermediate of the carotenoid pathway, is considered to be a major rate-determining step regulating the metabolic flux through this pathway (Fraser *et al.*, 2002). In tomato (*Solanum lycopersicum*), three PSY-encoding genes control carotenoid biosynthesis in different tissues. *PSY1* expression is boosted during ripening to produce carotenoids involved in the pigmentation of the fruit (Bartley *et al.*, 1992; Fray & Grierson, 1993; Giorio *et al.*, 2008; Kachanovsky *et al.*, 2012). *PSY2* is expressed in all tissues, including fruits, but transcript levels are much higher than those of *PSY1* in photosynthetic tissues, where carotenoids are required for photosynthesis and photoprotection (Bartley & Scolnik, 1993; Giorio *et al.*, 2008). Lastly, *PSY3* is mainly expressed in roots and it is induced during mycorrhization (Walter *et al.*, 2015; Stauder *et al.*, 2018), when carotenoid biosynthesis is upregulated to produce strigolactones and apocarotenoid molecules essential for the establishment of the symbiosis (Fester *et al.*, 2002, 2005; Baslam *et al.*, 2013; Ruiz-Lozano *et al.*, 2016; Stauder *et al.*, 2018). Whether the corresponding PSY isoforms use GGPP supplied by different GGPPS isoforms remains unknown.

Several GGPPS paralogues have been retained in plants during evolution (Beck *et al.*, 2013; Zhang *et al.*, 2015; Ruiz-Sola *et al.*, 2016a,b; Zhou *et al.*, 2017; Wang *et al.*, 2018). However, a single GGPPS isoform appears to produce the GGPP substrate needed for the production of carotenoids and other plastidial isoprenoids in *Arabidopsis thaliana,* rice (*Oryza sativa*) and pepper (*Capsicum annuum*), the three plant species whose GGPPS families have been best characterised to date (Ruiz-Sola *et al.*, 2016a, b; Zhou *et al.*, 2017; Wang *et al.*, 2018). While tomato has become a model plant systems to study the biosynthesis of carotenoids and its regulation, we still have an incomplete picture of the GGPPS family in this plant. Recent work has determined that five genes encoding GGPPS homologues exist in the tomato genome, three of which were confirmed to produce GGPP *in vitro* and localise in plastids (Zhou & Pichersky, 2020). Which of these plastidial GGPPS isoforms are required for the production of carotenoids in photosynthetic tissues (e.g. for photoprotection), fruits (e.g. for pigmentation) or roots (e.g. for mycorrhization) remains unknown. Here we characterised the *in vivo* role of these plastidial GGPPS enzymes and provide clues to understand how the supply of plastidial GGPP for the synthesis of carotenoids with different biological functions in particular tomato tissues is regulated in this important crop plant.

Materials and Methods

Plant material

Tomato (*Solanum lycopersicum* var. MicroTom) plants were used for most experiments. Seed germination, plant growth and sample collection were carried out as described (Supporting Information Methods S1). *Agrobacterium tumefaciens* GV3101 strain was used to stably transform tomato MicroTom cotyledons with plasmids harbouring two sgRNAs to disrupt *SlG2* and *SlG3* genomic sequences as described previously (Fernandez *et al.*, 2009). The sgRNAs were designed for each gene to create short deletions using the CRISPR P 2.0 online tool (http://crispr.hzau.edu.cn/CRISPR2/; Liu *et al.*, 2017). Cloning of the sgRNA sequences was performed as described previously (Schiml *et al.*, 2016) using a pDE-Cas9 plasmid providing kanamycin resistance (Methods S2). Primers and cloning steps are detailed in Tables S1 and S2, respectively. *In vitro* regenerated T1 lines were identified based on kanamycin resistance (100 μg ml^{-1}), PCR genotyping and restriction analyses. Homozygous T2 lines lacking Cas9 were obtained after segregation. Stable T3 offspring was used for further experiments. Methods S2 and Tables S1 and S2 describe the generation of the rest of the constructs. *Nicotiana benthamiana* plants were grown and used for transient expression assays (agroinfiltration) as previously described (Llorente *et al.*, 2020).

Gene co-expression network (GCN) analyses

GCN analyses were performed as previously described (Ahrazem *et al.*, 2018). Pairwise Pearson correlations between each GGPPS gene and each selected isoprenoid biosynthetic input gene were computed for leaf and fruit tissues throughout their development and Fisher's Z-transformation was used to test their statistical significance.

RNA analyses

RNA isolation, cDNA synthesis, and RT-qPCR analyses were carried out as described (Methods S3). Normalised transcript abundances were calculated as described previously (Simon, 2003) using tomato *ACT4* (*Solyc04g011500*) or *EXP* (*Solyc07g025390*) as endogenous reference genes. Three biological replicates of cDNA samples from roots of nonmycorrhized and mycorrhized tomato plants (Ruiz-Lozano *et al.*, 2016) were kindly provided by Juan Antonio López-Ráez.

Protein analyses

In vitro GGPPS activity determination was performed as described (Methods S4). Purified enzymes were used to calculate kinetic parameters as described previously (Barja & Rodríguez-Concepción, 2020). Protein concentration was determined according to the Bradford method (Bradford, 1976). GGPPS activity assays in *E. coli* were carried out as described previously (Beck *et al.*, 2013). Subcellular localisation assays were performed using *A. tumefaciens*-mediated transient expression in *N. benthamiana* leaves (Sparkes *et al.*, 2006). Leaves were co-infiltrated with strains carrying appropriate constructs (Methods S2) and a HC-Pro silencing suppressor (Goytia *et al.*, 2006) as described (Methods S5). Subcellular localisation of GFP fusion proteins was determined 3 d post infiltration with an Olympus

© 2021 The Authors
New Phytologist © 2021 New Phytologist Foundation

FV 1000 confocal laser-scanning microscope (Methods S5). Co-immunoprecipitation (Co-IP) assays were performed in *N. benthamiana leaves* as described previously (Muñoz & Castellano, 2018; Methods S6). Immunoblot analyses were performed as described previously (Pulido *et al.*, 2013).

Metabolite analysis

Detection of prenyl diphosphates was carried out as described previously (Ruiz-Sola *et al.*, 2016a). Carotenoids, chlorophylls and tocopherols were extracted as described (Methods S7). Separation and detection were next performed using an Agilent 1200 series HPLC system (Agilent Technologies) as previously reported (Fraser *et al.*, 2000). ABA levels were determined as described previously (Diretto *et al.*, 2020). Primary metabolites were extracted, annotated and quantified as described previously (Llorente *et al.*, 2020).

Results

SlG1, SlG2 and SlG3 are GGPP-producing plastidial enzymes with similar kinetic properties

Several genes encoding proteins with homology to GGPPS enzymes are found in the tomato genome (Ament *et al.*, 2006; Fraser *et al.*, 2007; Stauder *et al.*, 2018; Zhou & Pichersky, 2020). From these, three have been found to localise in plastids and produce GGPP *in vitro*, namely *GGPPS1* (*Solyc11g011240*), *GGPPS2* (*Solyc04g079960*) and *GGPPS3* (*Solyc02g085700*), here referred to as *SlG1*, *SlG2* and *SlG3* (Table S3). We confirmed the plastidial targeting of these three isoforms by expressing constructs encoding GFP fusions of the full-length SlG1-3 proteins in agroinfiltrated tobacco (*Nicotiana benthamiana*) leaves. In all three cases, fluorescence corresponding to the GFP fusion proteins co-localised with chlorophyll autofluorescence (Fig. S1), and supported the conclusion that they were all efficiently targeted to chloroplasts. We also experimentally confirmed the ability of purified SlG1-3 proteins to produce GGPP *in vitro*. The three tomato isoforms were expressed in *Escherichia coli* cells without their predicted plastid-targeting sequences (Fig. S2) and whole-cell protein extracts were directly used for activity assays in the presence of IPP and DMAPP followed by the analysis of the reaction products by LC-MS (Fig. S3). As positive and negative controls, we used the Arabidopsis AtG11 (active) and AtG11s (inactive) proteins (Ruiz-Sola *et al.*, 2016a). This experiment confirmed that SlG1, SlG2, SlG3 and AtG11 (but no AtG11s) produced only GGPP (Fig. S3a), in agreement with recently reported data (Zhou & Pichersky, 2020). To gain new knowledge on the biochemical properties of these enzymes, we used purified proteins to calculate their kinetic parameters. Enzymatic assays performed as described previously (Barja & Rodríguez-Concepción, 2020) showed that all tested GGPPS proteins exhibited a similar optimal pH around 7.5 (Fig. S3b), as expected for stromal enzymes (Höhner *et al.*, 2016). The parameters Km (an estimator of the apparent affinity for the IPP and DMAPP substrates) and Vmax exhibited very similar values among the three tomato enzymes (Table 1). They were also similar to those obtained for AtG11 here and elsewhere (Wang & Dixon, 2009; Camagna *et al.*, 2019). We therefore concluded that tomato SlG1, SlG2 and SlG3 and Arabidopsis AtG11 are plastidial GGPPS enzymes with very similar kinetic properties.

Gene expression profiles suggest a major role of SlG2 and SlG3 in chloroplasts and chromoplasts

Analysis of public gene expression databases showed that the genes encoding SlG1-3 enzymes were expressed in roots, leaves and flowers (Fig. S4). Of these, the most highly expressed gene was *SlG3* followed by *SlG2*, while *SlG1* transcripts were present at very low levels. *SlG2* and *SlG3*, but not *SlG1*, were also expressed at high levels in fruit pericarp and seed tissues (Fig. S4). As an initial approach to gain an insight into the possible functions of these individual isoforms, we performed a GCN analysis. This is a powerful tool to infer biological functions that we previously used to identify AtG11 as the main GGPPS isoform for plastidial isoprenoid production in Arabidopsis (Ruiz-Sola *et al.*, 2016b). By using publicly available databases for plant comparative genomics (*PLAZA 4.0*, *Phytozome*), we searched for tomato homologues of the plastidial pathways that supply GGPPS substrates (MEP pathway) and consume GGPP to produce carotenoids, chlorophylls, tocopherols, phylloquinone, plastoquinone, gibberellins, strigolactones and ABA (Table S4). We retrieved their expression data from TomExpress database (Zouine *et al.*, 2017) experiments carried out using either leaf or fruit samples at different developmental stages (Table S5). Then, we calculated their correlation with *SlG1*, *SlG2* and *SlG3* expression using pairwise Pearson correlations. The results of the GCN analyses are shown in Fig. 1 and Fig. S5, and correlations are listed in Table S6. It was not possible to obtain correlation data for tomato roots as only two experiments using root samples are deposited in the TomExpress database. In leaves and fruits, *SlG1* was poorly co-expressed with the query genes. By contrast, and similar to that observed with *AtG11* (Ruiz-Sola *et al.*, 2016b), *SlG2* and, to a lower extent, *SlG3* were highly connected to plastidial isoprenoid biosynthetic genes in leaf tissues. Connectivity was lower in fruit and, in this case, it was a bit higher for *SlG3* (Fig. 1). These results suggest that SlG2 and SlG3 might be the main GGPP-producing isoforms in leaf chloroplasts and fruit chromoplasts.

In tomato, carotenoids contribute to mycorrhizal associations, photoprotection and fruit pigmentation and, therefore, the levels of these GGPP-derived metabolites increase during root mycorrhization, seedling de-etiolation and fruit ripening. In agreement with the rate-determining role of PSY for carotenoid synthesis (Fraser *et al.*, 2002), the expression levels of PSY-encoding genes also increase during such carotenoid-demanding developmental processes. By using real-time quantitative PCR (qPCR) analysis, we experimentally confirmed the upregulation of *PSY1* during fruit ripening and *PSY3* in mycorrhized roots (Fig. 2). Furthermore, we found that the *PSY2* gene was more strongly upregulated than *PSY1* during tomato seedling de-etiolation (Fig. 2). Using the same samples, we observed that only *SlG1* was

© 2021 The Authors
New Phytologist © 2021 New Phytologist Foundation

Table 1 Kinetic parameters of tomato plastidial GGPPS enzymes.

	DMAPP (+100 μM IPP)		IPP (+100 μM DMAPP)	
	Km (μM)	V_{max} (nmol min^{-1} mg^{-1})	Km (μM)	V_{max} (nmol min^{-1} mg^{-1})
SlG1	31.82 ± 2.92	47.47 ± 1.40	74.18 ± 7.55	59.87 ± 2.73
SlG2	49.55 ± 5.31	38.87 ± 1.53	79.75 ± 8.33	36.73 ± 1.73
SlG3	45.75 ± 6.81	26.13 ± 1.40	45.92 ± 4.86	29.13 ± 1.13
AtG11	32.86 ± 4.86	21.53 ± 1.07	38.49 ± 4.94	24.13 ± 1.07

Values correspond to the mean ± SD of three independent experimental replicates ($n = 3$).

upregulated during root mycorrhization, showing an expression pattern similar to that observed for *PSY3* (Fig. 2). During fruit ripening, *SlG2* and, to a lower extent, *SlG3* were upregulated, but not as much as *PSY1* (Fig. 2). *SlG2* was also the most strongly upregulated GGPPS-encoding gene during seedling de-etiolation, paralleling *PSY2* induction. Interestingly, *SlG3* and *PSY1* were also induced with a similar profile during this process, even though induction levels were much lower than those observed for *SlG2* and *PSY2* (Fig. 2). Together, these data suggested that SlG1 might provide GGPP for PSY3 to produce carotenoids in roots, particularly when needed during mycorrhization, whereas both SlG2 and SlG3 would be required in leaves and fruits to support carotenoid production for photosynthesis (mostly by PSY2) and fruit pigmentation (by PSY1).

SlG2, but not SlG3, can interact with PSY1 and PSY2

A coordinated role for SlG1 and PSY3 in mycorrhization has already been proposed (Stauder *et al.*, 2018), but the possible connection between the other plastidial GGPPS and PSY isoforms remains unclear. GGPPS proteins can physically interact with PSY and other enzymes catalysing both upstream and downstream biosynthetic steps in the plastids of different plant species (Maudinas *et al.*, 1977; Dogbo & Camara, 1987; Camara, 1993; Fraser *et al.*, 2000; Ruiz-Sola *et al.*, 2016b; Zhou *et al.*, 2017; Wang *et al.*, 2018; Camagna *et al.*, 2019). This mechanism may facilitate channelling of precursors towards specific groups of plastidial isoprenoids. Protein complexes containing both GGPPS and PSY enzymes were isolated from tomato chloroplasts and fruit chromoplasts (Maudinas *et al.*, 1977; Fraser *et al.*, 2000), but the specific isoforms forming these protein complexes were never identified. Given the co-regulation of *SlG2* and *SlG3* with *PSY1* and *PSY2* genes in chloroplasts (i.e. photosynthetic tissues) and chromoplasts (i.e. fruits), we decided to test possible interactions of these isoforms in co-immunoprecipitation assays (Fig. 3). Constructs harbouring C-terminal Myc-tagged GGPPS and HA-tagged PSY sequences were combined and transiently co-expressed in *N. benthamiana* leaves. As a negative control, we used a Myc-tagged version of Arabidopsis phosphoribulokinase (PRK-Myc), a stromal enzyme of the Calvin cycle. Both PSY1-HA and PSY2-HA could be co-immunoprecipitated with SlG2-Myc, suggesting that they are present in the same complexes *in vivo* (Fig. 3). By contrast, none of these PSY isoforms could be detected in the samples co-immunoprecipitated with either SlG3-Myc or PRK-Myc. The same Myc-tagged SlG2 and SlG3 proteins used in these experiments were able to co-immunoprecipitate their HA-tagged counterparts (Fig. 3). This result, consistent with the ability of GGPPS proteins to form homodimers and also heterodimers, confirms that the observed lack of interaction of SlG3 with PSY enzymes was not due to SlG3-Myc having lost its capacity to interact with other proteins.

Loss of function mutants defective in SlG3, but not those impaired in SlG2, show lower levels of photosynthetic pigments and activity

To further explore the biological roles of SlG2 and SlG3, we generated CRISPR-Cas9 mutants defective in these enzymes (Fig. 4). We designed two single guide RNAs (sgRNA) for each gene with the aim of creating deletions encompassing unique restriction sites for rapid screening (Fig. 4a). Two independent deletion alleles that created premature translation stop codons were selected for each gene and named *slg2-1*, *slg2-2*, *slg3-1* and *slg3-2* (Figs 4a, S6–S8). To confirm that the truncated proteins lacked GGPPS activity, we tested them in *E. coli* strains that synthesised the red carotenoid lycopene only when a source of GGPP was supplied (Ruiz-Sola *et al.*, 2016a). Transformation with constructs harbouring the mutant enzymes did not produce more lycopene than empty plasmid controls, indicating that they lacked GGPPS activity. (Fig. 4b). Once confirmed that the selected mutant alleles produced nonfunctional proteins, homozygous lines without Cas9 were obtained and used for further experiments.

The most obvious phenotype among the selected lines was the pale colour of *slg3* mutants compared with *slg2* alleles or azygous (wild-type (WT)) plants (Fig. 5). This phenotype was clear in emerging and young leaves, but it weakened as leaves grew and became mature (Fig. 5a). The pale colour correlated with significantly reduced levels of carotenoids and chlorophylls in young leaves of *sgl3-1* and *sgl3-2* lines compared with those of WT plants (Fig. 5b; Table S7). The differences were less clear for tocopherols, another group of GGPP-derived plastidial isoprenoids (Fig. 5b). Similar levels of carotenoids, chlorophylls and tocopherols were detected in mature leaves of WT, *slg2* and *slg3* plants (Fig. 5b; Table S7). To test whether the reduced accumulation of photosynthesis-related isoprenoids in *slg3* lines had an impact on photosynthesis, we quantified the effective quantum

© 2021 The Authors
New Phytologist © 2021 New Phytologist Foundation

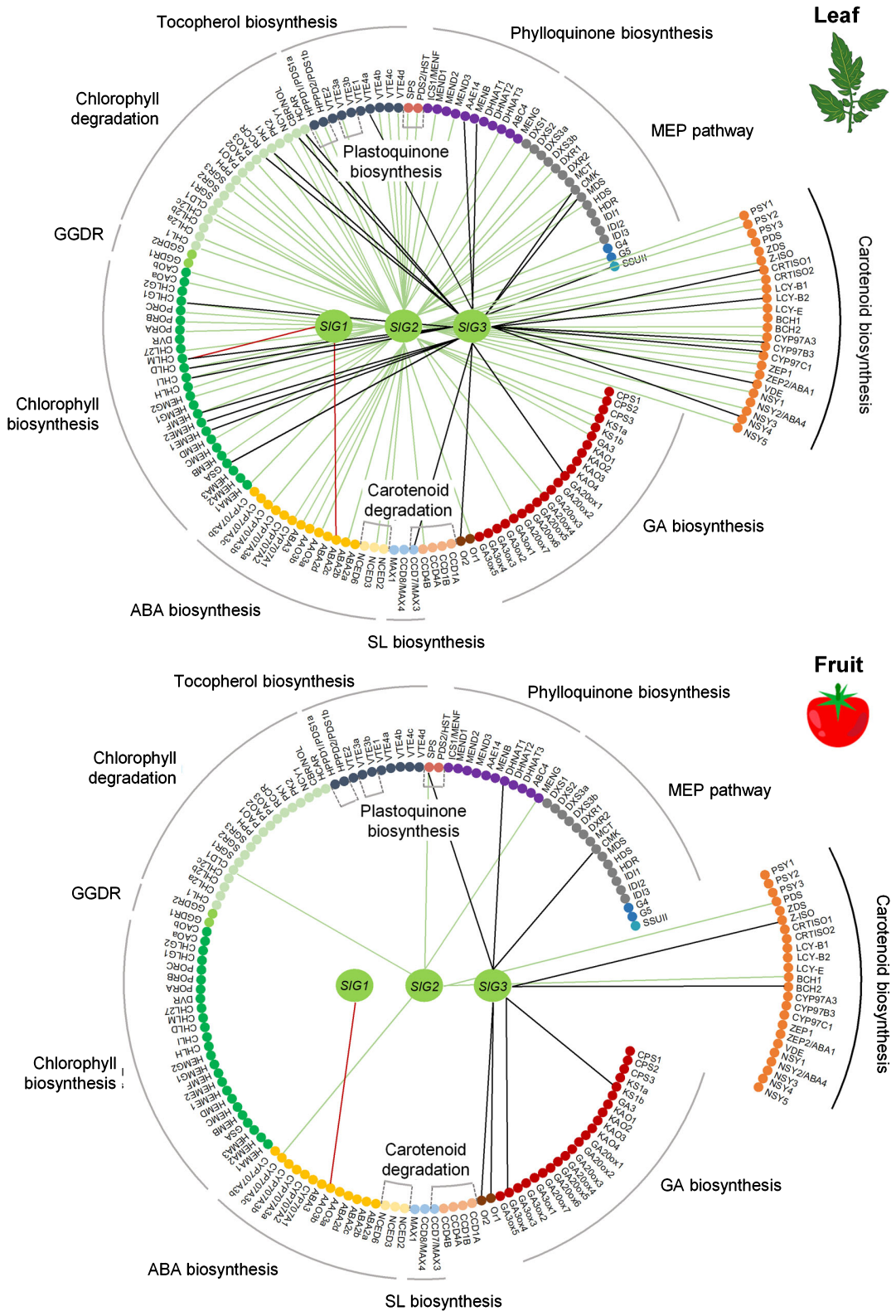

Fig. 1 Gene co-expression analysis of tomato genes encoding plastidial GGPPS isoforms in leaf and fruit tissues. Positive co-expression relationships ($P \geq 0.55$) are depicted in tissue-specific networks as edges. *SlG1*, *SlG2* and *SlG3* are depicted as central green nodes. Surrounding smaller nodes represent genes from the indicated isoprenoid pathways. Red, green and black edges indicate positive co-expression with *SlG1*, *SlG2* and *SlG3* genes, respectively. See Supporting Information Table S4 for gene accessions, Table S5 for leaf and fruit datasets used, and Table S6 for *P*-values.

© 2021 The Authors
New Phytologist © 2021 New Phytologist Foundation

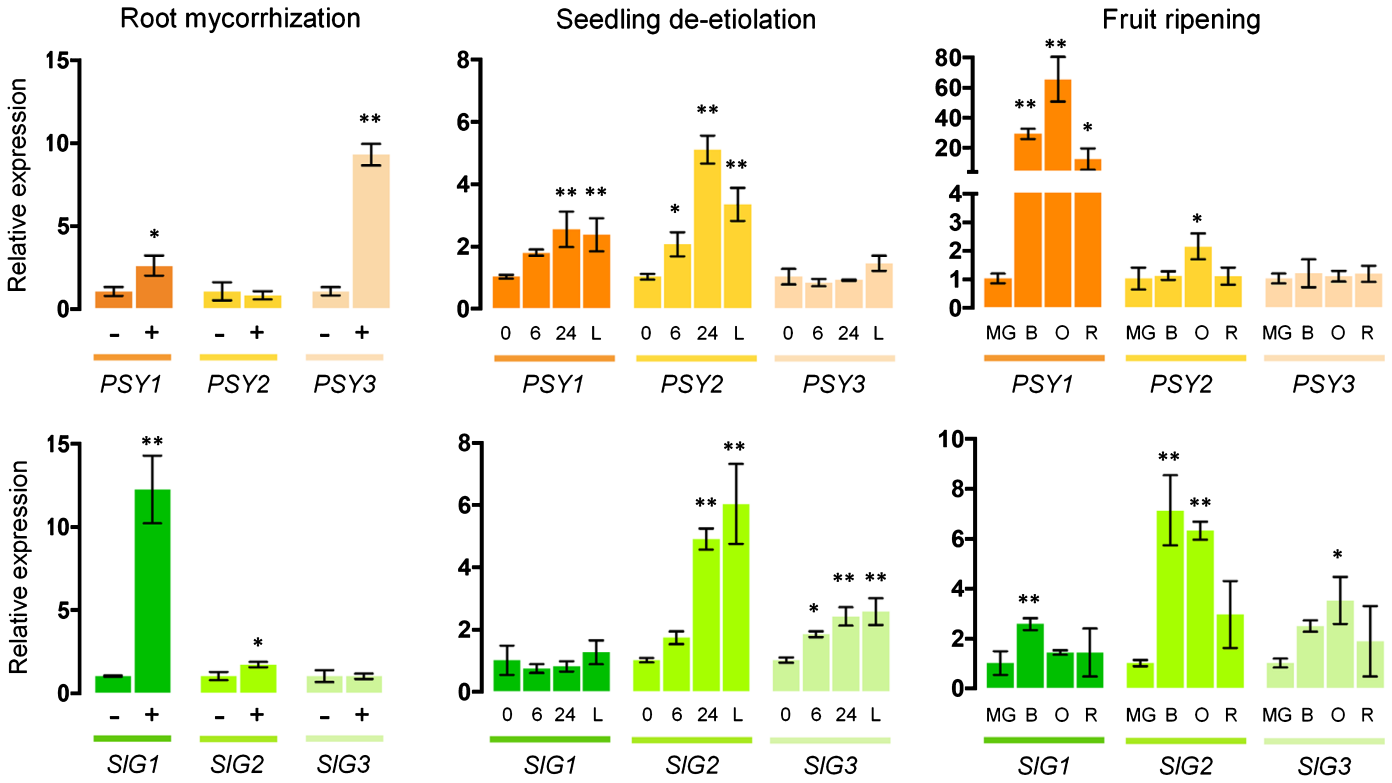

Fig. 2 Expression profiles of genes encoding tomato PSY and GGPPS paralogues during processes involving increased carotenoid production. First column corresponds to nonmycorrhized (−) and mycorrhized roots (+) at 6 wk postinoculation. Transcript levels were normalised using the tomato *EXP* gene and are shown relative to untreated root samples. Central column samples correspond to 7-d-old dark-grown seedlings at 0, 6 or 24 h after exposure to light and to seedlings continuously grown in the light (L). Transcript levels were normalised to the *EXP* gene and are represented relative to etiolated (0 h) samples. The third column depicts different fruit ripening stages: MG, mature green; B, breaker; O, orange; and R, red ripe. Levels were normalised using *ACT4* and are shown relative to MG samples. Expression values represent the mean ± SD of three independent biological replicates ($n = 3$). Asterisks indicate statistically significant differences relative to untreated (−), etiolated (0 h) or MG samples (*t*-test or one-way ANOVA with Dunnett's multiple comparisons test: *, $P < 0.05$; **, $P < 0.01$).

yield of photosystem II (ϕPSII) in both young and mature leaves (Fig. 5c). A 30% reduction in ϕPSII was observed in young leaves from *slg3* plants compared with those of WT or *slg2* lines, consistent with the *slg3*-specific reduction of GGPP-derived metabolites. Despite similar levels of photosynthetic pigments accumulated in the mature leaves of all genotypes tested, ϕPSII was slightly reduced in some mutants relative to WT lines (Fig. 5c).

We further explored the possible effects that the loss of SlG2 or SlG3 function might have on other metabolic pathways using the same samples of young leaves used for isoprenoid and ϕPSII determination (Fig. 6). GC-MS metabolite profiling showed strongly decreased levels of sucrose, glucose and fructose in SlG3-defective leaves, probably due to photosynthetic impairment. Mutant *slg3* leaves also displayed increased levels of amino acids derived from glycerate (Ser and Gly), shikimate (Phe, Trp and Tyr), pyruvate (Val, Ile and Ala), 2-oxoglutarate (Glu, Orn, His and GABA) and malate (Asp, Asn, Lys, Thr, Met, homoserine and beta-alanine). In line with some of these amino acid changes, SlG3-defective leaves displayed altered accumulation of tricarboxylic acid cycle-related intermediates (citrate and 2-oxoglutarate). Only a few common changes were detected in both *slg2* and *slg3* leaves. They included a decrease in putrescine and ascorbate levels (more pronounced in *slg3* leaves), as well as an altered accumulation of metabolites produced by the plastidial shikimate pathway, including the above-mentioned aromatic amino acids and phenylpropanoid derivatives such as caffeate and 3-caffeoyl-quinate (Fig. 6). The levels of the carotenoid-derived hormone ABA were similar in WT and mutant samples (Fig. 6; Table 2).

Ripening-associated fruit pigmentation is altered in *slg2* and *slg3* mutants in correlation with their carotenoid profile

Lines with reduced levels of plastidial GGPPS activity also showed changes in reproductive development (Fig. 7). Flowering time was similar in WT, *slg2* and *slg3* plants (Fig. 7a). However, pigmentation changes associated to fruit ripening were visually delayed in mutant fruits (Fig. 7b). Tomato fruits reach their final size at the mature green (MG) stage and then they start the ripening process. The first visual symptoms of ripening define the breaker (B) stage, when chlorophyll degradation and carotenoid biosynthesis change the fruit colour from green to yellow (Fig. 7c). As ripening advances, accumulation of orange and red carotenoids (β-carotene and lycopene, respectively) progressively change the fruit colour and define the orange (O) and eventually

© 2021 The Authors
New Phytologist © 2021 New Phytologist Foundation

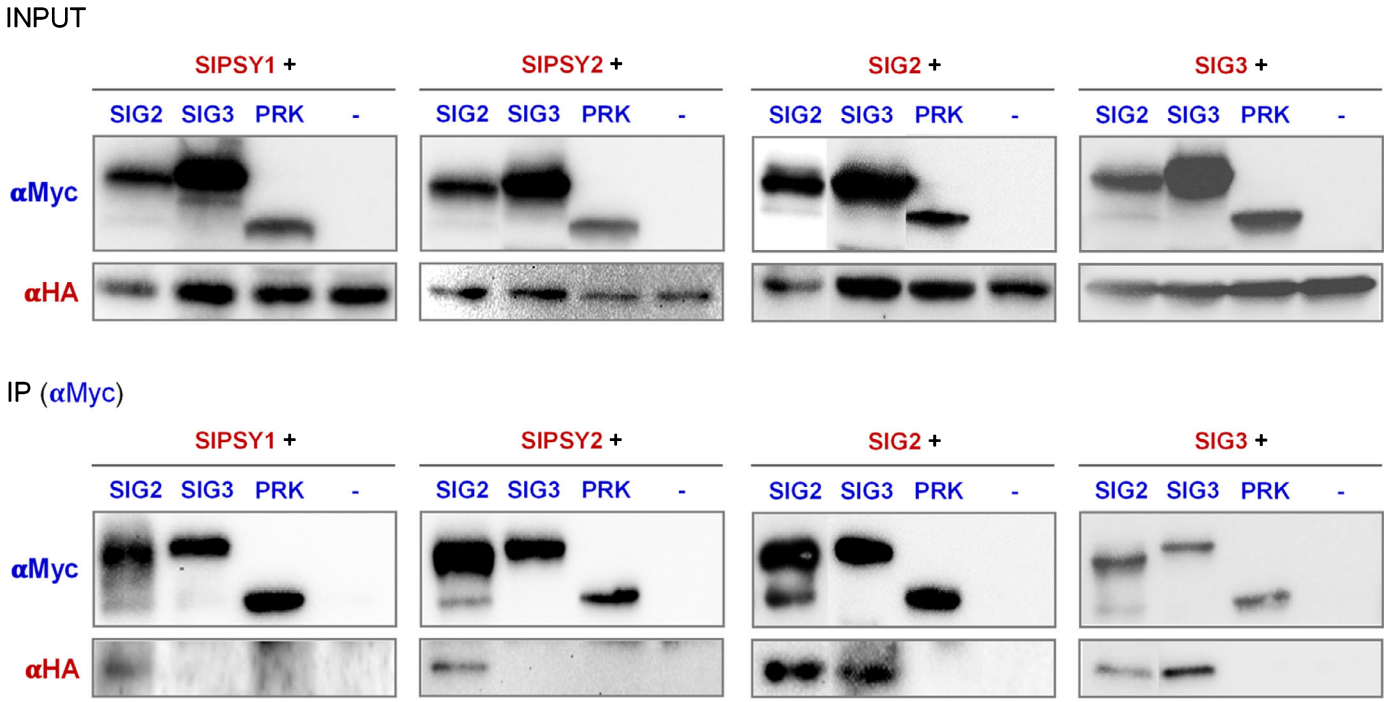

Fig. 3 Co-immunoprecipitation analyses. *Nicotiana benthamiana* leaves were co-agroinfiltrated with the indicated proteins tagged with C-terminal Myc (in blue) or HA (in red) epitopes. Controls agroinfiltrated only with the HA-tagged protein are indicated as (−). A fraction of the protein extracts (INPUT) was used to test protein production using immunoblot analyses using antibodies against Myc (αMyc) and HA (αHA). After immunoprecipitation (IP) of the remaining protein extracts using αMyc, samples were used for immunoblot analyses with αMyc (to confirm successful IP) and αHA (to detect the presence of co-immunoprecipitated HA-tagged proteins).

red (R) stages (Fig. 7c). The time from anthesis to B was similar in WT and SlG2-defective fruits, but it was longer in the *slg3* mutants (Figs 7b, S9). Fruits from lines defective in SlG3, but also those defective in SlG2, showed a pigmentation delay in the transition from B to O. The delay was observed both on vine (i.e. in fruits attached to the plant) and off vine (i.e. in fruits detached from the plant at the B stage; Figs 7b, S9). Both on-vine and off-vine measurements revealed that *slg2* mutants also took longer to reach the R stage compared with WT fruits (Fig. S9), whereas *slg3* mutants did not reach a proper R stage, as they developed a dark-orange colour when ripe and never turned fully red (Fig. 7c).

WT and mutant fruits showed similar levels of carotenoids, chlorophylls and tocopherols at the MG stage (Fig. S10), but clear differences were detected in ripe fruits at B + 10, i.e. 10 d after B (Figs 6, 7d; Table S7). Phytoene and lycopene were decreased in all mutants, although the effect was higher for *slg3* fruits. No significant differences were found for β-carotene, although the levels of this orange carotenoid tended to be higher in *slg3* mutants. This, together with the lower levels of the red carotenoid lycopene, may explain the dark-orange colour of B + 10 *slg3* fruits (Fig. 7c). Tocopherols also showed a trend towards higher abundance in SlG3-deficient fruits, a change that was statistically significant in the *slg3-1* allele (Fig. 7d) or when *slg3-1* and *slg3-2* samples were considered together (Fig. 6).

Unlike that observed in young leaves, ABA levels were reduced in B + 10 fruits of *slg2* and, most strongly, *slg3* mutants compared with WT controls (Fig. 6; Table 2). At the level of primary metabolites, B + 10 fruits from both *slg2* and *slg3* mutants exhibited increased levels of raffinose, galacturonate, pyruvate and Asp and lower levels of Ser, Gly, Tyr, Val, Ala, Glu and GABA compared with WT controls (Fig. 6). The changes in these metabolites were typically stronger for *slg3* fruits, paralleling that observed for carotenoids and derived ABA levels.

Double mutants defective in both SlG2 and SlG3 are not viable

To assess the impact of simultaneous disruption of both *SlG2* and *SlG3* genes, alleles *slg2-2* and *slg3-1* were crossed using the former as female parent and the latter as male parent or *vice versa*. Double heterozygous F1 plants from each cross were allowed to self-pollinate and the resulting seeds were used to screen the F2 population for double homozygous plants, which were expected to occur at a Mendelian frequency of 6.25% (1 in 16). We performed two rounds of screening. In the first one, 200 seeds (100 from each cross) were plated and all of them germinated and produced green seedlings. In the second round, carried out with older seeds, 80 seeds were plated and 76 (95%) germinated (Table 3). The seeds that failed to germinate (four) were manually open and found to contain either albino/pale (three) or green (one) embryos (Fig. S11). PCR genotyping of these embryos (Fig. S11) and of the remaining 276 seedling did not identify double homozygous mutants (Table 3). A chi-squared goodness-of-fit test performed with 8 degrees of freedom and 95% interval of confidence confirmed that the observed genotype frequencies

© 2021 The Authors
New Phytologist © 2021 New Phytologist Foundation

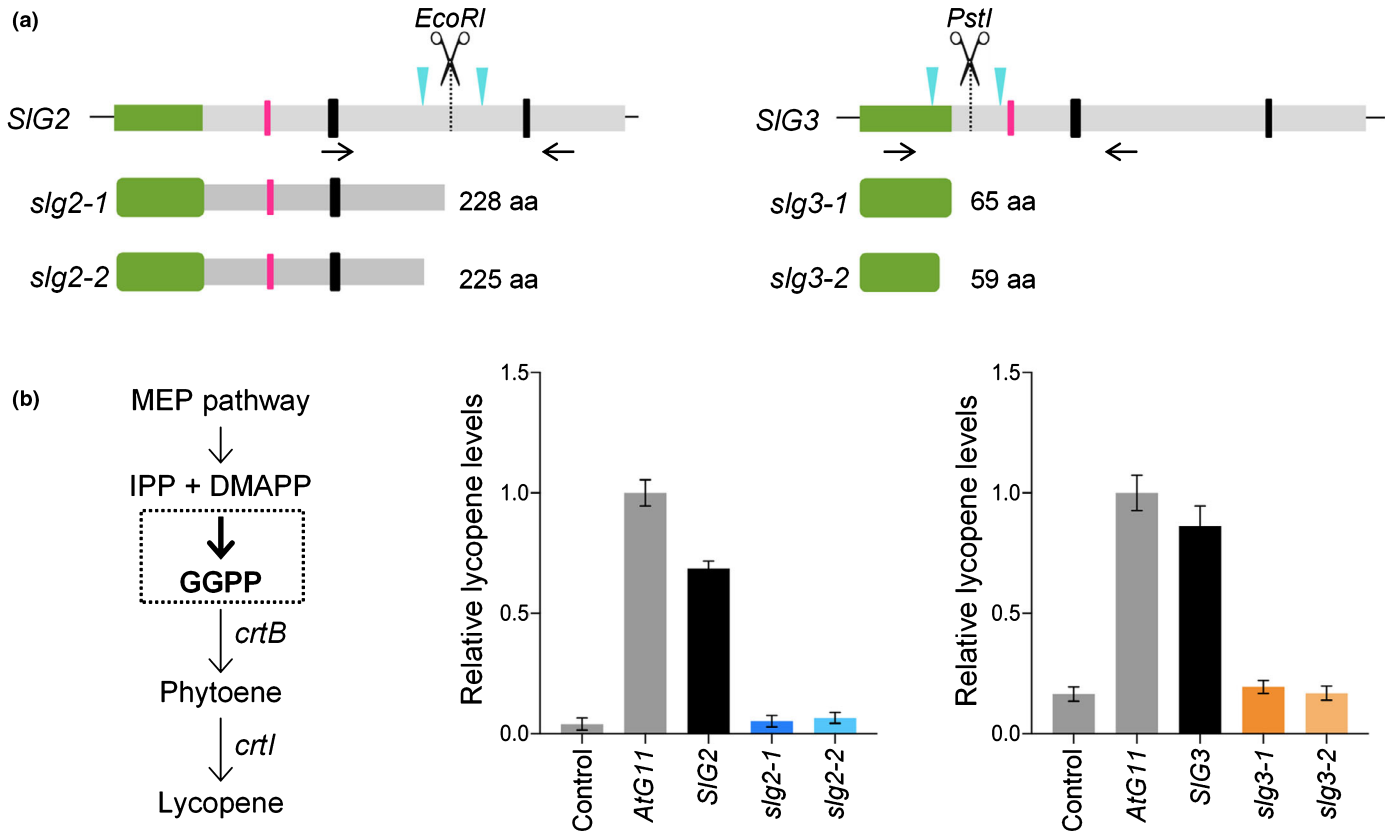

Fig. 4 CRISPR-Cas9 mutagenesis of tomato *SlG2* and *SlG3* genes. (a) Scheme representing the designed strategy to generate deletions on *SlG2* and *SlG3* genes and the resulting proteins in selected mutant alleles (see Supporting Information Figs S6–S8 for further details). Green, pink and black boxes represent transit peptides, protein–protein interaction motifs, and catalytic domains (FARM and SARM), respectively. Blue arrowheads indicate the position of the designed sgRNAs encompassing specific restriction sites, and black arrows represent primer pairs used for genotyping. (b) Activity assays of wild-type (WT) and mutant GGPPS enzymes in *E. coli* strains expressing bacterial genes for lycopene biosynthesis (*crtB* and *crtI*) but lacking GGPPS activity. Lycopene production after transformation with an empty vector (labelled as 'Control' in the plots) or plasmid constructs harbouring the indicated sequences is represented relative to the levels obtained with the true GGPPS enzyme AtG11. Values represent the mean ± SD of at least three independent transformants ($n = 3$).

did not follow the expected Mendelian segregation in any of the two experiments or when considering all data together (Table 3). In addition to the absence of double *slg2-2 slg3-1* mutants (here referred to as *g2g2 g3g3*), lines with one of the two genes in homozygosis and the second one in heterozygosis (i.e. *g2g2 G3g3* and *G2g2 g3g3*) were found at lower frequencies than predicted (Table 3), suggesting a gene dosage effect. Our interpretation of these results is that the absence of both *SlG2* and *SlG3* results in a lethal phenotype that is partially rescued by incorporating one copy of any of these two genes (as in *g2g2 G3g3* or *G2g2 g3g3* plants), and fully rescued when two copies are present in the genome (as in double heterozygous or single homozygous mutants). These results, together with the similar expression levels of both genes in developing tomato seeds (Fig. S4), suggest that SlG2 and SlG3 contribute similarly and additively to embryo or/and seed development.

The phenotypes of single *slg3* mutants are exacerbated in lines with the *SlG2* gene in heterozygosis

Plants segregating from double heterozygous F1 plants (*G2g2 G3g3*) that showed a single mutant genotype (i.e. *g2g2 G3G3* and *G2G2 g3g3*) or one of the two genes in homozygosis and the second one in heterozygosis (i.e. *g2g2 G3g3* and *G2g2 g3g3*) were transferred to soil and used to carefully examine their phenotype. Consistent with that described for the *slg2-2* and *slg3-1* parentals (Fig. 5), young leaves of *g2g2 G3G3* plants showed unchanged pigmentation and WT levels of photosynthetic pigments (chlorophylls and carotenoids) and photosynthetic activity (ϕPSII), whereas those of *G2G2 g3g3* plants were paler and displayed a reduction of photosynthetic pigments and activity (Fig. 8). Most interestingly, the phenotypes of the *slg3* mutants were intensified when one of the two genomic copies of *SlG2* was inactivated in the *G2g2 g3g3* line (Fig. 8). Loss of an *SlG3* gene copy in the *slg2* mutant background, however, was not sufficient to trigger statistically significant changes in young leaves compared with WT or *slg2* lines. This result indicates that a single copy of the *SlG3* gene is sufficient to provide GGPP for the production of photosynthetic pigments in chloroplasts, even when no SlG2 activity is available. For mature leaves, no significant differences were observed between WT and any of the mutant lines (Fig. 8).

At the level of fruit ripening, quantification of fruit colour using the TomatoAnalyzer 4.0 tool (Gonzalo *et al.*, 2009) confirmed the pigmentation delay previously observed in single mutants defective

© 2021 The Authors
New Phytologist © 2021 New Phytologist Foundation

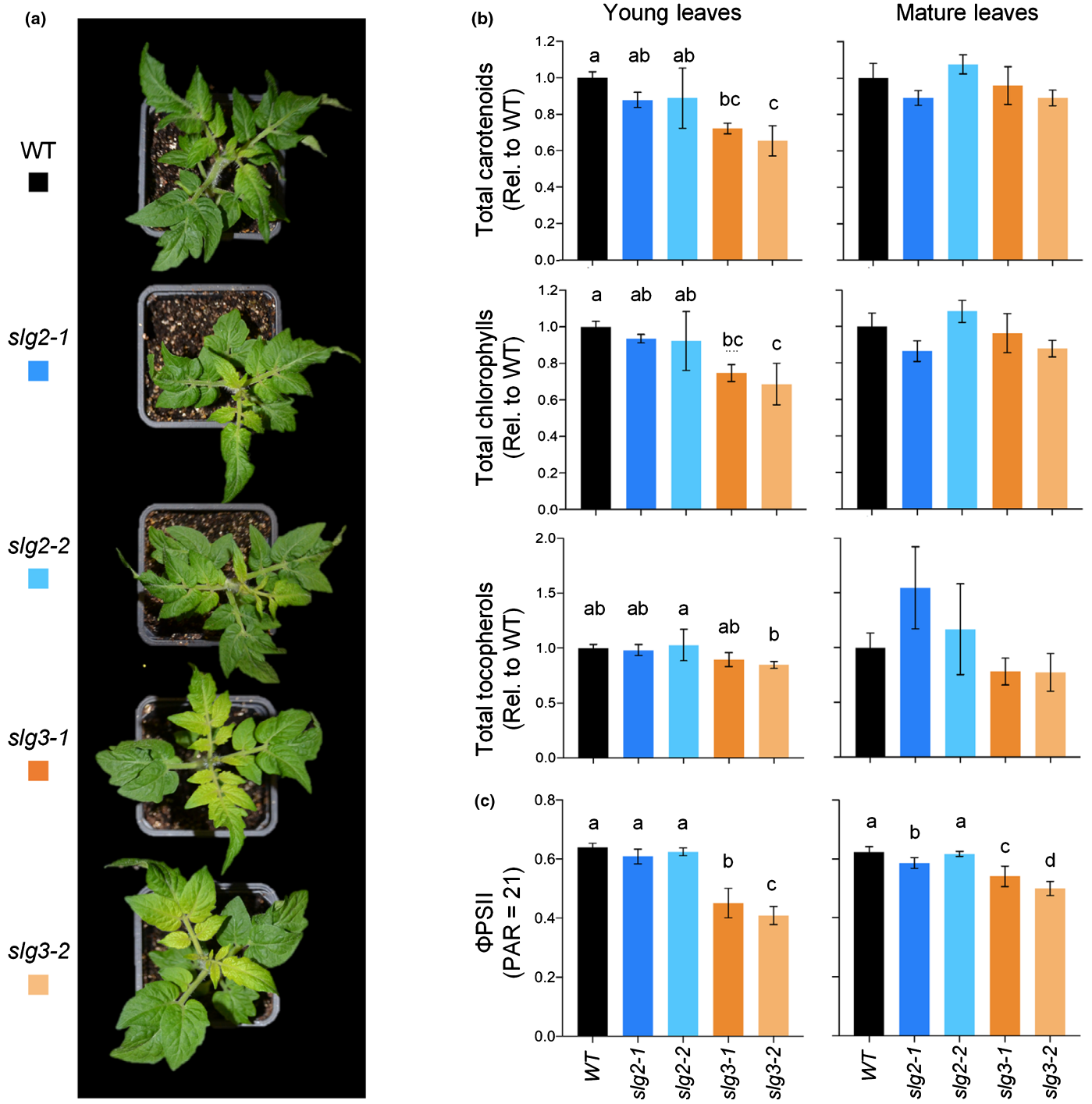

Fig. 5 Leaf phenotypes of mutant tomato lines defective in SlG2 or SlG3. (a) Representative images of 4-wk-old plants of the indicated lines. (b) Relative levels of total carotenoids, chlorophylls and tocopherols in young and mature leaves of wild-type (WT) and mutant lines. Values are represented relative to WT levels and they correspond to the mean ± SD of at least three independent biological replicates ($n = 3$). See Supporting Information Table S7 for absolute values. (c) ϕPSII in young and mature leaves of the indicated lines. Values represent the mean ± SD of four different leaf areas from three different plants. In all cases, different letters represent statistically significant differences ($P < 0.05$) among means according to post hoc Tukey's tests run when one-way ANOVA detected different means.

in SlG2 or, to a higher extent, SlG3 (Fig. 7) and further showed a stronger effect when one of the two genomic copies of *SlG2* was additionally inactivated in the *slg3* background (Fig. 9a). Analysis of the expression of ripening marker genes such as *E8* and *ACS2* (Estornell *et al.*, 2009; Llorente *et al.*, 2016; D'Andrea *et al.*, 2018) showed that the peak of *E8* and *ACS2* expression observed at the onset of ripening (Fig. S4) was reduced in the mutants (Fig. 9b). Again, the stronger effect was observed in lines without SlG3 activity and tended to be higher in *G2g2 g3g3* compared with *G2G2 g3g3* lines (Fig. 9b).

© 2021 The Authors
New Phytologist © 2021 New Phytologist Foundation

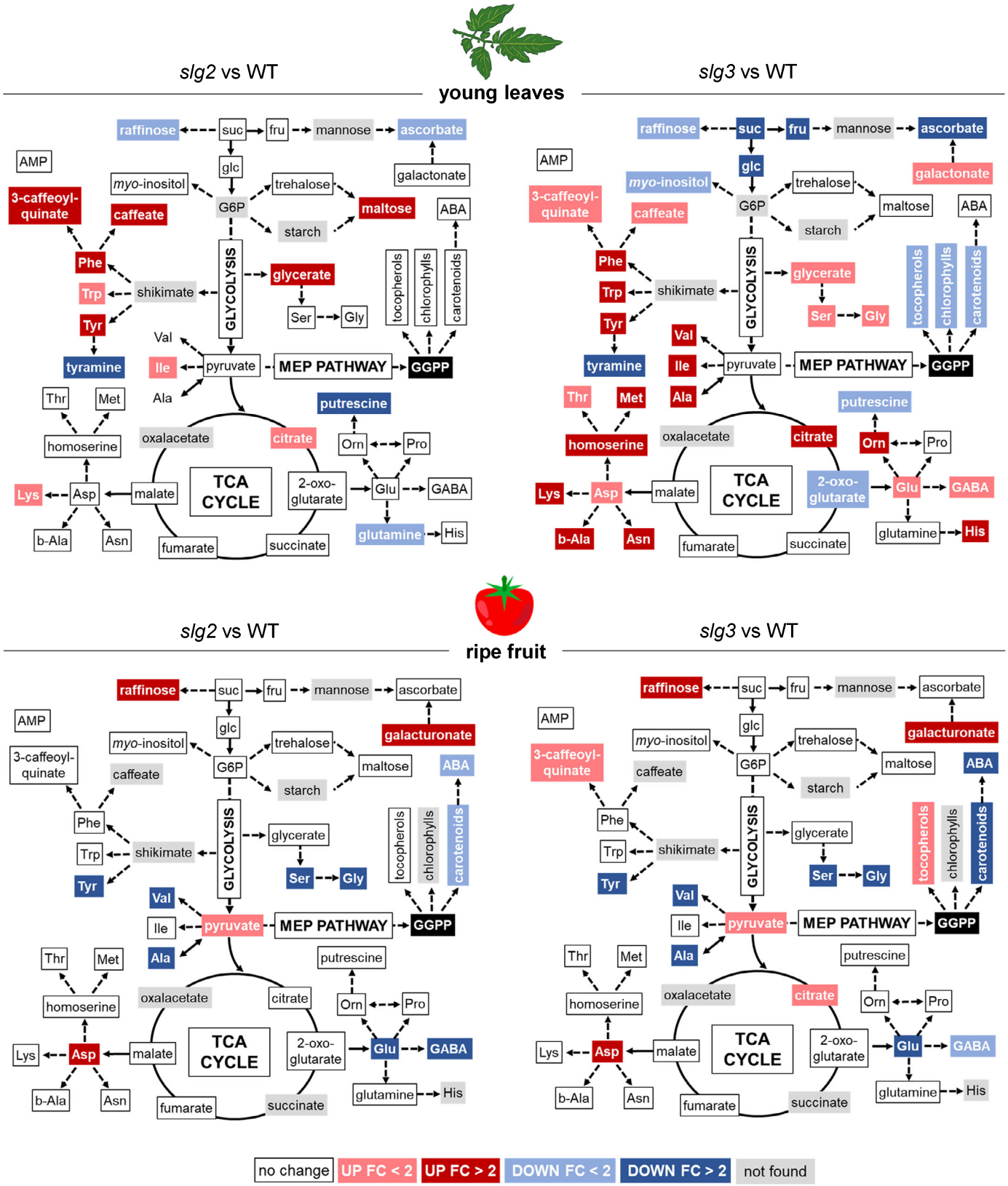

Fig. 6 Metabolic changes in *slg2* and *slg3* mutants. Colours represent statistically significant fold-change (FC) values (*t*-test, $P < 0.05$) of metabolite levels in young leaves or ripe fruit (B + 10) from mutant tomato plants relative to those in wild-type (WT) controls. Quantitative and technical data are detailed in Supporting Information Tables S8 and S9 for leaves and Tables S10 and S11 for fruit.

© 2021 The Authors
New Phytologist © 2021 New Phytologist Foundation

Table 2 ABA levels in GGPPS-defective tomato leaves and fruit.

	Young leaves	B + 10 fruit
WT	1.67 ± 0.19	0.63 ± 0.13
slg2-1	1.69 ± 0.10	0.55 ± 0.12
slg2-2	1.98 ± 0.39	**0.30 ± 0.08**
slg3-1	1.96 ± 0.09	**0.16 ± 0.04**
slg3-2	1.61 ± 0.29	**0.08 ± 0.01**

Values (μg g^{-1} dry weight) correspond to the mean ± SD of four independent samples ($n = 4$). Statistically significant changes in mutants compared with wild-type (WT) samples (*t*-test, $P < 0.01$) are indicated in bold.

Discussion

The fundamental basis for our knowledge of the regulation of GGPP biosynthesis in plants mainly comes from the characterisation of the Arabidopsis GGPPS family (Zhu *et al.*, 1997a,b; Okada *et al.*, 2000; Beck *et al.*, 2013; Nagel *et al.*, 2015; Wang *et al.*, 2016; Ruiz-Sola *et al.*, 2016a,b). In this model plant, there are two plastid-targeted GGPPS paralogues (AtG2 and AtG11) but only AtG11 appears to be required for the production of plastidial isoprenoids (Beck *et al.*, 2013; Nagel *et al.*, 2015; Ruiz-Sola *et al.*, 2016a,b). The gene encoding AtG11 is ubiquitously expressed at high levels and can generate long transcripts encoding the plastid-targeted isoform, but also short transcripts encoding a cytosolic enzyme that retains enzymatic activity and is essential for embryo development (Ruiz-Sola *et al.*, 2016a). The production of GGPP has also been studied in a few crop plants (Wang & Dixon, 2009; Zhang *et al.*, 2015; Zhou *et al.*, 2017; Wang *et al.*, 2018, 2019). Similar to Arabidopsis, rice and pepper contain only one enzymatically active GGPPS isoform localised in plastids, named OsGGPPS1 (OsG1 in short) and CaGGPPS1 (CaG1), respectively (Zhou *et al.*, 2017; Wang *et al.*, 2018). Strikingly, only scattered information has been available to date on the tomato GGPPS family, despite this species being a well established model plant that accumulates high amounts of GGPP-derived metabolites of human interest such as carotenoids in fruits. Here we demonstrate that, in tomato, two plastidial isoforms (SlG2 and SlG3) co-ordinately supply GGPP to produce carotenoids and other isoprenoids essential for photosynthesis, fruit pigmentation and seed viability.

Subfunctionalisation of plastidial GGPPS paralogues in tomato might involve several mechanisms with a major role for differential gene expression

The three plastid-targeted GGPPS homologues present in tomato (SlG1-3) produce GGPP with similar kinetic parameters and an optimal pH around 7.5 (Fig. S3; Table 1). Several mechanisms might allow enzymatically similar GGPPS isoforms to acquire new functions, including: (a) localisation in distinct subcellular compartments, (b) specific interactions with other protein, and (c) diversification of spatio-temporal gene expression patterns. Despite the clear plastidial localisation observed here (Fig. S1) and elsewhere (Zhou & Pichersky, 2020) for GFP fusions of the SlG1-3 isoforms, we cannot exclude the possibility that shorter extraplastidial versions of these proteins could also be produced *in vivo*, paralleling that observed for AtG11 (Ruiz-Sola *et al.*, 2016a). Indeed, several M residues can be found in the N-terminal region of both SlG2 and SlG3 enzymes (Fig. S8); they could be used as alternative translation start sites to produce catalytically active GGPPS enzymes with an absent or shorter (i.e. dysfunctional) plastid-targeting domain.

In addition to localisation in distinct subcellular compartments, subfunctionalisation of GGPPS paralogues might also involve isoform-specific interactions with other proteins. The enzymatic properties of GGPPS proteins change to produce GPP upon heterodimerisation with members of the GPP synthase small subunit type I (SSU-I) subfamily (Orlova *et al.*, 2009; Wang & Dixon, 2009). This occurs upon interaction of SlG1-3 enzymes with the tomato SSU-I protein (Solyc07g064660; Zhou & Pichersky, 2020). Multienzymatic complexes appear to be particularly important for metabolic channelling of GGPP. In particular, PSY cannot access freely diffusible GGPP or time-displaced GGPP supply by GGPPS (Camagna *et al.*, 2019). Arabidopsis AtG11 and pepper CaG1 can directly interact with PSY proteins (Ruiz-Sola *et al.*, 2016b; Wang *et al.*, 2018; Camagna *et al.*, 2019). We found that tomato SlG2, but not SlG3, is able to interact with PSY1 and PSY2 *in planta* (Fig. 3). However, tomato SlG3 might deliver GGPP to PSY enzymes by heterodimerisation with PSY-interacting SlG2 (Fig. 3). An alternative possibility involves interaction with members of another catalytically inactive SSU subfamily, named type II (SSU-II). Similar to AtG11 and CaG1, OsG1 is the only GGPPS enzyme producing GGPP for carotenoid biosynthesis in rice. Strikingly, OsG1 does not interact with PSY, but heterodimerises with a SSU-II homologue, resulting in its delivery to a large protein complex in thylakoid membranes (Zhou *et al.*, 2017). The interaction with SSU-II proteins was also shown to enhance not only the GGPP-producing activity of rice OsG1 but also of pepper CaG1 (Wang *et al.*, 2018) and tomato SlG1-3 isoforms (Zhou & Pichersky, 2020). Interestingly, the pepper SSU-II protein also interacts with PSY, suggesting that binding of CaG1 to SSU-II might stimulate both its GGPPS activity and its interaction with PSY (Wang *et al.*, 2018). It is therefore possible that heterodimerisation with tomato SSU-II (Solyc09g008920) might also deliver SlG3 to PSY-containing protein complexes and enhance interaction of SlG2 with PSY isoforms.

Regardless of other possible mechanisms discussed above, it appears that a major determinant defining the biological roles of plastidial GGPPS isoforms in tomato is their distinct expression profiles. Mining of public tomato gene expression databases, GCN analyses and qPCR assays led us to conclude that SlG1 is likely to contribute to carotenoid biosynthesis in roots together with PSY3. This conclusion is supported by a recent study showing that the expression of *PSY3* and *SlG1* co-ordinately responds to tomato root mycorrhization and phosphate starvation (Stauder *et al.*, 2018). The SlG1–PSY3 tandem might be channelling the flux of MEP-derived precursors towards the synthesis of carotenoid-derived molecules, such as strigolactones and apocarotenoids, that are crucial for the establishment of symbiosis

© 2021 The Authors
New Phytologist © 2021 New Phytologist Foundation

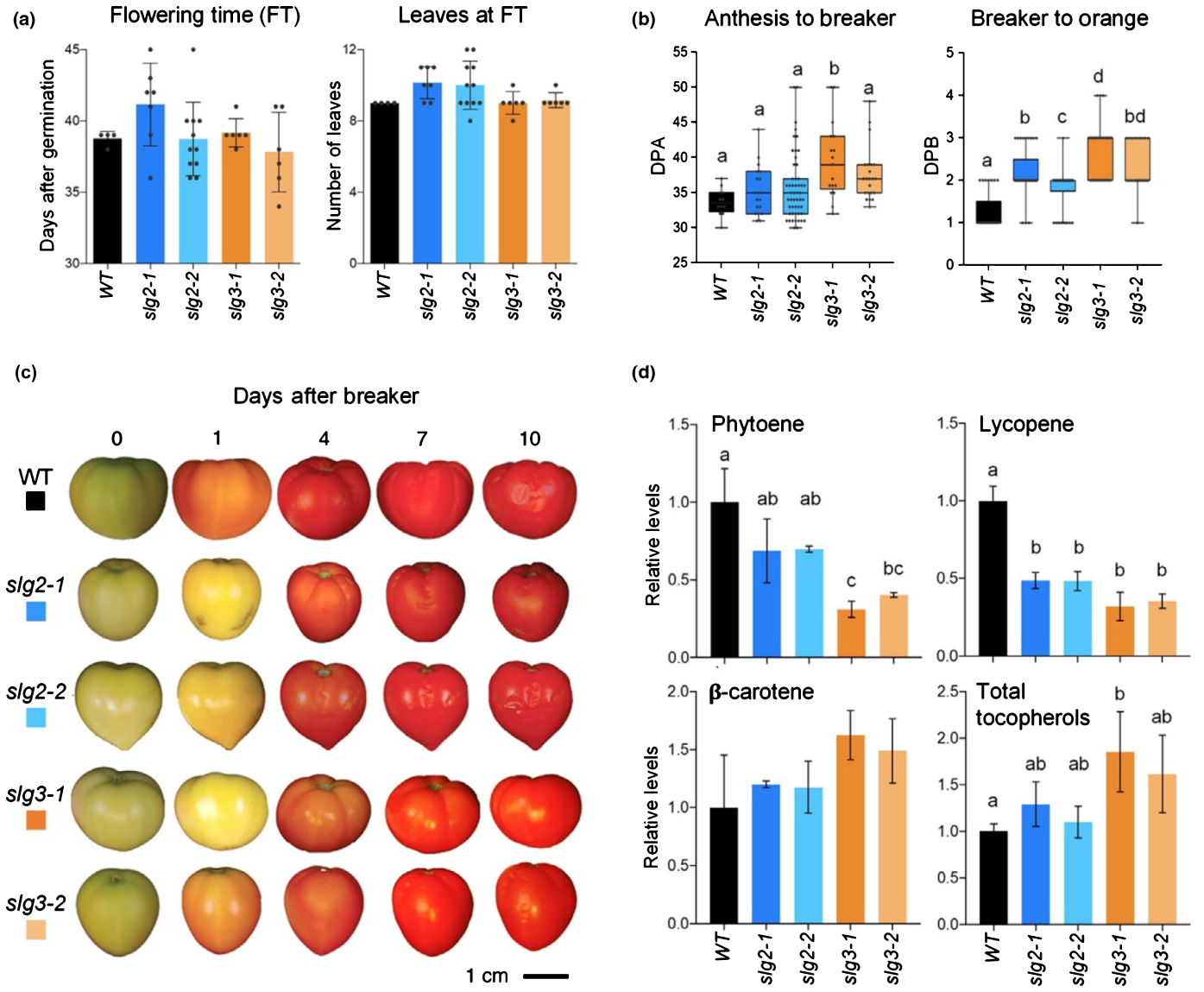

Fig. 7 Flowering and fruit phenotypes of mutant tomato lines defective in SlG2 or SlG3. (a) Flowering time measured as days after germination (left) or number of leaves (right). Values correspond to the mean ± SD of at least $n = 4$ independent biological replicates. (b) Number of days to reach the indicated ripening stages represented as days post anthesis on vine (DPA, left) and days post breaker off vine (DPB, right). In both box-plots, the lower boundary of the boxes indicates the 25th percentile, the black line within the boxes marks the median, and the upper boundary of the boxes indicates the 75th percentile. Dots mark data values and whiskers above and below the boxes indicate the minimum and maximum values. (c) Representative images of fruit from WT and mutant lines harvested from the plant at the breaker stage. (d) Relative levels of individual carotenoids (phytoene, lycopene and β-carotene) and total tocopherols in fruits of wild-type (WT) and mutant linesat the B+10 stage. Values are represented relative to those in WT samples and correspond to the mean ± SD of $n = 3$ independent biological replicates. See Supporting Information Table S7 for absolute values. In all plots, different letters represent statistically significant differences (one-way ANOVA followed by Tukey's multiple comparisons test, $P < 0.05$).

(Stauder *et al.*, 2018). Unlike *SlG1*, *SlG2* and *SlG3* are constitutively expressed, with *SlG3* being the paralogue with the highest expression level in all plant tissues (Fig. S4). In leaves, *SlG2* is more strongly co-expressed than *SlG3* with genes from photosynthesis-related isoprenoid pathways (Fig. 1). This suggests that the expression of the *SlG2* gene changes more than that of *SlG3* to adapt to conditions requiring a re-adjustment of the gene expression network regulating the metabolism of isoprenoids such as carotenoids. In agreement, *SlG2* was much more upregulated than *SlG3* during seedling de-etiolation (Fig. 2) and leaf development (Fig. S4c), in which an enhanced production of carotenoids and other photosynthesis-related isoprenoids contributes to assemble a functional photosynthetic machinery. *SlG2* was also much more induced than *SlG3* during fruit ripening, when carotenoid biosynthesis is boosted thanks to the upregulation of the PSY1 isoform. *PSY1* and *SlG2*, but not *SlG3*, are coordinately regulated by FUL and RIN transcription factors that control the expression of ripening-related genes, including many of the MEP and carotenoid pathway genes (Fujisawa *et al.*, 2013, 2014).

© 2021 The Authors
New Phytologist © 2021 New Phytologist Foundation

Table 3 Expected and observed frequencies of the F2 population from the crosses of *slg2-2* and *slg3-1* mutant tomato plants.

		Round 1		Round 2		Combined	
Genotypes	Expected (%)	*n*	%	*n*	%	*n*	%
G2g2 G3g3	25	52	26	15	20	67	24
G2g2 G3G3	12.5	26	13	18	24	44	16
G2G2 G3g3	12.5	35	17.5	10	13	45	16
g2g2 G3g3	12.5	18	9	6	8	24	9
G2g2 g3g3	12.5	16	8	5	7	21	8
g2g2 g3g3	6.25	0	0	0	0	0	0
g2g2 G3G3	6.25	17	8.5	5	7	22	8
G2G2 g3g3	6.25	14	7	8	11	22	8
G2G2 G3G3	6.25	22	11	9	12	31	11
Total plants (*n*)		200		76		276	
Chi-square			30.84		22.68		45.17
P-value			0.0002		0.0038		< 0.0001

Mutant alleles are marked in red. A chi-squared goodness-of-fit test was performed with 8 degrees of freedom and 95% confidence interval to check the Mendelian segregation of the mutant alleles. *n*, number of plants.

All these expression data showed that *SlG2* expression is more responsive to sudden demands of precursors for the production of isoprenoids, including carotenoids. By contrast, *SlG3* expression is higher and does not change as much, suggesting a housekeeping role to maintain a continuous supply of GGPP in plastids for basal production of carotenoids and other isoprenoids. According to this model, SlG1 and SlG2 would help SlG3 to supply GGPP when a boost in carotenoid production is needed. The very low and restricted expression level of *SlG1*, however, strongly suggests that SlG2 is the main helper isoform for SlG3 in chloroplasts of cotyledons and expanding leaves and chromoplasts of ripening fruit.

GGPPS isoforms SlG2 and SlG3 have functionally interchangeable roles in chloroplasts and chromoplasts

Analysis of tomato mutants defective in gene copies for SlG2 or/and SlG3 further suggested that these are functionally exchangeable isoforms that participate in the same biological processes. This might not be obvious when analysing leaves, as only *slg3* alleles were found to display reduced levels of GGPP-derived isoprenoids and subsequent inhibition of photosynthesis (Figs 5, 8). However, the effects of reduced isoprenoid synthesis could also be indirectly detected in *slg2* leaves. Our GC-MS analysis showed higher levels of all aromatic amino acids derived from the shikimate pathway (Trp, Tyr and Phe) as well as Phe-derived phenylpropanoids caffeate (caffeic acid) and 3-caffeoyl-quinate (chlorogenic acid) in both *slg2* and *slg3* mutant lines (Fig. 6). This might be a physiological response to cope with photo-oxidative stress caused by lower levels of carotenoids in the mutants, as phenylpropanoids (including Phe-derived flavonoids and anthocyanins) can also function as photoprotective metabolites (Muñoz & Munné-Bosch, 2018). Reduced levels of well known metabolites associated with oxidative stress such as ascorbate and putrescine in leaves from both mutant lines would also support this view.

Loss of one *SlG3* gene copy in the *slg2* mutant background failed to cause a statistically significant decrease in the levels of photosynthetic pigments or activity, even though a trend towards reduction of chlorophyll and carotenoid levels was observed (Fig. 8). However, complete loss of SlG3 activity in lines with one or two functional *SlG2* copies was sufficient to reduce levels of GGPP-derived photoprotective isoprenoids such as carotenoids and tocopherols to an extent that became detectable and affected photosynthesis (Fig. 5), causing sugar starvation and the subsequent metabolic changes observed only in the *slg3* mutant (Fig. 6). In agreement, the increased accumulation of most amino acids in *slg3* leaves suggested a high proteolytic activity to generate an alternative respiratory source, a probable response to sugar starvation derived from reduced photosynthesis and/or photo-oxidative stress (Araújo *et al.*, 2011; Obata & Fernie, 2012; Galili *et al.*, 2016).

The absence of any of the two individual enzymes also decreases plastidial GGPP production in fruit, as deduced from the levels of the main GGPP-derived metabolites (Fig. 7d; Table S7). Tocopherol levels did not decrease in mutant fruit, perhaps because they are mostly produced by recycling the phytyl chain released from the chlorophylls degraded during fruit ripening. By contrast, lycopene (by far the most abundant carotenoid in ripe fruit) and, to a lower extent, phytoene, showed reduced levels in both mutants (Fig. 7d; Table S7). Similar to that observed in leaves, the effect is stronger in *slg3* mutants, consistent with the higher expression levels of the *SlG3* compared with *SlG2* in young leaves and MG fruits (Fig. S4). While altered levels of 3-caffeoyl-quinate and citrate were detected only in fruit of the *slg3* mutant, the rest of the metabolic changes were similar in *slg2* and *slg3* lines (Fig. 6), again supporting the conclusion that these enzymes are redundant and interchangeable. In particular, both *slg2* and *slg3* fruit showed pigmentation defects that were associated with a decreased carotenoid accumulation (Figs 7, 9a). Because ABA is synthesised from carotenoids, its reduced levels in GGPPS-defective ripe fruits, but not in leaves (Table 2),

© 2021 The Authors
New Phytologist © 2021 New Phytologist Foundation

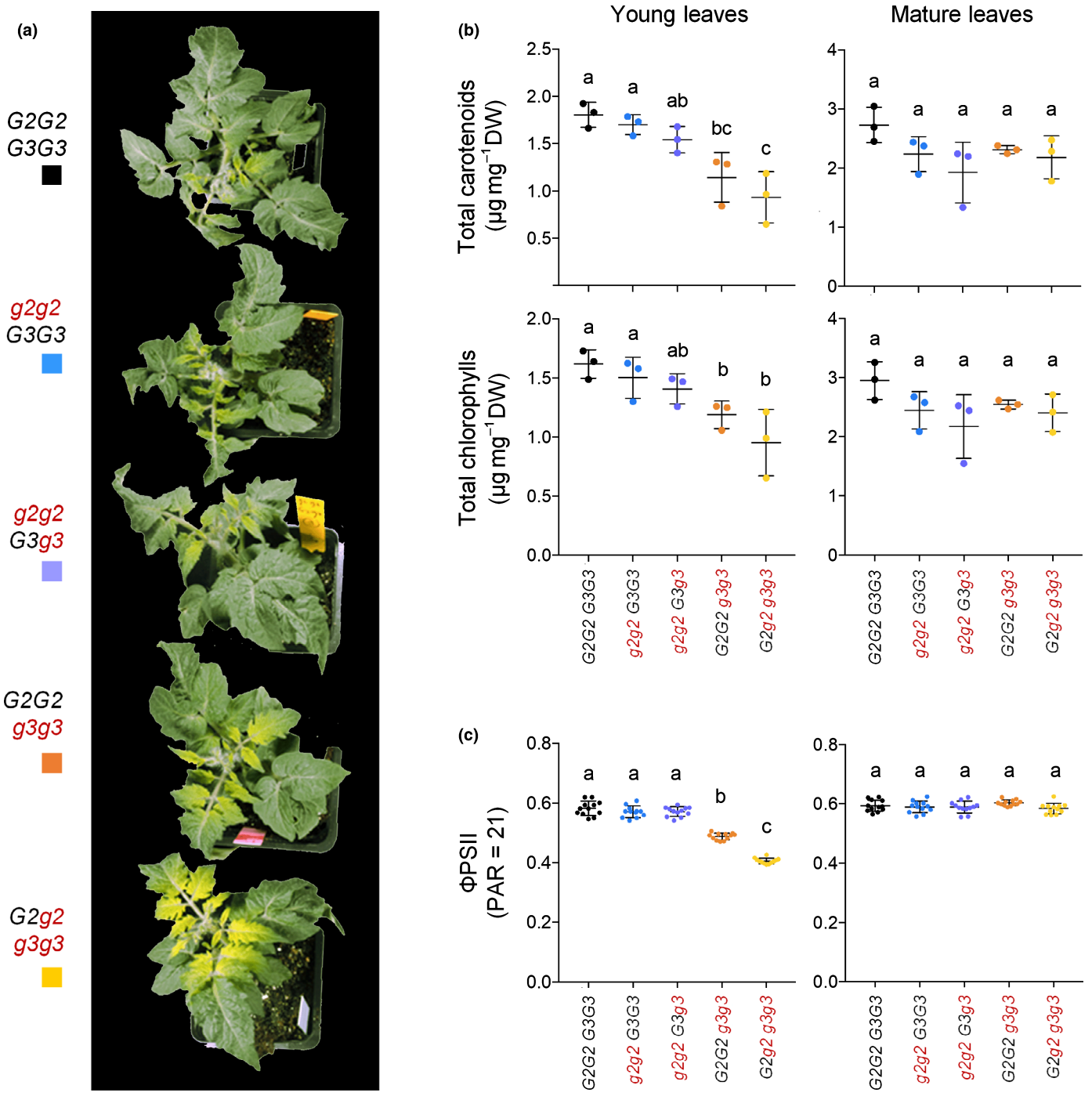

Fig. 8 Leaf phenotypes of tomato lines with different combinations of *slg2* and *slg3* mutations. (a) Representative images of 4-wk-old plants of the indicated lines. Mutant alleles are marked in red. (b) Total levels of photosynthetic pigments (carotenoids and chlorophylls) in young and mature leaves of wild-type (WT) and mutant lines. Values, mean and SD of $n = 3$ independent biological replicates are represented. (c) ϕPSII in young and mature leaves of the indicated lines. Values, mean and SD of four different leaf areas from three different plants are shown. In all plots, different letters represent statistically significant differences ($P < 0.05$) among means according to post hoc Tukey tests that were run once the existence of different means was established using one-way ANOVA.

may be the result of a more substantial reduction in carotenoid contents in mutant fruit (Fig. 7) compared with leaves (Fig. 5; Table S7). A role for ABA in promoting tomato fruit ripening has been proposed based on the analysis of mutants or external application of hormones and inhibitors. This, together with the observed downregulation of ethylene-related ripening marker genes (*E8* and *ACS2*) in GGPPS-defective fruit (Fig. 9b), allowed us to speculate that reduced ABA levels in the mutant fruit may contribute to a delay in ripening, either directly or indirectly by ethylene (Zhang *et al.*, 2009; McQuinn *et al.*, 2020).

© 2021 The Authors
New Phytologist © 2021 New Phytologist Foundation

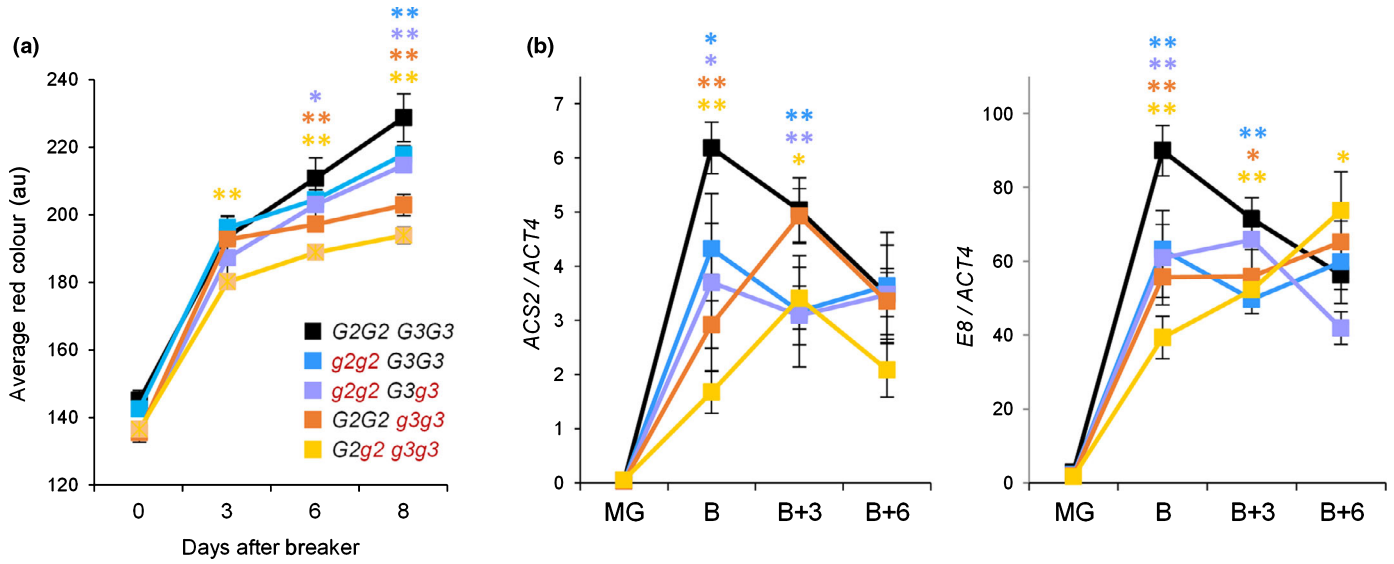

Fig. 9 Ripening-associated pigmentation and marker gene expression in tomato fruits with different combinations of *slg2* and *slg3* mutations. (a) Average red colour quantification (arbitrary units) of on-vine fruit from wild-type (WT) and mutant lines at the indicated times. Values represent the mean ± SD of three different fruits ($n = 3$) for each point. (b) RT-qPCR analysis of *ACS2* and *E8* transcript levels in WT and mutant fruits collected at the indicated developmental stages. Expression values were normalised using *ACT4* and represent the mean ± SD of $n = 3$ independent biological replicates. In all plots, asterisks indicate statistically significant differences among means relative to WT samples (*t*-test: *, $P < 0.05$; **, $P < 0.01$). Asterisk colour represents the genotype.

Additionally, metabolic roles of SlG2 and SlG3 in addition to their GGPPS activity in plastids might play a role in fruits but also in developing seeds, therefore explaining why we could not isolate a double *slg2 slg3* mutant (Table 3). The observation that the lethal phenotype is dose dependent in an isoform-independent fashion (i.e. can be rescued by a single genomic copy of either *SlG2* or *SlG3*) reinforces our conclusion that SlG2 and SlG3 have functionally interchangeable roles.

Concluding remarks

Retention of multiple gene copies after duplication events may allow the acquisition of new functions (neofunctionalisation) or partitioning the ancestral functions between duplicate partners (subfunctionalisation), by evolution of coding sequence and/or regulatory regions. The work reported here demonstrates that the bulk of GGPP production in tomato leaf chloroplasts and fruit chromoplasts relies on two redundant, but cooperating, GGPPS paralogues, SlG2 and SlG3. Additionally, the SlG1 isoform might contribute to GGPP synthesis in root plastids. This subfunctionalisation scenario contrasts with that described to date in other plant species such as Arabidopsis, rice or pepper, which produce their essential plastidial isoprenoids using a single GGPPS isoform. However, it is likely that tomato is not an exception. Examples of gene families encoding enzyme isoforms located in the same cell compartment, but differing in gene expression profiles abound in the literature. They include deoxyxylulose 5-phosphate synthase (DXS) and PSY, the rate-determining enzymes of the MEP and carotenoid pathways, respectively (Walter *et al.*, 2015). Both DXS and PSY are encoded by single genes in Arabidopsis, but several differentially expressed genes in tomato. Subfunctionalisation is also widespread beyond the isoprenoid pathway, contributing to the huge diversity of specialised metabolism in plants (Moghe & Last, 2015). Deciphering how different plants regulate plastidial GGPP production and channelling will be useful for future metabolic engineering approaches targeted to manipulate the accumulation of specific groups of GGPP-derived isoprenoids without negatively impacting the levels of others.

Acknowledgements

We greatly thank Juan Antonio López-Ráez for providing cDNA samples of nonmycorrhized and mycorrhized tomato roots; Ernesto Llamas for providing the pGWB417_AtPRK construct, and Albert Ferrer and Laura Gutiérrez for the pDE-Cas9 (with kanamycin resistance) plasmid. The technical support of M. Rosa Rodríguez-Goberna and all CRAG services is also appreciated. This work was funded by the European Regional Development Fund (FEDER) and the Spanish Agencia Estatal de Investigación (grants BIO2017-84041-P and BIO2017-90877-REDT) and Generalitat de Catalunya (2017SGR-710) to MRC. Support by the collaborative European Union's Horizon 2020 (EU-H2020) ERA-IB-2 (Industrial Biotechnology) BioProMo project to MRC (PCIN-2015-103), RK and JB (053-80-725) is also acknowledged. CRAG is financially supported by the Severo Ochoa Programme for Centres of Excellence in R&D 2016–2019 (SEV-2015-0533) and the Generalitat de Catalunya CERCA Programme. MVB was funded with a Spanish Ministry of Education, Culture and Sports PhD fellowship (FPU14/05142) and a EU-H2020 COST Action CA15136 (EuroCaroten) short-stay fellowship. ME is supported by a Spanish Agencia Estatal de Investigación (BES-2017-080652) PhD fellowship. IFS is supported by the EU-H2020 Marie S. Curie Action 753301 (Arcatom).

© 2021 The Authors
New Phytologist © 2021 New Phytologist Foundation

Author contributions

MVB, ME and MRC designed the research; MVB, ME, SB, GD, IFS, EF and AF performed research; RK, ARF and JB contributed analytic tools; MVB, ME, SB, GD, IFS, EF, AF, RK, ARF, JB and MRC analysed data; MVB and MRC wrote the paper. MVB and ME contributed equally to this work.

ORCID

M. Victoria Barja https://orcid.org/0000-0002-3846-4885
Jules Beekwilder https://orcid.org/0000-0003-3238-4427
Gianfranco Diretto https://orcid.org/0000-0002-1441-0233
Miguel Ezquerro https://orcid.org/0000-0002-3051-5502
Elisenda Feixes https://orcid.org/0000-0003-0285-1979
Alisdair R. Fernie https://orcid.org/0000-0001-9000-335X
Igor Florez-Sarasa https://orcid.org/0000-0002-1862-7931
Rumyana Karlova https://orcid.org/0000-0003-0230-6428
Manuel Rodríguez-Concepción https://orcid.org/0000-0002-1280-2305

REFERENCES

Ahrazem O, Argandoña J, Fiore A, Aguado C, Luján R, Rubio-Moraga Á, Marro M, Araujo-Andrade C, Loza-Alvarez P, Diretto G *et al.* 2018. Transcriptome analysis in tissue sectors with contrasting crocins accumulation provides novel insights into apocarotenoid biosynthesis and regulation during chromoplast biogenesis. *Scientific Reports* **8**: 1–17.

Ament K, Van Schie CC, Bouwmeester HJ, Haring MA, Schuurink RC. 2006. Induction of a leaf specific geranylgeranyl pyrophosphate synthase and emission of (E,E)-4,8,12-trimethyltrideca-1,3,7,11-tetraene in tomato are dependent on both jasmonic acid and salicylic acid signaling pathways. *Planta* **224**: 1197–1208.

Araújo WL, Tohge T, Ishizaki K, Leaver CJ, Fernie AR. 2011. Protein degradation – an alternative respiratory substrate for stressed plants. *Trends in Plant Science* **16**: 489–498.

Barja MV, Rodríguez-Concepción M. 2020. A simple *in vitro* assay to measure the activity of geranylgeranyl diphosphate synthase and other short-chain prenyltransferases. *Methods in Molecular Biology* **2083**: 27–38.

Bartley G, Scolnik P. 1993. cDNA cloning, expression during development, and genome mapping of a second phytoenen synthase. *Biochemistry* **268**: 25718–25721.

Bartley GE, Viitanen PV, Bacot KO, Scolnik PA. 1992. A tomato gene expressed during fruit ripening encodes an enzyme of the carotenoid biosynthesis pathway. *Journal of Biological Chemistry* **267**: 5036–5039.

Baslam M, Esteban R, García-Plazaola JI, Goicoechea N. 2013. Effectiveness of arbuscular mycorrhizal fungi (AMF) for inducing the accumulation of major carotenoids, chlorophylls and tocopherol in green and red leaf lettuces. *Applied Microbiology and Biotechnology* **97**: 3119–3128.

Beck G, Coman D, Herren E, Ruiz-Sola MA, Rodríguez-Concepción M, Gruissem W, Vranová E. 2013. Characterization of the GGPP synthase gene family in *Arabidopsis thaliana*. *Plant Molecular Biology* **82**: 393–416.

Bradford MM. 1976. A rapid and sensitive method for the quantitation of microgram quantities of protein utilizing the principle of protein-dye binding. *Analytical Biochemistry* **72**: 248–254.

Camagna M, Grundmann A, Bär C, Koschmieder J, Beyer P, Welsch R. 2019. Enzyme fusion removes competition for geranylgeranyl diphosphate in carotenogenesis. *Plant Physiology* **179**: 1013–1027.

Camara B. 1993. Plant phytoene synthase complex: component enzymes, immunology and biogenesis. *Methods in Enzymology* **214**: 352–365.

D'Andrea L, Simon-Moya M, Llorente B, Llamas E, Marro M, Loza-Alvarez P, Li L, Rodriguez-Concepcion M. 2018. Interference with Clp protease impairs carotenoid accumulation during tomato fruit ripening. *Journal of Experimental Botany* **69**: 1557–1568.

Diretto G, Frusciante S, Fabbri C, Schauer N, Busta L, Wang Z, Matas AJ, Fiore A, Rose JKC, Fernie AR *et al.* 2020. Manipulation of β-carotene levels in tomato fruits results in increased ABA content and extended shelf life. *Plant Biotechnology Journal* **18**: 1185–1199.

Dogbo O, Camara B. 1987. Purification of isopentenyl pyrophosphate isomerase and geranylgeranyl pyrophosphate synthase from *Capsicum* chromoplasts by affinity chromatography. *Biochimica et Biophysica Acta (BBA)/Lipids and Lipid Metabolism* **920**: 140–148.

Estornell LH, Orzáez D, López-Peña L, Pineda B, Antón MT, Moreno V, Granell A. 2009. A multisite gateway-based toolkit for targeted gene expression and hairpin RNA silencing in tomato fruits. *Plant Biotechnology Journal* **7**: 298–309.

Fernandez AI, Viron N, Alhagdow M, Karimi M, Jones M, Amsellem Z, Sicard A, Czerednik A, Angenent G, Grierson D *et al.* 2009. Flexible tools for gene expression and silencing in tomato. *Plant Physiology* **151**: 1729–1740.

Fester T, Schmidt D, Lohse S, Walter MH, Giuliano G, Bramley PM, Fraser PD, Hause B, Strack D. 2002. Stimulation of carotenoid metabolism in arbuscular mycorrhizal roots. *Planta* **216**: 148–154.

Fester T, Wray V, Nimtz M, Strack D. 2005. Is stimulation of carotenoid biosynthesis in arbuscular mycorrhizal roots a general phenomenon? *Phytochemistry* **66**: 1781–1786.

Fraser PD, Enfissi EMA, Halket JM, Truesdale MR, Yu D, Gerrish C, Bramley PM. 2007. Manipulation of phytoene levels in tomato fruit: effects on isoprenoids, plastids, and intermediary metabolism. *Plant Cell* **19**: 3194–3211.

Fraser PD, Romer S, Shipton CA, Mills PB, Kiano JW, Misawa N, Drake RG, Schuch W, Bramley PM. 2002. Evaluation of transgenic tomato plants expressing an additional phytoene synthase in a fruit-specific manner. *Proceedings of the National Academy of Sciences, USA* **99**: 1092–1097.

Fraser PD, Schuch W, Bramley PM. 2000. Phytoene synthase from tomato (*Lycopersicon esculentum*) chloroplasts – partial purification and biochemical properties. *Planta* **211**: 361–369.

Fray RG, Grierson D. 1993. Identification and genetic analysis of normal and mutant phytoene synthase genes of tomato by sequencing, complementation and co-suppression. *Plant Molecular Biology* **22**: 589–602.

Fujisawa M, Nakano T, Shima Y, Ito Y. 2013. A large-scale identification of direct targets of the tomato MADS box transcription factor RIPENING INHIBITOR reveals the regulation of fruit ripening. *Plant Cell* **25**: 371–386.

Fujisawa M, Shima Y, Nakagawa H, Kitagawa M, Kimbara J, Nakano T, Kasumi T, Ito Y. 2014. Transcriptional regulation of fruit ripening by tomato FRUITFULL homologs and associated MADS box proteins. *Plant Cell* **26**: 89–101.

Galili G, Amir R, Fernie AR. 2016. The regulation of essential amino acid synthesis and accumulation in plants. *Annual Review of Plant Biology* **67**: 153–178.

Giorio G, Stigliani AL, D'Ambrosio C. 2008. Phytoene synthase genes in tomato (*Solanum lycopersicum* L.) - new data on the structures, the deduced amino acid sequences and the expression patterns. *FEBS Journal* **275**: 527–535.

Gonzalo MJ, Brewer MT, Anderson C, Sullivan D, Gray S, Van Der Knaap E. 2009. Tomato fruit shape analysis using morphometric and morphology attributes implemented in tomato analyzer software program. *Journal of the American Society for Horticultural Science* **134**: 77–87.

Goytia E, Fernández-Calvino L, Martínez-García B, López-Abella D, López-Moya JJ. 2006. Production of plum pox virus HC-Pro functionally active for aphid transmission in a transient-expression system. *Journal of General Virology* **87**: 3413–3423.

Höhner R, Aboukila A, Kunz H-H, Venema K. 2016. Proton gradients and proton-dependent transport processes in the chloroplast. *Frontiers in Plant Science* **7**: 1–7.

Kachanovsky DE, Filler S, Isaacson T, Hirschberg J. 2012. Epistasis in tomato color mutations involves regulation of phytoene synthase 1 expression by *cis*-carotenoids. *Proceedings of the National Academy of Sciences, USA* **109**: 19021–19026.

Liu H, Ding Y, Zhou Y, Jin W, Xie K, Chen LL. 2017. CRISPR-P 2.0: an improved CRISPR-Cas9 tool for genome editing in plants. *Molecular Plant* **10**: 530–532.

© 2021 The Authors
New Phytologist © 2021 New Phytologist Foundation

Llorente B, D'Andrea L, Ruiz-Sola MA, Botterweg E, Pulido P, Andilla J, Loza-Alvarez P, Rodriguez-Concepcion M. 2016. Tomato fruit carotenoid biosynthesis is adjusted to actual ripening progression by a light-dependent mechanism. *The Plant Journal* **85**: 107–119.

Llorente B, Torres-Montilla S, Morelli L, Florez-Sarasa I, Matus JT, Ezquerro M, D'Andrea L, Houhou F, Majer E, Picó B *et al.* 2020. Synthetic conversion of leaf chloroplasts into carotenoid-rich plastids reveals mechanistic basis of natural chromoplast development. *Proceedings of the National Academy of Sciences, USA* **117**: 21796–21803.

Maudinas B, Bucholtz ML, Papastephanou C, Katiyar SS, Briedis AV, Porter JW. 1977. The partial purification and properties of a phytoene synthesizing enzyme system. *Archives of Biochemistry and Biophysics* **180**: 354–362.

McQuinn RP, Gapper NE, Gray AG, Zhong S, Tohge T, Fei Z, Fernie AR, Giovannoni JJ. 2020. Manipulation of ZDS in tomato exposes carotenoid- and ABA-specific effects on fruit development and ripening. *Plant Biotechnology Journal* **18**: 2210–2224.

Moghe GD, Last RL. 2015. Something old, something new: conserved enzymes and the evolution of novelty in plant specialized metabolism. *Plant Physiology* **169**: 1512–1523.

Muñoz A, Castellano MM. 2018. Coimmunoprecipitation of interacting proteins in plants. *Methods in Molecular Biology* **1794**: 279–287.

Muñoz P, Munné-Bosch S. 2018. Photo-oxidative stress during leaf, flower and fruit development. *Plant Physiology* **176**: 1004–1014.

Nagel R, Bernholz C, Vranová E, Košuth J, Bergau N, Ludwig S, Wessjohann L, Gershenzon J, Tissier A, Schmidt A. 2015. *Arabidopsis thaliana* isoprenyl diphosphate synthases produce the C 25 intermediate, geranylfarnesyl diphosphate. *The Plant Journal* **84**: 847–859.

Nisar N, Li L, Lu S, Khin NC, Pogson BJ. 2015. Carotenoid metabolism in plants. *Molecular Plant* **8**: 68–82.

Obata T, Fernie AR. 2012. The use of metabolomics to dissect plant responses to abiotic stresses. *Cellular and Molecular Life Sciences* **69**: 3225–3243.

Okada K, Saito T, Nakagawa T, Kawamukai M, Kamiya Y. 2000. Five geranylgeranyl diphosphate synthases expressed in different organs are localized into three subcellular compartments in Arabidopsis. *Plant Physiology* **122**: 1045–1056.

Orlova I, Nagegowda DA, Kish CM, Gutensohn M, Maeda H, Varbanova M, Fridman E, Yamaguchi S, Hanada A, Kamiya Y *et al.* 2009. The small subunit of snapdragon geranyl diphosphate synthase modifies the chain length specificity of tobacco geranylgeranyl diphosphate synthase *in planta*. *Plant Cell* **21**: 4002–4017.

Pulido P, Perello C, Rodríguez-Concepción M. 2012. New insights into plant isoprenoid metabolism. *Molecular Plant* **5**: 964–967.

Pulido P, Toledo-Ortiz G, Phillips MA, Wright LP, Rodríguez-Concepción M. 2013. Arabidopsis J-protein J20 delivers the first enzyme of the plastidial isoprenoid pathway to protein quality control. *Plant Cell* **25**: 4183–4194.

Rodriguez-Concepcion M, Avalos J, Bonet ML, Boronat A, Gomez-Gomez L, Hornero-Mendez D, Limon MC, Meléndez-Martínez AJ, Olmedilla-Alonso B, Palou A *et al.* 2018. A global perspective on carotenoids: metabolism, biotechnology, and benefits for nutrition and health. *Progress in Lipid Research* **70**: 62–93.

Rodríguez-Concepción M, Boronat A. 2015. Breaking new ground in the regulation of the early steps of plant isoprenoid biosynthesis. *Current Opinion in Plant Biology* **25**: 17–22.

Ruiz-Lozano JM, Aroca R, Zamarreño ÁM, Molina S, Andreo-Jiménez B, Porcel R, García-Mina JM, Ruyter-Spira C, López-Ráez JA. 2016. Arbuscular mycorrhizal symbiosis induces strigolactone biosynthesis under drought and improves drought tolerance in lettuce and tomato. *Plant, Cell & Environment* **39**: 441–452.

Ruiz-Sola MÁ, Barja MV, Manzano D, Llorente B, Schipper B, Beekwilder J, Rodriguez-Concepcion M. 2016a. A single arabidopsis gene encodes two differentially targeted geranylgeranyl diphosphate synthase isoforms. *Plant Physiology* **172**: 1393–1402.

Ruiz-Sola MÁ, Coman D, Beck G, Barja MV, Colinas M, Graf A, Welsch R, Rütimann P, Bühlmann P, Bigler L *et al.* 2016b. Arabidopsis GERANYLGERANYL DIPHOSPHATE SYNTHASE 11 is a hub isozyme required for the production of most photosynthesis-related isoprenoids. *New Phytologist* **209**: 252–264.

Ruiz-Sola MÁ, Rodríguez-Concepción M. 2012. Carotenoid biosynthesis in Arabidopsis: a colorful pathway. *The Arabidopsis book* **10**: e0158.

Sandmann G. 2015. Carotenoids of biotechnological importance. *Advances in Biochemical Engineering/Biotechnology* **148**: 449–467.

Schiml S, Fauser F, Puchta H. 2016. CRISPR/Cas-mediated site-specific mutagenesis in *Arabidopsis thaliana* using Cas9 nucleases and paired nickases. *Methods in Molecular Biology* **1469**: 111–122.

Simon P. 2003. Q-Gene: processing quantitative real-time RT-PCR data. *Bioinformatics* **19**: 1439–1440.

Sparkes IA, Runions J, Kearns A, Hawes C. 2006. Rapid, transient expression of fluorescent fusion proteins in tobacco plants and generation of stably transformed plants. *Nature Protocols* **1**: 2019–2025.

Stauder R, Welsch R, Camagna M, Kohlen W, Balcke GU, Tissier A, Walter MH. 2018. Strigolactone levels in dicot roots are determined by an ancestral symbiosis-regulated clade of the PHYTOENE SYNTHASE gene family. *Frontiers in Plant Science* **9**: 255.

Sun T, Yuan H, Cao H, Yazdani M, Tadmor Y, Li L. 2018. Carotenoid metabolism in plants: the role of plastids. *Molecular Plant* **11**: 58–74.

Tholl D. 2015. Biosynthesis and biological functions of terpenoids in plants. *Advances in Biochemical Engineering/Biotechnology* **148**: 63–106.

Vranová E, Coman D, Gruissem W. 2013. Network analysis of the MVA and MEP pathways for isoprenoid synthesis. *Annual Review of Plant Biology* **64**: 665–700.

Walter MH, Stauder R, Tissier A. 2015. Evolution of root-specific carotenoid precursor pathways for apocarotenoid signal biogenesis. *Plant Science* **233**: 1–10.

Wang C, Chen Q, Fan D, Li J, Wang G, Zhang P. 2016. Structural analyses of short-chain prenyltransferases identify an evolutionarily conserved GFPPS Clade in Brassicaceae plants. *Molecular Plant* **9**: 195–204.

Wang G, Dixon RA. 2009. Heterodimeric geranyl(geranyl)diphosphate synthase from hop (*Humulus lupulus*) and the evolution of monoterpene biosynthesis. *Proceedings of the National Academy of Sciences, USA* **106**: 9914–9919.

Wang J, Lin H-X, Su P, Chen T, Guo J, Gao W, Huang L-Q. 2019. Molecular cloning and functional characterization of multiple geranylgeranyl pyrophosphate synthases (ApGGPPS) from *Andrographis paniculata*. *Plant Cell Reports* **38**: 117–128.

Wang Q, Huang X-Q, Cao T-J, Zhuang Z, Wang R, Lu S. 2018. Heteromeric geranylgeranyl diphosphate synthase contributes to carotenoid biosynthesis in ripening fruits of red pepper (*Capsicum annuum* var. *conoides*). *Journal of Agriculture and Food Chemistry* **66**: 11691–11700.

Yuan H, Zhang J, Nageswaran D, Li L. 2015. Carotenoid metabolism and regulation in horticultural crops. *Horticulture Research* **2**: 15036.

Zhang M, Su P, Zhou Y-J, Wang X-J, Zhao Y-J, Liu Y-J, Tong Y-R, Hu T-Y, Huang L-Q, Gao W. 2015. Identification of geranylgeranyl diphosphate synthase genes from *Tripterygium wilfordii*. *Plant Cell Reports* **34**: 2179–2188.

Zhang M, Yuan B, Leng P. 2009. The role of ABA in triggering ethylene biosynthesis and ripening of tomato fruit. *Journal of Experimental Botany* **60**: 1579–1588.

Zhou F, Pichersky E. 2020. The complete functional characterisation of the terpene synthase family in tomato. *New Phytologist* **226**: 1341–1360.

Zhou F, Wang C-Y, Gutensohn M, Jiang L, Zhang P, Zhang D, Dudareva N, Lu S. 2017. A recruiting protein of geranylgeranyl diphosphate synthase controls metabolic flux toward chlorophyll biosynthesis in rice. *Proceedings of the National Academy of Sciences, USA* **114**: 6866–6871.

Zhu XF, Suzuki K, Okada K, Tanaka K, Nakagawa T, Kawamukai M, Matsuda K. 1997a. Cloning and functional expression of a novel geranylgeranyl pyrophosphate synthase gene from *Arabidopsis thaliana* in *Escherichia coli*. *Plant and Cell Physiology* **38**: 357–361.

Zhu XF, Suzuki K, Saito T, Okada K, Tanaka K, Nakagawa T, Matsuda H, Kawamukai M. 1997b. Geranylgeranyl pyrophosphate synthase encoded by the newly isolated gene GGPS6 from *Arabidopsis thaliana* is localized in mitochondria. *Plant Molecular Biology* **35**: 331–341.

Zouine M, Maza E, Djari A, Lauvernier M, Frasse P, Smouni A, Pirrello J, Bouzayen M. 2017. TomExpress, a unified tomato RNA-Seq platform for visualization of expression data, clustering and correlation networks. *The Plant Journal* **92**: 727–735.

© 2021 The Authors
New Phytologist © 2021 New Phytologist Foundation

Supporting Information

Additional Supporting Information may be found online in the Supporting Information section at the end of the article.

Fig. S1 Subcellular localisation of tomato GGPPS proteins.

Fig. S2 Purification of recombinant GGPPS proteins for *in vitro* activity assays.

Fig. S3 Biochemical activity of purified recombinant GGPPS proteins.

Fig. S4 Transcript levels of tomato genes in different tissues.

Fig. S5 Gene co-expression network (GCN) analysis of tomato plastidial *GGPPS* genes in leaf and fruit tissues.

Fig. S6 DNA sequence alignment of *SlG2* CRISPR mutants.

Fig. S7 DNA sequence alignment of *SlG3* CRISPR mutants.

Fig. S8 Protein alignments of WT and mutant SlG2 and SlG3 sequences.

Fig. S9 Fruit ripening initiation and progression in WT and mutant plants.

Fig. S10 Relative levels of plastidial isoprenoids in mature green fruits from WT and mutant lines.

Fig. S11 PCR-based genotyping of nongerminating F2 seeds from the cross of *slg2-2* and *slg3-1* mutant plants.

Methods S1 Growth conditions, sample collection and phenotypic analyses.

Methods S2 Constructs.

Methods S3 RNA isolation and cDNA synthesis.

Methods S4 GGPPS activity determination.

Methods S5 Subcellular localisation assays.

Methods S6 Co-immunoprecipitation assays.

Methods S7 Isoprenoid analysis.

Table S1 Primers used in this work.

Table S2 Constructs and cloning details.

Table S3 List of tomato GGPPS-like sequences.

Table S4 List of plastidial isoprenoid-related genes used for the tomato GGPPS GCN analyses.

Table S5 List of expression datasets in the TomExpress database used for the generation of the tomato GGPPS GCN in leaf and fruit tissues.

Table S6 Co-expression of tomato GGPPS paralogues (guide genes) with isoprenoid-related genes (query genes) in leaf and fruit tissues.

Table S7 Levels of GGPP-derived metabolites detected by HPLC.

Table S8 Relative levels of metabolites detected by GC-MS in samples from WT and mutant young leaves.

Table S9 Parameters used for peak annotation in leaves.

Table S10 Relative levels of metabolites detected by GC-MS in samples from WT and mutant B + 10 fruit.

Table S11 Parameters used for peak annotation in B + 10 fruit.

Please note: Wiley Blackwell are not responsible for the content or functionality of any Supporting Information supplied by the authors. Any queries (other than missing material) should be directed to the *New Phytologist* Central Office.

© 2021 The Authors
New Phytologist © 2021 New Phytologist Foundation

SUPPORTING INFORMATION

Several geranylgeranyl diphosphate synthase isoforms supply metabolic substrates for carotenoid biosynthesis in tomato

M. Victoria BARJA, Miguel EZQUERRO, Stefano BERETTA, Gianfranco DIRETTO, Igor FLOREZ-SARASA, Elisenda FEIXES, Alessia FIORE, Rumyana KARLOVA, Alisdair R. FERNIE, Jules BEEKWILDER, Manuel RODRIGUEZ-CONCEPCION

Article acceptance date: 08 February 2021

METHODS

Method S1. Growth conditions, sample collection and phenotypic analyses. Tomato (*Solanum lycopersicum* var. MicroTom) seeds were surface-sterilized by a 15 min incubation in 25 mL of 40% bleach containing a drop of Tween-20 followed by 3 consecutive 10 min washes with sterilized milli-Q water. Sterile seeds were germinated on plates with solid 0.5x Murashige and Skoog medium without vitamins or sucrose. The medium was supplemented with kanamycin (100 µg/mL) when required to select transgenic plants. After stratification at 4 °C in the dark for at least 3 days, plates were incubated in a climate-controlled growth chamber at 24 °C with a photoperiod of 10 h of darkness for 14 h of fluorescent white light at a photosynthetic photon flux density of 140 µmol m^{-2} s^{-1}. After 1 to 2 weeks, seedlings were transferred to soil and grown under standard greenhouse conditions (14 h light at 27 ± 1 °C and 10 h dark at 22 ± 1 °C). Photosynthetic activity was assessed by measuring chlorophyll *a* fluorescence with a MAXI-PAM fluorometer (Walz). The effective quantum yield ϕPSII (ΔF/Fm') of young and mature tomato leaves was measured as (Fm'−Fs)/Fm', where Fm' and Fs are the maximum and the minimum fluorescence of light exposed plants, respectively. The light intensity chosen was 21 PAR (actinic light, AL=2). The results are presented as the average of three biological replicates and four different leaf areas for each replicate. For the analysis of flowering time, at least five independent plants of each genotype were used. Flowering time was assessed by counting the number of days from germination until the first flower was fully opened (anthesis) or the number of leaves in the plant at this first anthesis day. Fruit pigmentation was measured using the TomatoAnalyzer 4.0 software (https://vanderknaaplab.uga.edu/tomato_analyzer.html). Average Red Color of three different whole tomatoes was quantified using the default red color calibrator sorted by the software as standard. For deetiolation experiments, seeds were sown on sterile water-soaked cotton in plastic containers. After stratification, seeds were exposed to fluorescent white light for 2-4 hours at 22°C to induce germination. The containers were then covered with a double layer of aluminum foil and kept in darkness at 22 °C. After one week, seedlings were exposed to light and samples were harvested after 0, 6 and 24 h. Control samples were germinated and grown under continuous light and collected at the 0 h time point. Leaf samples were collected from four-week-old plants. Young leaf samples correspond to growing leaflets from the fifth and sixth true leaves, and mature leaf samples correspond to fully expanded leaflets from the third or fourth leaf. Tomato fruit pericarp samples were collected at four ripening stages based on days post-anthesis (DPA) or days post-breaker (DPB): mature green (~30 DPA), breaker (~35 DPA), orange (~38-40 DPA) and red (~45-50 DPA or 10 DPB). Full seedlings, leaflets, and pericarp samples were frozen in liquid nitrogen immediately after collection, freeze-dried and stored at -80 °C.

Method S2. Constructs. Full-length cDNAs encoding SlG1-5 and PSY1-2 proteins without their stop codons were amplified by PCR and cloned via BP clonase into pDONR207 entry plasmid using Gateway (GW) technology (Invitrogen). Full-length sequences were then subcloned through an LR reaction into pGWB405 plasmid for subcellular localization assays, or into pGWB414 and pGWB420 plasmids for co-immunoprecipitation experiments. Constructs in pGWB405, pGWB414 and pGWB420 vectors harbor GFP, 3x-HA and 10x-Myc tags, respectively. These tag sequences are fused to the C-terminus of each cloned element and the expression module is controlled by the CaMV 35S promoter. For recombinant protein production in *E. coli*, SlG1-3 versions lacking the predicted transit peptide for plastid import were amplified from pGWB405 constructs, cloned into pDONR207 plasmid, and then subcloned into pET32-GW plasmid (fusing a 6x-His tag at the N-terminal end of the cloned fragments) under the control of the T7 promoter. For CRISPR-Cas9-mediated disruption of *SlG2* and *SlG3*, two single guide RNAs (sgRNA) sequences were designed encompassing an *EcoRI* and a *PstI* restriction site for *SlG2* and *SlG3* genes, respectively (Figures S6 and S7). A pair of primers for each guide was designed, denaturalized and assembled into pENC1.1 (pENTRY) vector previously digested with *BbsI.* The entry vectors contained the corresponding sgRNA expression cassette flanked by *Bsu36I* and *MluI* restriction sites, and by GW recombinant sites to allow both types of interchange with a pDE-Cas9 plasmid providing kanamycin resistance (pDESTINY). The final binary vectors were generated in a two-step cloning process that involved *Bsu36I* and *MluI* digestion-ligation of the first sgRNA into the pDE-Cas9 vector followed by an LR reaction to subclone the second sgRNA of each gene into the pDE-Cas9 vector already containing the first sgRNA. For activity assays in *E. coli*, full-length *SlG2*, *SlG3*, *slg2-1*, *slg2-2*, *slg3-1* and *slg3-2* sequences were amplified from genomic DNA of the corresponding lines and cloned into the *SmaI* site of the pBluescript SK+ plasmid. All constructs were confirmed by restriction mapping and DNA sequencing. Information about primers used and cloning details are described in Tables S1 and S2, respectively.

Method S3. RNA isolation and cDNA synthesis. Total RNA was isolated from tomato freeze-dried tissue (seedlings, leaves or fruit pericarp) using the Maxwell® RSC Plant RNA Kit with the Maxwell® RSC Instruments (Promega) following the manufacturer's instructions. RNA was quantified using a NanoDropTM 8000 spectrophotometer (ThermoFischer Scientific) and checked for integrity by agarose gel electrophoresis. The Transcriptor First Strand cDNA Synthesis Kit (Roche) was used to reverse transcribe 0.5 µg of extracted RNA into 20 µL of cDNA, which was subsequently diluted ten-fold and stored at -20 °C for further analysis. Relative mRNA abundance was evaluated via Real-Time Quantitative Polymerase Chain Reaction (RT-qPCR) in a reaction volume of 20 µL containing 10 µL of the LightCycler 480 SYBR Green I Master Mix (Roche), 0.3 µM of each specific forward and reverse primer (Table S1) and 5 µL of cDNA. The RT-qPCR was carried out on a LightCycler 480 Real-Time PCR System (Roche). Three independent biological replicates of each condition and at least two technical replicates of each biological replicate were performed. Primer efficiencies were calculated using serial dilutions of genomic or plasmidic DNA.

Method S4. GGPPS activity determination. Constructs to produce different truncated GGPPS protein versions were generated in the pET32-GW vector (Table S2). Competent *E. coli Rosetta 2* (DE3) cells (Novagen) were separately transformed with each construct and single transformants were grown overnight at 37 °C in 5 mL of LB medium supplemented with appropriate antibiotics. Then, 250 µL of each overnight culture were diluted in 25 mL 2xYT medium with the required antibiotics and incubated at 37 °C and 250 rpm until reaching an OD600 between 0.5 and 0.8. After inducing the production of the recombinant proteins with 1 mM IPTG, the cultures were grown overnight at 18 °C and 250 rpm. Bacterial cells were harvested by centrifugation at 2,000 *g* for 15 min and pellets were resuspended in 1 mL *Assay* buffer (15 mM MOPSO, 12.5% v/v glycerol, 1 mM ascorbic acid, pH 7.0, 1 mM $MgCl_2$, 2 mM DTT). About 0.2 g of

zirconium/silica beads 0.1 mm (BioSpec Products) were added and bacterial lysis was carried out in two rounds of shaking for 10 s at a speed of 6.5 in a FastPrep machine (FP120 Bio101 Savant). Cell lysates were subsequently centrifuged for 10 min at 13,000 g and 4 °C, and supernatants were collected for SDS-PAGE and GGPP activity assays. Enzymatic assays were performed in Eppendorf tubes in a final volume of 200 µL containing 25 µL of cell extract, 150 µM IPP and 50 µM DMAPP in *Assay* buffer supplemented with 5 mM Na_3O_4V. The reaction mix was incubated for 2 h at 30 °C in mild agitation and stopped by adding 800 µL of 100% methanol / 0.5% formic acid. After vortexing, samples were sonicated for 15 min and centrifuged at maximum speed for 10 min. Supernatants were then evaporated in a SpeedVac concentrator and 80 µL of 100% methanol / 0.65% formic acid were added to the remnant sample. After centrifugation at maximum speed for 15 min, the supernatants were transferred to glass vials. The detection of prenyl diphosphate products by Liquid Chromatography-Mass Spectrometry (LC-MS) using XcaliburTM software (ThermoFischer Scientific) for data acquisition and visualization. Kinetic parameters were calculated using 3 µg of purified SlG1, SlG2, SlG3 and AtG11 enzymes. pET32 constructs were used to produce 6xHis-tagged recombinant enzymes (Table S2) and protein purification from *E. coli Rosetta* cells was carried out using nickel-nitrilotriacetic acid (Ni-NTA) agarose (Qiagen) (Barja and Rodríguez-Concepción, 2020). IPP and DMAPP substrates and FPP and GGPP standards were obtained from Echelon Biosciences.

Method S5. Subcellular localization assays. *A. tumefaciens* GV3101 cells were transformed with pGWB405-based constructs (Table S2) and grown on LB plates at 28 °C for 3 days. A single PCR-confirmed colony per construct was grown overnight at 28 °C in 5 mL antibiotic-supplemented LB media and 500 µL of the grown culture were then inoculated in 20 mL of fresh medium. After another overnight incubation, bacterial cells were pelleted and resuspended in infiltration buffer (10 mM MES pH5.5-6, 10 mM $MgSO_4$, 150 µM acetosyringone) to a final OD600 of 0.5. To prevent silencing, *N. benthamiana* leaves were co-infiltrated with a second *Agrobacterium* strain harboring a HC-Pro silencing suppressor. A 1:1 mixture of the two cultures was infiltrated with a syringe in the abaxial part of leaves from 4 to 6-week old *N. benthamiana* plants. GFP signal and chlorophyll autofluorescence were detected with an Olympus FV 1000 confocal laser-scanning microscope using an argon laser for excitation (at 488 nm) and a 500–510 nm filter (for GFP) or a 610–700 nm filter (for chlorophyll). All images were acquired using the same confocal parameters.

Method S6. Co-immunoprecipitation assays. Constructs encoding Myc- and HA-tagged tomato GGPPS and PSY proteins (Table S2) were transformed into *A. tumefaciens* GV3101 strains. A plasmid containing the Arabidopsis phosphoribulokinase protein with a Myc tag (pGWB417_PRK-Myc) was kindly provided by Dr. Ernesto Llamas and used as a negative control. Different *Agrobacterium* infiltration mixtures were prepared and infiltrated into *N. benthamiana* leaves, and 3 days later 1.2 g of agroinfiltrated leaf tissue was frozen in liquid nitrogen and directly stored at -80 ºC until use. For crude extracts preparation, frozen leaf samples were ground in liquid nitrogen and incubated in 4 ml lysis buffer (50 mM Tris-HCl pH7.5, 150 mM NaCl, 5% glycerol, 0.05% NP-40, 1 mM $MgCl_2$, 0.5 mM PMSF, 1X Sigma protease inhibitor, 10 mM DTT, 2% PVPP) at 4 ºC for 15 min using a rotator to form a homogeneous suspension, that was then pre-clarified at 3,000 g for 15 min. Supernatants were cleaned by centrifugation at 16,000 g for 30 min and used for protein quantification. Crude extracts were then adjusted to the same volume and protein concentration with lysis buffer lacking PVPP. An aliquot of each adjusted crude extract was boiled for 10 min in SDS-loading buffer and stored at -20 ºC as input sample. 500 µL of each crude extract were incubated overnight with 1 µL of monoclonal αMyc antibody (Sigma) in a rotator at 4 ºC. Immunoprecipitation of αMyc interacting protein/complexes was carried out using Pierce Protein A/G Magnetic Beads (ThermoFischer Scientific). After pre-washing the magnetic beads (50 mM Tris-HCl pH7.5, 500 mM NaCl, 5% glycerol, 0.05% NP-40, 1 mM $MgCl_2$,

0.5 mM PMSF, 1X Sigma protease inhibitor, 10 mM DTT), the Co-IP sample (crude extract + αMyc antibody) was added and incubated with the beads at room temperature for 1 h with shaking. The beads were then collected with a magnetic stand and repeatedly washed with washing buffer and water. After removing the water from the last washing step, 100 µL of SDS-PAGE loading buffer were added to the beads and boiled for 10 min. Afterwards, the beads were magnetically removed from the supernatants containing the immunoprecipitated complexes and stored at -20 ºC. The presence of Myc- and HA-tagged proteins in input and Co-IP samples were detected by immunoblot analyses using 1:5000-diluted αMyc (Sigma) and 1:1000-diluted αHA (Roche) as primary antibodies. Horseradish peroxidase (HRP)-conjugated secondary antibodies against mouse and rat IgGs were used in a 1:10000 dilution. WesternBright ECL Western blotting detection kit (Advansta) and Amersham ECL Prime Western Blotting Detection Kit (GE Healthcare) were used for detection and the signal was visualized using the ChemiDoc Touch Imaging System (Bio-Rad).

Method S7. Isoprenoid analysis. Carotenoids, chlorophylls and tocopherols were extracted as follows. A mix was prepared in 2 mL Epperdorf tubes with ca. 4 mg of freeze-dried leaf tissue, 375 µL of methanol as extraction solvent and 25 µL of a 10 % (w/v) solution of canthaxanthin (Sigma) in chloroform as internal control. After vortexing the samples for 10 s and lysing the tissue with 4 mm glass beads for 1 min at 30 Hz in the TissueLyser II (Qiagen), 400 µL of Tris-HCl pH:7.5 were added and the samples were again mixed for 1 min in the TissueLyser. Next, 800 µL of chloroform were added and the mixture was again shaken for 1 min in the TissueLyser. Samples were then centrifuged for 5 min at maximum speed at 4 ºC. The lower organic phase was placed in a new 1.5 mL tube and evaporated using a SpeedVac. Fruit isoprenoids were extracted using 15 mg of freeze-dried tissue and 1 ml of hexane/acetone/methanol 2:1:1 as extraction solvent. After vortexing and lysing the tissue with the TissueLyser as described for leaves, 100 µL of milli-Q water were added. Then, 1 min of TissueLyser was carried out again and samples were centrifuged for 3 min at 500 *g* and 4 ºC. The organic phase was transferred to a 1.5 mL tube and the rest was re-extracted by adding 1 mL of hexane/acetone/methanol 2:1:1 solvent, TissueLyser-mixing for 1 min and centrifuging for 5 min at maximum speed and 4 ºC. The new organic phase was mixed with that previously extracted and evaporated using the SpeedVac system. Extracted metabolites from leaf and fruit pericarp samples were resuspended in 200 µL of acetone by using an ultrasound bath (Labolan) and filtered with 0.2 µm filters into amber-colored 2 mL glass vials. Separation and detection was next performed using an Agilent 1200 series HPLC system (Agilent Technologies). Eluting chlorophylls and carotenoids were monitored using a photodiode array detector whereas tocopherols were identified using a fluorescence detector. Peak areas of chlorophylls (650 nm), carotenoids (470 nm for lycopene, lutein, β-carotene, violaxanthin, neoxanthin and canthaxanthin or 280 nm for phytoene), and tocopherols (330 nm) were determined using the Agilent ChemStation software. Quantification was performed by comparison with commercial standards (Sigma).

FIGURES

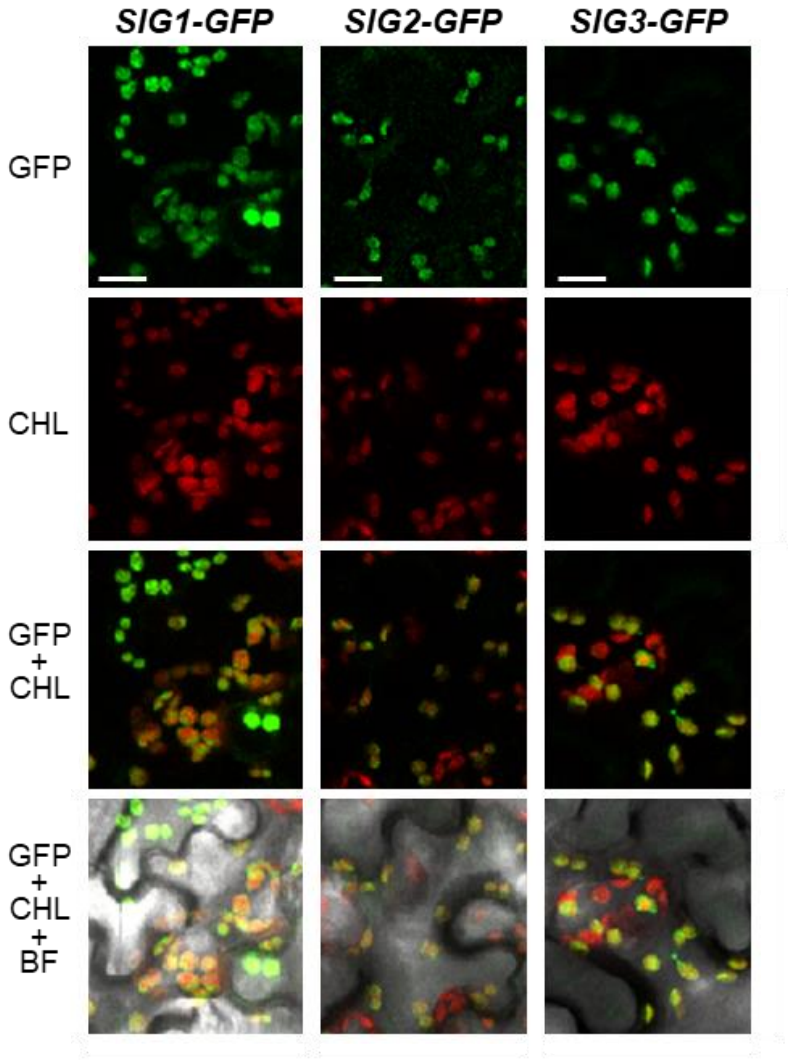

Figure S1. Subcellular localization of tomato GGPPS proteins. Representative confocal microscopy images of *N. benthamiana* leaf cells transiently expressing the indicated GFP fusion proteins are shown. For each construct, GFP fluorescence (GFP), chlorophyll autofluorescence (CHL) and merged images of them either alone (GFP+CHL) or overlapped with the bright field image (GFP+CHL+BF) are shown for the same field. Bars, 10 µm.

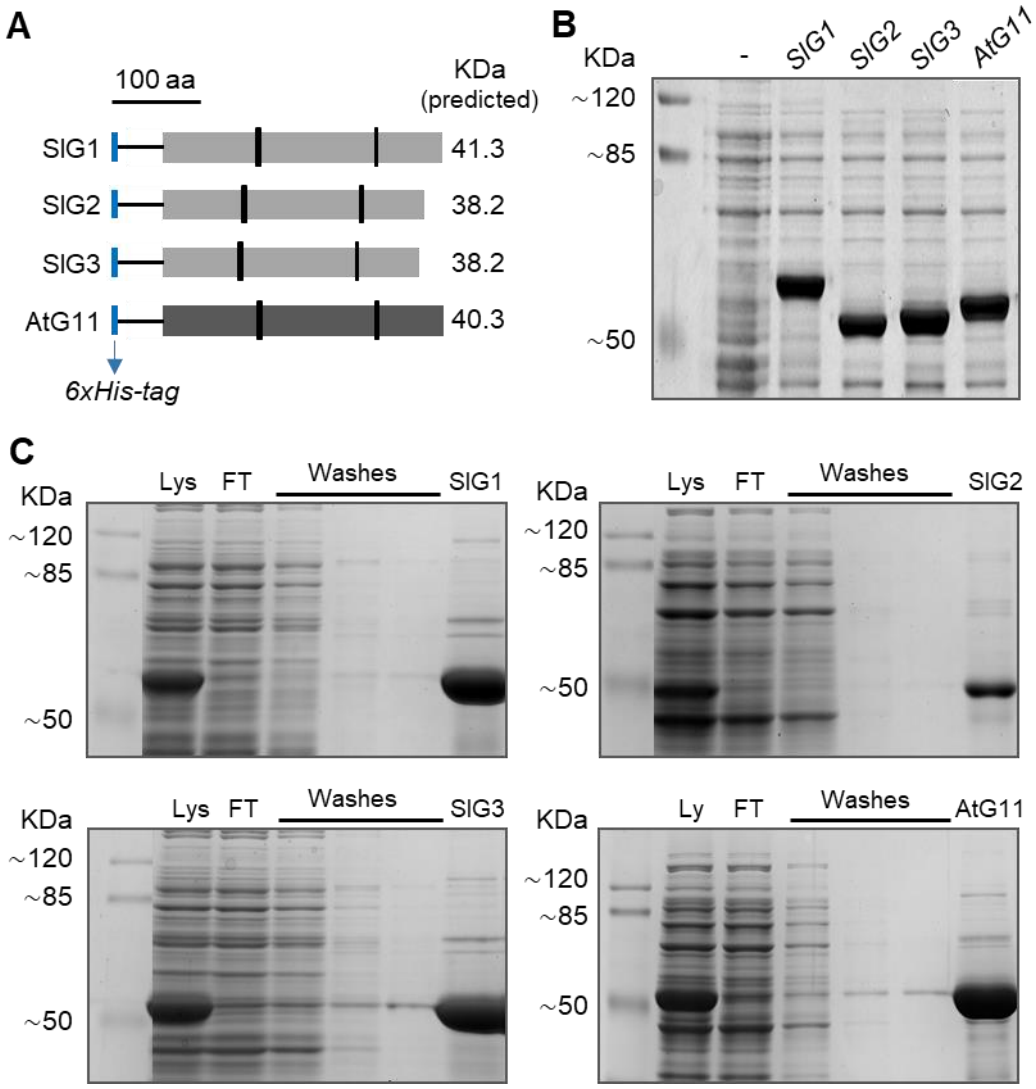

Figure S2. Purification of recombinant GGPPS proteins for *in vitro* activity assays. **(A)** Schematic representation of the purified GGPPS enzyme versions lacking the predicted plastid-targeting peptide and fused to a 6xHis-tag (blue) in the N-terminal end. **(B)** Coomassie-Blue stained SDS-PAGE of total protein extracts from *E. coli Rosetta* cells transformed with constructs to express the indicated GGPPS versions or an empty plasmid (marked as "-"). After IPTG induction, a 10 µL aliquot of each culture was boiled for 10 min in SDS-loading buffer and run in a gel. A protein size ladder is shown in the left. **(C)** Coomassie-Blue stained gels showing the purification steps of the indicated proteins. The enzymes were purified from soluble lysates (Lys) of *E. coli* cells overproducing the corresponding recombinant protein. Lysates were separately incubated with Ni-NTA beads and the staining of the flow-through (FT) shows that most of the recombinant protein was retained in the Ni-NTA column. After several washes with 20 mM imidazole to remove non-specific proteins attached to the column, His-tagged enzymes were eluted using 150 mM imidazole. Purified proteins were then desalted, quantified and stored with glycerol 40% in the freezer until use for activity assays.

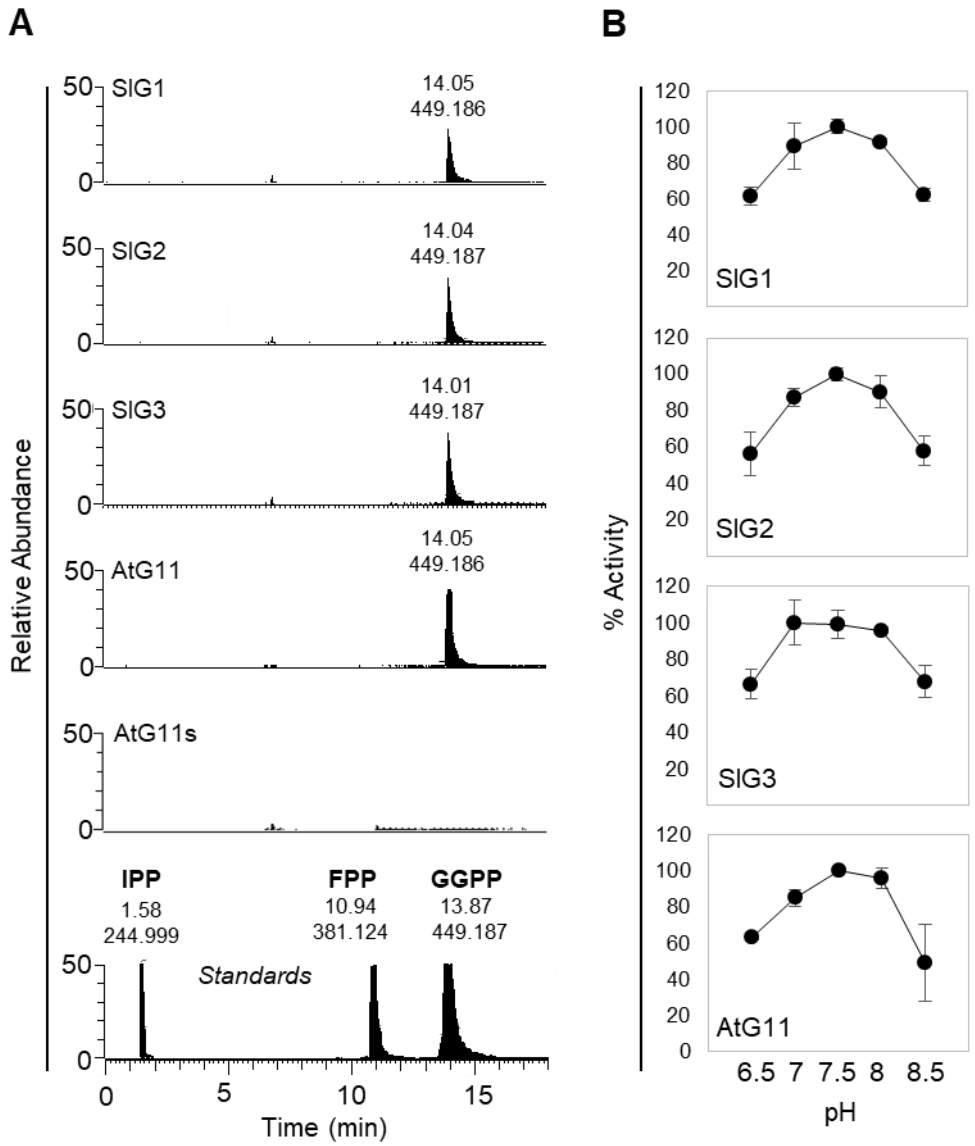

Figure S3. Biochemical activity of purified recombinant GGPPS proteins. (A) LC-MS chromatograms of reaction products. Extracts of *E. coli* cells overproducing the indicated recombinant proteins (with an N-terminal 6x-His tag instead of their predicted plastid-targeting peptide) were incubated with IPP and DMAPP. Prenyl diphosphate products in the *in vitro* assays were detected by LC-MS using mass-to-charge (m/z) ratios of 313.061 (GPP), 381.123 (FPP), 449.186 (GGPP) and 518.254 (GFPP). Retention times and m/z values of available standards is also shown in the bottom plot. **(B)** Optimal pH determination for the activity of each GGPPS assayed. Purified recombinant proteins were incubated with IPP and DMAPP under different pH conditions. Activity values are represented as the percentage of activity relative to the maximum activity obtained. Data correspond to the mean ± SD of n=3 independent replicates.

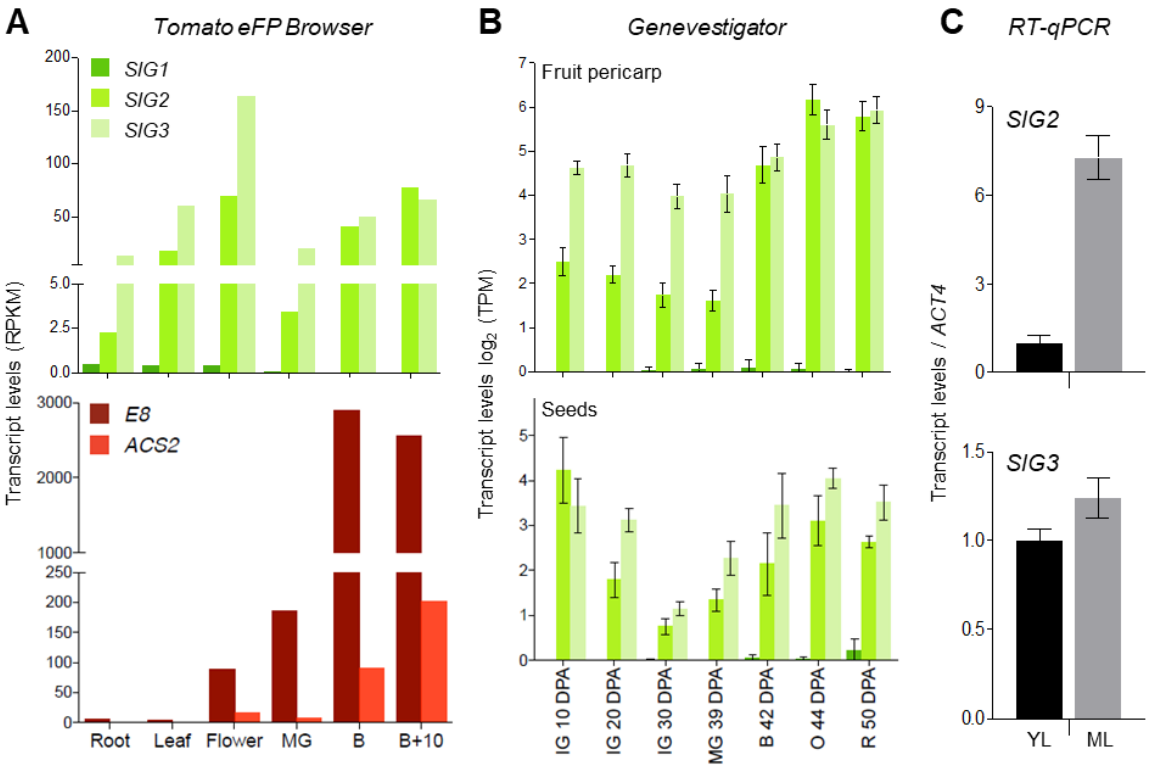

Figure S4. Transcript levels of tomato genes in different tissues. Abbreviations: DPA, days post-anthesis; IG, immature green; MG, mature green; B, breaker; O, orange, R, red; YL, young leaves; ML, mature leaves. **(A)** RNAseq data retrieved from the *Tomato eFP Browser* database (http://bar.utoronto.ca/efp_tomato/cgi-bin/efpWeb.cgi). Plots show the transcript levels of *SlG1-3, E8 (Solyc09g089580)* and *ACS2 (Solyc01g095080)* genes in root, leaf, flower and fruit pericarp during ripening. Expression data are represented as RPKM (Reads per Kilobase of transcript per Million mapped reads). **(B)** RNAseq data obtained from GeneInvestigator (https://genevestigator.com/). Plots show the transcript levels of *SlG1-3* genes in fruit pericarp and seeds during development. Levels are represented as $\log_2$ TPM (Transcripts per Million mapped reads). **(C)** RT-qPCR analysis of *SlG2* and *SlG3* transcript levels in young and mature leaves from WT plants. Expression values were normalized using *ACT4* and and they are shown relative to YL samples. Data correspond to the mean±SD of n=3 independent biological replicates.

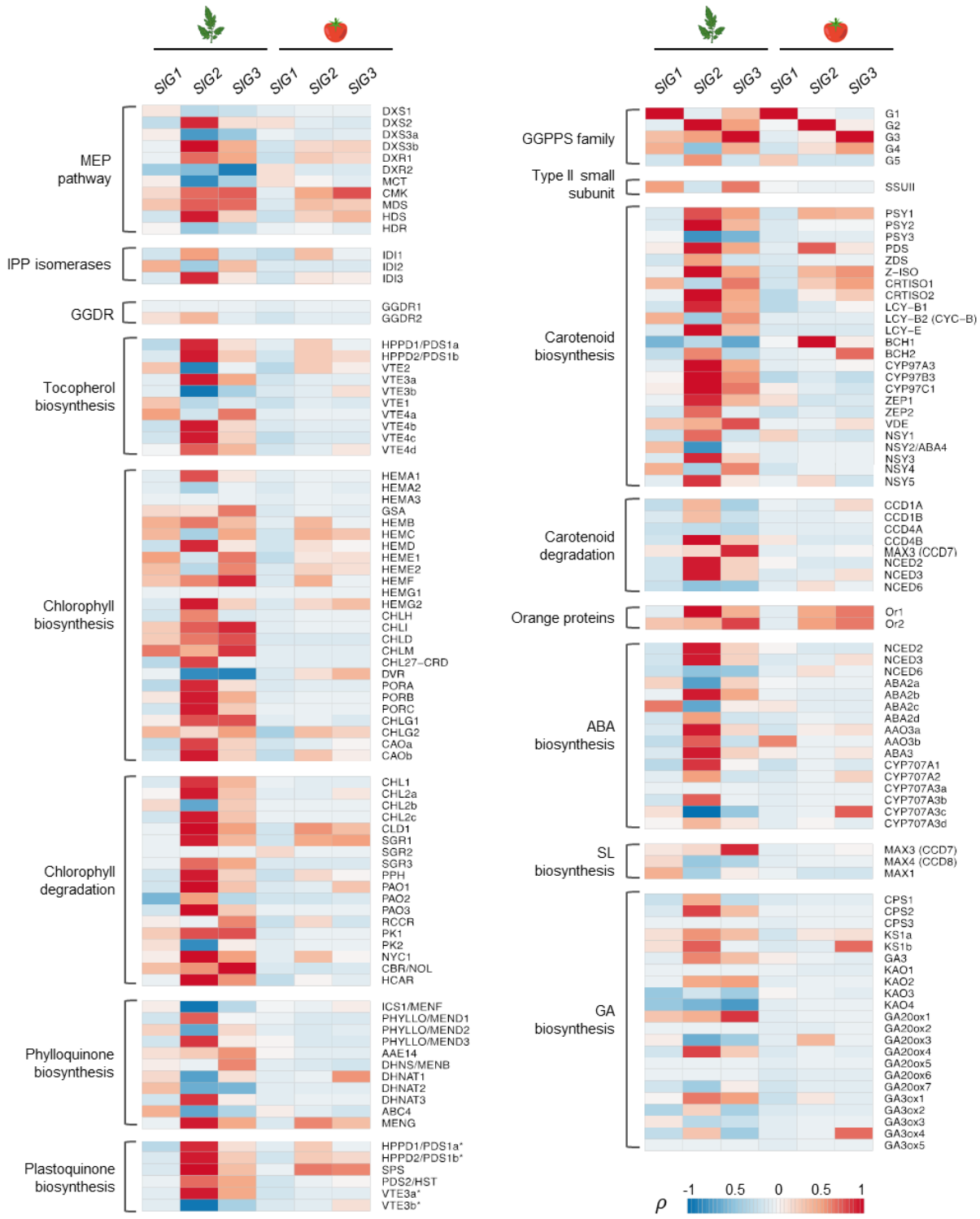

Figure S5. Gene co-expression network (GCN) analysis of tomato plastidial *GGPPS* genes in leaf and fruit tissues. Pairwise Pearson correlations (ρ) between the expression of genes encoding GGPPS isoforms and enzymes from the indicated plastidial isoprenoid pathways upstream and downstream of GGPP are represented as a heatmap. Gene abbreviations and accessions are listed in Table S4, leaf and fruit datasets used for the analysis are indicated in Table S5, and positive co-relation ρ values are shown in Table S6.

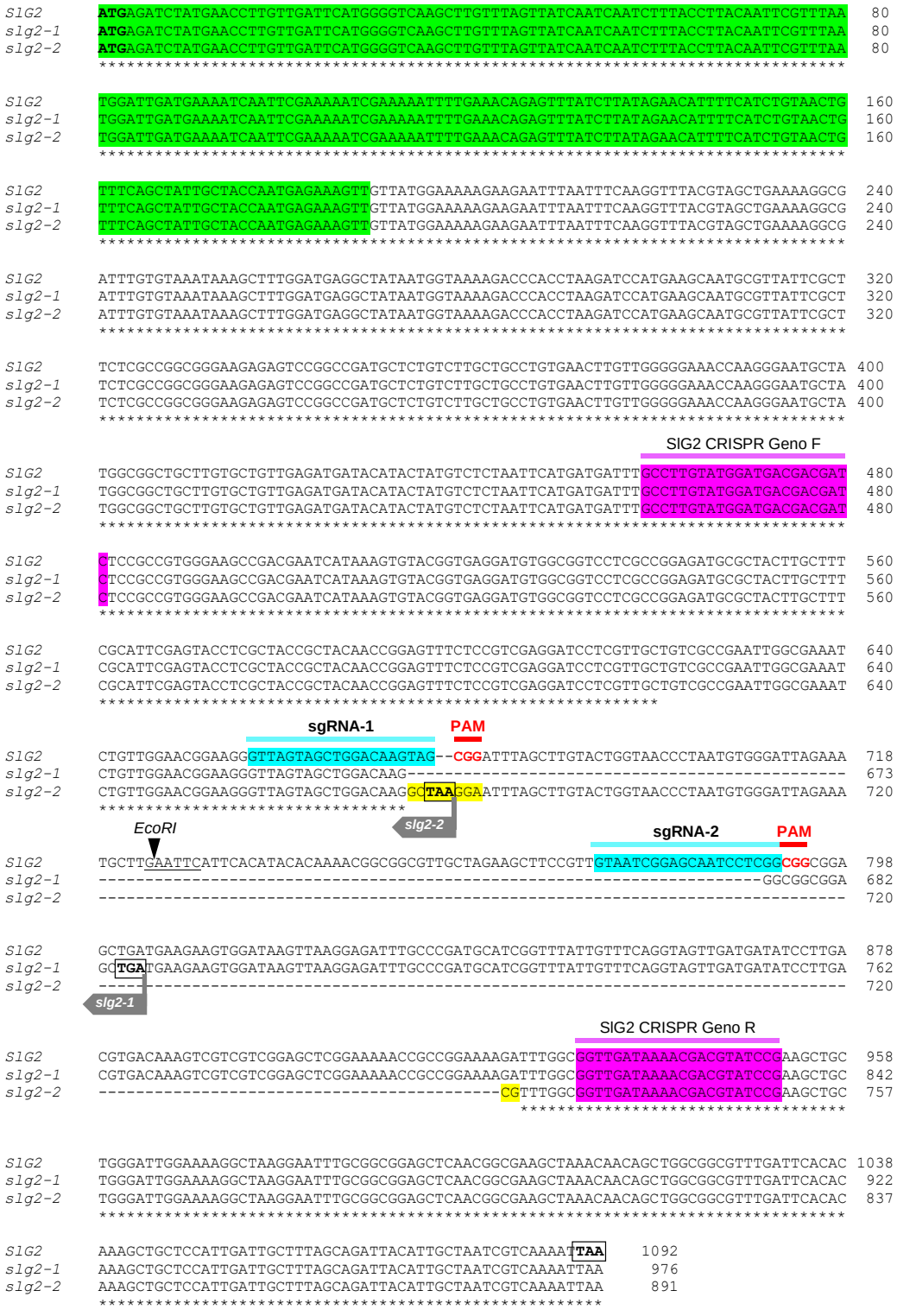

Figure S6. DNA sequence alignment of *SlG2* CRISPR mutants. Alignment was performed using *Clustal Omega* (https://www.ebi.ac.uk/Tools/msa/clustalo/) with default settings. The sequence encoding the predicted plastid-targeting peptide is boxed in green. Designed single-guide RNAs (sgRNA) and genotyping oligonucleotides are highlighted in blue and purple, respectively. The designed sgRNAs encompass an *EcoRI* restriction site (underlined in black). Protospacer adjacent motifs (PAM) are highlighted in red. Translation stop codons are boxed and marked in bold. Sequences changes due to CRISPR-Cas9 are depicted in yellow. Numbers at the end of each sequence indicate DNA sequence length.

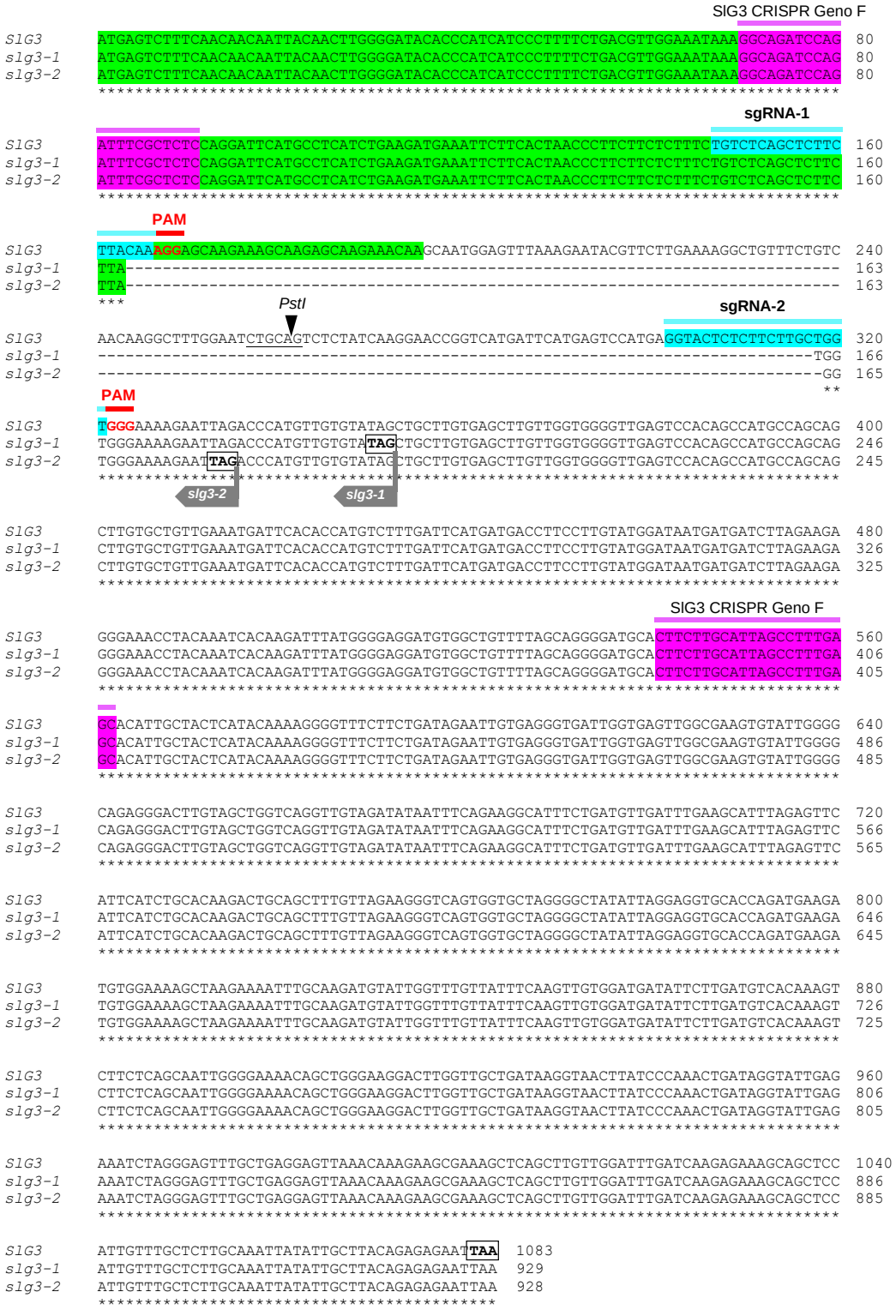

Figure S7. DNA sequence alignment of *SlG3* CRISPR mutants. Alignment was performed using *Clustal Omega* (https://www.ebi.ac.uk/Tools/msa/clustalo/) with default settings. The sequence encoding the predicted plastid-targeting peptide is boxed in green. Designed single-guide RNAs (sgRNA) and genotyping oligonucleotides are highlighted in blue and purple, respectively. The designed sgRNAs encompass a *PstI* restriction site (underlined in black). Protospacer adjacent motifs (PAM) are highlighted in red. Translation stop codons are boxed and marked in bold. Numbers at the end of each sequence indicate DNA sequence length.

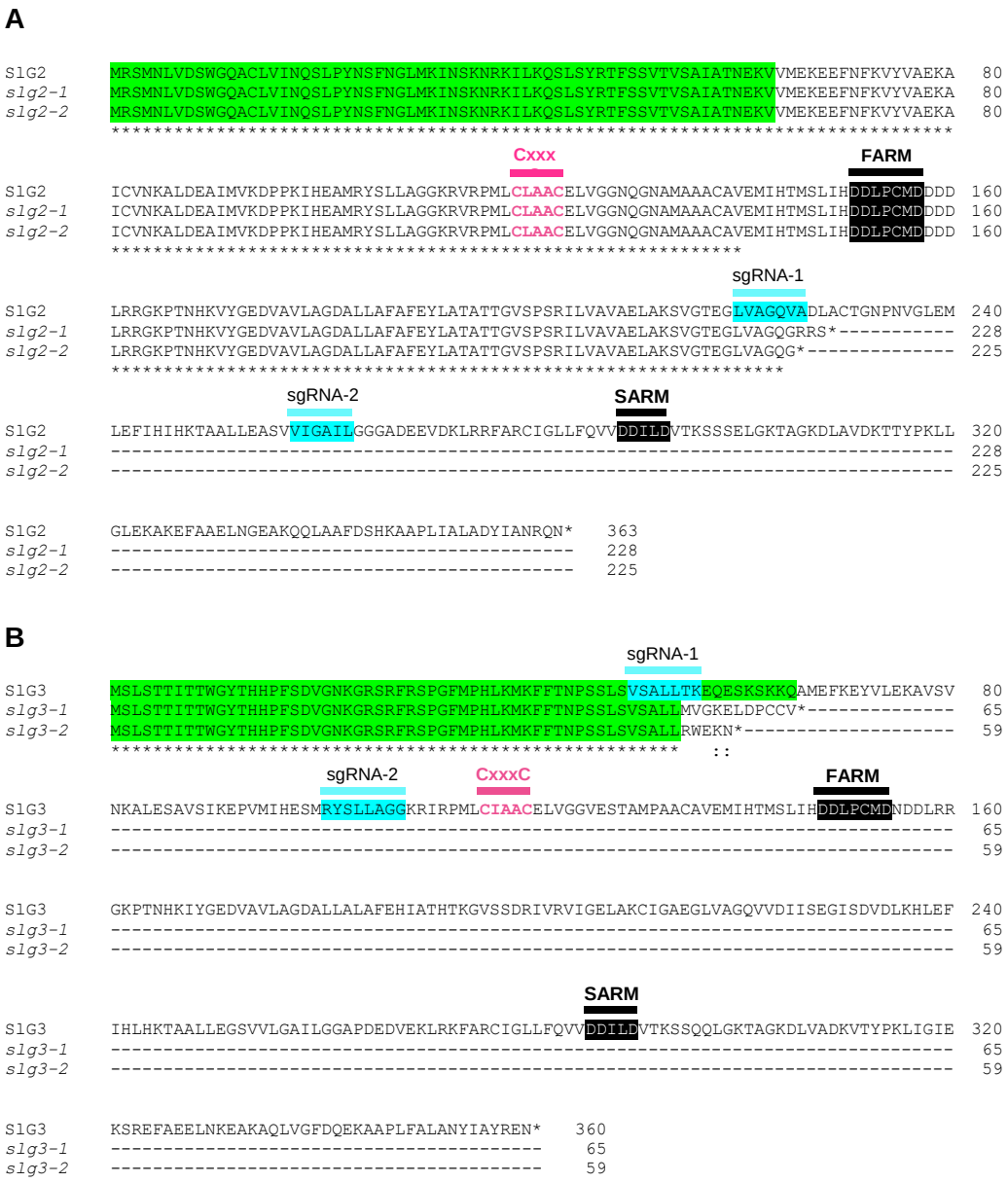

Figure S8. Protein alignments of WT and mutant SlG2 (A) and SlG3 (B) sequences. *Clustal Omega* (https://www.ebi.ac.uk/Tools/msa/clustalo/) with default settings was used for the alignment. The predicted targeting peptide, the region of the designed sgRNAs and the catalytic motifs FARM and SARM are boxed in green, blue and black, respectively. The protein-protein interaction CxxxC motifs (x = any hydrophobic residue) are highlighted in pink. Numbers at the end of each sequence indicate protein length.

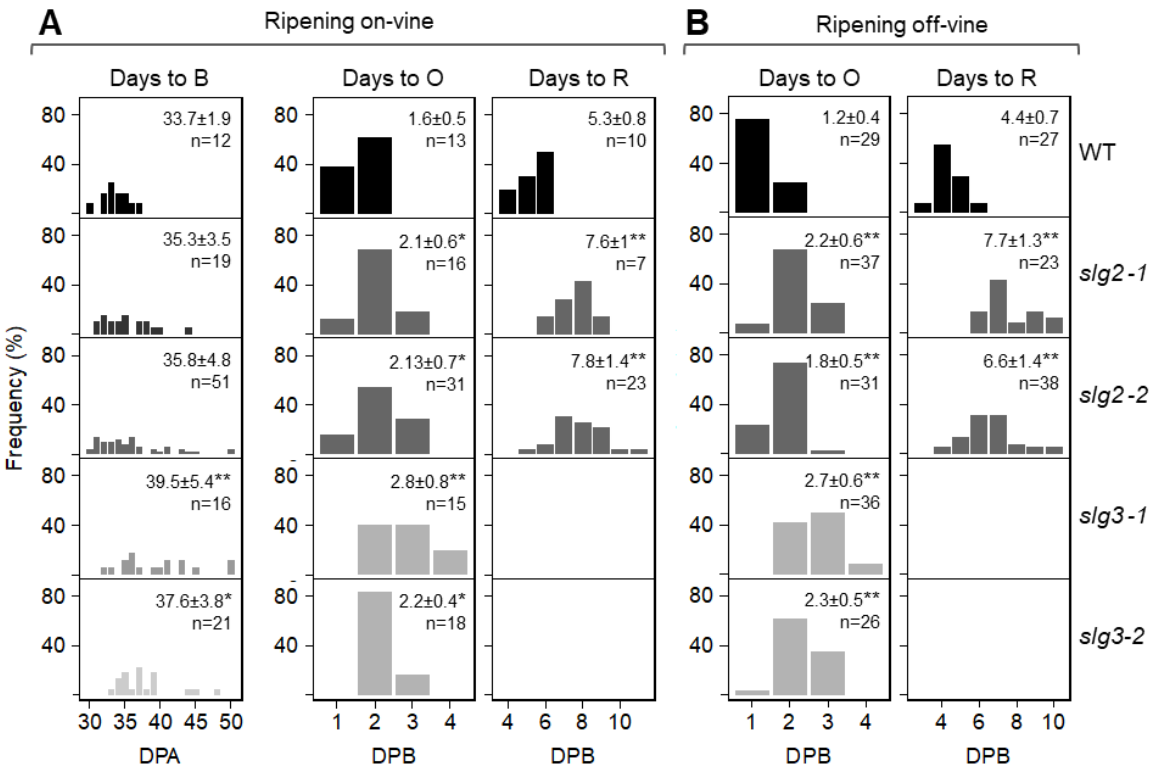

Figure S9. Fruit ripening initiation and progression in WT and mutant plants. Histograms represent the number of days to reach Breaker (B), Orange (O) and Red (R) fruit stages represented as days post-anthesis (DPA) or days post-breaker (DPB). On-vine **(A)** and off-vine **(B)** measurements are shown. For on-vine measurements, flowers were marked in anthesis and followed *in planta*. For off-vine measurements fruits were harvested at the B stage. The mean±SD values and the sample size (n) are shown in each histogram. Asterisks indicate statistically significant differences among means relative to WT samples (one-way ANOVA followed by Dunnett's multiple comparisons test, *p<0.05, **p<0.01).

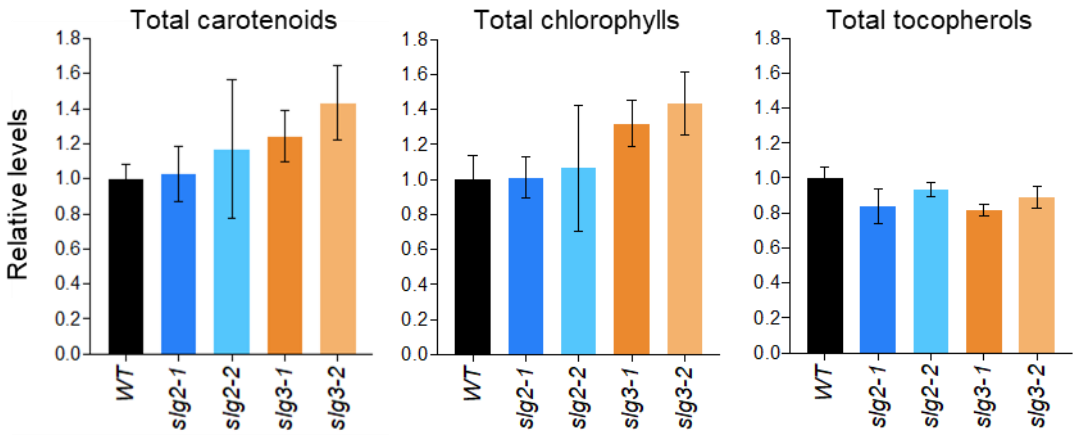

Figure S10. Relative levels of plastidial isoprenoids in mature green fruits from WT and mutant lines. Values correspond to the mean±SD of at least three independent biological replicates (n=3) relative to WT levels. No statistically significant differences among means were found (one-way ANOVA).

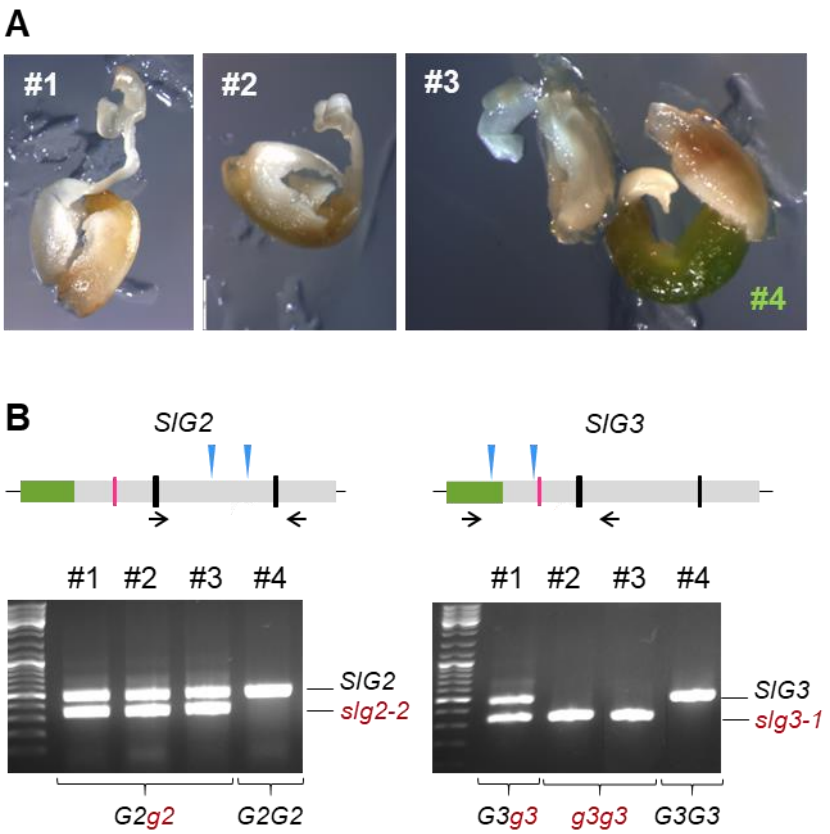

Figure S11. PCR-based genotyping of non-germinating F2 seeds from the cross of *slg2-2* and *slg3-1* mutant plants. (A) Non-germinating seeds were manually open to show the phenotype of their embryos. Only seed #4 showed a green embryo. **(B)** Scheme representing the *SlG2* and *SlG3* genes and the genotyping results. Blue arrowheads indicate the position of the designed sgRNAs to generate deletions, and black arrows represent primer pairs used for PCR-based genotyping. Gel pictures show the PCR amplification products from samples of the embryos shown in (A). The position of amplicons from WT and mutant genes (in black and red, respectively) is indicated.

TABLES S1-S11– see Excel file